

TECHNISCHE UNIVERSITÄT MÜNCHEN

Wissenschaftszentrum Weihenstephan für Ernährung, Landnutzung und Umwelt
Lehrstuhl für Entwicklungsgenetik

The role of *Glypican 4* during mouse brain development

Stefan Johann Andreas Weiß

Vollständiger Abdruck der von der Fakultät Wissenschaftszentrum Weihenstephan für Ernährung, Landnutzung und Umwelt der Technischen Universität München zur Erlangung des akademischen Grades eines

Doktors der Naturwissenschaften

genehmigten Dissertation.

Vorsitzender: Univ.-Prof. Dr. B. Schusser
Prüfer der Dissertation: 1. Univ.-Prof. Dr. W. Wurst
2. Univ.-Prof. A. Schnieke, PhD

Die Dissertation wurde am 12.01.2017 bei der Technischen Universität München eingereicht und durch die Fakultät Wissenschaftszentrum Weihenstephan für Ernährung, Landnutzung und Umwelt am 26.05.2017 angenommen.

Table of contents

Abstract.....	1
Zusammenfassung.....	1
I. Introduction.....	1
1. The extracellular matrix	1
2. The extracellular matrix of the central nervous system	2
3. Glypicans	3
3.1 Glypican structure	3
3.2 Glypican function during embryonic development.....	5
3.3 Glypican function in Wnt signaling modulation	5
3.4 Glypican function in Hedgehog (Hh) signaling modulation.....	7
3.5 Glypican function in Fgf signaling modulation	11
4. <i>Glypican 4</i> expression during mouse development and in the adult.....	12
5. Early development of the mammalian brain.....	14
5.1 Anterior neural induction by inhibition of posterior signals	14
5.2 Anterior-posterior forebrain patterning by Wnt and Fgf signaling	15
5.3 Dorso-ventral forebrain patterning by Hh signaling	16
6. Holoprosencephaly – defects in forebrain separation.....	17
7. Ciliopathies – primary cilium defects can cause holoprosencephaly.....	19
8. Pluripotent stem cells as a model of early neuroectoderm differentiation	20
9. Aims of the thesis	22
II. Results	23
1. Analysis of <i>Glypican 4</i> in mice	23
1.1 <i>Gpc4</i> expression in the developing and the adult brain.....	23
1.2 Generation of the <i>Gpc4</i> loss-of-function mouse line (<i>Gpc4</i> ^{-/-})	25
1.3 <i>Gpc4</i> ^{-/-} embryos show a broad spectrum of severe developmental defects.....	28
1.4 Holoprosencephaly in <i>Gpc4</i> ^{-/-} embryos	31
1.5 Phenotype penetrance is increased in <i>Gpc4</i> ^{-/-} females	35
1.6 <i>Gpc4</i> ^{-/-} phenotype expressivity is genetic background dependent	36
1.7 Impaired neural differentiation in the cortex of <i>Gpc4</i> ^{-/-} embryos.....	36
1.8 Wnt and Hh are misregulated candidate pathways in <i>Gpc4</i> ^{-/-} embryos.....	37
1.9 <i>Gpc4</i> does not act as an anterior Wnt signaling repressor	39
1.10 <i>Gpc4</i> ^{-/-} embryos show loss of anterior SHH domains.....	40
1.11 Hh signaling activity is impaired upon loss of <i>Gpc4</i> <i>in vitro</i>	42

Table of contents

1.12	Co-expression of <i>GPC4</i> with <i>BOC</i> in the human developing cortex	45
1.13	Cleavage resistant GPC4 can be expressed in primary cilia <i>in vitro</i>	46
1.14	<i>Gpc4</i> ^{-/-} embryos develop primary cilia in the node.....	47
2.	Analysis of <i>Gpc4</i> knockdown mouse embryonic stem cells (shGpc4).....	50
2.1	Optimization of a mESC-based neural differentiation protocol.....	50
2.2	shGpc4 mESCs show no differences in stem cell marker expression.....	53
2.3	shGpc4 mESCs show no differences in proliferation and cell death	54
2.4	shGpc4 mESCs show impaired neural differentiation	56
2.5	Impaired neural differentiation is not the result of increased colony numbers.....	56
2.6	Impaired neural differentiation is not due to a developmental delay.....	57
2.7	Impaired mesoderm differentiation of <i>Gpc4</i> knockdown mESCs	60
2.8	GPC4 treatment of shGpc4 mESCs does not rescue neural differentiation.....	61
2.9	Hh signaling is impaired in differentiating shGpc4 mESCs	62
2.10	Inhibition of Fgf signaling phenocopies <i>Gpc4</i> knockdown defects	65
III.	Discussion	67
	Summary of the results	67
1.	<i>Gpc4</i> modulates mouse forebrain development	69
1.1	<i>Gpc4</i> is specifically expressed in the developing anterior forebrain	69
1.2	The loss of <i>Gpc4</i> ^{-/-} can cause HPE	69
1.3	Female <i>Gpc4</i> ^{-/-} embryos have a higher phenotype penetrance.....	70
1.4	<i>Gpc4</i> controls different signaling pathways during mouse brain development	71
1.4.1	<i>Gpc4</i> does not repress Wnt signaling in the developing forebrain	72
1.4.2	Impaired Hh signaling most likely causes HPE in <i>Gpc4</i> ^{-/-} embryos	73
1.4.3	Other impaired signaling pathways might cause HPE.....	75
1.4.4	Diabetes in <i>Gpc4</i> ^{-/-} mothers might cause HPE in <i>Gpc4</i> ^{-/-} embryos	76
1.4.5	<i>Gpc4</i> ^{-/-} forebrain truncations and neural tube defects are not mediated by impaired Hh signaling	76
1.5	Phenotype variability of <i>Gpc4</i> ^{-/-} mice	78
1.5.1	Variability in human HPE	78
1.5.2	Impact of genetic background of <i>Gpc4</i> ^{-/-} mice	79
1.5.3	Variability of <i>Gpc3</i> ^{-/-} mice	79
1.5.4	Variability in defined genetic background and <i>Gpc</i> redundancy	80
1.5.5	Potential strategies to homogenize the <i>Gpc4</i> ^{-/-} phenotype	81
2.	<i>GPC4</i> mutations in humans – Simpson-Golabi-Behmel-Syndrome.....	82

Table of contents

2.1	Hh-mediated overgrowth by mutations in <i>GPC4</i>	82
2.2	Severe forms of SGBS are caused by impaired ciliogenesis	83
3.	<i>Gpc4</i> is required for early stem cell differentiation	85
3.1	Limitations of early <i>Gpc4</i> ^{-/-} embryo analysis	85
3.2	Early brain development is modeled by neural <i>in vitro</i> differentiation protocol	85
3.3	<i>Gpc4</i> is not required for mESC maintenance	86
3.4	<i>Gpc4</i> is required for early mESC differentiation.....	87
3.5	Released GPC4 does not rescue defects which are caused by the loss of <i>Gpc4</i>	89
3.6	Impaired Hh signaling does not cause differentiation defects in shGpc4 mESCs	90
3.7	Impaired Fgf signaling in shGpc4 mESCs might cause differentiation defects.....	91
4.	Conclusion	93
IV.	Materials and methods	96
1.	Materials.....	96
1.1	Equipment	96
1.2	Consumables	98
1.3	Kits.....	98
1.4	Chemicals.....	99
1.5	Buffers and solutions.....	102
1.6	Enzymes.....	104
1.7	Software	104
1.8	Primary antibodies	105
1.9	Secondary antibodies	105
1.10	Bacteria and bacteria culture media	105
1.11	Eukaryotic cell lines and cell media.....	106
1.12	Mouse lines	107
2.	Methods	107
2.1	Embryology.....	107
2.1.1	Ethics statement.....	107
2.1.2	Husbandry and matings.....	107
2.1.3	Generation of <i>Gpc4</i> loss-of-function mice.....	108
2.1.4	Genotyping	108
2.1.5	<i>In situ</i> hybridization on histological sections	109
2.1.6	X-ray micro-computed tomography (μ – CT)	110
2.1.7	μ -CT data analysis.....	110

Table of contents

2.1.8	Scanning electron microscopy.....	111
2.1	Generation of viral <i>Gpc4</i> knockdown and overexpression particles.....	111
2.1.1	Re-transformation of sh <i>Gpc4</i> and shScr constructs.....	111
2.1.2	Growth of bacteria	111
2.1.3	Plasmid DNA preparation.....	111
2.1.4	Lentivirus production	112
2.2	Cell culture.....	112
2.2.1	Production of irradiated mouse embryonic fibroblasts	112
2.2.2	Production of irradiated MS5 cells.....	113
2.2.3	Freezing and thawing of cells	113
2.2.4	mESC maintenance.....	113
2.2.5	Generation of <i>Gpc4</i> knockdown mESCs	114
2.2.6	mESC differentiation	114
2.2.7	Treatment of <i>Gpc4</i> knockdown mESCs with GPC4 conditioned medium	114
2.2.8	Inhibition of <i>in vitro</i> neural differentiation by signaling pathway inhibitors	115
2.2.9	Luciferase assay.....	116
2.2.10	GPC4 expression in primary cilia	117
2.3	Molecular Biology.....	117
2.3.1	RNA isolation	117
2.3.2	cDNA synthesis	117
2.3.1	mRNA expression analysis by PCR.....	117
2.3.2	<i>In situ</i> probe generation	120
2.3.3	Generation of the pCDH-HA- <i>Gpc4</i> -AISA construct.....	121
2.3.1	Sanger sequencing.....	121
2.3.2	Microarray expression profiling	122
2.3.3	Microarray statistical transcriptome analysis.	122
2.3.1	Human single cell RNAseq analysis	122
2.4	Methods in protein biochemistry.....	123
2.4.1	Western blot analysis	123
2.4.2	Immunocytochemistry stainings	125
2.4.1	Cell death analysis	125
2.4.1	<i>LacZ</i> staining	126
2.4.1	Whole mount immunohistochemistry	126
2.4.2	Immunohistochemistry stainings	127

Table of contents

2.4.1	Fluorescence microscopy.....	127
2.4.2	High-content imaging analysis	127
2.5	Statistical evaluation	127
	List of figures	129
	List of tables	130
	List of abbreviations	131
	References.....	134
	Appendix.....	
	Curriculum vitae.....	
	List of conference contribution.....	
	Danksagung.....	

Abstract

The development of the mammalian brain is a complex process which requires a tightly controlled spatial and temporal orchestration of different signaling pathways. Hence, a misbalance of this developmental program can cause severe brain malformations which are mostly not compatible with life. The release of signaling ligands, their spatial distribution and their activity on receiving cells are regulated by a dynamic network of extracellular matrix proteins and polysaccharides. One of the most abundant extracellular matrix proteins is *Gpc4*, which has been identified to modulate Hedgehog-, Wnt-, Fgf- and Bmp signaling during non-mammalian development. All of these pathways are required for normal brain development – from its early initiation to complex patterning. In mice, *Gpc4* is specifically expressed in the early forebrain and in the (sub) ventricular zones of the developing cortex. Additionally, *Gpc4* has been suggested to play a role in neural subtype specification during mouse embryonic stem cell differentiation.

To investigate the potential function of *Gpc4* as a signaling modulator during mouse brain development, I created a loss-of-function mouse line (*Gpc4*^{-/-}). *Gpc4*^{-/-} embryos showed a broad spectrum of phenotype expressivity with reduced penetrance. Most commonly, I observed an impaired separation of the forebrain midline, defined as holoprosencephaly, which was concomitant with eye defects such as cyclopia, micro- and anophthalmia. In addition, neural tube closure defects leading to exencephaly were frequent. Homozygous *Gpc4*^{-/-} females were about eight times more often affected than hemizygous males and phenotype expressivity was strongly dependent on genetic modifiers. To unravel the underlying affected signaling pathways, I performed transcriptome analysis of E9.5 embryo heads, which identified the Wnt- and Hedgehog signaling pathways to be potentially misregulated. *In situ* analysis of the diencephalic *Wnt1* expression was not altered, indicating a normal Wnt signaling repression in the forebrain of *Gpc4*^{-/-} embryos. In contrast, a lack of the Sonic Hedgehog domain “anterior entopeduncular area” in truncated *Gpc4*^{-/-} embryo brains was observed. Furthermore, in a collaborative effort, I performed single cell RNAseq analysis, which revealed a strong co-expression of *GPC4* with the positive Hedgehog modulator *brother of CDO precursor (BOC)* in the ventricular and sub ventricular zones of the human developing cortex. This co-expression might be the first evidence for an interaction between GPC4 and BOC, suggesting a similar role in the human brain. Moreover, I confirmed that *Gpc4* knockdown causes impaired Hedgehog signaling activity by using a Hedgehog activity reporter cell line. Accordingly, overexpressed GPC4 was partially localized in primary cilia, the main site of Hedgehog signaling. In summary, my data strongly suggest an important role of *Gpc4* as a positive Hedgehog modulator during mouse forebrain development, potentially through the co-regulation with BOC.

Additionally to midline defects, truncated forebrains and empty deciduae before E9.5 were observed upon loss of *Gpc4*, suggesting an early function of *Gpc4* already in neural plate induction. To analyze such a potential early role, I optimized a mouse embryonic stem cell (mESC)-based neural differentiation protocol and established two clonal *Gpc4* knockdown (shGpc4) mESC lines. In shGpc4 cells, no differences in proliferation, cell death or stem cell marker expression were detected in the undifferentiated state. In contrast, shGpc4 cells failed to differentiate to neural precursors and neurons. Impaired neural differentiation was neither caused by a general developmental delay nor by differentiation to non-neural cell types. Instead, shGpc4 cells retained stem cell fate. These results confirmed an impaired neural differentiation upon loss of *Gpc4*, which I also observed in the developing cortex of holoprosencephalic *Gpc4*^{-/-} mice. Furthermore, Hedgehog signaling was impaired in differentiating shGpc4 cells but seemed not to cause the observed differentiation defects. In contrast, I phenocopied shGpc4 differentiation defects by inhibiting Fgf signaling. These data suggest a role of *Gpc4* as a positive modulator of Fgf signaling during early neural induction *in vitro*, which might be the underlying cause for truncated forebrains of *Gpc4*^{-/-} embryos.

Taken together, my results indicate that the extracellular matrix member *Gpc4* is an important signaling modulator during mammalian forebrain development. The presented data suggest that *Gpc4* regulates the Hedgehog- and Fgf signaling pathways during different stages of anterior brain development. Furthermore, I show for the first time that *Gpc4* acts as a positive modulator of Hedgehog signaling in mammals. Thus, the loss of *Gpc4* function can cause holoprosencephaly in mice. It would be very interesting to investigate whether an impaired *GPC4* function might also cause human holoprosencephaly. An environmental risk factor to develop holoprosencephaly is diabetes in mothers. Because *Gpc4* was also described to sensitize insulin signaling, impaired *Gpc4* function might provide a molecular link between diabetes and holoprosencephaly. Thus, a better understanding of the role of *GPC4* in humans might be highly relevant regarding the exponential growth of diabetes in our modern society.

Zusammenfassung

Die Entwicklung des Säugergehirns folgt einem komplexen Ablauf, welcher eine strenge Kontrolle des räumlichen und zeitlichen Zusammenspiels verschiedener Signalwege erfordert. Folglich kann eine Störung dieser Entwicklungsprozesse schwere Fehlentwicklungen des Gehirns auslösen, welche meist zu einem vorzeitigen Tod im Embryonalstadium führen. Die Freisetzung von Signalliganden, ihre räumliche Verbreitung und ihre Wirkung auf Empfängerzellen werden durch ein dynamisches Netzwerk von extrazellulären Matrixproteinen und Polysacchariden reguliert. Eines der häufigsten vorkommenden extrazellulären Matrixproteine ist *Gpc4*, welches die Funktion von Hedgehog-, Wnt-, Fgf- und Bmp Signalwegen während der Entwicklung modulieren kann. Jeder dieser Signalwege wird für eine normale Gehirnentwicklung benötigt – angefangen bei der Initiierung bis hin zum Aufbau komplexer Hirnstrukturen. Bei Mäusen ist *Gpc4* spezifisch im frühen Vorderhirn und in den sich entwickelnden (sub) ventrikulären Zonen des Cortex exprimiert. Weiterhin wurde vorgeschlagen, dass *Gpc4* eine Rolle in der Spezifizierung zu neuronalen Subtypen während der Differenzierung von embryonalen Mausstammzellen spielen könnte.

Um die potentielle Funktion von *Gpc4* in der Modulation von Signalwegen während der Mausentwicklung zu untersuchen, stellte ich eine *Gpc4* loss-of-function-Mauslinie her (*Gpc4*^{-/-}). *Gpc4*^{-/-} Embryonen zeigten ein breites Spektrum an Phänotypen mit reduzierter Penetranz. Am häufigsten beobachtete ich eine unvollständige Trennung der Mittellinie des Vorderhirns, was als Holoprosenzephalie definiert ist. Diese Missbildungen des Gehirns wurden von Augendefekten, einschließlich Zyklopie, Mikro- und Anophthalmie begleitet. Außerdem wurden häufig Neuralrohrdefekte beobachtet, die zu Exenzephalie führten. Homozygote *Gpc4*^{-/-} Weibchen waren achtmal häufiger betroffen als hemizygoten Männchen und die Ausprägung des Phänotyps war sehr abhängig von genetischen Modifikatoren. Um die zugrundeliegenden betroffenen Signalwege zu identifizieren, führte ich eine Analyse des Transkriptoms von E9.5 Embryoköpfen durch, welche eine potentielle Fehlregulierung der Wnt- und Hedgehog Signalwege aufzeigte. Die *in situ* Expressionsanalyse von *Wnt1* im Dienzephalon zeigte keine Veränderungen, was auf eine normale Aktivität des Wnt Signalwegs im Vorderhirn von *Gpc4*^{-/-} Embryonen hinweist. Im Gegensatz dazu fehlte die Sonic Hedgehog Domäne „anterior entopeduncular area“ (AEP) in trunkierten Gehirnen von *Gpc4*^{-/-} Embryonen. Weiterhin führte ich im Rahmen einer Kollaboration eine Einzelzell-RNAseq-Analyse durch, welche eine starke Koexpression von *GPC4* mit dem positiven Hedgehog Modulator *brother of CDO precursor* (*BOC*) in den (sub) ventrikulären Zonen des sich entwickelnden menschlichen Cortex aufzeigte. Diese Koexpression könnte der erste Beweis für eine Interaktion zwischen *GPC4* und *BOC* sein und darauf hinweisen, dass auch *Gpc4* als ein positiver Modulator des Hedgehog Signalweges agiert. In Übereinstimmung mit dem (sub) ventrikulären Expressionsmuster von *GPC4* wurde eine

Reduktion der neuronalen Differenzierung im Cortex von *Gpc4*^{-/-} Embryos mit Holoprosenzephalie beobachtet.

Weiterhin konnte ich durch die Analyse einer Reporterzelllinie für Hedgehog Aktivität bestätigen, dass der Verlust von *Gpc4* eine Verminderung der Hedgehog Signalaktivität auslöst. Entsprechend einer Rolle von *Gpc4* als positivem Hedgehog Modulator, war überexprimiertes *GPC4* zum Teil in primären Zilien lokalisiert, welches das primäre Organell für Hedgehog Aktivität ist. Zusammenfassend weisen meine Daten stark auf eine wichtige Rolle von *Gpc4* als positivem Hedgehog Modulator während der Vorderhirnentwicklung der Maus hin, welche vermutlich durch eine Koregulierung mit *Boc* gesteuert wird.

Zusätzlich zu Mittelliniendefekten wurden trunkierte Vorderhirne und leere Deciduae vor E9.5 durch den Funktionsverlust von *Gpc4* beobachtet, was auf eine frühe Funktion von *Gpc4* schon während der Induktion der Neuralplatte hindeutet. Um zu untersuchen ob *Gpc4* während der frühen Entwicklung eine Rolle spielt, optimierte ich ein auf embryonalen Stammzellen von Mäusen (mESCs) basierendes Differenzierungsprotokoll und etablierte zwei klonale *Gpc4* knockdown mESC Linien (sh*Gpc4*). sh*Gpc4* Zellen zeigten im undifferenzierten Stadium keine Unterschiede in der Proliferation, im Zelltod oder in der Expression von Stammzellmarkern, wogegen sh*Gpc4* Zellen nicht zu neuronalen Vorläuferzellen und Neuronen differenzierten. Die neuronalen Differenzierungsdefekte wurden weder durch eine generelle Verzögerung der Entwicklung, noch durch eine Differenzierung zu nicht-neuronalen Zelltypen verursacht. Stattdessen verblieben sh*Gpc4* Zellen im undifferenzierten Stammzellstadium. Diese Ergebnisse bestätigte eine Störung der neuralen Differenzierung durch den Verlust von *Gpc4*, die ich auch im Cortex von *Gpc4*^{-/-} Embryonen mit Holoprosenzephalie beobachtete. Wie in *Gpc4*^{-/-} Embryonen, war der Hh Signalweg in differenzierenden sh*Gpc4* Zellen in seiner Funktion beeinträchtigt, was aber nicht zu den beobachteten neuronalen Differenzierungsdefekten dieser Zellen zu führen schien. Stattdessen wurden ähnliche Differenzierungsdefekte durch die Inhibierung des Fgf Signalweges ausgelöst. Diese *in vitro* Daten sprechen für eine Rolle von *Gpc4* als positivem Modulator des Fgf Signalweges während der frühen neuralen Induktion, welche für die Trunkierung der Vorderhirne von *Gpc4*^{-/-} Embryonen verantwortlich sein könnte.

Zusammenfassend weisen meine Ergebnisse darauf hin, dass das extrazelluläre Matrix Mitglied *Gpc4* ein wichtiger Modulator von Signalwegen während der Vorderhirnentwicklung von Säugern ist. Weiterhin deuten die gezeigten Ergebnisse darauf hin, dass *Gpc4* die Hedgehog- und Fgf Signalwege während verschiedener Stadien der Vorderhirnentwicklung reguliert. Außerdem konnte ich als Erster zeigen, dass *Gpc4* auch in Säugetieren als ein positiver Modulator von Hedgehog Aktivität agiert, was beim Verlust von *Gpc4* in Mäusen zu Holoprosenzephalie führen kann.

Als nächsten Schritt wäre es sehr interessant zu untersuchen, ob ein Funktionsverlust von *GPC4* auch bei menschlicher Holoprosenzephalie festgestellt werden könnte. Ein Umweltrisikofaktor für Holoprosenzephalie ist Diabetes in Müttern. Da *Gpc4* auch als Sensibilisator für den Insulin-Signalweg beschrieben wurde, könnte eine Störung von *Gpc* eine molekulare Verknüpfung zwischen Diabetes und Holoprosenzephalie darstellen. Aufgrund der exponentiell wachsenden Anzahl von Diabetespatienten in unserer modernen Gesellschaft wäre ein besseres Verständnis der *Gpc4* Funktion im Menschen höchst relevant.

I. Introduction

1. The extracellular matrix

The extracellular matrix (ECM) is a three-dimensional, non-cellular structure that is present in all tissues and is essential for life. Every organ has a unique composition of the ECM which is generated early on during development (Bonnans, Chou, & Werb, 2014). The structure of the ECM is highly dynamic and adapts its composition to maintain tissue homeostasis during development and in adulthood. The fundamental role of the ECM during development is shown by lethality caused by loss-of-function mutations of specific ECM proteins like fibronectin and collagens (reviewed in Rozario and DeSimone, 2010). In the adult, a dysregulation of the composition, stiffness or abundance of the ECM can contribute to severe diseases like cancer and fibrosis (reviewed in Bonnans et al., 2014).

The mammalian ECM comprises more than 300 proteins, the so called “core matrisome” (reviewed in Hynes and Naba, 2012), which can be divided into two main classes of macromolecules: fibrous proteins including collagens and glycoproteins including laminins, fibronectin and proteoglycans (Mecham, 2012). The specific composition of each individual ECM compartment is highly adapted to the requirements of its surrounding tissue. Therefore, the three-dimensional protein structure of the ECM is closely linked to its specific function (Fratzl et al., 1998).

Since the 1960s, the ECM is known for its role as a supportive framework between cells, established by fibrillary collagen. This structural function is particularly well depicted in the ECM which surrounds cartilage, tendons and ligaments (reviewed in Mouw et al., 2014). These tissues are exposed to strong mechanical forces. Thereby, the ECM encompassing cartilage predominantly consists of collagens which are organized in parallel fibrillar bundles. This allows a high absorbance of mechanical forces and thereby is crucial for the prevention of injuries.

Additionally to its well-known role as a passive physical scaffold, the function of the ECM goes far beyond holding cells and tissues in place. In contrast to the structural function of fibrous proteins, the second class of ECM proteins, the glycoproteins, are mainly involved in processes like proliferation, cell survival and differentiation by modulating cell signaling pathways. The most prominent characteristic of the subgroup of proteoglycans are sugar chains, the so called glycosaminoglycan (GAG) components. GAG chains bind with high affinity to a broad spectrum of ligands, including growth factors, cell adhesion molecules and ECM enzymes. By these interactions, proteoglycans can modulate signaling pathways and are therefore important during development and homeostasis (reviewed in Bandtlow and Zimmermann, 2000). Interestingly, also ECM proteins themselves often carry domains of canonical growth factors and might therefore act as autonomous signaling ligands (e.g. laminins contain epidermal growth factor-like domains). However, to which extent these proteins can activate signaling pathways independently is still not fully understood.

2. The extracellular matrix of the central nervous system

Until 1971, the existence of the ECM in the central nervous system (CNS) was mainly neglected due to the low abundance of typical macromolecules like laminins, fibronectin and collagens in the brain (reviewed in Tani and Ametani, 1971 and Zimmermann and Dours-Zimmermann, 2008). However, further studies discovered that the ECM of the CNS makes up 10 – 20 % of the total brain volume and shows a highly different composition compared to cartilage ECM (Bignami, Hosley, & Dahl, 1993; Cragg, 1979; Nicholson & Sykova, 1998). The ECM of the adult CNS can be subdivided into three compartments which are characterized based on their different molecular compositions and thus on their functions (Fig 1; reviewed in Lau et al., 2013).

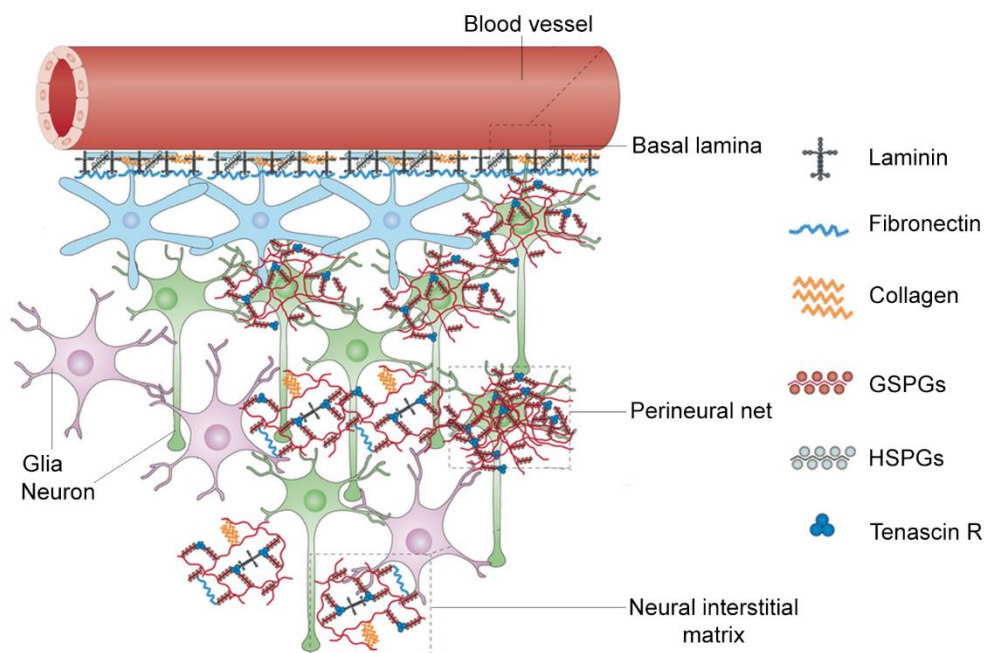


Figure 1 The three compartments of the ECM of the CNS. The fibrous protein-rich basal lamina outlines blood vessels and maintains the blood-brain-barrier. The proteoglycan-rich perineurial net surrounds neural somata and is involved in synaptic plasticity regulation. The neural interstitial matrix comprises additionally hyaluronan. CSPGs: Chondroitin sulfate proteoglycans, HSPGs: Heparan sulfate proteoglycans. Adapted from in Lau et al., 2013.

The basal lamina of the CNS lines the parenchymal side of the cerebral blood vessels and is required for the maintenance of the blood-brain-barrier integrity. This is the only compartment which comprises fibrous proteins like laminins, fibronectin and collagens. These proteins establish a boundary between endothelial cells and CNS parenchymal tissue. In contrast, the other two compartments are rich in proteoglycans and surround neurons and glia cells. The dense, mesh-like second compartment, the so called perineurial net, surrounds cell bodies of neurons and proximal dendrites. This net mainly consist of proteoglycans, tenascin R and link proteins and is thought to be

involved in synaptic plasticity maintenance and neuronal survival (Kwok, Dick, Wang, & Fawcett, 2011). The third compartment, the neural interstitial matrix, consists additionally to proteoglycans of hyaluronan, an anionic nonsulphated GAG which acts as a central hub for proteoglycans. The ECM of this compartment is not tightly packed and surrounds neurons diffusely. However, its exact physiological role remains unknown.

The group of proteoglycans can be subdivided according to their attached sugar chains. The two main proteoglycans in the CNS are heparan sulfate proteoglycans (HSPGs) and chondroitin sulfate proteoglycans (CSPGs). Both families are involved in regulating neuronal growth and guidance, though with opposing effects. CSPGs are upregulated in glial scar tissue after neural injury and inhibit axonal outgrowth. Therefore, they are considered as a limiting factor in axonal sprouting and CNS regeneration (reviewed in Sugahara and Mikami, 2007). In contrast, HSPGs stimulate neurite outgrowth and increase synaptic plasticity (Coles et al., 2011). These distinguished effects indicate the importance of the attached sugar in the specific function of the different proteoglycan families.

3. Glypicans

3.1 Glypican structure

Within the family of HSPGs, Glypicans (*Gpcs*) and Syndecans are the two family members which are most strongly expressed in the CNS (Siddiqui et al., 2013). In the mouse and human genome, six family members of Glypicans have been described (*Gpc1* to *Gpc6*), one in zebrafish (*knypek*), two in *Drosophila* (*dally*, *dally-like* (*dlp*)) and two in *Xenopus laevis* (*gpc2.L* and *gpc4.L*) (reviewed in Filmus et al., 2008). Mammalian *Gpcs* can be classified into two evolutionary conserved subfamilies: The first group is derived from the *Drosophila* orthologue *dally* which includes *Gpc3* and *Gpc5*. The other group comprises *Gpc1/2/4/6* and is derived from *Drosophila dally-like*. Within the latter group, *Gpc4* and *6* are most closely related to each other and share 64 % amino acid identity (reviewed in Filmus et al., 2008). Interestingly, there are two clusters of closely linked genes in the mouse and human genome: *Gpc3/4* on the X-Chromosome and *Gpc5/6* on mouse chromosome 14. Therefore, each cluster contains one member of each evolutionary subfamily, suggesting an ancient linkage of these genes (reviewed in Filmus et al., 2008).

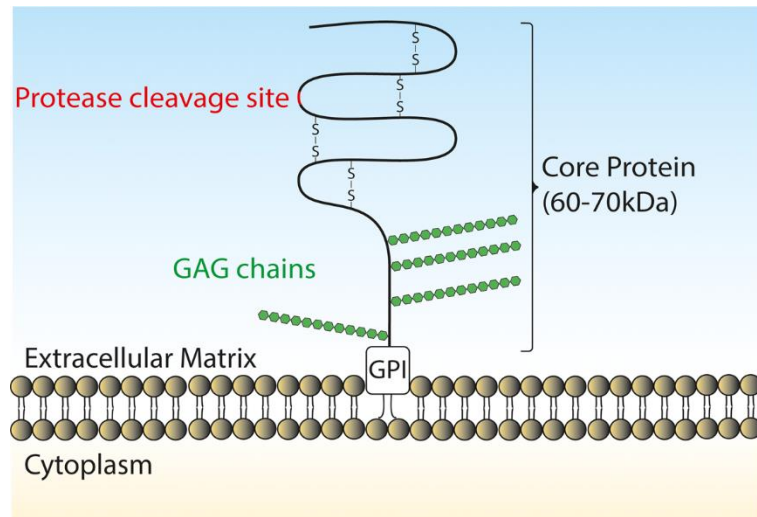


Figure 2 Glypican structure. The 60 – 70 kDa Glypican core protein is GPI-linked to the cell surface and can be cleaved into an N-terminal and C-terminal fragment by extracellular proteases. The proximal part of the C-terminus is highly glycosylated by 2 – 5 unbranched sugar chains (GAG chains). GPI: glycosylphosphatidylinositol; GAG: Glycosaminoglycan.

The core proteins of mouse *Gpcs* consist of a 60 – 70 kDa core protein which is synthesized as a precursor peptide bearing an N-terminal secretory signal sequence and a hydrophobic C-terminus (Fig 2). In the mature protein, the latter is replaced by a covalently-linked glycosylphosphatidylinositol (GPI) anchor, which mediates the anchorage of the core protein to the outer leaflet of the plasma membrane.

In a recent study, the crystal structure of a fragment of the N-terminal sequence of the *d/p* core protein revealed an elongated α -helical structure with no significant homology to any described protein domains, suggesting a unique function of *Gpcs* (Kim, Saunders, Hamaoka, Beachy, & Leahy, 2011). Due to a strong sequence conservation of the investigated fragment, including 14 Cysteine-residues, a conserved function of this protein was suggested in humans (Kim et al., 2011; Veugelers et al., 1999). An important although not mandatory regulation step of *Gpc* function is the shedding of the core protein from the cell surface. *Gpc* cleavage has been observed *in vitro* and *in vivo* (Ford-Perriss et al., 2003; Ko et al., 2015). The *Gpc* core protein can be shed by extracellular lipases which cleave the GPI anchor and thereby release the complete core protein. Additionally, extracellular proteases can recognize a *furin*-like convertase cleavage motif (Arg-X-Arg-Arg) of the core protein and can cut the full-length protein in an N-terminal (about 37 kDa) and a C-terminal domain (about 23 kDa) (De Cat & David, 2001; Ford-Perriss et al., 2003; Hosaka et al., 1991; Kreuger, Perez, Giraldez, & Cohen). The long-believed idea that Notum acts as a sheddase of *Gpcs* has been questioned lately (Kakugawa et al., 2015; Traister, Shi, & Filmus, 2008). Instead, it has been suggested that Notum acts more specifically as a carboxylesterase which inhibits Wnt signaling by deacylation (Kakugawa et al., 2015). Dynamic expression patterns and different binding properties of cleaved and full-length *Gpcs* have been identified during development (Hagihara, Watanabe, Chun, & Yamaguchi, 2000; Ko et al., 2015; Watanabe, Yamada, & Yamaguchi, 1995). In post-natal rat brain development, a shift between cleaved and full-length GPC4 occurs, which changes its functionality (Ko et al., 2015). Only the cleaved N-

terminal fragment of GPC4 is able to bind to the pre-synaptic adhesion molecule *PTP σ* and thereby regulates *trans-synaptic* synapse formation (Ko et al., 2015).

Covalently linked to the *Gpc* core protein are 2 – 5 HS GAG chains. These sugar chains are *O*-linked by serine residues close to the C-terminus of *Gpcs* and can be modified by deacetylation, epimerization and sulfation at different positions (reviewed in Poulain and Yost, 2015). The unique composition of GAGs varies between distinct tissues and changes during embryonic development. As the interaction of *Gpcs* is highly dependent on their specific GAG chains, changes in the composition of these chains are considered to lead to a completely different set of interaction partners (B. L. Allen & Rapraeger, 2003; Ledin et al., 2004). Therefore, this ‘sugar code’ of *Gpc* GAG chains might represent another level of *Gpc* function regulation.

3.2 Glypican function during embryonic development

The family of *Gpcs* and their orthologues are strongly expressed during embryonic development. After their discovery in *Drosophila*, their role during development has been extensively studied. *Dally* and *dlp* have been associated with the modulation of major developmental signaling pathways, like Wingless/INT proteins (Wnt) (Dani, Nahm, Lee, & Broadie, 2012), Hedgehog (Hh) (Desbordes & Sanson, 2003; Lum et al., 2003), fibroblast growth factor (Fgf) (Yan & Lin, 2007) and bone morphogenetic proteins (Bmp) (Akiyama et al., 2008; Fujise et al., 2003). Thereby *Gpcs* have been shown to modulate developmental processes like proliferation, differentiation, migration and axonal growth.

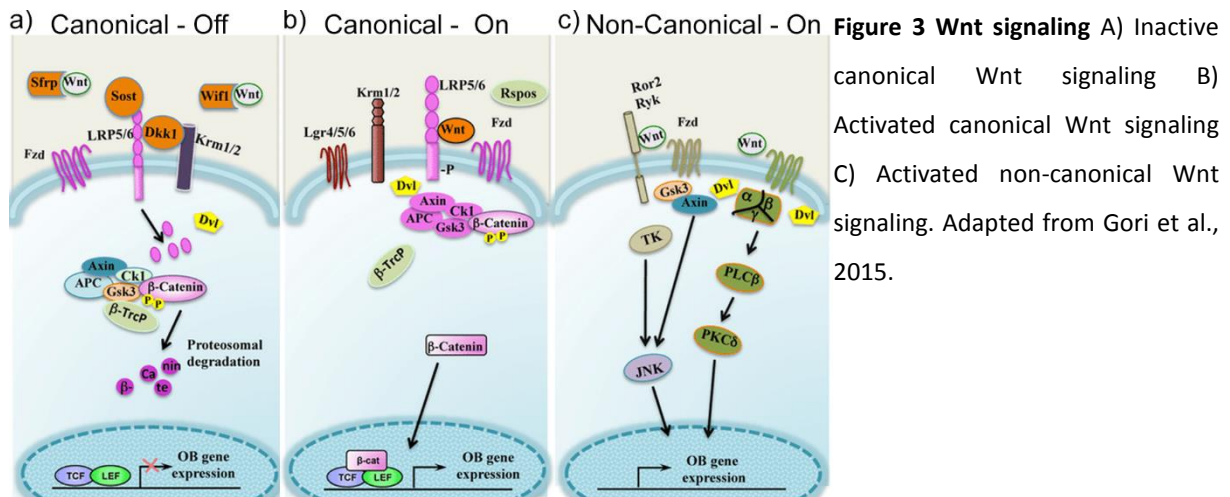
During the last years, major advancements in the understanding of the role of vertebrate *Gpcs* in Wnt and Hh signaling were achieved. It was shown that *Gpc1* controls the switch between Hh-mediated attraction and repulsion of spinal cord axons during development (Wilson & Stoeckli, 2013). Additionally, several reports identified a new role of *Gpc4* during *trans-synaptic* differentiation in mice (N. J. Allen et al., 2012; de Wit et al., 2013; Siddiqui et al., 2013).

The best studied signaling pathways which are modulated by *Gpcs* are the Wnt and Hh signaling pathways. They will be summarized in the following chapter with a focus on the modulation of morphogen secretion and reception.

3.3 Glypican function in Wnt signaling modulation

The Wnt signaling pathways are activated by different Wnt ligands which bind to Frizzleds (*Fzds*), their primary cell surface receptors. In humans, 19 Wnt ligands, 10 *Fzds* receptors and various co-receptors have been identified (reviewed in Gerdes et al., 2009). Their function is summarized in Figure 3 (reviewed in Gori et al., 2015).

I. Introduction



Canonical Wnt signaling can be activated by different ligands, including WNT3a and WNT1 and requires the presence of the co-receptors lipoprotein receptor-related protein (LRP)-5/6. The LRP receptors are phosphorylated by GSK3 which leads to the recruitment of dishevelled segment polarity protein 1 (DVL1) to the plasma membrane where it gets activated. In a next step, DVL1 inactivates the destruction complex of β -Catenin, which leads to the accumulation and nuclear translocation of β -Catenin. Subsequently, nuclear β -Catenin activates TCF/LEF dependent transcription of target genes. In contrast, non-canonical Wnt pathways including planar cell polarity and non-canonical Wnt/ Ca^{2+} Wnt pathways are activated by WNT5A and WNT11, independently of LRP5/6. These pathways require other co-receptors including lgr receptor tyrosine kinase-like orphan receptor 2 (ROR2) and RYK. Downstream signaling is independent of β -Catenin and mediated by protein kinases including Rho kinase, Jun N-terminal kinase or by intracellular release of Ca^{2+} , which activates kinases like calcium/calmodulin-dependent kinase (CaMK)II and calcineurin.

Both signaling pathways are thought to be initiated by endocytosis of the WNT-FZD-complex. However, signaling occurs in different microdomains of the plasma membrane. Canonical signaling occurs mainly within lipid rafts whereas non-canonical signaling is associated to non-lipid raft microdomains (Sakane, Yamamoto, Matsumoto, Sato, & Kikuchi, 2012).

In a recent study it was shown that WNT3A-mediated canonical- and also WNT5A-mediated non-canonical Wnt signaling was enhanced *in vitro* by overexpression of GPC4 (Sakane et al., 2012). Furthermore, upon stimulation with WNT3A and WNT5A, GPC4 co-internalized together with FZD2 and ROR2 respectively (Sakane et al., 2012).

In vivo analysis of *knypek*, the *Gpc4* orthologue in zebrafish, revealed the role of *Gpc4* in Wnt signaling during embryonic development. The loss-of-function of *knypek* led to a shortening of the anterior-posterior (A-P) axis and caused severe forebrain defects including an impaired separation of the eye fields (cyclopia) (Topczewski et al., 2001). The expressivity of the cyclopia phenotype was further increased by the additional removal of Wnt11, a member of the planar-cell-polarity Wnt signaling pathway. Very similar defects in anterior-posterior axis formation due to impaired non-canonical Wnt

signaling were observed in *Xenopus* (Ohkawara, Yamamoto, Tada, & Ueno, 2003). However, the observed forebrain defects were suggested to be mediated by impaired Fgf signaling, which will be described in chapter 3.5 (Galli, Roue, Zeller, & Dono, 2003).

In summary, these data suggest that *Gpc4* might act as a positive regulator of canonical and non-canonical Wnt signaling which enhances the interaction between growth factors and signaling receptors.

Additionally to *Gpc4*, the role of *Gpc3* has been studied intensively in the context of Wnt signaling by the group of Dr. Filmus (M. Capurro, Martin, Shi, & Filmus, 2014; M. I. Capurro, Xiang, Lobe, & Filmus, 2005; Song, Shi, Xiang, & Filmus, 2005). They identified *Gpc3* as a positive regulator of canonical Wnt signaling in hepatocellular carcinomas (M. I. Capurro et al., 2005). GPC3 bound to FZDs in a GAG chain dependent manner and interacted also with Wnt ligands (M. I. Capurro et al., 2005). Furthermore, the overexpression of *Gpc3* increased canonical signaling activity by boosting endocytosis of GPC3-FZD-WNT complexes (M. Capurro et al., 2014; M. I. Capurro et al., 2005). *In vivo*, the situation seems to be more complex. *Gpc3* loss-of-function mice show severe overgrowth defects additionally to decreased non-canonical but increased canonical Wnt signaling (Song et al., 2005). However, later studies suggest abnormal Hh signaling in these mice as the major cause of body overgrowth (described in the next chapter) (M. I. Capurro, Li, & Filmus, 2009).

Interestingly, in contrast to *Gpc3* and *Gpc4*, *Gpc6* seems to inhibit canonical Wnt signaling (M. Capurro et al., 2014). Although GPC6 binds to Wnt ligands, it lacks interaction with *Fzd* receptors and is therefore considered as a negative regulator of canonical Wnt signaling.

In summary, *Gpcs* have been identified as important regulators of Wnt signaling *in vitro* and *in vivo*. Interestingly, the *Gpc* family members *Gpc3*, 4 and 6 have highly different functions as Wnt signaling modulators. However, the exact role of *Gpc4* on Wnt signaling during mammalian brain development has not been investigated so far and remains elusive.

3.4 Glypican function in Hedgehog (Hh) signaling modulation

The immature HH ligands (in *Drosophila* HH; in vertebrates *Sonic Hedgehog* (SHH), *Indian Hedgehog* (IHH), *Desert Hedgehog* (DHH)) undergo several post-translational modifications before they are secreted from producing cells (Fig 4, reviewed in Briscoe and Therond, 2013). First, the premature HH is proteolytically cleaved into an N-terminal peptide (HH-N), which acts as the future morphogen, and a C-terminal fragment which catalyzes this self-cleavage event (X. Chen et al., 2011).

Subsequently, HH-N undergoes further modifications by dual lipidation of a palmitic acid group and cholesterol (reviewed in Mann and Beachy, 2004). Once the modified HH-N reaches the cell surface, it is released to the ECM. Thereby, the transmembrane proteins Dispatched (DISP) and SCUBE2 have

been shown to play an important role in releasing HH-N from the cell surface (reviewed in Tukachinsky et al., 2012 and Creanga et al., 2012).

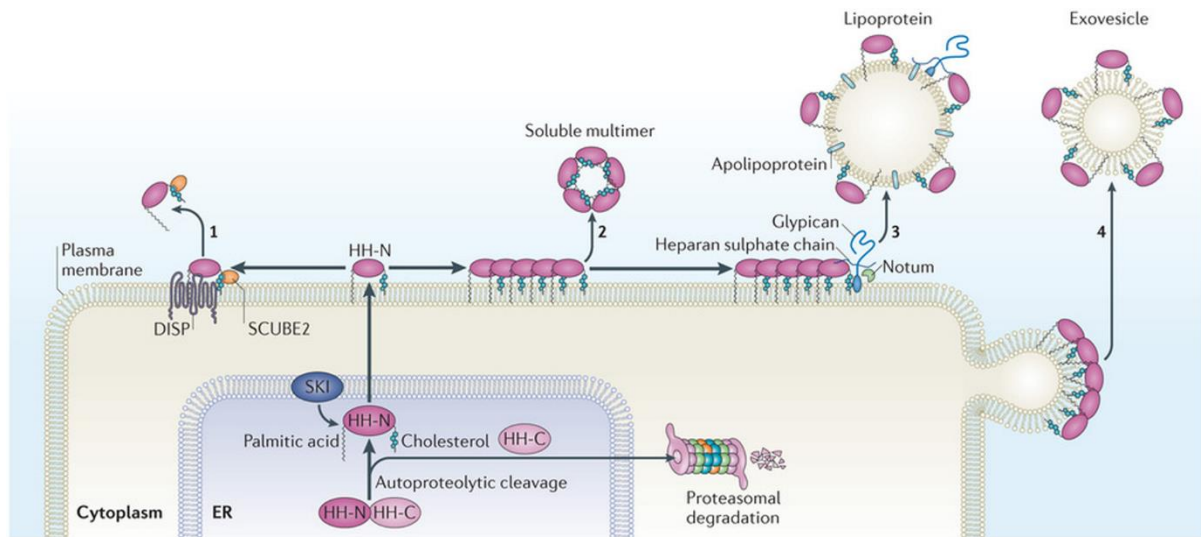


Figure 4 Release of HH from secreting cells. After self-cleavage of the HH precursor protein, the HH-N fragment undergoes dual lipidation by a palmitic acid group and cholesterol. Once dually lipid-modified HH-N reaches the cell surface it is released by different mechanisms (1 – 4). HH-N monomers can be released by interacting with DISP and SCUBE2 (1). HH-N monomers can also form soluble multimers that are released from the cell surface (2). These oligomers can interact with *Gpcs* by their GAG chains to recruit lipophorin apolipoproteins and assemble into lipoprotein particles (3). Furthermore, HH-N may be released at the surface of exovesicles (4). Adapted from Briscoe & Therond, 2013.

It has been shown before that secreted HHs can spread up to 300 μm through the vertebrate limb and thereby establish long gradients of signaling activity (Yang et al., 1997). Importantly, in *Drosophila*, *dally* is involved in the regulation of long-range travel of HH (Ayers, Gallet, Staccini-Lavenant, & Therond, 2010). It recruits the circulating apolipoprotein LIPOPHORIN to cell surface bound HH-N oligomers in a GAG dependent manner (Ayers et al., 2010). This interaction leads to the assembly into lipoprotein particles which can undergo long distance travel (Eugster, Panakova, Mahmoud, & Eaton, 2007; Panakova, Sprong, Marois, Thiele, & Eaton, 2005). However, the function of *Gpcs* to modulate morphogen travel seems not to be exclusive for HHs, but includes also Tgf- β and Wnt signaling ligands (Akiyama et al., 2008; Belenkaya et al., 2004; Fujise et al., 2003; Kirkpatrick, Dimitroff, Rawson, & Selleck, 2004).

Once HH ligands reach their target cells, they bind to their main receptor patched1 (PTC, Fig 5). Upon binding, the HH-PTC-complex is removed from the cell surface by endocytosis. Subsequently, the inhibitory action of PTC on the transmembrane protein smoothed (SMO) is removed which leads to the translocation of SMO to the primary cilium. The disinhibited SMO initiates an intracellular signaling cascade which is followed by the stimulation of GLI transcriptional activators and the inhibition of GLI

transcriptional repressors. These activating transcription factors are then translocated to the nucleus where they initiate the transcription of downstream target genes.

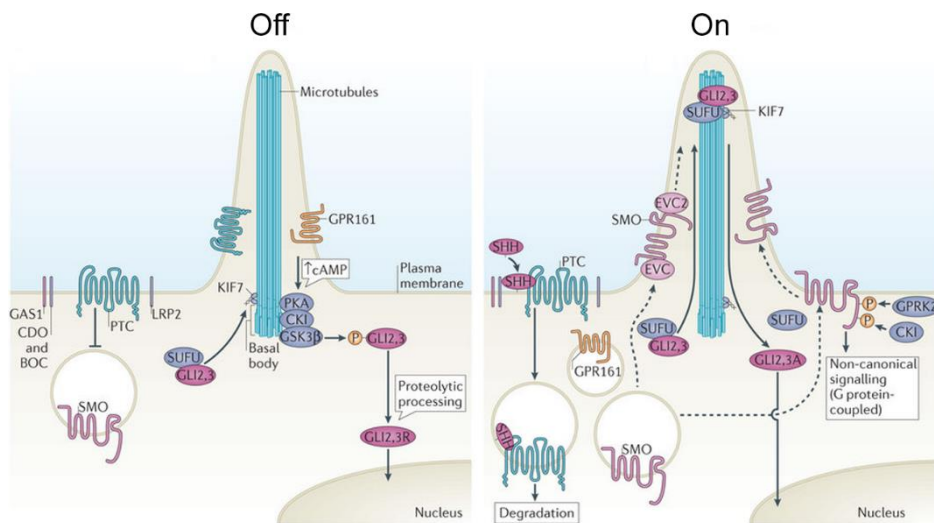


Figure 5 Hh signaling pathway Upon binding of HH-ligands to PTC, the complex gets endocytosed leading to the disinhibition and of SMO. Subsequent ciliar translocation of SMO stimulates GLI transcription activators which initiate target gene transcription upon nuclear localization. Adapted from Briscoe & Therond, 2013.

The Hh signaling activity on signal receiving cells is regulated by several modulators in a spatial and temporal manner during embryonic development (Bae et al., 2011; Martinelli & Fan, 2007). So far, five interaction partners of HH on signal receiving cells have been identified in vertebrates (Fig 6, reviewed in Beachy et al., 2010 and Briscoe and Therond, 2013). Four of them increase Hh signaling and therefore act as positive modulators: CAM-related/downregulated by oncogenes (*Cdo*) (B. L. Allen, Tenzen, & McMahon, 2007; Zhang, Kang, Cole, Yi, & Krauss, 2006), brother of CDO (*Boc*) (Yao, Lum, & Beachy, 2006), growth arrest-specific 1 (*Gas1*) (B. L. Allen et al., 2007), and low-density lipoprotein receptor-related protein 2 (*Lrp2*, also called *Megalin*) (McCarthy, Barth, Chintalapudi, Knaak, & Argraves, 2002). Additionally, Hh-interacting protein (*Hhip*) has been described as a negative Hh modulator (P. T. Chuang & McMahon, 1999). CDO, BOC and MEGALIN are single pass transmembrane proteins whereas GAS1 and HHIP are linked to the cell surface by a GPI-anchor.

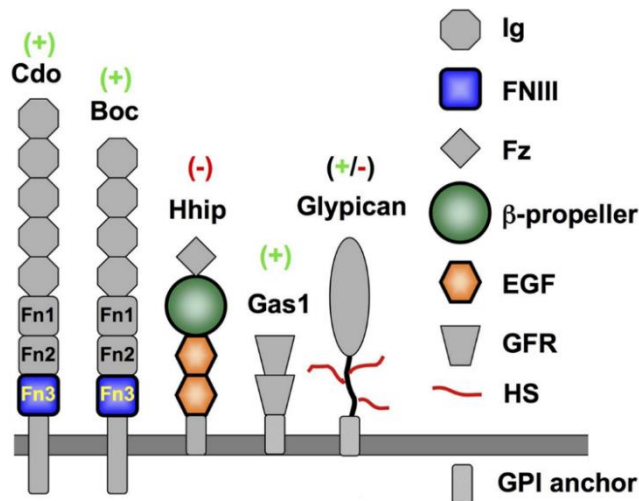


Figure 6 Hh signaling modulators on signal receiving cells. Five HH interaction partners have been identified to modulate signaling either positively (+) or negatively (-). Domains for which high-resolution structures have been determined are shown in color. In *dlp*, the *Gpc4/6* orthologue in *Drosophila*, no known functional domains have been identified, indicating a unique function of *Gpcs*. The positive modulator Megalin/LRP2 is missing in this scheme. Adapted from Beachy et al., 2010.

Upon ablation of one of these positive modulators, Hh signaling is impaired but not completely lost. Consequently, only the simultaneous absence of *Gas1*, *Boc* and *Cdo* resulted in the complete loss of Hh activity (B. L. Allen et al., 2011; Izzi et al., 2011). It was concluded that GAS1-PTC, BOC-PTC and CDO-PTC complexes act most likely collectively as co-receptors in Hh signaling (Izzi et al., 2011).

Importantly, also *Gpcs* have been identified to modulate Hh signaling on receiving cells (reviewed in Filmus et al., 2008 and Filmus and Capurro, 2014).

The loss-of-function of *Gpc3* led to significant body overgrowth of about 30 % in mice (Cano-Gauci et al., 1999; Chiao et al., 2002; Paine-Saunders, Viviano, Zupicich, Skarnes, & Saunders, 2000). This phenotype does not seem to be caused by the originally suggested misregulation of insulin-like growth factor-II (Cano-Gauci et al., 1999; Chiao et al., 2002; Pilia et al., 1996). In fact, body overgrowth was partially rescued by the additional removal of *Ihh*, the main Hh ligand in cartilage (M. I. Capurro et al., 2009). Therefore, *Gpc3* was suggested to act as a negative modulator of Hh signaling in mice (M. I. Capurro et al., 2008). Further evidence came from cell culture experiments which showed that GPC3 competes with PTC for HH binding (M. I. Capurro et al., 2008). Upon HH binding to GPC3 over GAG chains, the HH-GPC3 complex is endocytosed by the low-density-lipoprotein receptor-related protein-1 (LRP1) (M. I. Capurro, Shi, & Filmus, 2012). The endocytosed complex is then degraded without activation of the Hh pathway. Interestingly, shedding of GPC3 by convertases seems to be required for the specific inhibitory function of *Gpc3* on Hh signaling (M. Capurro, Shi, Izumikawa, Kitagawa, & Filmus, 2015). In contrast to endogenous GPC3, a cleavage-resistant mutant form boosts Hh signaling by increasing pathway activating endocytosis of the HH-PTC-GPC3 complex (M. Capurro et al., 2015). Although *Gpc3* and *Gpc5* are members of the same evolutionary conserved subfamily, they show opposite functions as Hh signaling modulators. *Gpc5* is significantly upregulated in rhabdomyosarcoma, a malignant tumor in muscles, which has been associated with a hyper activation of the Hh pathway (Hahn et al., 1998; Williamson et al., 2007). In contrast to *Gpc3*, *Gpc5* increases Hh signaling by binding to SHH and PTC which is mediated by GAG chains (F. Li, Shi, Capurro, & Filmus, 2011).

The exact mechanism, whereby *Gpc3* and *Gpc5* modulate Hh signaling in opposing ways is not yet clear. Since their core protein structure is largely conserved, current explanations focus on differences in their HS GAG chains (see 'sugar code' described in chapter 3.1). *Gpc3* carries two HS GAG chains compared to three in *Gpc5*. The HS GAG chains of GPC5 showed higher levels of post-translational sulfate modifications in comparison to the ones of GPC3 (F. Li et al., 2011). The negative charge of sulfate groups is thought to be the main mediator for molecular interactions between GAG chains and PTC (M. Capurro et al., 2015). Therefore, differences in GAG chain sulfation might lead to a change of GPC-PTC binding affinity resulting in opposing effects on Hh signaling. Taking into consideration the opposing effect between cleavable and cleavage-resistant GPC3, it was proposed that inhibiting cleavage might induce structural changes of the core protein. This could lead to a hypersulfation of the GAG chains and thus, mediate the new established interaction between PTC and HH (M. Capurro et al., 2015). However, the exact roles of GAG chain sulfation and core protein shedding remain elusive. So far, the role of *Gpc4* in mammalian Hh signaling has not been investigated. However, several lines of evidence from the *Drosophila* orthologue *dlp*, suggest a role of *Gpc4* as a positive modulator of Hh signaling (Desbordes & Sanson, 2003; Gallet, Staccini-Lavenant, & Therond, 2008; Lum et al., 2003; Yan et al., 2010). In *Drosophila*, *dlp* has been identified as an important positive Hh modulator during embryonic development and *in vitro* (Desbordes & Sanson, 2003; Lum et al., 2003). It was shown that *dlp* can physically interact with HH and PTC and thereby boost the endocytosis of this complex (Yan et al., 2010). However, the role of the HS GAG chains in this interaction remains still controversial (Kim et al., 2011; Williams et al., 2010; Yan et al., 2010). In contrast to *Gpc3* in MEFs, furin-like shedding of *dlp* does not influence its function on Hh signaling (M. Capurro et al., 2015; Williams et al., 2010). In a recent study, structure-guided mutagenesis identified the region which mediates *dlp* function in Hh signaling. However, no high-affinity interaction between *dlp* and HH was found in this region (Kim et al., 2011).

3.5 Glypican function in Fgf signaling modulation

In comparison to the role of *Gpcs* in Hh and Wnt, less is known about their function in Fgf signaling. It was shown that recombinant GPC4 can bind to FGF2 by GAG chains (Hagihara et al., 2000). *In vivo* analysis of the *Xenopus* orthologue of *Gpc4* revealed an important function during forebrain development in addition to the formation of the A-P axis described in chapter 3.3 (Galli et al., 2003). Downregulation of *Gpc4* led to a loss of dorsal forebrain markers by increased cell death. On a functional level, it was suggested that the observed brain defects are mediated by the loss of Fgf signaling because high doses of the Fgf-receptor inhibitor SU5402 phenocopied the observed misdevelopment. *In vitro* analysis confirmed reduced Fgf activity upon reduction of *Gpc4*, which could be rescued by mouse GPC4 (Galli et al., 2003).

These studies suggest a role of *Gpc4* as a positive Fgf signaling regulator during brain development in *Xenopus*. However, if this role is conserved in mammals has not been investigated so far.

Apart from a direct regulation of developmental signaling pathways, growing evidence indicates a role of *Gpc4* in mammalian synapse formation. Two studies showed that pre-synaptic GPC4 interacts *trans-synaptically* with LRRTM4 in the dentate gyrus of the hippocampus, thereby promoting bi-directional development of excitatory synapses (de Wit et al., 2013; Siddiqui et al., 2013). It was also shown that GPC4 and GPC6 are secreted from mouse astrocytes and are sufficient to increase synaptic strength in the adult hippocampus (N. J. Allen et al., 2012). Although both functions seem to be GAG chain dependent, their mechanisms – including potentially involved signaling pathways – is not yet understood.

4. *Glypican 4* expression during mouse development and in the adult

The expression of *Gpc4* during mouse embryo development shows a specific and highly dynamic expression pattern suggesting a role during brain development (Fig 7, Table 1).

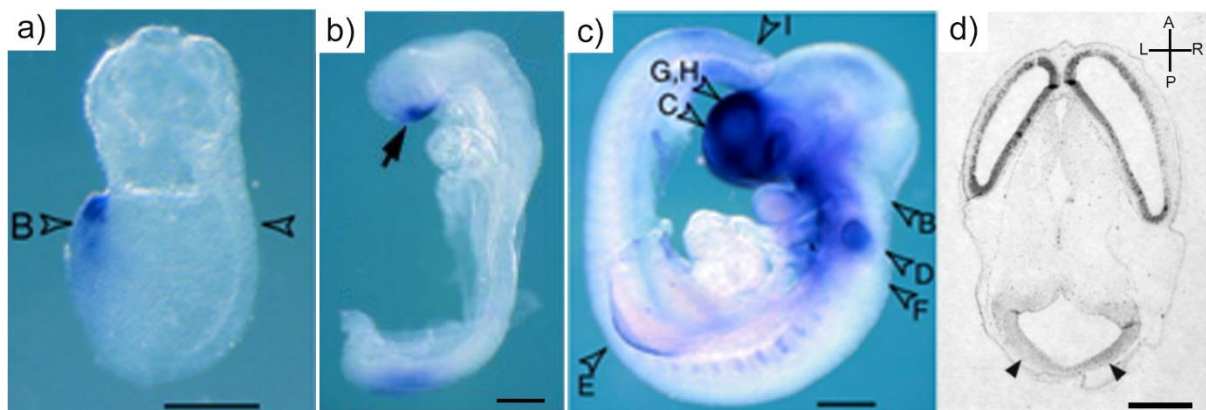


Figure 7 *Gpc4* mRNA expression during mouse embryo development. a) E7.0 embryo, b) E8.5 embryo, c) E10.0 embryo, d) E13.0 embryo. Scale bar: a: 25 μ m, b: 30 μ m, c: 50 μ m, d: 1 mm. Adapted from Ybot-Gonzalez, Copp, & Greene, 2005 and Hagihara et al., 2000.

Embryonic stage	<i>Gpc4</i> in CNS	<i>Gpc4</i> in other organs	Source
E6.5 (ES) – E7.5 (LHF)	AVE and midline neuroepithelium		(Luxardi et al., 2007; Ybot-Gonzalez et al., 2005)
E7.5 (LHF) – E9.5	Midline neuroepithelium, eye and ventral forebrain	Rhombomeres, brachial arches	(Jen, Musacchio, & Lander, 2009; Ybot-Gonzalez et al., 2005)
E10.0 – E13.0 and primary cells	- Periventricular neuroepithelium of telencephalon -NPCs and young neurons		(Hagihara et al., 2000) (Ford-Perriss et al., 2003; Watanabe et al., 1995)
E15.0 + E16.0	VZ and SVZ of the telencephalic lateral ventricles	- Facial mesenchyme - Kidney - Aorta - Adrenal gland	(Watanabe et al., 1995)
P6 – P24	Pre-synapse and astrocytes within hippocampus	Kidney	(N. J. Allen et al., 2012; de Wit et al., 2013; Hagihara et al., 2000)

Table 1 *Gpc4* mRNA expression during mouse embryo development. ES: early streak, LS: late streak, LHF: late head fold, AVE: anterior visceral endoderm, (S)VZ: (sub) ventricular zone. NPCs: Neural precursor cells.

Within the family of *Gpcs*, *Gpc4* is the strongest expressed member in the developing mouse brain (Ford-Perriss et al., 2003). In contrast to other *Gpcs*, the early expression pattern of *Gpc4* is highly specific to the developing head and strongly expressed in ventral areas of the future forebrain (Ford-Perriss et al., 2003; Hagihara et al., 2000; Luxardi et al., 2007; Watanabe et al., 1995; Ybot-Gonzalez et al., 2005). Importantly, *Gpc4* is strongly expressed in key signaling centers which regulate anterior brain development. The exact expression pattern of *Gpc4* during embryo development will be reviewed below.

In the early mouse embryo between E6.5 (early streak) until E7.25 (late streak – early head fold), *Gpc4* mRNA is strongly expressed in the anterior visceral endoderm (AVE) but not in the underlying epiblast (Fig 7 a)) (Luxardi et al., 2007). The AVE acts as a main signaling center for early head formation and underlies the most anterior part of the neural plate. At E7.5, *Gpc4* switches expression from developing endoderm to the neuroectoderm which forms the future forebrain. There, it is strongly expressed in the midline of the neuroepithelium and expands subsequently laterally into the anterior neural ridge (7.5 – E8.0, Fig 7a) and b)). This structure is the most rostral junction between neural and non-neural ectoderm and represents another key signaling center for forebrain patterning (Rubenstein, Shimamura, Martinez, & Puellas, 1998; Ybot-Gonzalez et al., 2005). Subsequently, the expression of *Gpc4* expands caudally throughout the neuroepithelium of the entire telencephalon (E9.0, Fig 7c), including the developing eye (optic and otic vesicles) and other ventral areas like the future anterior pituitary gland, brachial arches and rhombomeres (E10.5) (Ybot-Gonzalez et al., 2005). During further development, *Gpc4* is strongly expressed in the ventricular- (VZ) and sub ventricular zone (SVZ) of the lateral telencephalic ventricles, main sites of neurogenesis of the developing cortex (Fig 7d)) (Ford-Perriss et al., 2003; Hagihara et al., 2000; Watanabe et al., 1995). Consistent with the expression

pattern *in vivo*, *Gpc4* is strongly expressed in *Nestin* positive neural precursors (NPCs) and partially in *Tubb3* positive young neurons. However, no expression was detected in *Map2* positive mature neurons (Hagihara et al., 2000). Additionally to the expression in the brain, *Gpc4* expression spreads to the facial mesenchyme, the aorta, the adrenal gland and the developing kidney (E15.0) (Watanabe et al., 1995).

In the adult, *Gpc4* remains strongly expressed in the kidney and the brain. Within the adult brain, *Gpc4* is highly expressed in the dentate gyrus (DG) of the hippocampus, a structure important for memory formation (N. J. Allen et al., 2012). *Gpc4* has been suggested to be stronger expressed in astrocytes than in neurons of postnatal mouse brains (P6 – P24) (N. J. Allen et al., 2012). Another study identified GPC4 being expressed in the pre-synapse to promote *trans-synaptic* differentiation during synaptogenesis in the DG (P7 – P14) (de Wit et al., 2013).

5. Early development of the mammalian brain

As reviewed before, *Gpc4* is specifically expressed in the brain during early development. The development of this most complex organ of a mammalian organism requires a tightly regulated orchestration of developmental signaling pathways. For a deeper understanding of the role of *Gpc4* during brain development, the key signaling centers and -pathways which are required for early neural development will be reviewed in detail.

5.1 Anterior neural induction by inhibition of posterior signals

The development of the neural plate is intimately linked to the establishment of the embryonic axes and the formation of the three principle germ layers (reviewed in Andoniadou and Martinez-Barbera, 2013). Between E5.5 and E6.5, visceral endoderm cells locate to the prospective anterior side of the embryo and form the anterior visceral endoderm (AVE) (Takaoka, Yamamoto, & Hamada, 2011). This structure is essential for the A-P axis formation and is also a key signaling center which induces neural fate in the overlaying anterior epiblast (Tam & Steiner, 1999). The specific regulation of signaling pathways by the AVE remains still poorly understood. However, a broadly accepted concept suggests that anterior neural fate requires the inhibition of posteriorizing signals (Fig 8). In the anterior neural plate, Wnt, Bmp, Nodal, and retinoic acid activity is antagonized by *Lefty1*, *Dkk1* (Dickkopf), *Cer1* (Cerberus) and *Tlc* (Bouwmeester, Kim, Sasai, Lu, & De Robertis, 1996). In contrast, distal areas escape this inhibition which leads to the formation of the primitive streak at the posterior side of the embryo (reviewed in Takaoka and Hamada, 2012).

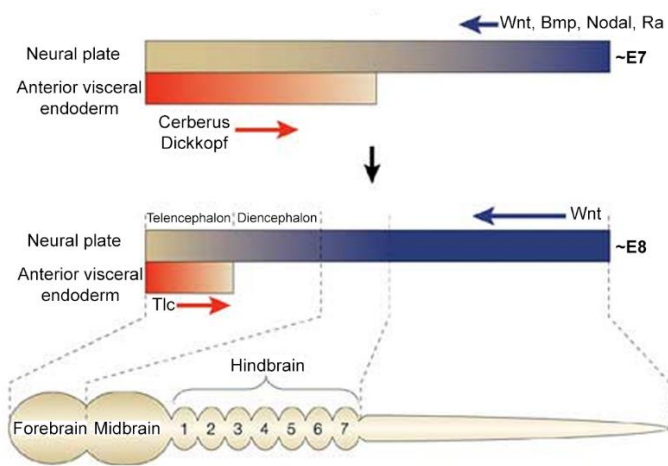


Figure 8 Anterior neural induction by inhibition of posterior signals. Wnt, Bmp, Nodal and retinoic acid (Ra) induce posterior fate in the developing neural plate. These signals are antagonized by Cerberus, Dickkopf and Tlc in the anterior neural plate which are secreted from the anterior visceral endoderm. Adapted from Rallu, Corbin, & Fishell, 2002.

Additionally to the AVE, the node is required as a late gastrula organizer for neural patterning (Kinder et al., 2001). Together with the AVE, it secretes antagonists of the Wnt and Nodal pathways. Furthermore, *Shh* and the Bmp antagonists *Chrd* (chordin) and *Nog* (noggin) are secreted by the node. Therefore, the AVE and the node act together to induce early head formation mainly by inhibiting posteriorizing signals.

5.2 Anterior-posterior forebrain patterning by Wnt and Fgf signaling

After the neural plate has been induced, this originally flat structure is bended to form the neural tube. During this process defined as neurulation, the neural tube specifies along the A-P- and dorso-ventral (D-V) axis. Along the A-P axis, three primary vesicles are originally formed, the prosencephalon, the mesencephalon and the rhombencephalon. The prosencephalon or forebrain further separates into the telencephalon and the diencephalon. Due to the specific expression of *Gpc4* in the anterior brain, only the development of this brain area will be described further.

Essential for the development of the telencephalon is a rising signaling center at the most anterior tip of the neural tube, the anterior neural ridge (ANR, Fig 9).

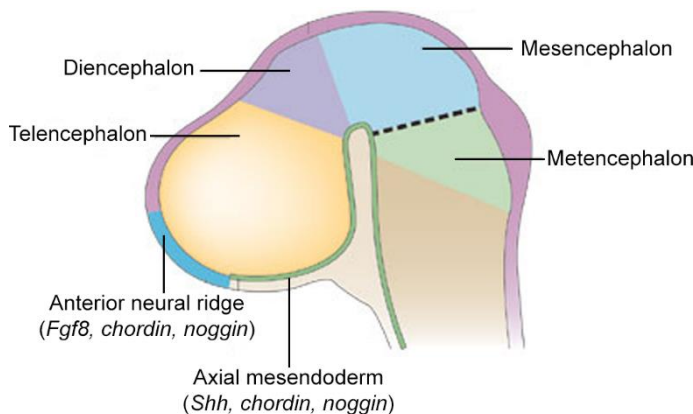


Figure 9 A-P forebrain specification by Wnt and Fgf signaling. The anterior neural ridge maintains anterior fate by Wnt- and Bmp inhibition. Secreted *Fgf8* is required for midline formation and lateral development of the telencephalon. Adapted from Liu & Niswander, 2005.

Similarly to early signaling centers, the ANR maintains anterior fate by secreting Wnt- and Bmp antagonists including *Axin*, *Chrd* (chordin) and *Nog* (noggin) (Heisenberg et al., 2001; Houart et al., 2002). Importantly, the ANR also secretes *Fgf8* which is essential for midline formation and lateral development of the telencephalon (Okada, Okumura, Motoyama, & Ogawa, 2008; Shimamura & Rubenstein, 1997). Therefore, activation of Fgf signaling is essential for normal development of the anterior forebrain.

5.3 Dorso-ventral forebrain patterning by Hh signaling

During neurulation, the anterior forebrain specifies also along its dorsal-ventral (D-V) axis (reviewed in Le Dreau and Marti, 2012 and Hébert und Fishell, 2008). D-V patterning is mainly controlled by two opposing signaling sites: the axial mesendoderm, which underlies the neural tube ventrally and the dorsal roof plate of the neural tube. The axial mesendoderm comprises the prechordal plate and the notochord which release *Shh* and thereby induce ventral fate marked by expression of *Nkx2.1* and *Gsh2* (Fig 10 a) and b)) (Chiang et al., 1996). Subsequently, ventral domains including the medial ganglionic eminence develop (Fig 10 c)) (Shimamura, Hartigan, Martinez, Puelles, & Rubenstein, 1995).

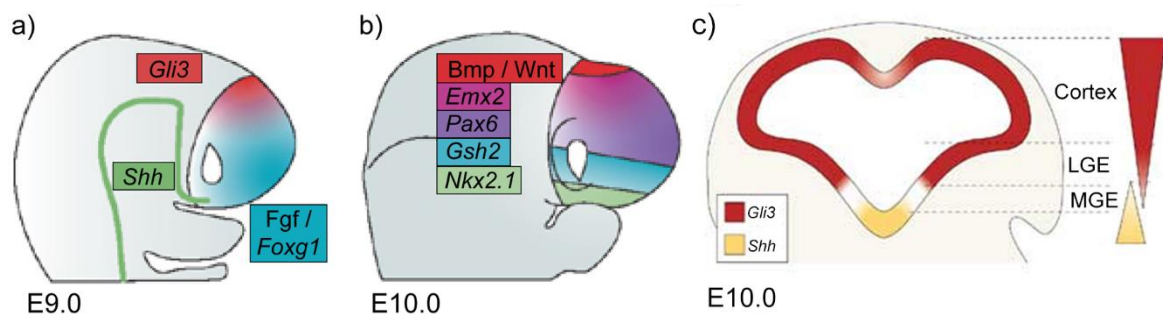


Figure 10 Dorso-ventral patterning of the anterior brain. The axial mesendoderm induces ventral fate by secreting *Shh*. Ventral domains including the medial ganglionic eminence (MGE) express high levels of *Nkx2.1* and *Gsh2*. The floor plate expresses high levels of the Hh repressor *Gli3* leading to expression of Bmps and Wnts and therefore to the development of the dorsal domains including the cortex and lateral ganglionic eminence (LGE). Adapted from Hébert & Fishell, 2008 and Rallu et al., 2002.

In contrast, dorsal structures including the developing cortex and the lateral ganglionic eminence (LGE) lack *Shh* expression but express Wnt- and Bmp agonists (Theil, Aydin, Koch, Grotewold, & Ruther, 2002; Timmer, Wang, & Niswander, 2002). These agonists are activated by insufficient Hh activation from ventral *Shh*, leading to high levels of the Hh repressor *Gli3* which induces dorsal fate in the anterior brain.

In summary, Hh signaling is not only controlling ventral fate but it regulates also indirectly dorsal differentiation. Additionally to these main signaling cues, the retinoic acid signaling pathway and members of the Tgf- β superfamily have been implicated to D-V patterning. However, they are

considered to have a rather short range of activity compared to *Shh* (Hogan, 1996; Marklund et al., 2004).

6. Holoprosencephaly – defects in forebrain separation

The Hh signaling pathway is important for many aspects of brain development. Consequently, defects in the Hh pathway can cause severe misdevelopment of the brain, including holoprosencephaly (HPE). HPE is the most common developmental defect of the forebrain and midface with an incidence of 1:250 in conceptuses and 1:16.000 in newborn infants (reviewed in Orioli and Castilla, 2010). It is characterized by an inadequate or absent division of the anterior CNS into two cerebral hemispheres (reviewed in Petryk et al., 2015). An important feature of HPE is its highly variable expressivity and incomplete penetrance (Fig 11).

Interestingly, HPE has been reported to be about twice as common in females than in males (Croen, Shaw, & Lammer, 2000; Olsen, Hughes, Youngblood, & Sharpe-Stimac, 1997). Clinical phenotypes vary from lethal alobar HPE without midline separation, to very mild forms with a cleft lip or single central tooth.

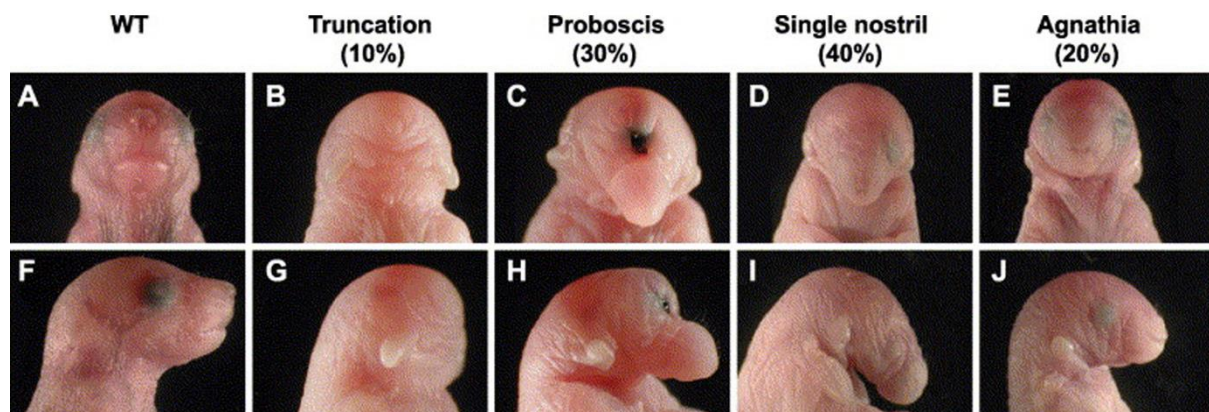


Figure 11 Mouse model of HPE. *Twsg*^{-/-} embryos show severe forebrain defects including truncations of anterior head (B, G), HPE including cyclopia with proboscis (C, H), a single nostril (D, I) or agnathia (no lower mandibular; E, J). Adapted from A. Petryk et al., 2004.

The most common genetic cause of HPE are chromosomal abnormalities such as trisomy 13, 18 and triploidy, causing 24 – 45 % of all cases (reviewed in Roessler & Muenke, 2010). Additionally, nine genes and four non-annotated genetic loci have been associated with HPE in humans (Table 2). The first discovered mutated gene leading to HPE was *Shh*, which was confirmed one month later in human cases of HPE (Chiang et al., 1996; Roessler et al., 1996). Loss-of-function mutations in *Shh* lead to severe midline defects including alobar HPE and are the most common HPE-causing mutations in humans (Chiang et al., 1996; Roessler et al., 1996).

Human gene	Chromosome	Molecular function
<i>CDON</i>	11q24.2	Positive modulator of Hh signaling
<i>DISP1</i>	1q42	Release of Hh ligands
<i>DLL1</i>	6q27	NOTCH-Signaling member
<i>FGF8</i>	10q24	Lateral development of the anterior forebrain
<i>FOXH1</i>	8q24.3	Transcription factor for nodal signaling
<i>GAS1</i>	9q21.33	Positive modulator of Hh signaling
<i>GLI2</i>	2q14	Transcription factor mediating HH signaling
<i>NODAL</i>	10q	Tgf- β -like ligand involved in midline and laterality establishment
<i>PTCH1</i>	9q22.3	Receptor for Hh ligands
<i>SHH</i>	7q36	Ventral CNS patterning Hh signaling ligands
<i>SIX3</i>	2p21	Upstream activator of Hh and anterior Wnt repressor
<i>TDGF1 (CRIPTO)</i>	3p23-p21	Positive modulator of Nodal signaling
<i>TGIF</i>	18p11.3	Transcriptional repressor including retinoids
<i>ZIC2</i>	13q32	Axis formation and dorsal brain development, FGF8 downstream target

Table 2 Human HPE-associated gene loci. 14 genes have been identified so far in human HPE. Blue: Hh signaling members and modulators. Adapted from Roessler & Muenke, 2010.

In contrast to the *Shh*^{-/-} mouse model which shows a full phenotype penetrance, only 37 % of human carriers of loss-of-function mutations in *SHH* manifest HPE (reviewed in Cohen, 1989). Therefore, additional factors modulate the phenotypic spectrum of *SHH*-mediated HPE in humans. Most identified genes so far are direct members of the Hh signaling pathway including *SHH*, *PTCH1*, *GLI2* and *DISP1* (Ma et al., 2002; Ming et al., 2002; Rahimov, Ribeiro, de Miranda, Richieri-Costa, & Murray, 2006; Ribeiro, Murray, & Richieri-Costa, 2006; Roessler et al., 1996; Roessler et al., 2003; Roessler et al., 2005; Roessler, Ma, et al., 2009).

Importantly, also mutations in modulators of Hh signaling can cause HPE in humans, including the positive modulator *CDON* (in mice: *Cdo1*) (Ribeiro, Queizi, Nascimento, Bertolacini, & Richieri-Costa, 2010) and *GAS1* (Pineda-Alvarez et al., 2012). HPE has also been observed in loss-of-function mice for any of the described Hh signaling modulators with an exception for *Boc1*. *Megalin*^{-/-} mice show alobar HPE, exencephaly and eye defects (Willnow et al., 1996). 80 % of *Cdo1*^{-/-} embryos develop HPE, which can be rescued by the removal of one *Ptc* allele (M. Hong & Krauss, 2013; Zhang, Kang, et al., 2006; Zhang, Yi, et al., 2006). *Gas1*^{-/-} embryos show a mild form of HPE, which is further boosted by the additional removal of *Cdo1* (B. L. Allen et al., 2007). Although *Boc1*^{-/-} embryos do not develop HPE, the additional removal of *Cdo1* leads to severe alobar HPE (Zhang, Hong, Bae, Kang, & Krauss, 2011). These studies indicate that the modulators of Hh signaling are not only fine-tuning the pathway activity but are an essential requirement for normal brain development.

Apart from Hh signaling, other key developmental pathways have been identified, e.g. *DLL1* (Notch pathway) (Dupe et al., 2011), *NODAL* (Nodal pathway) (Roessler, Pei, et al., 2009), *TGIF* (Retinoic acid pathway) (Gripp et al., 2000) and *ZIC2* (Brown et al., 1998), a downstream target of *FGF8* signaling.

Also the loss of Bmp/Tgf- β antagonists *Chordin* and *Noggin* (Anderson, Lawrence, Stottmann, Bachiller, & Klingensmith, 2002) as well as the Bmp-binding protein *Twsg1* (A. Petryk et al., 2004) lead to HPE in mice.

Additionally to genetic mutations, environmental factors are very important for the manifestation of HPE. Diabetes in mothers increases the risk of HPE in fetuses by 200-fold in comparison to healthy mothers (Barr et al., 1983). Furthermore, exposure to teratogens like ethanol (Ronen & Andrews, 1991), retinoic acid (Lammer et al., 1985) and low levels of cholesterol (Lanoue et al., 1997) increase the HPE risk, potentially by reducing *SHH* levels during development.

Although many members of developmental signaling pathways have been identified to contribute to HPE, the genetic cause of about 75 % of human HPE cases remains unknown (reviewed in Winter et al., 2015).

7. Ciliopathies – primary cilium defects can cause holoprosencephaly

In vertebrates, Hh signaling and Wnt signaling require a specialized organelle for proper signaling, the primary cilium (Fig 12, reviewed in Gerdes et al., 2009 and Nozawa et al., 2013).

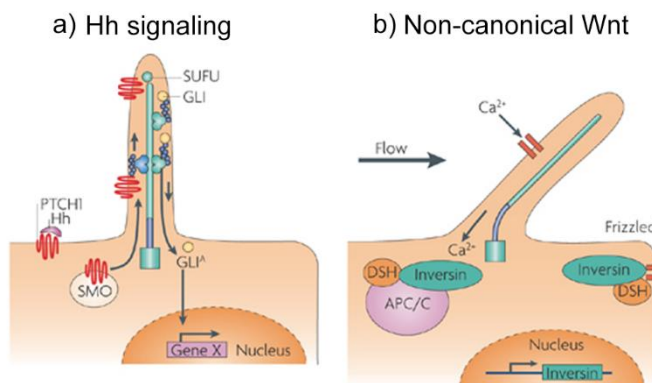


Figure 12 Signaling pathway activity on primary cilium. a) Hh signaling requires the primary cilium. b) Non-canonical Wnt signaling requires the primary cilium. Adapted from Fliegau, Benzing, & Omran, 2007.

The primary cilium is a highly dynamic, antenna-like organelle which is present on most mammalian cell types. It is formed upon cell cycle exit and disassembled upon cell cycle entrance and has a central role in translating extracellular signaling cues to intracellular responses (reviewed in Gerdes et al., 2009). Thereby, important developmental processes like the establishment of planar cell polarity and the regulation of proliferation, but also DNA damage response and autophagy, are controlled by the primary cilium. Given its central role during development, defects in their structure and function lead to pleiotropic congenital disorders summarized as ciliopathies (reviewed in Waters and Beales, 2011). An important aspect of these diseases is the highly variable expressivity of the clinical phenotype which typically, but not always, includes polydactyly, renal defects and CNS misdevelopment (reviewed in Cortes et al., 2015). Mutations in more than 80 genes have been associated to ciliopathic features. Thereby most of the affected proteins are involved in the structure and the intraflagellar transport

system of the cilium, which is required for its assembly and maintenance (Fig 13; reviewed in Waters and Beales, 2011 and Guo et al., 2015).

Because the primary cilium is the main site for Hh signaling, loss-of-function of ciliar transport proteins lead to severe embryonic patterning defects which overlap with defects observed in Hh pathway member mutations. Strikingly, HPE, neural tube closure defects like exencephaly and preaxial polydactyly are observed in *Shh*^{-/-} mice as well as in loss-of-function mutant mice of the intraflagellar transport proteins *Ift88* and *Ift172* (Chiang et al., 1996; Huangfu et al., 2003).

Additionally to Hh signaling, the primary cilium seems to be involved in Wnt signaling. Although its role is not yet completely understood, it is believed that the primary cilium inhibits canonical Wnt signaling whereas it is required for non-canonical PCP signaling (Corbit et al., 2008; Gerdes et al., 2007).

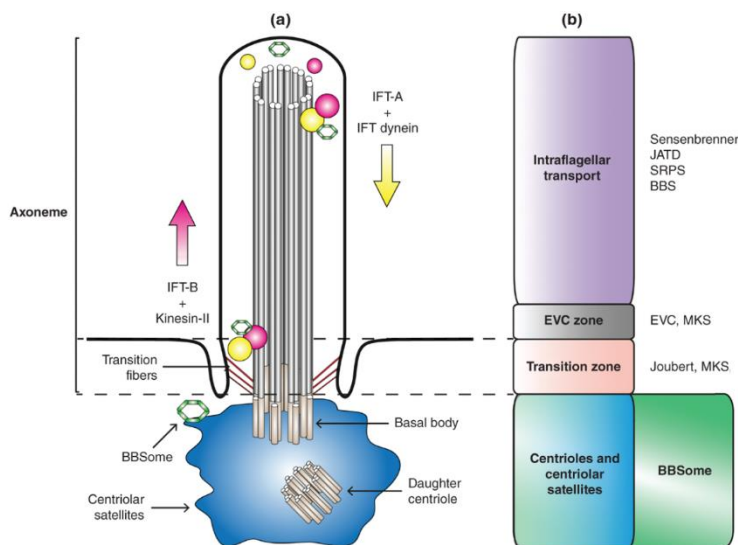


Figure 13 Structure and disease-associated compartments of the primary cilium. Most disease-associated genes have been identified in intraflagellar transport proteins which are trafficked along the ciliar axoneme. Additionally mutations in other ciliar compartments including the EVC- (Ellis-van Creveld) and transition zone as well as in centrioles and the BBSome can cause ciliopathies. Adapted from Cortes et al., 2015.

8. Pluripotent stem cells as a model of early neuroectoderm differentiation

Fundamental developmental cues and mechanisms involved in early embryo patterning and development were discovered through the investigation of model organisms. However, our understanding of the mammalian brain is still very basic due to the complex interplay of signaling pathways *in vivo*. This disadvantage can be circumvented by the use of cell culture models with defined experimental setups. This approach seems to be especially tempting in the field of ECM research, because it allows to investigate the effects of specific ECM components on cellular processes. Modeling early neural development by differentiating pluripotent stem cells (PSCs) provides the opportunity to study specific aspects of complex development and thereby extend our understanding of brain development.

Mouse and human embryonic stem cells (mESC and hESCs) are PSCs derived from the inner cell mass of blastocyst staged embryos. Since 2006, PSCs can additionally be generated from somatic cells circumventing the technically and ethically problematic use of embryonic tissue (Takahashi & Yamanaka, 2006). Thereby, differentiated cells like fibroblasts are reprogrammed to an embryonic-like

state by a transient activation of a specific set of transcription factors. These cells are termed induced pluripotent stem cells, iPSCs (Takahashi & Yamanaka, 2006). Hallmarks of PSCs include their potential to differentiate to all derivatives of the three primary germ layers and their ability to expand indefinitely. Therefore, PSCs represent an ideal source to model and study early developmental processes *in vitro*.

The differentiation of PSCs to specific cell types *in vitro* require the presence of specific signaling pathway agonists and antagonists. Thereby, the *in vivo* development of an embryo is mimicked in a cell culture dish. A common strategy to differentiate PSCs to neuroectoderm is to co-culture PSCs on neural-inducing stromal cells like MS5 (Barberi et al., 2003) or PA6 cells (Kawasaki et al., 2000). These cells induce exclusively neuroectoderm fate in a highly efficient manner in mouse and human PSCs (Lee et al., 2007). Furthermore, feeder-free differentiation of hPSCs to neuroectoderm can be achieved by the inhibition of meso- and endodermal differentiation by dual SMAD inhibition (Chambers et al., 2009). The differentiation of PSCs to specific neural subpopulations requires further refined protocols which mimic the development of specific brain areas. These strategies allow the creation of highly specific cell types including ventral midbrain dopaminergic neurons which have the potential to replace degenerated neurons in Parkinson's disease (Kriks et al., 2011).

The control of stem cell maintenance and differentiation has been classically based on the activation or inhibition of signaling pathways by soluble growth factors (Agarwal, Holton, & Lanza, 2008; Kattman et al., 2011; Zimmer et al., 2016). However, other microenvironmental factors including the ECM gain increasing attention as major modulators of stem cell maintenance and differentiation (reviewed in Guilak et al., 2009 and Mummery et al., 2012). Depending on its molecular composition, the ECM can modulate binding kinetics between the signaling pathway ligands and their receptors by GAG chains. In mESCs, 80 % of the GAG chains are heparan sulfates whose abundance is increasing and constantly changed during differentiation in a cell type-specific manner (Johnson et al., 2007; Nairn et al., 2007). Although heparan sulfate GAG chains seem not to be required for mESC maintenance, they are mandatory to induce differentiation to all three germ layers (Johnson et al., 2007; Kraushaar, Yamaguchi, & Wang, 2015). However, which specific members of the ECM are involved in the regulation of early differentiation has only begun to be investigated.

Gpc4 has been identified to be among the most abundant HSPGs in hESCs (Harkness et al., 2008). Two studies investigated the role of *Gpc4* in mESCs. In 2012, it was proposed that *Gpc4* might be required for mESC self-renewal by facilitating canonical Wnt signaling (Fico et al., 2012). Reduction of *Gpc4* in mESCs led to accelerated differentiation to mesoderm and neuroectoderm. Furthermore, it was reported that decreased levels of *Gpc4* led to a specific increase of ventral midbrain dopaminergic neurons but did not affect the GABAergic neuronal subpopulation (Fico et al., 2014). However, no modified pathway mediating these effects was suggested.

A recent study investigated the expression pattern of various HSPGs in human neural stem cells, neurons and astrocytes. The authors suggested the family of *Gpcs* as cell surface markers for specific cell types, including *GPC4* as a cell-surface marker for neural stem cells and astrocytes (Oikari et al., 2016). However, the function of *GPC4* on these cells as a potential signaling modulator have not been addressed in these study.

9. Aims of the thesis

Despite the strong and specific expression of *Gpc4* in the developing mouse brain and the known function of its orthologues as modulators of developmental signaling pathways, its role during mouse brain development remains elusive.

My PhD project was aimed to investigate the expression of *Gpc4*, its modulated developmental processes and the involved signaling pathways during mouse brain development.

As a first step, the *Gpc4* mRNA and protein expression patterns were analyzed in the developing mouse brain and during early neural development, modeled by mESCs differentiation. Secondly, the role of *Gpc4* during brain development was studied in two different models. *Gpc4* was downregulated in mESCs and analyzed in the undifferentiated state and during neural differentiation *in vitro*. Additionally, a *Gpc4* loss-of-function mouse line (*Gpc4*^{-/-}) was created which was analyzed during embryo development. Thirdly, the developmental signaling pathways which are modulated by *Gpc4* and hence are underlying the identified defects were analyzed in both models.

II. Results

1. Analysis of *Glypican 4* in mice

1.1 *Gpc4* expression in the developing and the adult brain

The expression of *Gpc4* during mouse embryo development and in the adult mouse has been described before (Ford-Perriss et al., 2003; Hagihara et al., 2000; Luxardi et al., 2007; Watanabe et al., 1995; Ybot-Gonzalez et al., 2005). To verify published data, *Gpc4* mRNA expression was analyzed by *in situ* hybridization at E12.5, E17.5 and in the adult mouse 42 days after birth (in collaboration with Ms Anna Truckenbrodt, lab manager in our group; P 42, Fig 14 a), c), f)). The mRNA expression patterns were then verified on protein level by western blot analysis of different brain areas (Fig 14 b), d)).

At all analyzed embryonic stages, *Gpc4* mRNA was expressed strongest in the developing forebrain compared to all other analyzed brain areas. At E12.5, *Gpc4* mRNA was almost exclusively expressed in the ventricular and sub ventricular zones surrounding the lateral ventricles (Fig 14 a)). Additionally, a lower, but specific expression of *Gpc4* was detected at the ventral midline of the mid- and hindbrain. Accordingly, *GPC4* protein was strongly expressed in the anterior areas of the brain, the snout and the cortex. In contrast, almost no expression was detected in the mid- and hindbrain (Fig 14 b)).

At E17.5, the expression of *Gpc4* mRNA expanded to newly developed cortical layers (Fig 14 c)). Although the expression remained strong in the ventricular and sub ventricular zone, also single cells of the subplate zone and cells of the cortical plate expressed *Gpc4*. On protein level, strong expression of *GPC4* were observed in the eyes. In addition, the cortex showed high levels of expression compared to the mid- and hindbrain (Fig 14 d)). Accordingly to the pattern at E12.5, the expression in the mid- and hindbrain was low in comparison to strong levels in the forehead.

In the adult mouse, *Gpc4* was strongly expressed in the dentate gyrus and the region I of hippocampus proper (CA1) of the hippocampus (Fig 14 e) and f)). Strong expression was also observed in the postpiriform transition area of the olfactory areas and in the cortical layers 5 and 6. Apart from single cells in the cerebellum, the *Gpc4* expression was limited to the anterior areas of the adult brain (Fig 14 f)).

II. Results

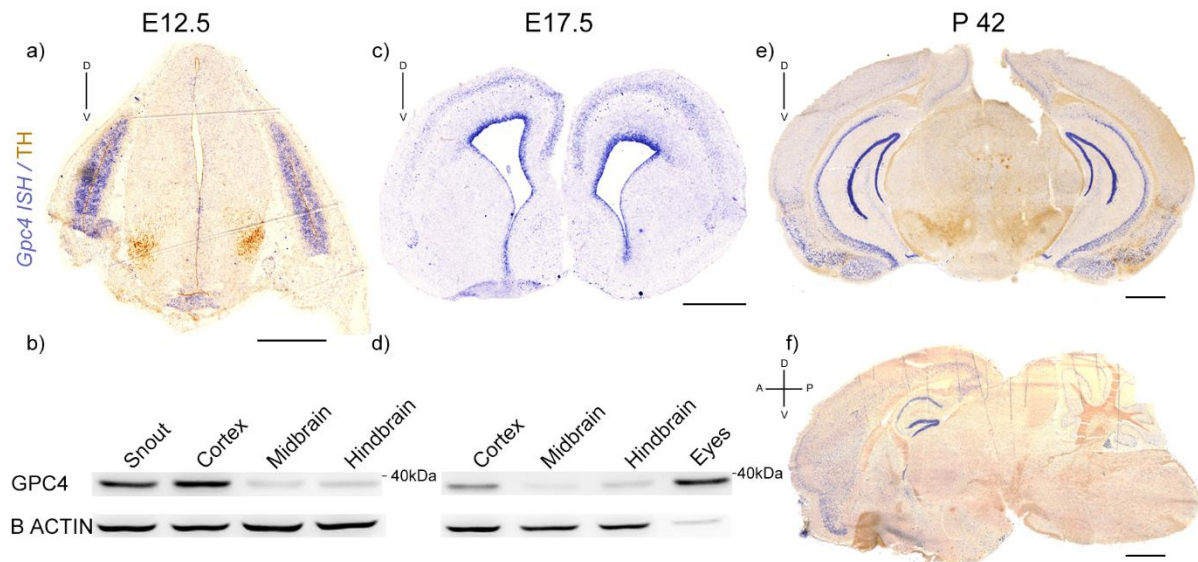


Figure 14 *Gpc4* expression in the developing and the adult brain. a) – d) Specific *Gpc4* expression in the ventricular and sub ventricular zones of the developing cortex and in the snout at E12.5 and E17.5 (purple). e) and f) Expression in the hippocampal regions dentate gyrus and CA1 additionally to expression in specific cortical layers of adult mice (P 42). a), e) and f) were co-stained by the midbrain marker Tyrosine hydroxylase (TH, brown). Scale bar: a) 500 μ m c), e), f): 1 mm.

Gpc4 and *Gpc6* are the most closely related members of the *Gpc* family and share about 64 % of their amino acid sequence. To exclude a non-specific detection of *Gpc6* mRNA, the expression patterns of both *in situ* hybridization probes were analyzed. Although an overlap between *Gpc4* and *Gpc6* expressing domains was observed in E17.5 brains, both probes detected exclusive expression regions. Therefore, the detected *Gpc4* signal was considered to be specific.

To visualize the expression of *GPC4* protein by immunofluorescence stainings, various commercial and non-commercial antibodies, which target different regions, were tested with different staining protocols. Although most antibodies stained specific cellular subpopulations, the detected patterns highly varied between the used antibodies and were not specific to *GPC4*. Furthermore, these antibodies were also tested by western blot analysis. Except for one non-commercial antibody which was used in Figure 14 and in all subsequent experiments, none of the antibodies detected *GPC4* exclusively. The specific antibody detected a 70 kDa, a 37 kDa and a 22 kDa band. Although the observed 70 kDa band theoretically corresponds to the potential full-length protein, this band was not specific to *GPC4*. Instead, the detected 37 kDa band was specific. This fragment is an N-terminal cleavage product of *GPC4*. Although it is shed from the cell surface, it remains bound in the cell lysate and was therefore detectable by western blot analysis. Considering the unspecific signal detected with all commercially available *Gpc4* antibodies, former published results based on these antibodies should be evaluated with caution.

Throughout development and in the adult brain, *Gpc4* mRNA and protein was mainly expressed in the anterior part of the head, including the snout, the eyes and in the developing cortex. In particular, *Gpc4* mRNA was strongly detected in the ventricular and sub ventricular zones around the developing lateral ventricles. These regions are main sites of neurogenesis during development and in the adult. To investigate the role of *Gpc4* during mouse brain development, mice with a loss-of-function of the *Gpc4* gene were created and analyzed during embryo development.

1.2 Generation of the *Gpc4* loss-of-function mouse line (*Gpc4*^{-/-})

To address the role of *Gpc4* during mouse brain development, a mouse line was created which carried a loss-of-function deletion of *Gpc4*. To achieve this, a targeted mESC clone from the European Conditional Mouse Mutagenesis Program (EUCOMM) was injected in blastocysts which were reimplanted in carrier mothers (detailed description in materials and methods chapter 2.1.3). The knockout of the *Gpc4* gene was mediated by a knockout-first conditional vector system (Fig 15 a) (Skarnes et al., 2011). This knockout-first allele of *Gpc4*, termed *Gpc4*^{tm1a(EUCOMM)Wtsi}, carries an *Engrailed-2* splice acceptor element (En2a) which traps normal transcription by alternative splicing to a *LacZ* cassette (*LacZ*). The *LacZ* gene codes for the β-Galactosidase which can be used to visualize the expression pattern of *Gpc4*. Premature truncation of the *GPC4* protein is mediated by a SV40 polyadenylation (pA) signal. Furthermore, 3 loxP sites are introduced flanking a neomycin selection cassette (NEO) and the critical Exon 3 of *Gpc4*. All injected mESCs and mouse lines which were used to create the *Gpc4* loss-of-function mouse line were strictly maintained on a C57BL/6N background if not otherwise indicated. Two carrier mothers gave birth to 6 pups out of which 1 chimeric male was born with 90 % chimerism which was used to establish the knockout-first mouse line. Correct targeting of the vector in knockout-first mice and the injected mESC clone were verified and confirmed by long-range polymerase chain reaction (PCR). To avoid potential residual expression of *Gpc4* by the *Gpc4*^{tm1a(EUCOMM)Wtsi} knockout-first allele, mice were further crossed with the *Gt(ROSA)26Sor*^{tm16(cre)Arte} mouse line. The ubiquitously active *ROSA26* locus drives the uniformly and constitutively expression of the *Cre* recombinase. The exposure of the *Gpc4*^{tm1a(EUCOMM)Wtsi} knockout-first allele to the *Cre* recombinase deletes the loxP-flanked Exon 3 and induces a frameshift mutation leading to nonsense decay of the mutant transcript (Skarnes et al., 2011). The resulting loss-of-function allele is termed *Gpc4*^{tm1b(EUCOMM)Wtsi}. To establish the *Gpc4*^{tm1b(EUCOMM)Wtsi} cohort, heterozygous *Cre* males (*Gpc4*^{wt/Y} / *Cre*^{+/wt}) were crossed with heterozygous *Gpc4*^{tm1a(EUCOMM)Wtsi/wt} knockout-first females (Fig 15 b)). Upon 51 adult animals, 22 males (43 %) and 29 females (57 %) were born. However, only one hemizygous *Gpc4*^{tm1b(EUCOMM)Wtsi/Y} male (2 %) and one heterozygous *Gpc4*^{tm1b(EUCOMM)Wtsi/wt} female (2 %) were viable to adulthood. This was in strong contrast to 12.5 %, corresponding to about six

II. Results

animals for each group which were expected from a normal distribution of allele inheritance. Additionally, one hemizygous $Gpc4^{tm1b(EUCOMM)Wtsi/Y}$ male was born but died after six weeks presumably due to hydrocephalic misdevelopment of the head. These results already suggested a potential role of $Gpc4$ during mouse brain development, which might cause embryonic lethality upon complete loss-of-function. The obtained hemizygous $Gpc4^{tm1b(EUCOMM)Wtsi/Y}$ male was used to expand the colony.

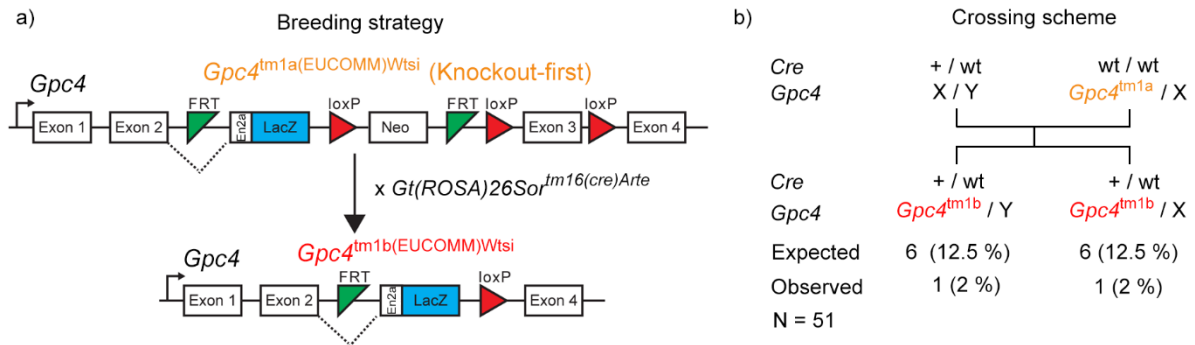


Figure 15 Generation of $Gpc4$ loss-of-function mice. a) Breeding strategy. Mice carrying the EUCOMM $Gpc4^{tm1a(EUCOMM)Wtsi}$ knockout-first allele were crossed with the $Gt(ROSA)26Sor^{tm16(cre)Arte}$ line to remove the floxed critical Exon 3 leading to the complete knockout of $Gpc4$ ($Gpc4^{tm1b(EUCOMM)Wtsi}$ allele). b) Crossing scheme to obtain $Gpc4^{tm1b(EUCOMM)Wtsi}$ founder animals. Heterozygous $Gt(ROSA)26Sor^{tm16(cre)Arte}$ males were crossed with heterozygous $Gpc4^{tm1a(EUCOMM)Wtsi/wt}$ knockout-first females. Out of 51 animals, only 1 hemizygous $Gpc4^{tm1b(EUCOMM)Wtsi/Y}$ male and one heterozygous $Gpc4^{tm1b(EUCOMM)Wtsi/wt}$ female were obtained compared to 6 expected animals for each group. **Yellow:** $Gpc4^{tm1a(EUCOMM)Wtsi}$ allele (Knockout-first); **red:** $Gpc4^{tm1b(EUCOMM)Wtsi}$ allele.

Once the mouse colonies were established, the functionality of both $Gpc4$ targeting alleles was analyzed by $Gpc4$ mRNA and protein expression (Fig 16). First, the LacZ reporter system of the $Gpc4^{tm1a(EUCOMM)Wtsi}$ knockout-first allele was used to verify the $Gpc4$ expression pattern previously obtained by *in situ* analysis in adult mice (Fig 16 a)). Both approaches showed identical expression patterns including a strong expression in the hippocampus and in ventral cortical layers. The $Gpc4$ expression pattern by β -Galactosidase was also tested on E8.0 – E10.0 sections and in whole embryos. In contrast to the adult brain, the signal in embryos was too weak to get a clear $Gpc4$ -driven β -Galactosidase expression pattern.

Next, the knockout efficiency of the $Gpc4$ targeting alleles was analyzed (Fig 16 b) - d)). In contrast to wildtype littermates, no expression of $Gpc4$ mRNA was detected in homozygous $Gpc4^{tm1b(EUCOMM)Wtsi/Y}$ embryos (E17.5) by *in situ* hybridization (Fig 16 b)). Furthermore, whole brain lysates of E12.5 male embryos were collected and $Gpc4$ mRNA and protein expression were analyzed (Fig 16 c) and d)). $Gpc4$ mRNA expression was not differently expressed between wildtype controls and littermates carrying the Cre recombinase (100.0 % vs. 103.8 %). In contrast, $Gpc4$ mRNA was strongly downregulated in

II. Results

Gpc4^{tm1a(EUCOMM)Wtsi/Y} knockout-first mice (12.3 %) and was almost completely absent in *Gpc4*^{tm1b(EUCOMM)Wtsi/Y} mice (2.4 %). These results indicated that the alternative splicing of the knockout-first vector was not complete, which led to residual expression of *Gpc4* mRNA. Therefore, the *Cre*-mediated removal of *Gpc4* Exon 3 was required for a complete loss-of-function. The absence of *Gpc4* on the protein level was verified by western blot analysis (Fig 16 e)). The 37 kDa cleavage product of GPC4 was completely absent in *Gpc4*^{tm1b(EUCOMM)Wtsi/Y} mice. However, as described in chapter 1.1, the non-specific 70 kDa band was not altered compared to wildtype controls.

Taken together, these results confirmed the expression of *Gpc4* mRNA obtained by *in situ* hybridization by *Gpc4*-driven β -Galactosidase expression. Furthermore, the remaining *Gpc4* expression observed in *Gpc4*^{tm1a(EUCOMM)Wtsi/Y} knockout-first animals was completely lost in *Gpc4*^{tm1b(EUCOMM)Wtsi/Y} mice on the mRNA and protein level. Hence, from here on the *Gpc4*^{tm1b(EUCOMM)Wtsi} loss-of-function mouse line will be referred to as *Gpc4*^{-/-} and the wildtype controls as *Gpc4*^{+/+}.

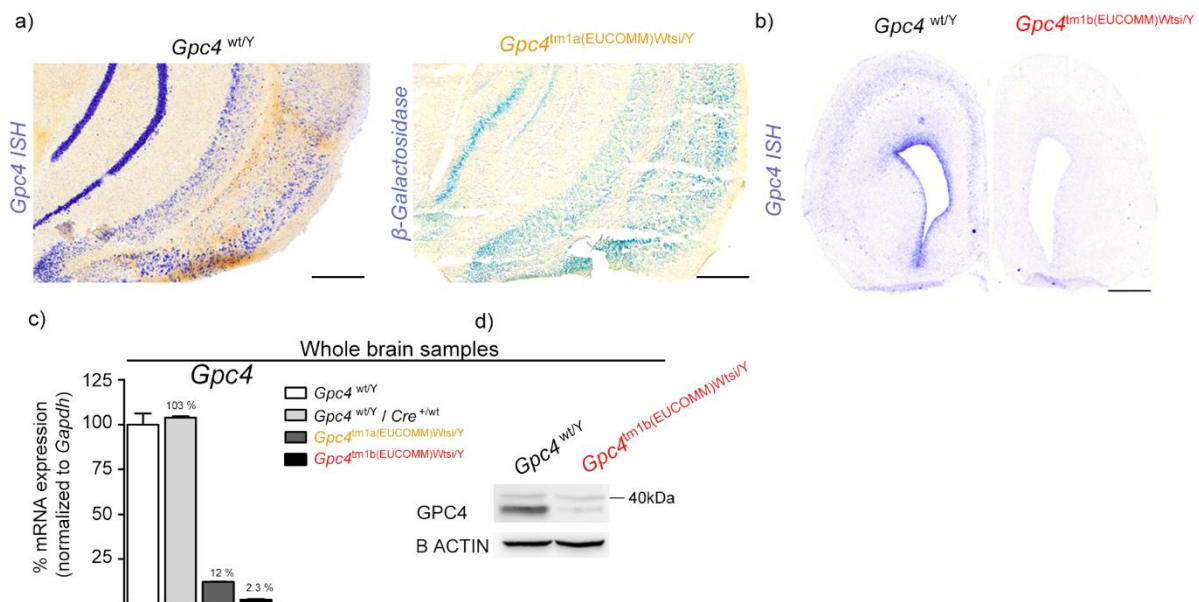


Figure 16 Confirmation of *Gpc4* knockout in mice. a) *Gpc4* mRNA expression by *in situ* analysis and *Gpc4*-driven β -Galactosidase expression of the *Gpc4*^{tm1a(EUCOMM)Wtsi} knockout-first vector in adults. Both methods showed identical expression patterns. b) Confirmation of *Gpc4*^{tm1b(EUCOMM)Wtsi/Y} loss-of-function by *in situ* hybridization on E17.5 sections. c) Quantitative PCR (qPCR) analysis of *Gpc4* mRNA expression in whole brain samples of E12.5 male mice. The *Cre* allele had no influence on *Gpc4* expression. The *Gpc4*^{tm1a(EUCOMM)Wtsi} knockout-first vector (yellow) led to residual levels of *Gpc4* mRNA in contrast to no expression in *Gpc4*^{tm1b(EUCOMM)Wtsi/Y} animals (red). d) Confirmation of complete loss-of-function of GPC4 by western blot analysis. The 37 kDa fragment was completely absent in *Gpc4*^{tm1b(EUCOMM)Wtsi/Y} embryos. Scale bar 500 μ m. Error bars of qPCR indicate minimum and maximum of technical replicates. **Yellow:** *Gpc4*^{tm1a(EUCOMM)Wtsi} allele (Knockout-first); **red:** *Gpc4*^{tm1b(EUCOMM)Wtsi} allele.

1.3 *Gpc4*^{-/-} embryos show a broad spectrum of severe developmental defects

After the complete absence of *Gpc4* was confirmed in the *Gpc4*^{-/-} line, mice were bred and analyzed at different embryonic stages. During embryo preparation at E12.5 and E15.5, many deciduae within the uteri of homo- and heterozygous *Gpc4* knockout females were empty or filled either with blood or reabsorbing embryonic tissue (Fig 17). Further analysis confirmed empty deciduae as early as E9.5. These results indicated that several embryos died already before E9.5. Furthermore, among surviving embryos, many *Gpc4*^{-/-} embryos showed severe developmental defects in the brain. Defects were often but not exclusively observed in embryos surrounding the reabsorbed sites (marked by asterix).

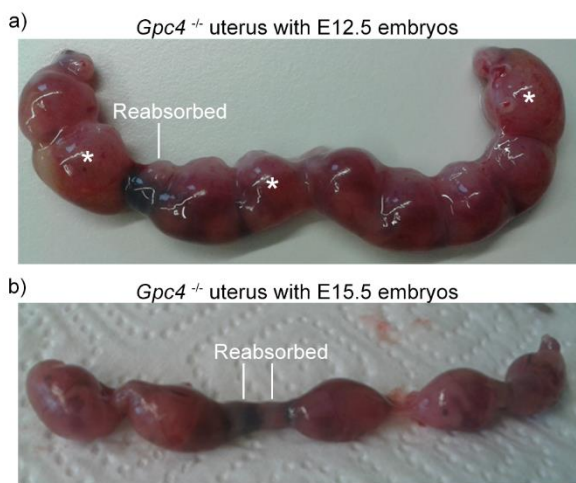


Figure 17 Reabsorbed embryos in *Gpc4*^{-/-} mothers. Reabsorption of embryos prepared at E12.5 (a) and E15.5 (b) led to blood-filled deciduae in *Gpc4*^{-/-} uteri. Misdeveloped embryos often but not exclusively surrounded reabsorbed embryos (marked by asterix).

The loss-of-function of *Gpc4* led to a broad spectrum of severe misdevelopment of the anterior brain and head (Fig 18). Common macroscopic features included a general developmental delay, hypoplasia of the eyes, neural tube defects (NTDs) including exencephaly and truncation of the anterior forebrain. At E12.5 and E15.5, embryos showed hypoplasia (Fig 18 b, c) or complete absence of the eyes (Fig 18 e, f)). Interestingly, the right eye was generally more affected than the left one. Additionally to the eyes, E12.5 embryos showed smaller forebrains (Fig 18 b)) or exencephaly (18 c)). In tissue sections of exencephalic embryos, an inversion of neural development was observed. Usually, neural precursor cells (PAX6 positive) surround the lateral ventricles and give rise to neurons by asymmetric division. Subsequently, maturing neurons migrate to outer cortical layers and start to express B3 TUBULIN. In exencephalic embryos, the outer-most layer of the cortex was positive for PAX6 and the inner-most was B3 TUBULIN positive, indicating the inversion of brain tissue. The embryo depicted in Fig 18 c) showed strong outgrowth of the dorsal brain whereas ventral parts were not affected. Similar exencephalic embryos have been observed at E15.5 (Fig 18 e)). Another animal had NTDs of the complete head with beginning tissue reabsorption (Fig 18 f)). Probably due to early lethality and reabsorption, no embryos with NTDs were obtained at later stages. Severe eye defects were also detected in E17.5 embryos (Fig 18 g – i). Interestingly, embryos with impaired separation of the eye

fields, resulting in cyclopia, were observed at E17.5 and P0 (Fig 18 i), l), q), r)). Preparation of the brains of these embryos confirmed anterior brain defects including the loss of the olfactory bulbs and cyclopia (Fig 18 k) – l)). Other *Gpc4*^{-/-} embryos completely lacked the anterior forebrain (Fig 18 o) – p)) indicating an impaired neural induction in these embryos. All severely affected embryos died either during embryogenesis, or shortly after birth (Fig 18 m) – r)). These embryos were quickly cannibalized by the mother.

To exclude potential effects of the remaining *LacZ* cassette in the investigated *Gpc4*^{-/-} line, another loss-of-function line which lacks the *LacZ* cassette was created by breeding *Gpc4*^{tm1a(EUCOMM)Wtsi} knockout-first animals first with *Tg(CAG-Flpe)2Arte* to create the floxed *Gpc4*^{tm1c(EUCOMM)Wtsi} allele (Skarnes et al., 2011). These mice were subsequently crossed with *Gt(ROSA)26Sor*^{tm16(cre)Arte} mice to create the loss-of-function allele without the *LacZ* cassette (*Gpc4*^{tm1d(EUCOMM)Wtsi}). Importantly, no differences in the phenotype expressivity and penetrance were observed between these two *Gpc4* loss-of-function lines. It was therefore concluded that the *LacZ* cassette is not affecting the phenotype of *Gpc4*^{-/-} mice.

In summary, the loss of *Gpc4*^{-/-} caused severe misdevelopment of the brain, whereas in almost all cases, the forebrain was strongly affected.

II. Results

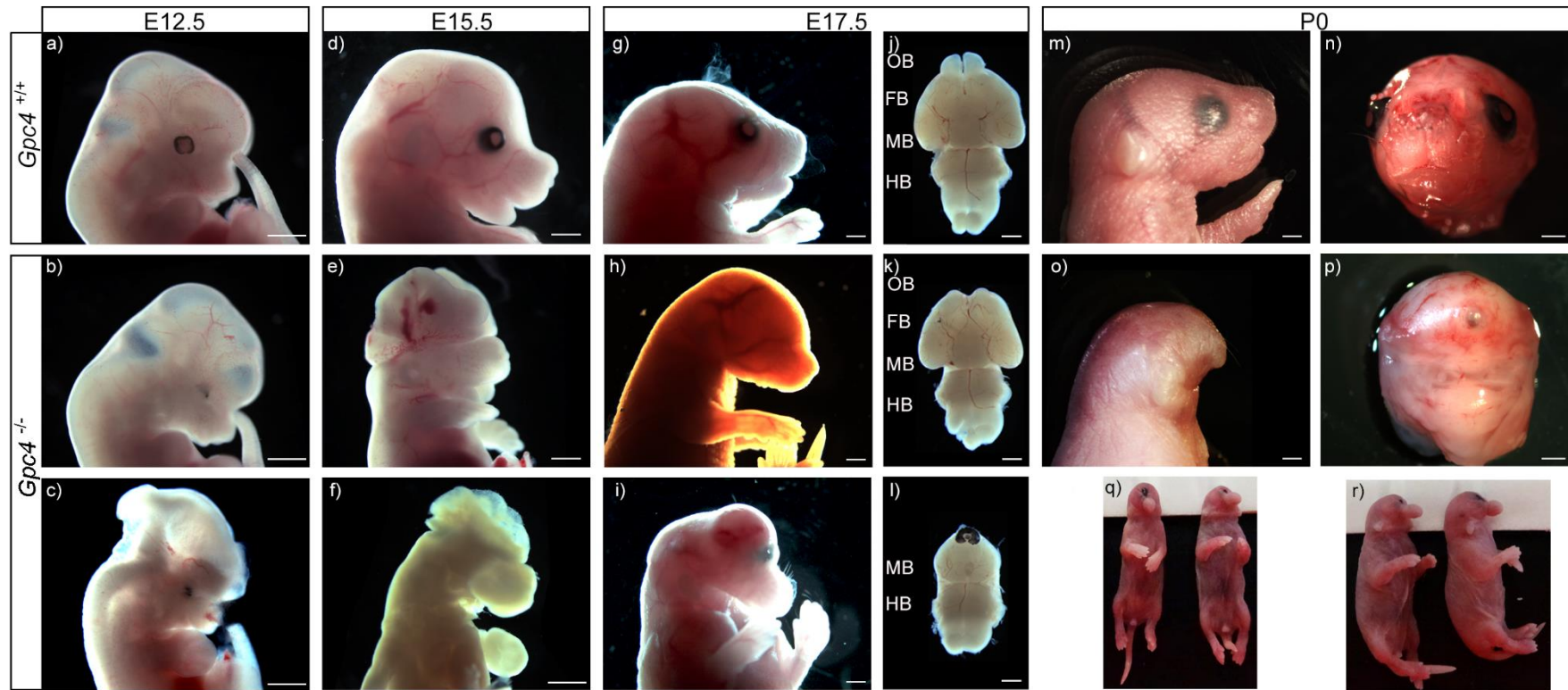


Figure 18 Overview of developmental defects in *Gpc4*^{-/-} embryos. Strong morphological phenotypes included neural tube closure defects (exencephalus: c, e, f)), developmental delay (b, c)), absent (e, f, h)), and non-separated eye fields (cyclopia; i, l, q, r)), absence of the olfactory bulbs (k) and absence of the anterior forehead (o, p)). Scale bar: 1 mm.

1.4 Holoprosencephaly in *Gpc4*^{-/-} embryos

To identify which specific brain areas are affected in *Gpc4*^{-/-} embryos, embryos at different developmental stages were analyzed by high-resolution μ -CT analysis. This method allows the analysis of body structures without destroying the tissue. Additionally, left and right defects were easier detectable than in cut brain sections. Several representative embryos were selected to depict the broad phenotypic spectrum of misdevelopment in *Gpc4*^{-/-} embryos (Fig 19).

3D surface reconstruction of E12.5 embryos visualized severe brain- and craniofacial misdevelopment. Virtual coronal sections showed no abnormalities in the posterior part of the head of *Gpc4*^{-/-} embryos (Fig 19 a sections). However, in the anterior brain, lateral ventricles were completely absent (Fig 19 b – d sections). The complete lack of separation of the anterior forebrain into left and right cerebral hemispheres had been described as alobar HPE, the most severe form of HPE. Consequently, the complete face including the eyes, snout and mandibular were not developed. In embryos without HPE, a strong thinning of the developing anterior cortex was observed indicating impaired neural differentiation.

At E14.5, another strong misdeveloped embryo was analyzed in detail. The 3D reconstruction indicated severe craniofacial defects, including cyclopia, an abnormal and elongated snout as well as a misdeveloped lower mandibular. Like in most other affected embryos, coronal sections did not identify defects in the posterior head, but confirmed anterior defects. In contrast to the E12.5 embryo, lateral ventricles were rudimentarily developed in this embryo. However, no separation into two cortical hemispheres occurred in the most anterior part of the brain. These defects are described as a milder, semilobar form of HPE. Additionally to brain misdevelopment, heart defects were detected in this embryo. The heart chambers were not separated into left and right ventricles due to an incomplete closure of the ventricular septum. However, this was the only animal out of nine *Gpc4*^{-/-} embryos analyzed by μ -CT which showed heart defects.

A very mild form of forehead misdevelopment was found in E17.5 embryos (Fig 19 c)). No macroscopic alterations were detected in this animal. However, μ -CT analysis allowed the identification of a very mild misdevelopment of the left olfactory epithelium of the snout, illustrated at transversal sections. In the 3D reconstruction, the left nostril was abnormally developed and seemed to be closed.

A severely affected dead born embryo was obtained before being cannibalized (Fig 19 d)). Although the brain seemed to be mostly developed, the snout was shortened and no lower mandibular and tongue was developed.

In summary, defects in anterior brain separation including the complete absence (alobar HPE) and a milder incomplete separation of lateral ventricles (semilobar HPE) were detected by μ -CT analysis. Although heart defects were found additionally to brain misdevelopment, these defects occurred only

in one embryo. Furthermore, no abnormalities in the morphology and position (*situs inversus*) of inner organs including lung, kidney and liver were detected by μ -CT analysis.

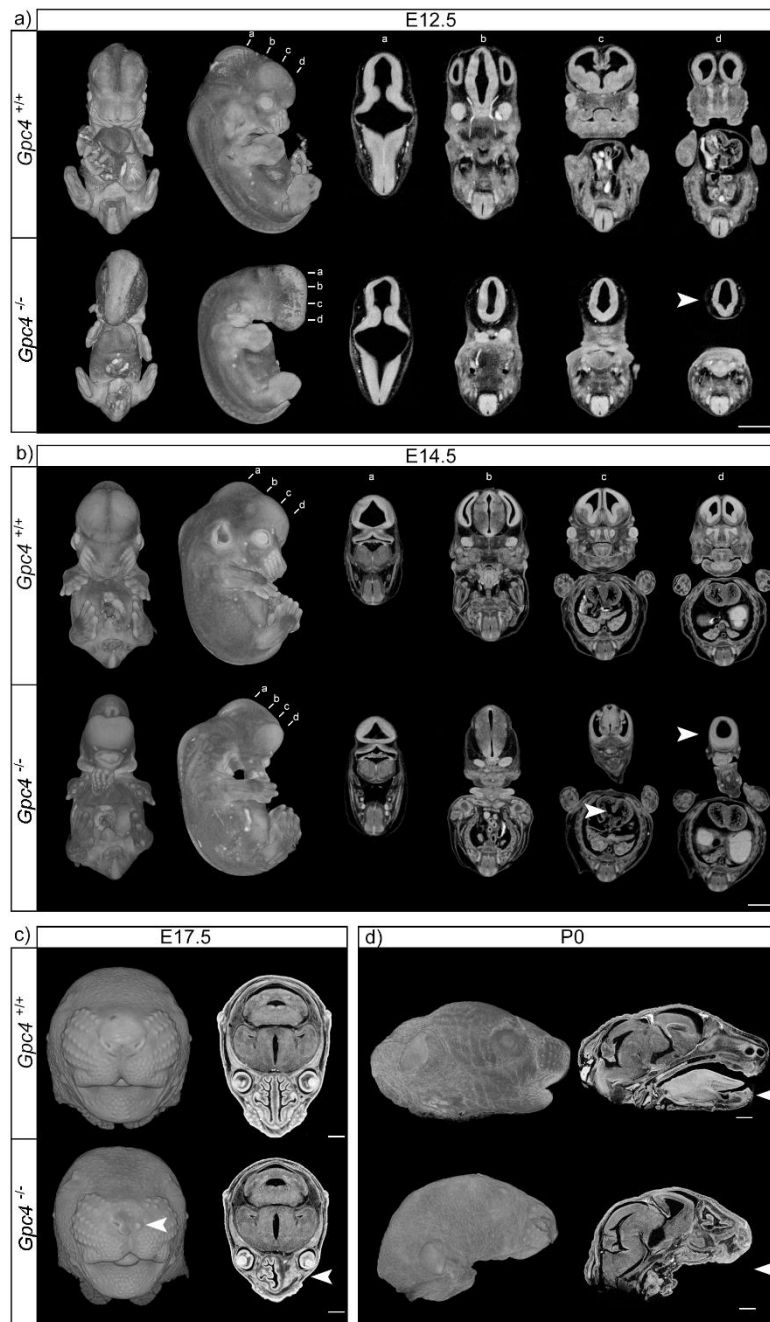


Figure 19 μ -CT analysis of *Gpc4*^{-/-} embryos. a) E12.5 embryo showed complete lack of lateral ventricle separation (alobar HPE). b) E14.5 embryo showed severe craniofacial defects including cyclopia and a partial lack of separation in the anterior forebrain (semilobar HPE) additionally to heart defects (arrow). c) E17.5 embryo showed mild misdevelopment affecting the left nasal area (arrow). d) Dead born embryo lacked the lower mandibular and tongue (arrow). Tails were partially removed for genotyping. Scale bar 1 mm.

The loss-of-function of *Gpc4* led to a broad spectrum of developmental defects ranging from mild misdevelopment of the left snout to severe and lethal forms including exencephaly, alobar HPE and cyclopia. To get an overview of the most pronounced hallmarks of this enormous spectrum, embryos between E12.5 and P0 were summarized and categorized based on their developmental defects (Table 3). The eyes are the most accessible part of the CNS. Eye development was affected in most embryos, ranging from hypoplasia to cyclopia and complete absence of the eyes (16 / 21). Interestingly, the right eye was generally more often affected than the left one. Most embryos with eye defects showed severe misdevelopment of the anterior brain including semilobar and alobar HPE (5/21). Additionally to defects in the anterior brain, NTDs including exencephaly and incomplete closure has often been observed (5 / 21).

II. Results

		Eyes	HPE	Neural Tube defects	Snout	Cortex	Jaw	OB	Heart defects	Reabsorption
E12.5	Em 1	Right eye underdeveloped		Exencephalus						
	Em 2	Left eye underdeveloped								
	Em 3			Exencephalus						Started
	Em 4	Right eye underdeveloped	Semilobar HPE							
	Em 5	both present, very low	Semilobar HPE							
	Em 6	No eyes	Alobar HPE							
	Em 7							Underdeveloped		
E14.5 + E15.5	Em 8	Cyclopia	Semilobar HPE		Elongated, Shh-KO-like				Non-separated ventricles	
	Em 9	No eyes		Exencephalus						
	Em 10	No right eye		No closure yet						
E17.5	Em 11	Cyclopia			Elongated, Shh-KO-like	Cortex absent				
	Em 12	No right eye	Semilobar HPE					Absent		
	Em 13				Left OB misdeveloped					
	Em 14									
	Em 15	Right eye underdeveloped								
	Em 16	Right eye underdeveloped								
	Em 17	No eyes		Exencephalus						
P0	Em 18	Cyclopia			Elongated, Shh-KO-like	Forehead absent				
	Em 19	Cyclopia			Elongated, Shh-KO-like					
	Em 20	No eyes				Forehead absent				
	Em 21						No lower jaw			

Table 3 Phenotype expressivity of *Gpc4*^{-/-} embryos. *Gpc4*^{-/-} embryos showed a very broad spectrum of phenotype expressivity including misdeveloped eyes, HPE and neural tube defects. Additionally, defects in the snout and the absence of the cortex, jaw and the olfactory bulbs (OB) were observed. Less frequently, embryos showed heart defects or died before E12.5 leading to tissue reabsorption.

1.5 Phenotype penetrance is increased in *Gpc4*^{-/-} females

Although many of the embryos showed severe brain misdevelopment, also hemi- and homozygous animals without any macroscopically detectable defects were obtained. To investigate the phenotype penetrance in detail, 61 embryos between E12.5 and E17.5 were analyzed based on macroscopic developmental defects (Fig 20 a)). These developmental stages were chosen due to a low endogenous variability of development between embryos of the same litter. Therefore, developmental defects were reliable distinguishable from endogenous developmental variability. Within 16 heterozygous females, two embryos showed detectable defects (13 %). Surprisingly, only two out of 26 hemizygous *Gpc4*^{-Y} males (8 %) had macroscopically misdeveloped brains. In contrast, 13 out of 19 homozygous females (68 %) showed severe defects. Therefore, homozygous loss-of-function females were much stronger affected compared to hemizygous male embryos. Importantly, mild defects e.g. in the snout were only detected by high-resolution μ -CT analysis. Only a portion of the 61 embryos were analyzed by this method. Therefore, hemizygous males might have developed mild, undetected defects.

One possibility for the observed increased phenotype penetrance in homozygous females was the loss of strongly misdeveloped hemizygous males before E12.5. Therefore, these embryos would have not contributed to the phenotype penetrance analysis leading to the observed data. Consequently, less hemizygous *Gpc4*^{-Y} males would have been expected to be born. To investigate this possibility, the distribution of genotypes, including loss-of-function animals which escaped the embryonic phenotype, was investigated (Fig 20 b)). Upon breeding of hemizygous *Gpc4*^{-Y} males with heterozygous females, there was a slight increase of wildtype males detected (35 % detected vs. 25 % expected). However, hemizygous *Gpc4*^{-Y} males as well as heterozygous and homozygous females were detected almost at expected values (21 % detected vs. 25 % expected). Therefore, it was concluded that the increased penetrance of the phenotype in homozygous females was most likely not the result of an early loss of male *Gpc4* mutants.

a)	Phenotype penetrance						b)	Genotype distribution of adult mice			
N = 61	E12.5	E14.5	E15.5	E17.5	Total						
X / X	1 / 10	0 / 1	1 / 1	0 / 4	2 / 16 (13 %)	N = 23	X / Y	X / Y	X / X	X / X	
X / Y	1 / 16	0 / 2	0 / 2	1 / 6	2 / 26 (8 %)	Expected %	25	25	25	25	
X / X	5 / 8	1 / 1	1 / 2	6 / 8	13 / 19 (68 %)	Observed %	35	21	21	21	

Figure 20 Phenotype penetrance analysis of *Gpc4*^{-/-} embryos. a) Within 61 analyzed embryos, two heterozygous *Gpc4*^{-wt} females (13 %) and two hemizygous *Gpc4*^{-Y} males (8 %) showed macroscopic developmental defects. In contrast, 13 homozygous *Gpc4*^{-/-} females (68 %) were misdeveloped. b) Adult *Gpc4* loss-of-function mice which escaped embryonic misdevelopment followed a mendelian distribution of the *Gpc4* genotype and sex. **Red X:** *Gpc4* loss-of-function allele (*Gpc4*^{tm1b(EUCOMM)Wtsi}); black X: *Gpc4* wt allele.

1.6 *Gpc4*^{-/-} phenotype expressivity is genetic background dependent

The *Gpc4*^{-/-} mouse line was generated and strictly maintained on the C57BL/6N background. To investigate the role of genetic modifiers on the phenotype expressivity, *Gpc4*^{-/-} were crossed with CD-1 wildtype mice to obtain animals with a mixed genetic C57BL/6N x CD-1 background. Mice of this F1 generation were crossed with each other and E14.5 embryos were analyzed for macroscopic defects (Fig 21). Interestingly, the obtained homozygous females showed no severe developmental defects as observed before. However, both homozygous females showed a complete lack of pigmentation in the left and right eyes. Taken together, these data suggest a strong dependency of the *Gpc4* phenotype expressivity on genetic modifiers which differ between the C57BL/6N and the CD-1 line.

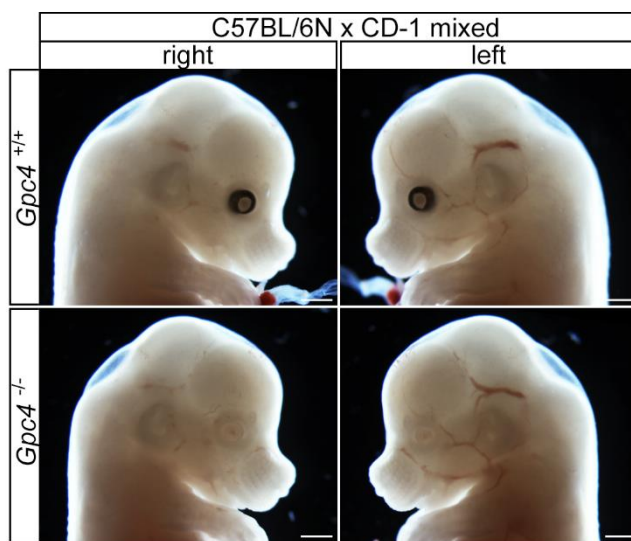


Figure 21 *Gpc4*^{-/-} phenotype expressivity is dependent on the genetic background. E14.5 *Gpc4*^{-/-} mice with a mixed C57BL/6N x CD-1 genetic background showed only mild misdevelopment by loss of pigmentation of the eyes. Scale bar: 1mm.

1.7 Impaired neural differentiation in the cortex of *Gpc4*^{-/-} embryos

Gpc4^{-/-} embryos on a pure C57BL/6 background showed severe defects in the lateral ventricles. To investigate the underlying mechanisms, E12.5 brain sections were analyzed for the proliferation rate of neural precursor cells (Fig 22 a)). In the anterior forebrain of control mice, a high amount of proliferation in the dorsal neural precursor cells of the lateral ventricles is observed by staining against phospho-Histone 3 (PHH3), whereas less expression is observed in the ventral parts of the ventricles. Although the illustrated *Gpc4*^{-/-} mouse showed a semilobar HPE phenotype with only one anterior ventricle, a similar proliferation rate in neural precursor cells was observed as in control animals. Furthermore, the neural precursor population and neural differentiation was analyzed by stainings against PAX6 and B3 TUBULIN (Fig 22 b)). Normal PAX6 expression was observed in the midline of the illustrated *Gpc4*^{-/-} mouse. In contrast, PAX6 expression was strongly decreased in the developing cortices. Consistently, the layer of B3 TUBULIN neurons was thinner compared to the control.

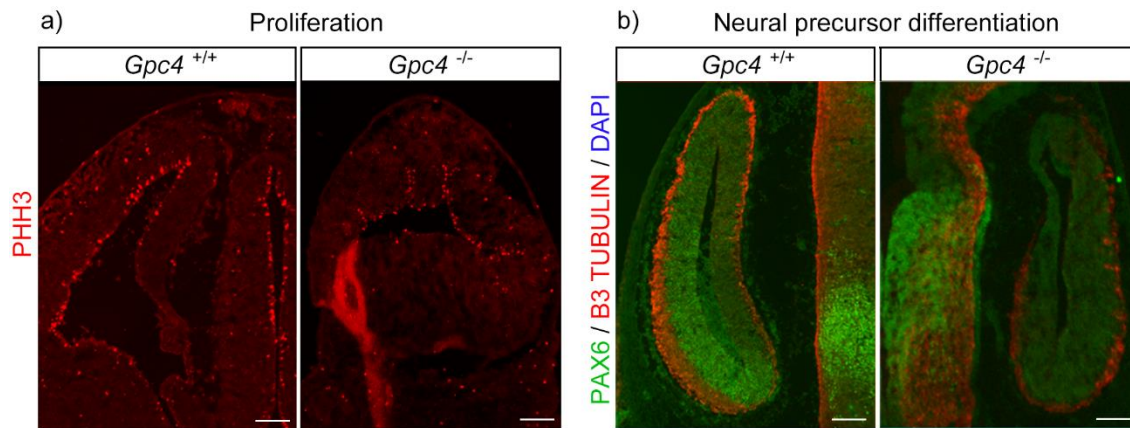


Figure 22 *Gpc4*^{-/-} mice show impaired neural differentiation in lateral ventricles. a) Similar proliferation rate by PHH positive cells in the single ventricle of *Gpc4*^{-/-} mice compared to control mice at E12.5. b) Strongly decreased expression of neural precursor marker PAX6 in the lateral ventricle of *Gpc4*^{-/-} mice with a HPE phenotype. Also the B3 TUBULIN positive cell layer was thinner. PAX6 expression in the midline was normal. Scale bar: 100 μm.

Taken together, these results indicate that *Gpc4* most likely does not control proliferation in the anterior forebrain of neural precursor cells at E12.5. However, impaired neural differentiation, specifically in the lateral ventricles, might be one of the reasons leading to the strong defects in the anterior forebrain of *Gpc4*^{-/-} embryos.

1.8 Wnt and Hh are misregulated candidate pathways in *Gpc4*^{-/-} embryos

Gpc4^{-/-} embryos showed severe defects in the separation of the brain midline into the left and right hemisphere. The separation of the midline is an early process during development. To identify the underlying misregulated signaling pathways leading to abnormal midline separation in *Gpc4*^{-/-} embryos, genome-wide mRNA expression analysis of early embryos was performed. Therefore, heads of E9.5 embryos and littermate controls were dissected and analyzed on microarray chips. Already at this stage, abnormal forebrain development was observed in analyzed animals (Fig 23 a)). By the application of strict parameters (> 1.3 fold expression change, $p < 0.01$, average expression > 10), 308 genes were significantly downregulated in *Gpc4*^{-/-} embryos compared to controls. 39 genes were downregulated stronger than 1.8 fold (Fig 23 b)). As expected, *Gpc4* mRNA was one of the top downregulated genes and therefore served as an internal control for the quality of the array. Importantly, no other *Gpc* family member was significantly up- or downregulated, indicating no compensation by *Gpcs* on the mRNA level. Most of the identified annotated genes are involved in forebrain and eye development, including *Aldh1a3*, *Lhx2*, *Dlk1*, *Six6*, *Emx2*, *Foxg1*, *Alx1* and *Rax*. The mRNA expression levels of the genes *Aldh1a3*, *Alx3*, *Lhx2*, *Dlk1*, *Six6*, *Alx1* and *Wnt7* were verified by qPCR (marked in bold in Fig 23b)). All tested genes were confirmed to be strongly downregulated in *Gpc4*^{-/-} embryos (Fig 23 c)).

II. Results

To identify misregulated signaling pathways, the data set of 308 downregulated genes was analyzed by the INGENUITY software. The underlying algorithm compares the dataset of misregulated genes to canonical pathways which are defined by a specific set of genes. If genes which define a pathway show significantly altered regulation, pathways are evaluated as significantly misregulated. Within the top five misregulated pathways, three pathways were members of the canonical and non-canonical Wnt signaling: Wnt/GSK- β Signaling ($p = 1.91 \times 10^{-3}$), Wnt/ β -catenin Signaling ($p = 2.57 \times 10^{-3}$) and Wnt/Ca $^{+}$ Signaling ($p = 1.09 \times 10^{-2}$). Additionally, the HIPPO Signaling pathway ($p = 5.13 \times 10^{-3}$) and Methylglyoxal Degradation VI ($p = 8.31 \times 10^{-3}$) were strongly misregulated.

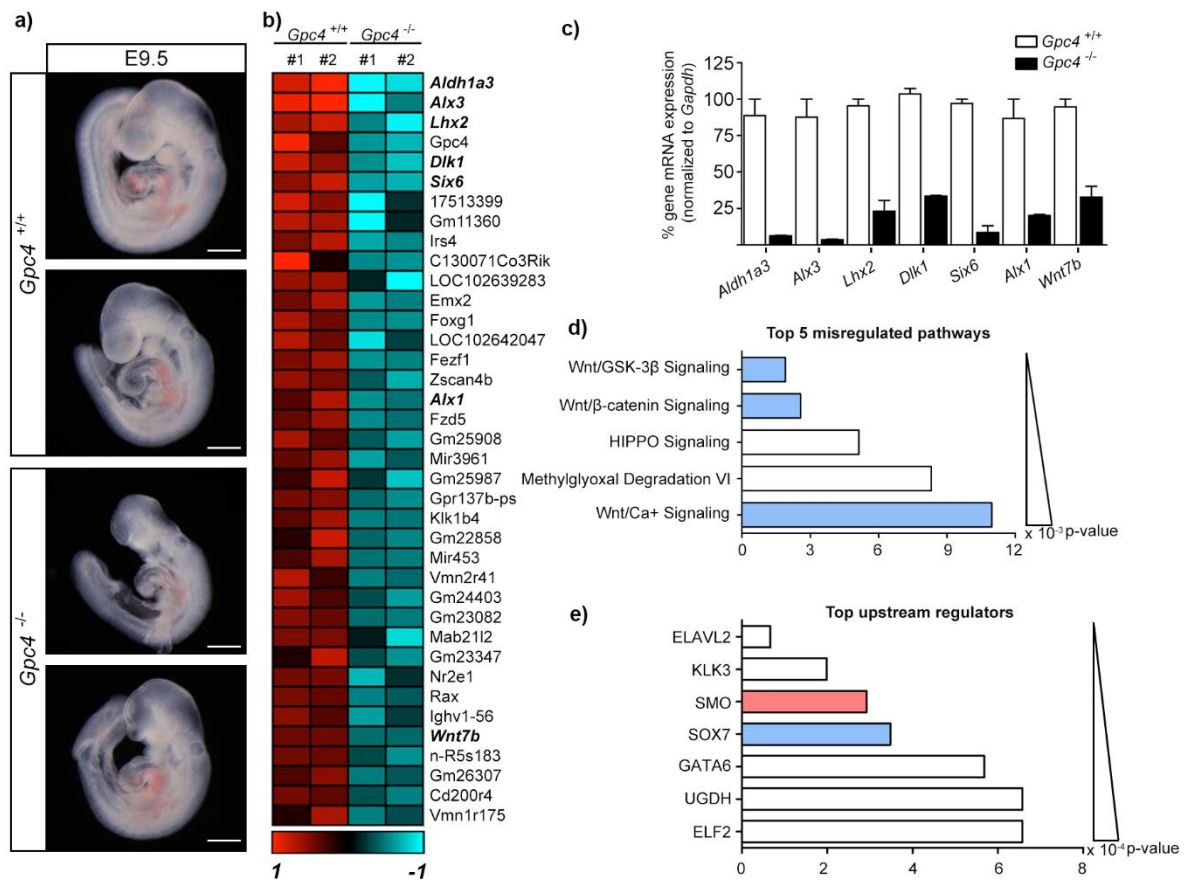


Figure 23 Wnt and Hh are misregulated candidate pathways in *Gpc4*^{-/-} embryos. a) mRNA expression of E9.5 heads of wildtype and *Gpc4*^{-/-} embryos were analyzed on microarray chips. *Gpc4*^{-/-} embryos showed strong forebrain defects. b) Top downregulated genes in *Gpc4*^{-/-} embryos genes are involved in forebrain and eye development. c) Verification of downregulated genes by qPCR analysis. d) INGENUITY analysis of Top 5 misregulated signaling pathways identified three Wnt signaling pathways (blue) additionally to HIPPO signaling and Methylglyoxal Degradation VI. e) Ingenuity analysis for misregulated upstream regulators identified members of the Hh signaling pathway (SMO, red) and of the Wnt signaling (SOX7, blue). Scale bar: 500 μ m. qPCR error bars indicate minimum and maximum of two biological replicates.

Furthermore, the top upstream regulators were analyzed by INGENUITY. This method identifies upstream regulators whose downstream targets were significantly regulated in the dataset. The

regulators themselves show no altered expression. The regulators with the most significantly regulated targets were ELAVL2 ($p = 6.00 \times 10^{-5}$) and KLK3 ($p = 1.90 \times 10^{-4}$). Furthermore, targets of the Hh signaling pathway member Smoothened (SMO, $p = 2.92 \times 10^{-4}$) and the Wnt signaling member Sox7 ($p = 3.48 \times 10^{-4}$) were significantly misregulated in addition to GATA6 ($p = 5.68 \times 10^{-4}$), UGHD ($p = 6.57 \times 10^{-4}$) and ELF2 ($p = 6.57 \times 10^{-4}$; Fig 23 e)).

In summary, microarray analysis of E9.5 embryo heads identified the Wnt and the Hh signaling pathways as potentially misregulated pathways in *Gpc4*^{-/-} mouse embryos.

1.9 *Gpc4* does not act as an anterior Wnt signaling repressor

The anterior repression of Wnt signaling is a requirement for the development of the anterior brain. Several repressors of Wnt signaling have been identified in the past, including *Dkk1* and *Six3*. Upon loss of those repressors, the posterior domain of the diencephalon expands to the anterior head due to the disinhibited spread of Wnt ligands like *Wnt1* (Fig 24 b) (Lagutin et al., 2003). Consequently, no forebrain is developed upon loss-of-function of these inhibitors.

We identified Wnt signaling in the microarray analysis as a potential misregulated signaling pathway in *Gpc4*^{-/-} embryos. *Gpc4* has been shown before to modulate canonical and non-canonical Wnt signaling *in vitro* and in *Xenopus* (Ohkawara et al., 2003; Sakane et al., 2012). To test if *Gpc4* might act as a negative regulator of Wnt signaling in the anterior mouse brain, I performed *in situ* analysis for the diencephalic marker *Wnt1* in E9.5 embryos (Fig 24 a)). *Wnt1* showed strong expression at the mid-hindbrain boundary and in the diencephalon of *Gpc4*^{-/-} embryos and littermate controls. One depicted embryo showed incomplete neural tube closure in the mid-hindbrain area, another one had an abnormally developed anterior head. Hence, both shown animals were considered to be severely misdeveloped at an early brain development stage. However, none of the analyzed *Gpc4*^{-/-} embryos showed an anterior expansion of the diencephalic *Wnt1* domain.

These data suggest that *Gpc4* does not act as an anterior repressor of Wnt signaling during mouse brain development.

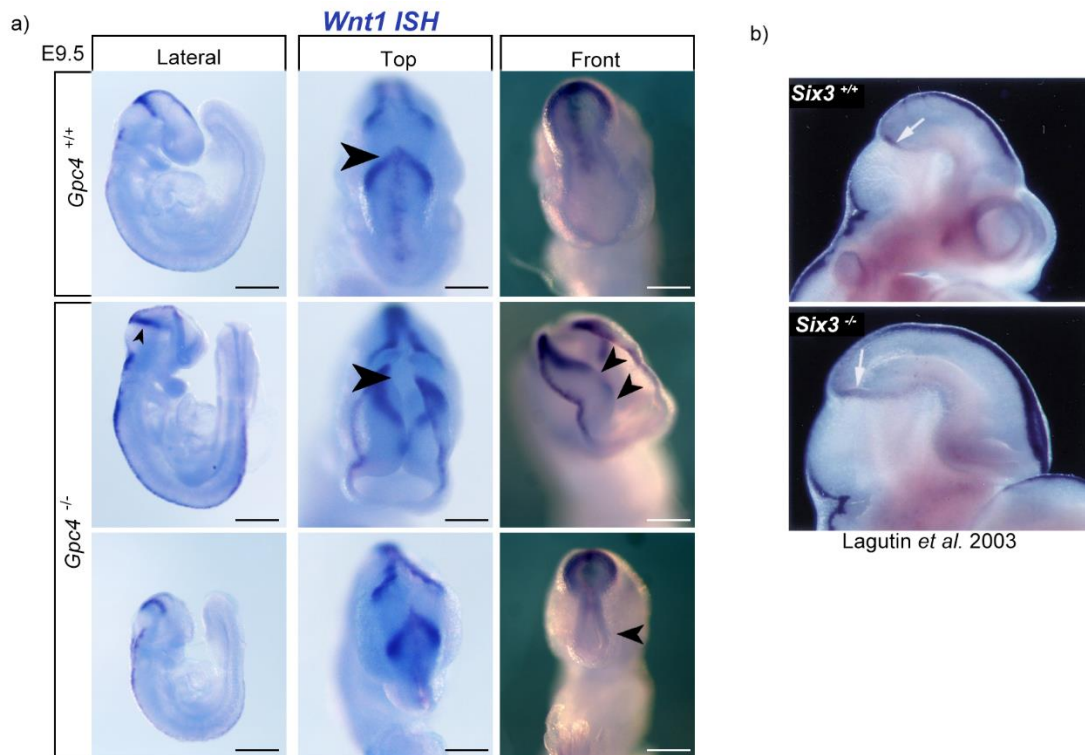


Figure 24 *Gpc4* does not act as an anterior repressor of Wnt signaling. a) *In situ* hybridization against *Wnt1* in E9.5 embryos showed a strong expression in the mid-hindbrain boundary and in the diencephalon. Although *Gpc4*^{-/-} embryos showed neural tube closure defects (arrow) and anterior head misdevelopment, no anterior extension of the diencephalic *Wnt1* domain was detected. Scale bar lateral: 500 μ m; Top and Front: 250 μ m. b) In contrast, the loss of the Wnt repressor *Six3* leads to a strong anterior expansion of the *Wnt1* domain and no induction of forebrain development. Adapted from Lagutin et al., 2003.

1.10 *Gpc4*^{-/-} embryos show loss of anterior SHH domains

The upstream regulator analysis of the microarray data discovered a misregulation of downstream targets of Smoothed (SMO), a direct member of the Hh signaling pathway. Loss-of-function mutations in Hh signaling members are the main genetic cause for human HPE, leading to craniofacial defects, cyclopia and to misdeveloped anterior forebrains. Furthermore, it has been shown before that the *Drosophila dlp* is an important positive regulator of Hh signaling *in vivo* (Desbordes & Sanson, 2003; Gallet et al., 2008; Yan et al., 2010). Additionally, I observed hallmark defects of Hh signaling pathway members including cyclopia and HPE (Chiang et al., 1996) in *Gpc4*^{-/-} mouse embryos. Therefore, I analyzed potentially misregulated Hh signaling in *Gpc4*^{-/-} embryos.

To visualize Hh activity in mice, whole E10.5 embryos were stained against SHH (Fig 25 a)). The expression pattern of SHH in the spinal cord, hindbrain and the ventral midbrain was not changed in *Gpc4*^{-/-} embryos. However, within the misdeveloped anterior forebrain, a diffused expression of SHH in the medial ganglionic eminence domain (MGE) was observed. Furthermore, the specific SHH domain

II. Results

anterior entopeduncular area (AEP, arrow) was absent in truncated forebrains (Fig 25 a)). Interestingly, mice lacking the *Megalin* gene, a positive modulator of Hh signaling on receiving cells, also show a specific loss of the AEP domain in the anterior forebrain (Fig 25 b)) (Spoelgen et al., 2005).

Taken together, these data suggest that at least part of the phenotypic spectrum observed in *Gpc4*^{-/-} embryos might be mediated by impaired Hh signaling in the anterior forebrain.

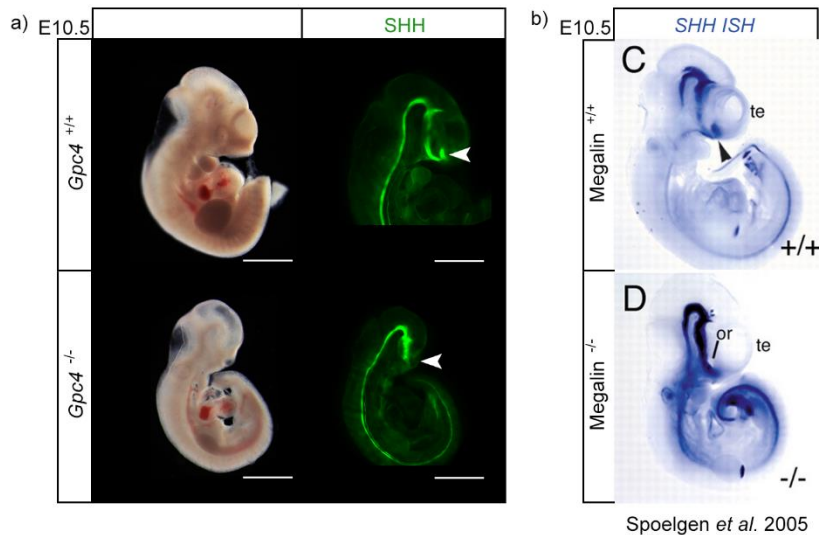


Figure 25 *Gpc4*^{-/-} embryos lack forebrain SHH domains. a) Loss of anterior SHH domain AEP (anterior entopeduncular area) in E10.5 *Gpc4*^{-/-} embryos. Shown are maximum projections of z-stacks. b) The AEP domain is specifically lost in *Megalin*^{-/-} embryos, a positive modulator of Hh signaling on receiving cells. Adapted from Spoelgen et al., 2005. Scale bar: 1 mm.

One approach to visualize Hh pathway activity *in vivo* is by the use of reporter mouse lines. A commonly used reporter mouse line is the *Tg(GBS-GFP)* line, created on the FVB/N genetic background, which carries eight concatemered binding sites for the Hh pathway downstream target *Gli*. Upon stimulation of the pathway, activated *Gli* transcription factors bind to their *Gli* binding motifs and thereby activate the expression of a GFP cassette (Balaskas et al., 2012). This *Tg(GBS-GFP)* line shows first *Gli* reporter activity within the ventral neural tube at the 3 – 4 somite stage (E8.0) and peaks at about the 16 somite stage (E8.7) slightly after the *Ptc* expression peak (Balaskas et al., 2012). The ventral expression pattern of this reporter mouse was confirmed in E8.5 and E9.5 embryos carrying one *GBS-GFP* allele. Next, this line was crossed to *Gpc4*^{-/-} mice, resulting in a mixed genetic background of FVB/N x C57BL/6N of the embryos which were analyzed at E8.5 and E9.5. Although the *GBS-GFP* allele was detected by genotyping, no GFP signal was observed in the obtained embryos. Importantly, this effect was independent of the *Gpc4* genotype. To analyze a potential weak GFP expression, coronal sections of *Gpc4*^{wt/y}; *GBS-GFP*^{wt/+} embryos were stained against GFP but did also not show any signal.

Furthermore, an influence of the *GBS-GFP* donor sex was investigated. Independent of the inheritance of a male or female allele, GFP expression was detected in the original *Tg(GBS-GFP)* line but not in embryos of the FVB/N x C57BL/6N genetic background. Hence, the genetic background seems to play an important role in the expression of the *Gli*-activation-driven GFP signal.

1.11 Hh signaling activity is impaired upon loss of *Gpc4* *in vitro*

To investigate the role of *Gpc4* in mammalian Hh signaling in more detail, a functional assay for Hh signaling was established *in vitro*. The gold standard to analyze cell signaling pathway activity in cells is the luciferase assay system. In regards of Hh signaling, eight repeats of *Gli* binding motifs are followed by a firefly luciferase cassette. Similar to the *Tg(GBS-GFP)* reporter mouse, activated *Gli* transcription factors bind to their *Gli* binding motifs and activate quantitatively the expression of the firefly luciferase. This signal can be measured with high sensitivity and a broad signal range with a lumino photometer. To analyze the role of *Gpc4* on Hh function *in vitro*, mouse embryonic fibroblasts (MEFs) were used which carry a stable inserted *Gli*-inducible firefly-luciferase element and a constitutively active renilla luciferase as a reference signal (LIGHT-II MEFs) (Taipale et al., 2000).

MEFs express high levels of *GPC4*. To downregulate *Gpc4* levels, cells were either transduced with 5 μ l per 96-well shRNA targeting *Gpc4* or with scrambled control shRNA. After serum starvation, Hh signaling was induced by recombinant SHH (rec. SHH) or vehicle. Alternatively, MEFs were stimulated by conditioned cell culture medium from SHH-overexpressing HEK293 cells. After 48 h stimulation, Hh activity was measured by the quantification of the *Gli*-driven luciferase signal. *Gpc4*-downregulated MEFs showed significantly reduced activation levels to 66 % after stimulation with rec. SHH compared to control transfected cells (Fig 26 a)). The activation with conditioned medium confirmed this result by a downregulation to 65% compared to control transfected cells (Fig 26 b)). Non-stimulated cells showed no alterations in Hh signaling, independent of the *Gpc4* expression levels.

To confirm that the observed effect was specific to downregulated *Gpc4*, the shRNA viral particles were titrated between 0.5, 2.5, 5 and 10 μ l per 96-well (Fig 26 c) and d)). The reduction of *Gpc4* mRNA to 29 % by 2.5 μ l virus was sufficient to decrease Hh signaling response to 68 %. Further downregulation to 11 % by 5 μ l virus, which was used as the standard condition, did not lead to a further decrease of Hh signaling response (66 %). Knockdown efficiency reached a plateau of 9 % knockdown even with 10 μ l virus. Interestingly, the reduction of *Gpc4* expression to 56 % by 0.5 μ l virus was not sufficient to decrease Hh signaling response. Therefore, the observed decrease of Hh signaling was considered as specific to the downregulation of *Gpc4*.

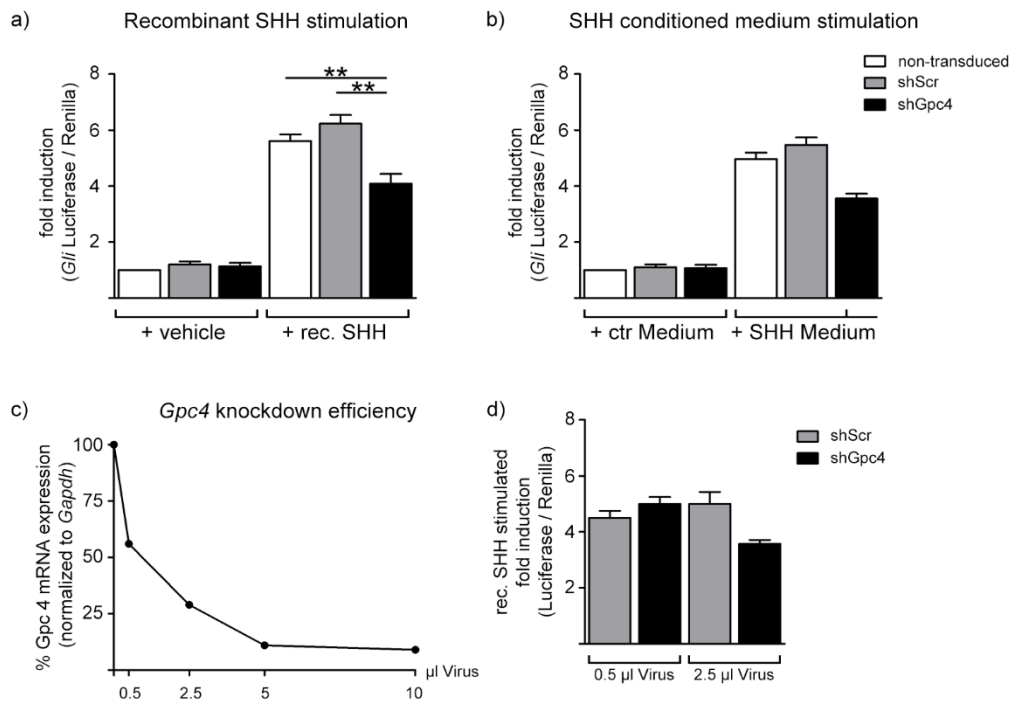


Figure 26 Hh signaling is impaired upon loss of *Gpc4* *in vitro*. a) Significant decrease of rec. SHH stimulation by *Gpc4* knockdown (non-transduced 5.60 fold \pm 0.23 vs. shGpc4 4.08 \pm 0.34, $p = 0.0067$ and shScr 6.22 fold \pm 0.31 vs. shGpc4 4.08 \pm 0.34, $p = 0.0018$; $n = 5$). No changes of non-stimulated Hh signaling (shScr 1.20 \pm 0.10 vs *Gpc4* 1.14 \pm 0.11, $p = 0.71$; $n = 5$). b) Strong decrease of conditioned SHH medium stimulation upon *Gpc4* knockdown (non-transduced 4.96 fold \pm 0.23 vs. shGpc4 3.55 \pm 0.17, $p = 0.10$ and shScr 5.47 \pm 0.26 vs. shGpc4 3.55 \pm 0.17, $p = 0.10$; $n = 3$). No changes of non-stimulated Hh signaling. c) and d) Decreased Hh signaling activity is dependent on *Gpc4* knockdown efficiency. 0.5 μ l shGpc4 virus led to a decrease of 57 % *Gpc4* mRNA which was insufficient to decrease Hh signaling activity (shScr 4.50 fold \pm 0.25 vs. shGpc4 5.00 \pm 0.25; $n = 3$). 2.5 μ l shGpc4 virus decreased *Gpc4* mRNA expression to 27 % which was sufficient to decrease Hh signaling activity (shScr 5.00 \pm 0.42 vs. shGpc4 3.57 \pm 0.14; $n = 3$). Further downregulation of *Gpc4* mRNA to 11 % and 9 % by 5 μ l and 10 μ l virus respectively did not further decrease Hh signaling activity.

To analyze at which level of the Hh signaling pathway *Gpc4* acts as a positive regulator, cells were stimulated with purmorphamine. This small molecule strongly activates the Hh pathway by directly targeting the downstream member *Smo* also in the absence of the upstream receptor *Ptc* (Sinha & Chen, 2006). Upon stimulation with purmorphamine, Hh signaling activity was decreased by *Gpc4* knockdown to 77 % (shScr 16.0 fold \pm 3.0 vs. shGpc4 12.43 fold \pm 2.9, Fig 27). These data suggest that *Gpc4* modulates *Smo* as a positive modulator of Hh signaling. However, no interaction between GPC4 and SMO has been reported so far. Furthermore, it is not clear whether purmorphamine acts exclusively by targeting *Smo* when *Ptc* is present (Sinha & Chen, 2006). Because PTC was present in the current system, it might have been the case that purmorphamine additionally acted on PTC to activate

II. Results

Hh signaling. Considering this, the reported results might not be sufficient to show exclusivity of *Gpc4* to SMO.

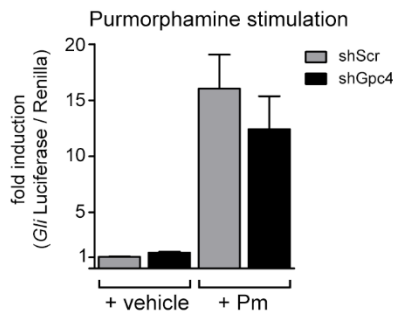


Figure 27 Impaired Hh activity upon *Gpc4* knockdown also by purmorphamine stimulation. After Pm stimulation: shScr 16.04 fold ± 3.03 vs. shGpc4 12.43 fold ± 2.92; n = 2. Error bars indicate minimum and maximum of two biological replicates. Pm: Purmorphamine.

Next, it was tested if Hh signaling activity was enhanced by the overexpression of wildtype (wt) or a mutated form of *Gpc4* lacking GAG chains (*Gpc4* ΔGAG) (Fig 28). Furthermore it was tested, if decreased Hh signaling upon *Gpc4* knockdown was rescued by overexpression of GPC4. Therefore, MEFs were first transduced with shScr or shGpc4 for 24 hours. The next day, wt or *Gpc4* ΔGAG was overexpressed by transduction. Both plasmids carried a hemagglutinin-Tag (HA-Tag) at the N-terminus of the *Gpc4* sequence and were not targeted by the shRNA sequence. Although *Gpc4* mRNA was strongly overexpressed (2.5 fold over wt), no enhancement of Hh signaling was observed in non-transduced and shScr transduced cells (Fig 28). Furthermore, no rescue of Hh signaling was detected in shGpc4 transduced cells. To exclude possible effects of the N-terminal HA-Tag, the experiment was additionally performed with wt *Gpc4* lacking the tag. Despite the mRNA overexpression, no increase or rescue was detected. Also the overexpression of *Gpc4* by transfection did not increase or restore Hh signaling.

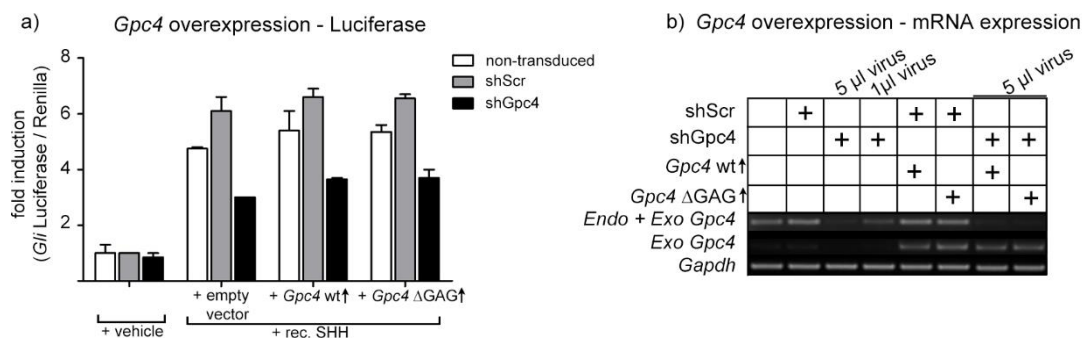


Figure 28 Overexpression of *Gpc4* did not rescue Hh signaling activity. a) Impaired Hh signaling activity upon knockdown of *Gpc4* was not rescued by overexpression of wt or *Gpc4* ΔGAG. Overexpression in non-transduced and shScr transduced cells did not increase Hh signaling activity (SHH stimulated: shGpc4 empty vector: 3.0 fold ± 0 vs. shGpc4+*Gpc4*wt: 3.65 fold ± 0.05 vs. shGpc4+*Gpc4*ΔGAG: 3.7 fold ± 0.3; n = 2).

b) ShGpc4 led to a concentration dependent knockdown of endogenous *Gpc4* mRNA. Overexpression of wt and *Gpc4* ΔGAG increased mRNA expression by 2.5 fold. Error bars indicate minimum and maximum of two biological replicates.

Taken together, these data support the role of *Gpc4* as a positive regulator of Hh signaling activity. The specific Hh pathway interaction partner of *Gpc4* was not specifically determined due to a potential direct activity of purmorphamine on PTC. Further enhancement of Hh signaling and a rescue by *Gpc4* overexpression were not detected, potentially due to a too strong overexpression of *Gpc4*. A similar biphasic mode of action has been observed in *Ihog*, a Hh modulator in *Drosophila* (Yan et al., 2010). Thereby, too strong and too little expression of *Ihog* reduced Hh signaling. The obtained results of my experiments might be explained by a similar biphasic mechanism of *Gpc4* in Hh signaling.

1.12 Co-expression of *GPC4* with *BOC* in the human developing cortex

In *Drosophila*, it has been shown that *dlp* acts as a positive regulator of Hh signaling at receiving cells (Desbordes & Sanson, 2003). Furthermore, *dlp* can bind to both, PTC and HH, supporting the hypothesis that *dlp* might act at the level of PTC (Yan et al., 2010). To identify potential interaction partners of *GPC4*, a data driven approach was chosen by single cell RNAseq analysis of the developing human cortex. *GPC4* has been identified as one of the most expressed ECM members in the developing human cortex and in cerebral organoids (Camp et al., 2015). A detailed analysis of this dataset confirmed the *Gpc4* mRNA expression pattern of the mouse in the human brain (Fig 29).

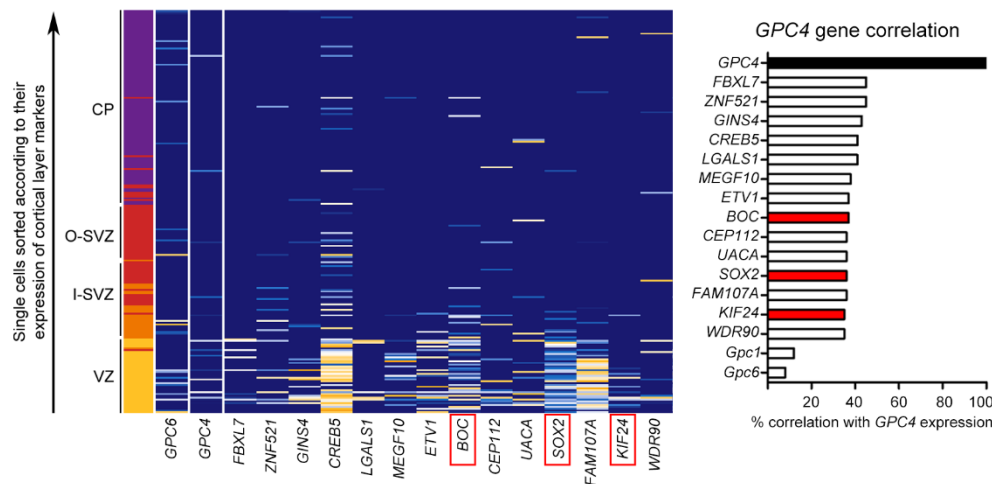


Figure 29 *BOC* mRNA expression correlates with *GPC4* in the human developing cortex. *GPC4* is strongly expressed in the VZ, whereas *GPC6* is additionally expressed in other cortical zones of the human cerebral cortex at gestational week 12. Within the top correlating genes, *BOC* (37 %), *SOX2* (36 %) and *KIF24* (35 %) has been identified. *GPC1* (12 %) and *GPC6* (8 %) were only weakly co-expressed with *GPC4*. VZ: ventricular zone, I-SVZ: inner sub ventricular zone, O-SVZ: outer sub ventricular zone, CP: cortical plate. Data analysis was performed by Dr. Camp (Camp et al., 2015).

Strong *GPC4* expression was observed in apical precursor cells of the ventricular zone. In contrast, although *GPC6* was also mostly expressed in the ventricular zone, its expression was more scattered

to other cortical layers. However, neither *GPC4* nor *GPC6* were expressed in a specific subpopulation of apical precursor cells.

To identify potential binding partners of *GPC4*, correlation analysis was performed to identify genes which showed the same expression pattern as *GPC4*. Among the top co-expressed genes was *Sox2* (36 %), a neural precursor marker and *KIF24* (35 %), which is involved in ciliogenesis. Within the family of *Gpcs*, *GPC1* (12 %) was the strongest correlating *Gpc* family member followed by *GPC6* (8 %). However, compared to the top regulated genes, the correlation was very low. Interestingly, one of the top correlating genes was *BOC* (37 %), which is a known positive modulator of Hh signaling by acting as a co-receptor to *Ptc* (Izzi et al., 2011). Due to the co-expression of *GPC4* and *BOC* in the same cells, which surround the lateral ventricles, both proteins might interact to regulate Hh signaling.

1.13 Cleavage resistant GPC4 can be expressed in primary cilia *in vitro*

The main site of Hh signaling is the primary cilium. Consequently, a ciliar localization of a protein is thought to be required for acting as a positive modulator of Hh signaling on receiving cells (M. Capurro et al., 2015). Because *Gpc4* might act as a positive regulator of Hh signaling, I tested if *GPC4* is located in this organelle. Endogenous *GPC4* in MEFs is efficiently cleaved by furin-like proteases, which results in a high abundance of the 37 kDa N-terminal fragment. To visualize endogenous levels of *GPC4* by immunofluorescence stainings on cells, different antibodies which were tested on tissue sections and in western blot analysis before were also tested in cultured cells. Like on tissue sections, none of the tested antibodies and conditions gave a clear and specific signal including the non-commercial antibody which was specific in western blot analysis. In contrast, overexpressed HA-tagged *GPC4* (HA-*GPC4*) stained by an antibody against the HA-Tag gave a strong signal which was absent in empty vector transfected cells. Therefore, overexpressed *GPC4* was analyzed for potential cilia localization instead of endogenous forms of the protein. To avoid a loss of the HA-Tag by furin-like cleavage of the N-Terminus, the protease cleavage consensus sequence R³⁵¹ISR³⁵⁴ was mutated to a cleavage resistant 351-AISA form (termed HA-*GPC4* in Fig 30 a)). This mutant form of *Gpc4* was overexpressed by transduction in LIGHT-II MEFs which were subsequently serum starved for three nights to induce primary cilia formation (Fig 30 a)). HA-*GPC4* was broadly expressed on MEFs and did not show a specific expression pattern on the cell surface. Interestingly, the overexpressed HA-*GPC4* was also localized in a proportion of primary cilia, marked by *ARL13B* expression (Fig 30 b)). Most *GPC4*-positive cilia showed expression in the axoneme, in rare cases *GPC4* was additionally expressed in the basal body. Quantification of *GPC4* expression revealed that in 23.3 % of the investigated cilia expressed *GPC4* (Fig 30 b)).

In summary, these data show that *GPC4* can be located to the primary cilium *in vitro*.

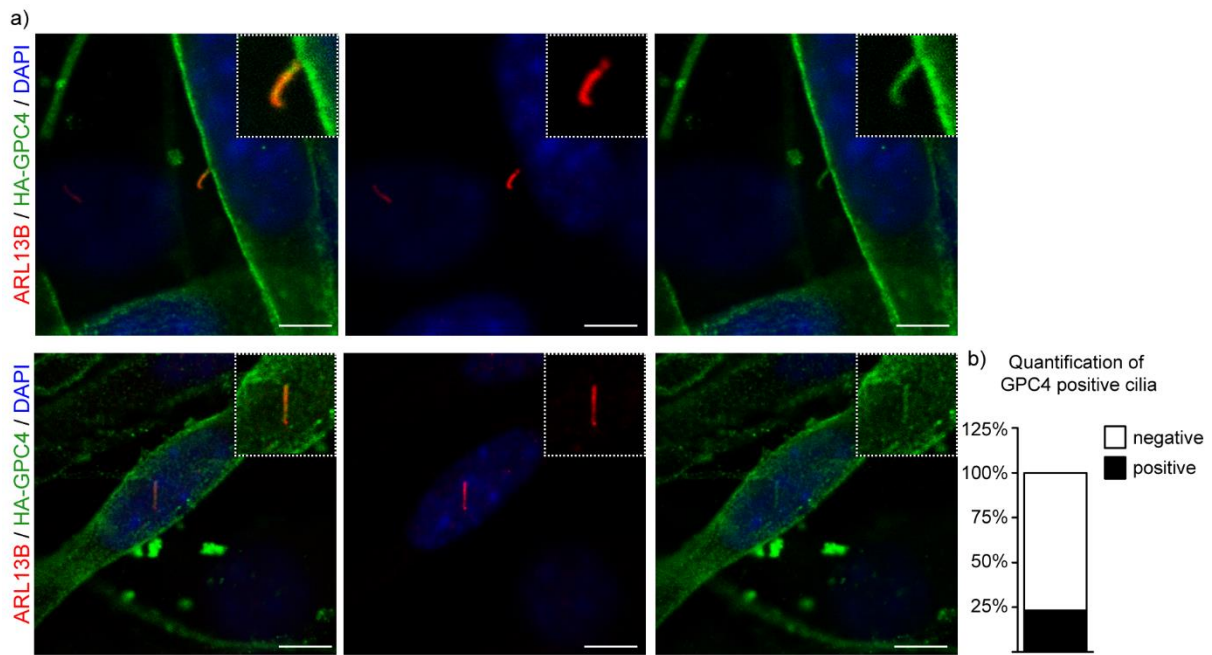


Figure 30 Cleavage resistant HA-GPC4 can be expressed in primary cilia. a) Two examples of fluorescence staining against the HA-Tag of GPC4 (green) and the primary cilium marker ARL13B (red). Nuclei are stained by DAPI (blue). b) Quantification of GPC4 expression in primary cilia: 23.3 % of the primary cilia expressed GPC4. n = 31.

1.14 *Gpc4*^{-/-} embryos develop primary cilia in the node

Primary cilia play an important role during early mouse embryo development. These organelles first appear in cells of the epiblast around E6.0 and are strongly expressed in cells of the node which is a key signaling center for anterior neural fate induction in embryos (Kinder et al., 2001). Within the node, two types of primary cilia are present. Motile cilia on crown cells are important for the establishment of left-right asymmetry by creating a unidirectional flow of extra-embryonic fluid from the right side. This signal is sensed by sensory primary cilia on pit cells at the left side of the embryo (reviewed in Shiratori and Hamada, 2006). Additionally to left-right signaling, primary cilia are mandatory for Hh signaling (Huangfu et al., 2003). The loss of cilia is associated with severe developmental defects. Hallmarks of ciliopathies are left-right defects including *situs inversus* and a very broad spectrum of phenotype expressivity with reduced penetrance (reviewed in Waters and Beales, 2011). As described in chapter 1.4, no forms of *situs inversus* were found in *Gpc4*^{-/-} embryos. However, a highly variable expressivity and reduced penetrance of the phenotype are strongly pronounced. Additionally, it was shown in the previous chapter that GPC4 was located on a proportion of primary cilia in MEFs *in vitro*. Therefore, the formation of primary cilia in the node of E7.5 *Gpc4*^{-/-} embryos was analyzed. Both embryos developed primary cilia on crown cells in the center region of the node and on pit cells at the periphery (Fig 31). Therefore, no complete absence of primary cilia was detected in *Gpc4*^{-/-} embryos.

However, primary cilia in *Gpc4*^{-/-} were shorter compared to the control embryo. Importantly, the control embryo was a few hours older, indicated by a more developed node structure with a deeper furrow of the axial mesoderm. Therefore, the shortened primary cilia in *Gpc4*^{-/-} might be attributed to a slight but important difference of the developmental stage. In the future, stage-matched embryos should be analyzed to conclude the impact of *Gpc4* on primary cilia formation in the node. Due to a limited penetrance of the phenotype, several embryos should be included in the analysis.

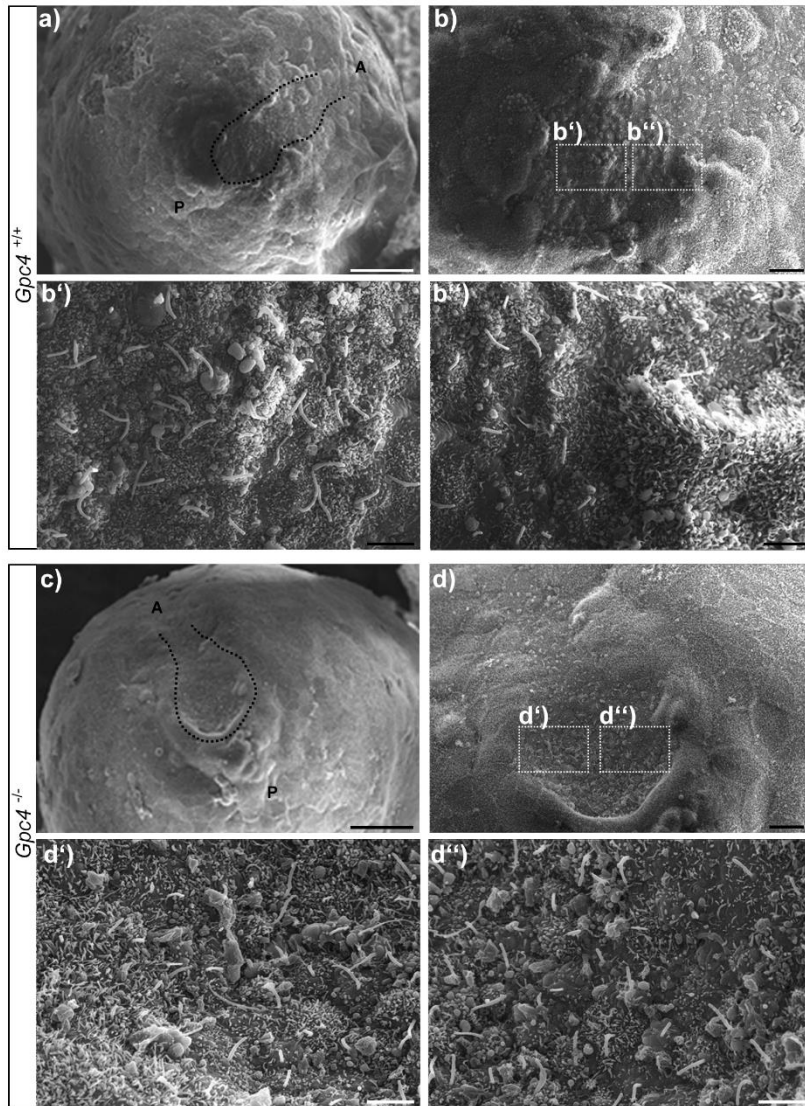


Figure 31 E7.5 *Gpc4*^{-/-} embryos develop primary cilia in the node. Primary cilia in the node of E7.5 control (a – b) appear longer than in *Gpc4*^{-/-} embryos (c – d). However, the control embryo is slightly further developed than the *Gpc4*^{-/-} embryos indicated by a smaller node. A: anterior, P: posterior. Scale bar: a), c): 50 μm; b), d): 10 μm; b'), b''), d'), d''): 3 μm.

2. Analysis of *Gpc4* knockdown mouse embryonic stem cells (shGpc4)

The loss-of-function of *Gpc4* can lead to severe developmental defects in mice. Among the most commonly observed defects are HPE with cyclopia, which are severe separation defects of the midline. However, as described earlier, some *Gpc4*^{-/-} embryos even lacked the complete anterior forebrain (Fig 18 p), q)). Furthermore, some *Gpc4*^{-/-} died before E9.5 indicated by empty deciduae. These results indicated that *Gpc4* might be involved in early neural induction of the forebrain. To model these very early developmental events, *Gpc4* knockdown mESCs lines were created and analyzed during neural differentiation *in vitro*.

2.1 Optimization of a mESC-based neural differentiation protocol

As a first step, the mRNA expression profile of *Gpcs* in MEFs (used for stem cell maintenance), MS5 cells (used for neural differentiation) and feeder-free mESCs themselves were analyzed (in collaboration with Ms Theresa Bäcker, PhD student in our group) (Fig 32 a)). In MEFs, all *Gpcs* except of *Gpc5* were expressed on the mRNA level. Within the family of *Gpcs*, *Gpc4* was the strongest expressed member followed by *Gpc1* and 3. *Gpc2* and 6 were expressed in low amounts. MS5 cells expressed only two *Gpcs* but in high amounts, *Gpc1* and 4. In mESCs, *Gpc4* was strongly expressed, additionally to *Gpc1* and 3. *Gpc2*, 5 and 6 were absent. Taken together, *Gpc4* was strongly expressed in mESCs and all cell types which were used for stem cell maintenance and differentiation.

II. Results

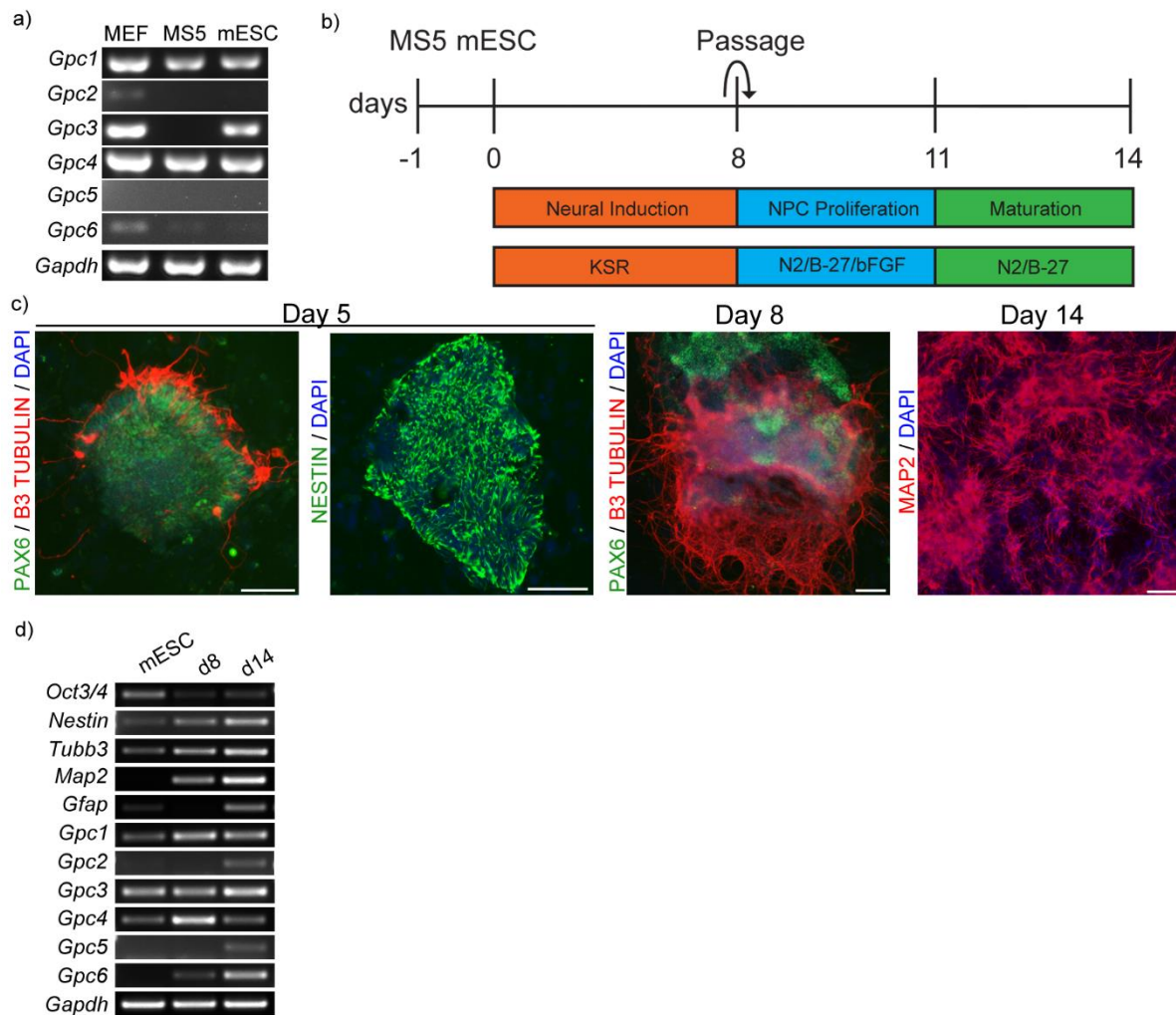


Figure 32 Optimization of a neural differentiation protocol for mESCs. a) mRNA expression analysis of *Gpcs* in mESCs, MEFs and MS5 cells showed strong expression of *Gpc4* in all three cell types. b) Scheme of neural differentiation on MS5 cells c) Efficient neural differentiation to the neural precursor stage (day 5), early neurons (day 8) and mature neurons (day 14). d) mRNA expression of *Gpcs* during neural differentiation. *Gpc4* mRNA was strongly expressed in neural precursor cells. Scale bar: 100 μ m.

Next, a neural differentiation protocol for mESCs was re-established and optimized (Fig 32 b)). Differentiation of mESCs to the neuroectoderm lineage was efficiently induced by removing LIF of the medium and co-culturing mESCs on an irradiated bone marrow stromal cell line (MS5) (Barberi et al. 2003). Other tested methods including the growth as embryoid bodies or low density growth on gelatin coated plates led either to additional non-specific differentiation to meso- and endoderm lineages or to complete cell death after several days. For the used differentiation protocol, mESCs were seeded at a single-cell density on MS5 cells and differentiated first for one week in knockout serum replacement medium (KSR) (Fig 32 b)). After five days, mESCs differentiated efficiently to neural precursor cells (NPCs) indicated by a strong expression of the neural precursor markers PAX6 and NESTIN (Fig 32 c)).

Consistently, neural differentiation did not yet progress to the early neuronal stage. This was indicated by the limited expression of the neural marker B3 TUBULIN to only few cells with short neurites at the edge of neural colonies (Fig 32 c)). Three days later, the neural colonies strongly increased their size and most cells within the colonies differentiated further to early neurons. However, parts of the colonies were still at the neural precursor stage. In the originally published protocol, cells were kept as colonies on MS5 cells for two weeks. However, a high amount of cell death was observed using these conditions presumably due to the massive size of single colonies and therefore limited access to nutrients in the center of colonies. Therefore, differentiating cells were gently dissociated to single cells on day 8 and passaged as a monolayer at high density on plates which were pre-coated with the ECM components poly-ornithin, laminin and fibronectin (Fig 32 c)). Additionally, the medium was changed to the neural medium N2-B27 and supplemented with bFGF to stimulate NPC proliferation. Due to this optimization step, differentiating cells showed strongly reduced levels of cell death compared to the growth in colonies. Furthermore, cells could be analyzed as a monolayer by stainings, which was not possible by reseeding them as high density droplets as this resulted in massive 3D overgrowth. Passaging cells at a lower density to facilitate the analysis of single cells was not possible due to a strong migration to cell clusters. From day 11 to day 14, cells developed further to mature neurons by removal of bFGF, which is indicated by the upregulation of MAP2 expression. Ascorbic acid (AA) and the brain-derived neurotrophic factor (BDNF), which were added in the original protocol, were not required for two weeks differentiations and were therefore only added in long-term differentiations.

The mRNA expression pattern during differentiation of the stem cell marker (*Oct3/4*), the neural precursor marker (*Nestin*), early and mature neural markers (*Tubb3* and *Map2*), the astrocyte marker (*Gfap*) and *Gpcs* are summarized in Fig 32 d). As expected, the expression of *Oct3/4* was strongly downregulated upon neural differentiation. *Nestin*, and *Tubb3* and *Map2* expression was strongly upregulated during the differentiation. Although the *Gfap* mRNA was weakly expressed on day 14, only single cells expressed the GFAP on a protein level. In contrast, additional passaging on day 14 and further differentiation until day 21 strongly enriched the astrocyte population.

During the two weeks of neural differentiation, the *Gpc* family members showed a dynamic mRNA expression pattern. *Gpc2* and *5* were weakly, but specifically expressed in mature neurons. Also *Gpc6* was strongly upregulated on day 14 with additional expression in neural precursor cells. *Gpc3* was strongly expressed at all tested stages. *Gpc1* and *Gpc4* showed similar expression patterns. Their mRNA was upregulated in neural precursor cells and downregulated in mature neurons.

Taken together, the optimized MS5-based co-culture differentiation protocol mimicked *in vivo* neural differentiation of mESC *in vitro*. Stem cells differentiated reliably to the neural precursor stage after

one week and matured to neurons after two weeks. The mRNA expression pattern of *Gpc4* during neural differentiation was highly different to each other. *Gpc4* mRNA was strongly upregulated in neural precursor cells and downregulated again in mature neurons. This expression pattern was in line with my previous results showing strong *Gpc4* mRNA expression in the ventricular and sub ventricular zone in the developing mouse cortex, the main sites of neurogenesis rising from neural precursor cells.

2.2 shGpc4 mESCs show no differences in stem cell marker expression

To investigate the role of *Gpc4* in undifferentiated mESCs and during neural differentiation, *Gpc4* mRNA was downregulated by shRNA. Thereby, mESCs were transduced either by shScr or ShGpc4 and subsequently selected for the expression of shRNA by antibiotics. 18 single clones of the original heterogeneous shGpc4 line were analyzed for their *Gpc4* knockdown efficiency by qPCR and compared to the expression of shScr cells (Fig 33 a)). The knockdown efficiency varied between clones from 79.1 % to 3.3 % compared to the shScr control line. The two clones with the lowest *Gpc4* expression, termed shGpc4 Clone 1 with 3.3 % and shGpc4 Clone 2 with 4.8 % were selected and further analyzed. The *GPC4* knockdown efficiency was verified on the protein level by western blot analysis (Fig 33 b) and c)). In both shGpc4 clones, the normalized GPC4 protein expression of the cleavage product at 37 kDa was almost completely absent (4.0 % and 5.1 % respectively) compared to wildtype and shScr mESCs (100 % and 101.8 % respectively). In contrast to mouse brain lysate and MEFs, mESCs do not show a 70 kDa band by immunoblotting against GPC4. Therefore, both shGpc4 mESC lines were considered to be completely deficient of GPC4 protein.

The established mESC lines were first analyzed at the undifferentiated state. mESCs grew as densely clustered colonies on irradiated MEFs. Interestingly, shGpc4 Clone 1 mESCs established even denser colonies compared to wildtype and shScr controls (Fig 33 d)). This effect was also observed in the second line, but to a lesser extent. These results suggest that loss of *Gpc4* might lead to increased stemness in mESCs and a potentially inhibited differentiation potential.

To analyze this approach in more detail, the mRNA expression levels of stem cell markers in undifferentiated mESCs were analyzed by qPCR. Although *Nanog* and *Oct3/4* mRNA was upregulated in Clone 2 and *Sox2* expression was reduced in both clones, the changes were minor and not significant (Fig 33 e)).

Taken together, although the colonies of the established shGpc4 clones grew in denser colonies, no differences in the mRNA expression levels of stem cell markers were observed.

II. Results

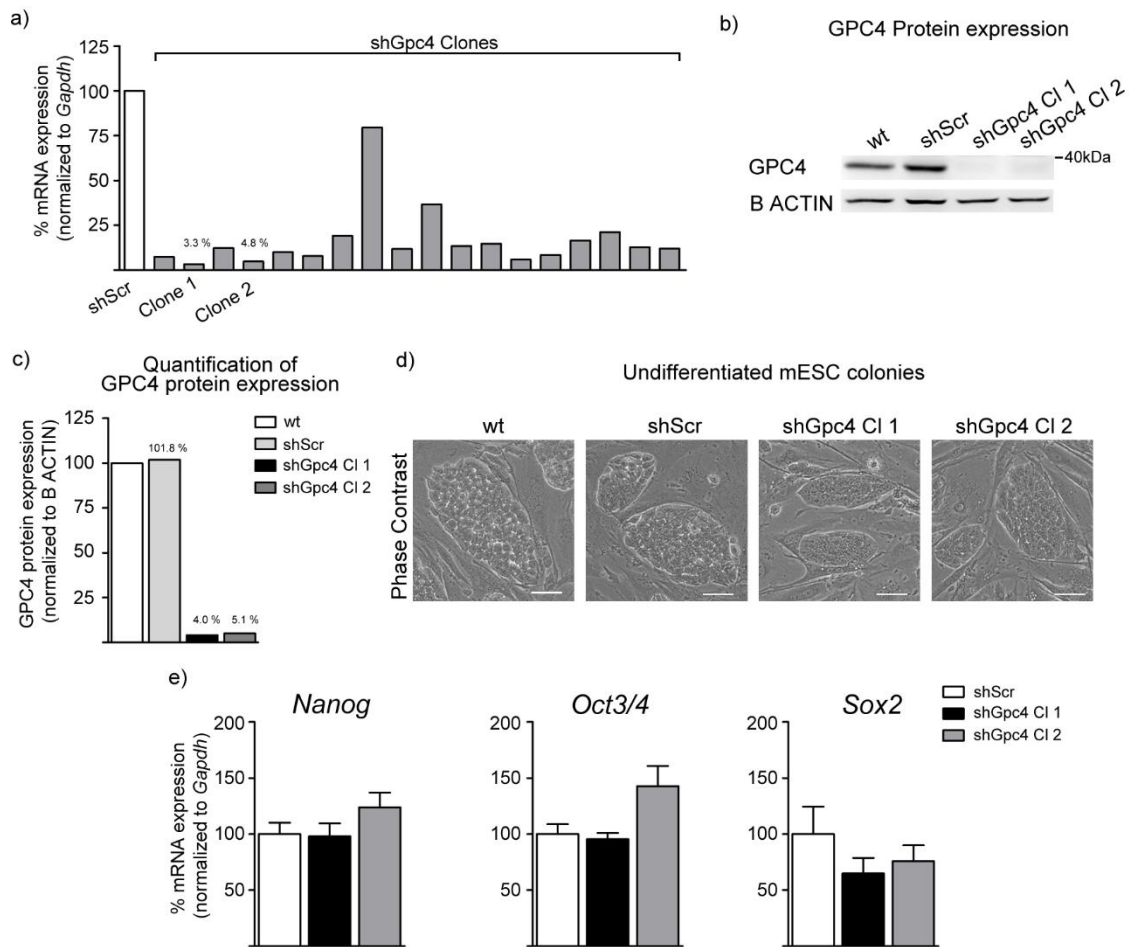


Figure 33 Generation of *Gpc4* knockdown mESCs. a) Out of 18 shGpc4 clones, two were selected and *Gpc4* knockdown was confirmed by WB analysis (b and c). Undifferentiated shGpc4 mESCs grew in denser colonies compared to control cells (d). e) Stem cell markers *Nanog*, *Oct3/4* and *Sox2* were not significantly altered in shGpc4 cells. n = 3. Scale bar: 50 μm.

2.3 shGpc4 mESCs show no differences in proliferation and cell death

To study potential effects of loss of *Gpc4* on proliferation in mESCs, a high-content imaging assay was established to quantify proliferation in mESCs (Fig 34 a)). Feeder-free mESCs were cultured on 96-well imaging plates for 48 hours. Cells were fixed and stained against the proliferation marker PHH3 and nuclei were visualized by DAPI. After image acquisition, single nuclei were defined by DAPI staining. Afterwards, PHH3 positive nuclei were selected by their signal intensity. PHH3 positive nuclei were then normalized to the total number of nuclei. By this method, thousands of cells were analyzed by the same parameters, which allowed the unbiased and highly sensible analysis of proliferation in the different cell lines. Although shGpc4 Clone 1 showed slightly decreased levels of proliferation compared to the control, the difference was not significant (Fig 34 b)).

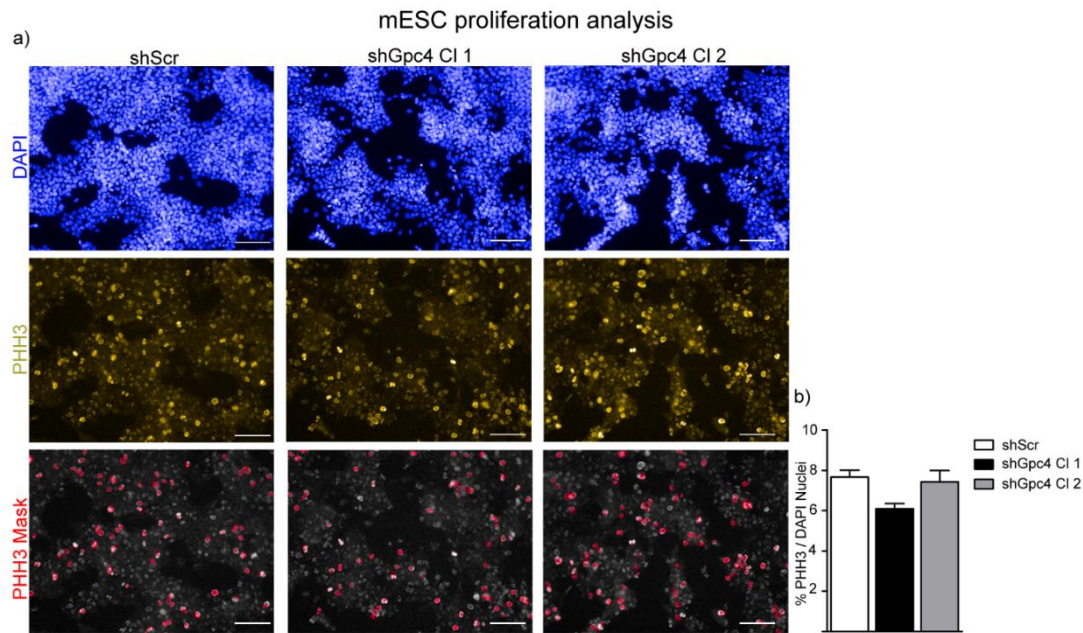


Figure 34 shGpc4 mESCs do not show altered levels of proliferation. a) Establishment of high-content imaging assay to detect PHH3 positive proliferating cells. b) No significant changes in proliferation were detected between shScr and shGpc4 lines. shScr: 7.6 % ± 0.34 % vs. shGpc4 CI 1: 6.1 % ± 0.26 % vs. shGpc4 CI 2 7.4 % ± 0.56 %; n = 3. Scale bar: 100 µm.

Furthermore, cell death was analyzed in mESCs by TdT-mediated dUTP-biotin nick end labeling (TUNEL) fluorescent stainings (Fig 35). On a qualitative level, no differences in cell death was observed between shGpc4 and control cells. Due to the strongly fragmented morphology of dying cells, a reproducible assay to quantify cell death was not possible to establish. Taken together, the loss of function of *Gpc4* did not lead to significant changes of proliferation and cell death in the undifferentiated state.

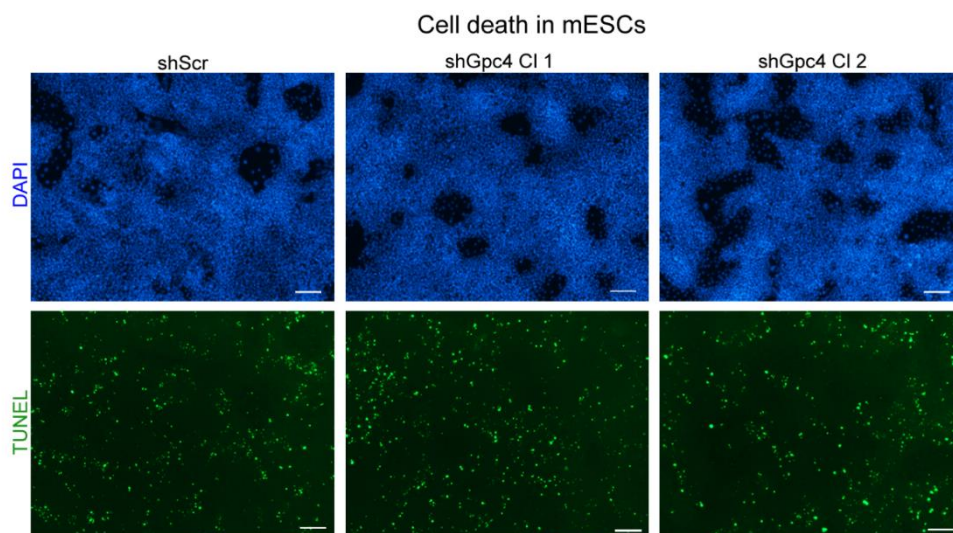


Figure 35 shGpc4 mESCs do not show altered levels of cell death. Similar levels of cell death were observed in shGpc4 lines and the control. Scale bar: 100 µm.

2.4 shGpc4 mESCs show impaired neural differentiation

Next, the role of *Gpc4* during neural differentiation was investigated. Therefore, the two shGpc4 clones and the shScr control were differentiated on MS5 cells for two weeks as described before. After 8 days of differentiation, cells were fixed and stained against B3 TUBULIN and DAPI (Fig 36 a)). shGpc4 cells showed a strong reduction of B3 TUBULIN expression compared to the shScr control. To quantify these results, mRNA expression of *Nestin*, *Tubb3*, *Oct3/4* and *Sox2* was analyzed by qPCR. The impaired neural differentiation in shGpc4 cells was also detected at the mRNA level (Fig 36 b)). Compared to the control, shGpc4 Clone 1 and 2 showed a significant reduction of *Nestin*. Due to a lack of neural precursors, also the neuronal population was strongly reduced, indicated by a decreased *Tubb3* expression respectively. In contrast, the *Oct3/4* expression was strongly increased in sh4*Gpc4* lines compared to the control. The *Sox2* expression, which is not exclusive to undifferentiated stem cells, was not significantly regulated.

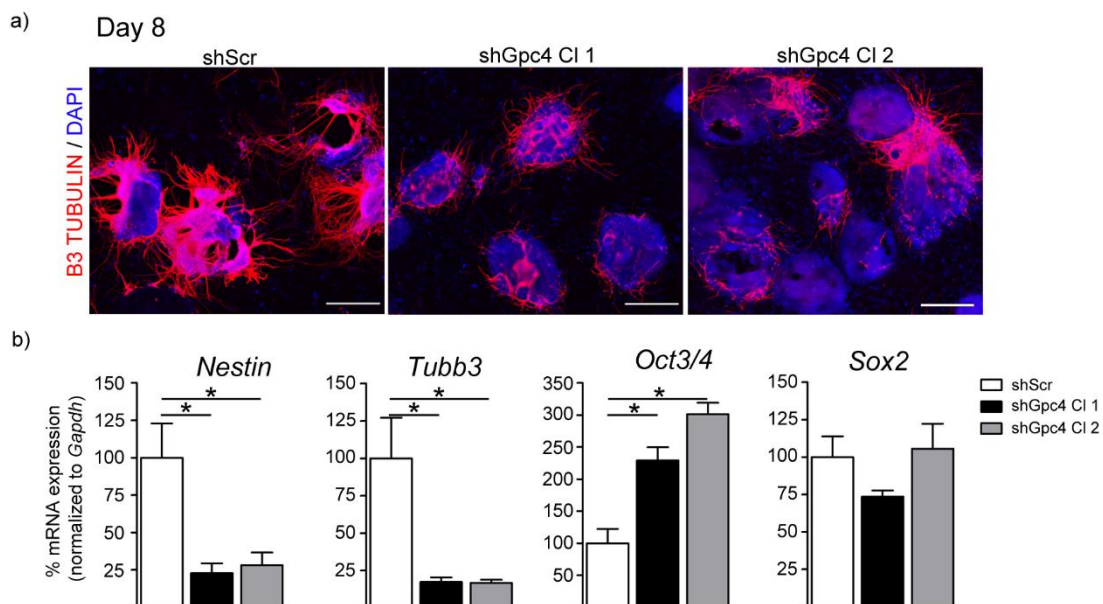


Figure 36 Impaired neural differentiation of shGpc4 cells on day 8. a) Staining against B3 TUBULIN showed impaired neural differentiation in shGpc4 cells. b) Quantification of significant differentiation defects by qPCR expression analysis of *Nestin*, *Tubb3*, *Oct3/4* and *Sox2* expression. *Nestin*: shScr vs. shGpc4 CI 1 ($p = 0.0286$) vs. shGpc4 CI 2 ($p = 0.0286$); *Tubb3*: shScr vs. shGpc4 CI 1 ($p = 0.0286$) vs. shGpc4 CI 2 ($p = 0.0286$); *Oct3/4*: shScr vs. shGpc4 CI 1 ($p = 0.0286$) vs. shGpc4 CI 2 ($p = 0.0286$); *Sox2*: shScr vs. shGpc4 CI 1 ($p = 0.40$) vs. shGpc4 CI 2 ($p = 1.0$); $n = 4$. Scale bar: 400 μm

2.5 Impaired neural differentiation is not the result of increased colony numbers

An important parameter for efficient neural differentiation is the density of seeded mESCs on MS5 cells. Overly dense colonies show decreased differentiation efficiency. Although cells were counted and the same amount was seeded for each differentiation, more colonies were observed in shGpc4

clones. To investigate this effect quantitatively, the amount of day 8 colonies and their size was determined by imaging complete 6 cm dishes and creating an analysis mask (Fig 37 a)). The shGpc4 lines showed a trend to an increased number of colonies compared to the control (shScr: 233 % vs. shGpc4 Clone 1 309 % vs. shGpc4 Clone 2 263 %; Fig 37 b)). However, these effects were not significant. Furthermore, shGpc4 Clone 1 showed a weak increase of total area covered by colonies which was less pronounced than the increase in number of colonies (Fig 37 c)).

Taken together, shGpc4 Clone 1 showed a trend to increased number of colonies but only weak increase of the area. This indicates that more but smaller colonies were present in this clone. In contrast, this trend was only very weakly pronounced in shGpc4 Clone 2. Importantly, this line showed equally strong impaired neural differentiation and even stronger expression in *Oct3/4* on day 8. Therefore, although more small colonies were present in shGpc4 clones, it was concluded that the colony size was not the main reason for impaired neural differentiation.

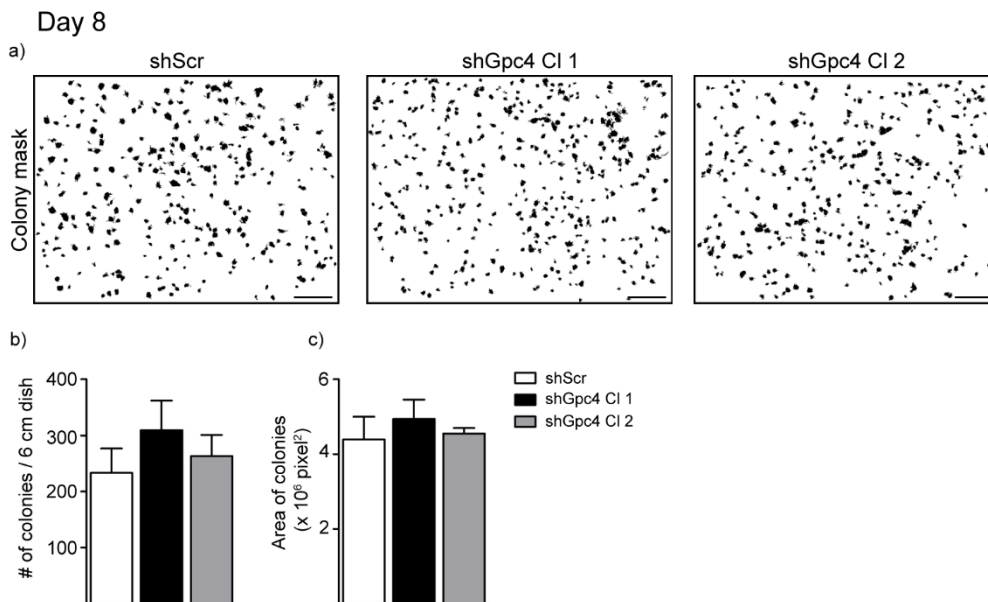


Figure 37 Impaired neural differentiation is not the result of increased colony numbers. a) Mask detecting size and area of neural colonies on day 8 of differentiation. Quantification of number (b) and size (c) of colonies showed no significant differences, n = 3. Scale bar: 1 mm.

2.6 Impaired neural differentiation is not due to a developmental delay

The observed decreased differentiation efficiency of shGpc4 mESCs might have been the result of a general delay of neural development. To address this, stem cells were further differentiated for another week as a monolayer and analyzed by qPCR for the mRNA expression levels of stem cell- and neural markers (Fig 38). Like on day 8, the expression of *Nestin* mRNA was strongly decreased in shGpc4 clones after two weeks of differentiation. The reduction of *Tubb3* expression was even more

II. Results

pronounced on day 14 compared to day 8. Consistently, *Oct3/4* was still stronger expressed in shGpc4 clones compared to the control.

Taken together, these data indicate that the decreased neural differentiation potential of shGpc4 cells is not mediated by a general delay of neural differentiation.

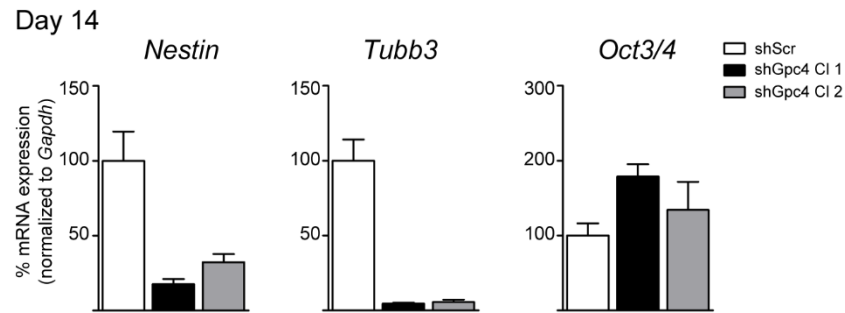


Figure 38 Impaired neural differentiation is not the result of developmental delay. Quantification of *Nestin*, *Tubb3* and *Oct3/4* confirmed sustained neural differentiation defects in shGpc4 cells. *Nestin*: shScr vs. shGpc4 Cl 1 ($p = 0.10$) vs. shGpc4 Cl 2 ($p = 0.10$); *Tubb3*: shScr vs. shGpc4 Cl 1 ($p = 0.10$) vs. shGpc4 Cl 2 ($p = 0.10$); *Oct3/4*: shScr vs. shGpc4 Cl 1 ($p = 0.10$) vs. shGpc4 Cl 2 ($p = 0.70$). $n = 3$.

To verify the obtained mRNA expression results quantitatively at protein levels, highly sensitive high-content imaging assays were developed to detect neural differentiation efficiency by stainings against the mature neural marker MAP2 and OCT3/4. The MAP2 expression was quantified by a specific mask which detects the MAP2 positive area. This area was then normalized to the total area of cells, stained by DAPI. Both shGpc4 clones showed a strongly reduced expression of MAP2 compared to the control (Fig 39 a)). The quantification detected a reduction to 4.3 % in the shGpc4 Clone 1 and 5.0 % in shGpc4 Clone 2 (Fig 39 b)).

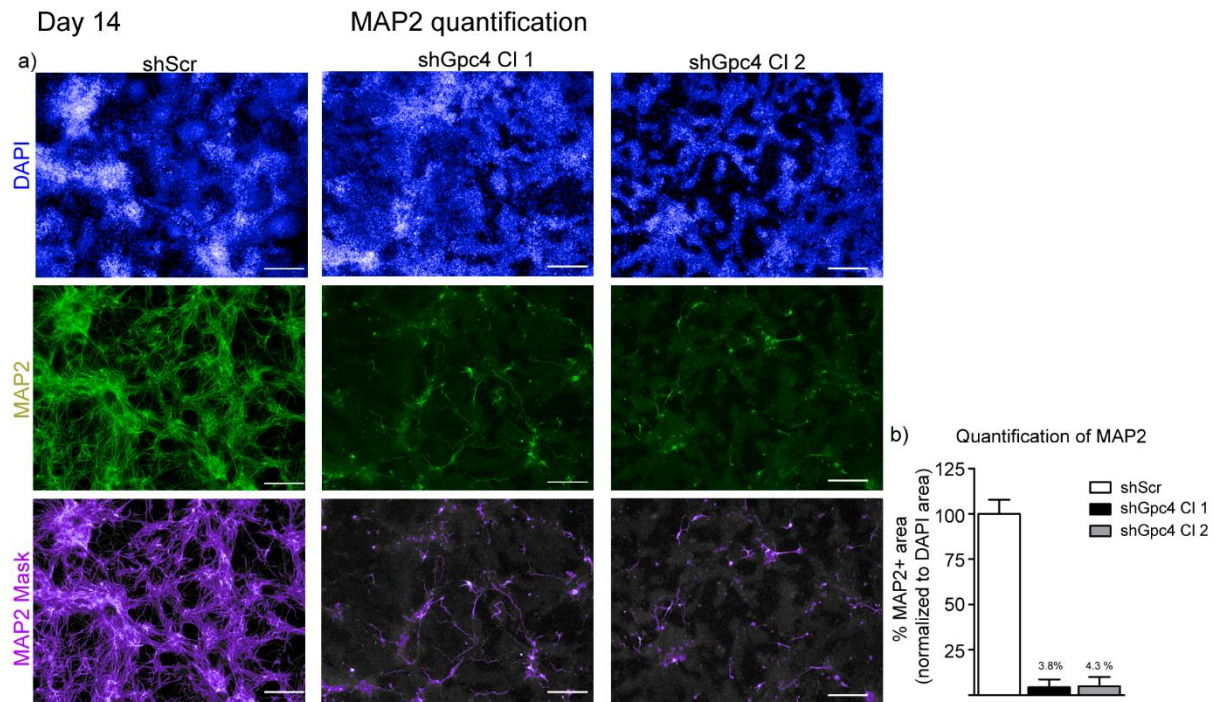


Figure 39 MAP2 quantification on day 14 of neural differentiation. Confirmation of impaired neural differentiation by strongly impaired MAP2 expression in shGpc4 cells. MAP2: shScr vs. shGpc4 CI 1 ($p = 0.10$) vs. shGpc4 CI 2 ($p = 0.10$). $n = 3$. Scale bar: 200 μm .

Although control cells showed a strong expression of MAP2 positive neurites all over the well, undifferentiated stem cells, marked by OCT3/4 expression were still present after two weeks of neural differentiation. However, these cells were exclusively organized in undifferentiated cell clusters in the shScr cell line. In contrast, almost all shGpc4 cells showed strong expression of OCT3/4, independent of local cell aggregates (Fig 40 a)).

As the area-based MAP2 assay was not sufficient to quantify a nuclear expression pattern, we chose an additional assay approach for the quantification of OCT3/4 expression. First, all DAPI positive cells were defined by masks of single cells. Depending on the expression intensity of OCT3/4, these single cells were divided in OCT3/4 expressing and not expressing cells. The positive population was then normalized to the total amount of cells.

As expected, both shGpc4 clones showed an increase in OCT3/4 positive neurons compared to the control. The population of OCT3/4 expressing cells was increased to 231.7 % in the shGpc4 Clone 1 and to 161.5 % in the shGpc4 Clone 2 (Fig 40 b)).

Taken together, these results show that the loss of *Gpc4* leads to a severe and significant impairment of neural differentiation *in vitro*. In particular, *Gpc4* seems to be required for early differentiation to neural precursor cells. This hypothesis is supported by a strongly reduced expression of *Nestin* upon *Gpc4* knockdown, which precedes *Tubb3* expression during development. Furthermore, this effect

II. Results

does not seem to be caused by a general delay of neural differentiation, because even after two weeks of differentiation no trend to recover was observed. The loss of neural differentiation was accompanied by a strong prolonged expression of the OCT3/4. Therefore, shGpc4 cells seem to be kept in the mESC stage and lack the potential to differentiate to the neuroectoderm lineage.

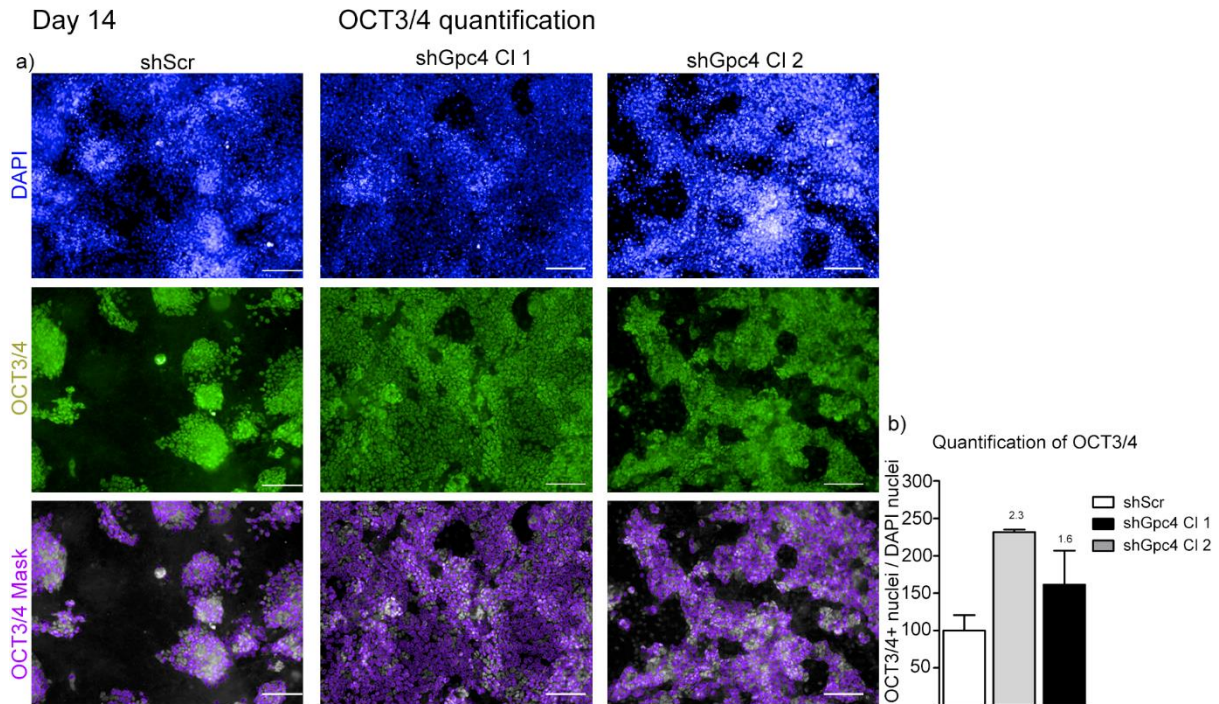
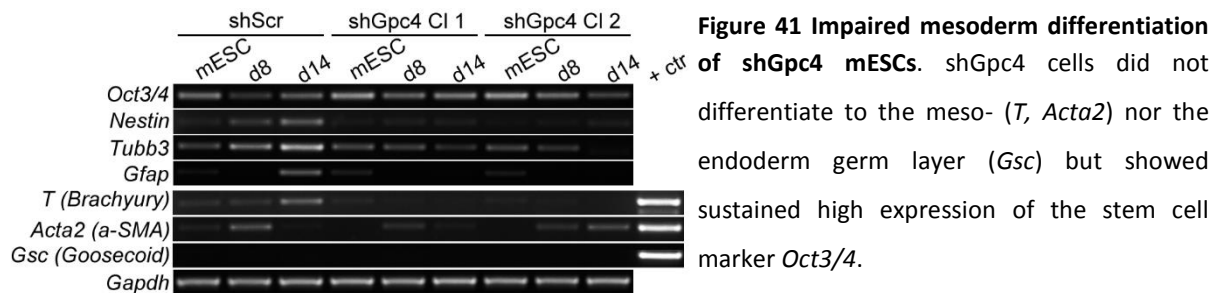


Figure 40 OCT3/4 quantification on day 14 of neural differentiation. a) Staining and b) quantification of OCT3/4 expression confirmed sustained high level in shGpc4 clones. OCT3/4: shScr vs. shGpc4 CI 1 ($p = 0.10$) vs. shGpc4 CI 2 ($p = 0.40$). $n = 3$. Scale bar: 100 μm .

2.7 Impaired mesoderm differentiation of *Gpc4* knockdown mESCs

Due to the strongly sustained expression of the stem cell marker Oct3/4, it was assumed that shGpc4 cells remain in the undifferentiated state rather than differentiate to other lineages. To verify this hypothesis, the mRNA expression of non-neural markers was tested in differentiating shScr and shGpc4 mESCs and compared to neural markers (Fig 41). Albeit a strong neuronal induction by MS5 cells, also non-neural markers were weakly upregulated during differentiation in shScr cells. On day 14, expression of *Gfap*, a marker for astrocytes, was detected in low levels. Additionally, early mesoderm markers including *T* (also called *Brachyury*) and *Acta2* (also called *alpha-SMA*), but not the mesoderm marker *Gsc* (*Gooseoid*) were weakly expressed in shScr cells (35 PCR cycles compared to 28 for neural markers). In contrast, both shGpc4 mESC lines showed no expression of *T* and strongly decreased levels of *Acta2* expression. These results indicate that *Gpc4* might have a more general role

in mediating mESC differentiation, which goes beyond the specific role in neural differentiation shown in the used *in vitro* model.



2.8 GPC4 treatment of shGpc4 mESCs does not rescue neural differentiation

As a next step, the impaired differentiation of shGpc4 cells was supposed to be rescued by the overexpression of *Gpc4* in mESCs. In the neuroblastoma line neuro-2a and in MEFs, *Gpc4* was strongly overexpressed by transfection or transduction of cytomegalovirus-(CMV)-promoter-driven expression of *Gpc4* cDNA. Overexpression was confirmed at mRNA and at protein level by stainings against the N-terminal HA-Tag and by western blot analysis. Because the *CMV* promoter is strongly silenced in undifferentiated stem cells (S. Hong et al., 2007), the promoter was exchanged by the elongation factor 1-alpha (*EF1a*) promoter which is robustly active in stem cells. The correct sequence of the obtained plasmid was confirmed by sequencing. The transduction and nucleofection of *EF1a*-driven *Gpc4* cDNA in mESCs resulted in a strong overexpression of *Gpc4* mRNA compared to endogenous levels. Furthermore, infected cells survived positive-selection by antibiotics. However, no overexpression of GPC4 protein was determined in mESCs, neither by HA-Tag antibodies nor by the *Gpc4* antibody. Interestingly, I could also not overexpress GPC4 protein in human neural precursor cells.

To circumvent this limitation, a mutant form of *Gpc4* (*Gpc4* ΔGPI) was overexpressed in HEK293T. This form carries a 6xHIS-Tag on the N- and C-terminus of the *Gpc4* sequence. The C-terminal 6xHIS-Tag destroys the GPI-anchorage site. Therefore, GPC4 ΔGPI is released to the cell culture medium. The efficiency of conditioning medium with GPC4 was investigated by western blot analysis. 40 μl of empty and GPC4 ΔGPI conditioned medium was loaded on a western blot gel. Even without concentration of the samples, a strong expression of the 37 kDa GPC4 band was detected in the GPC4 ΔGPI sample (Fig 42 a)). Interestingly, no band at 70 kDa was detected indicating a complete cleavage of overexpressed GPC4 ΔGPI. Conditioned media were 1:1 diluted with normal KSR and added to differentiating mESC lines from day 2 on (Fig 42 b)). On day 8, cells were harvested and the mRNA expression of *Tubb3*, *Nestin* and *Oct3/4* was analyzed by qPCR (Fig 42 c)). The expression of *Nestin* and *Tubb3* in control cells was weakly decreased by GPC4 ΔGPI medium. However, no rescue of neural

II. Results

differentiation in shGpc4 cells indicated by gene expression of *Nestin* and *Tubb3* were observed by treatment with GPC4 Δ GPI medium.

Taken together, these results might indicate that GPC4 needs to be GPI-anchored to the cell surface to rescue the impaired neural differentiation potential observed in shGpc4 clones. To exclude potential effects of the two 6xHIS-Tags on GPC4 functionality, a functional readout for GPC4 protein would be required in the future.

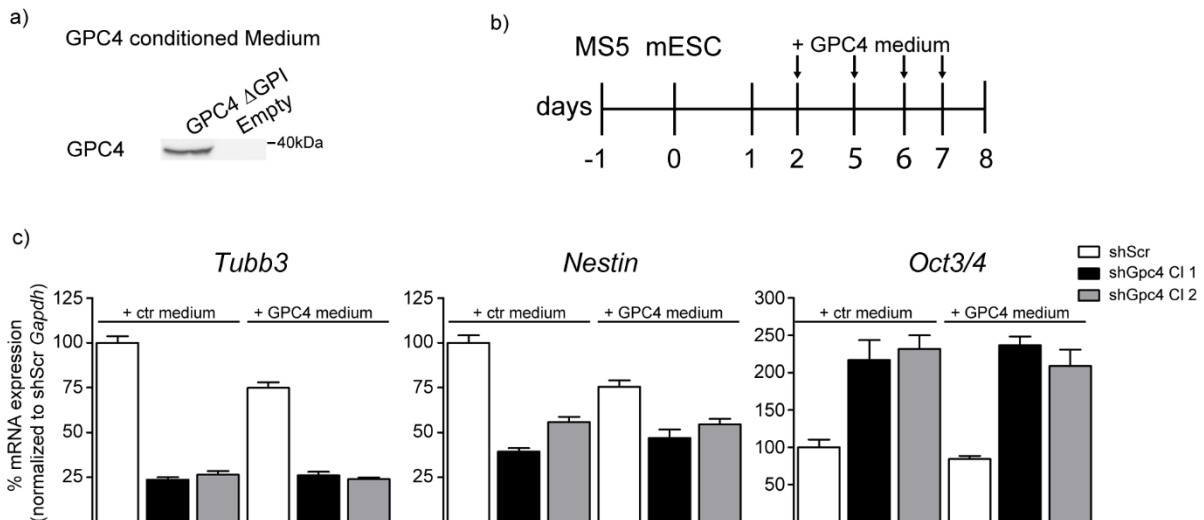


Figure 42 GPC4 treatment of shGpc4 mESCs does not rescue neural differentiation defects. a) *GPC4* conditioned medium showed high abundance of 37 kDa *GPC4* protein. b) *GPC4* conditioned medium was added on the four indicated days during differentiation and mRNA expression was analyzed on day 8. c) Quantification of *Tubb3*, *Nestin* and *Oct3/4* expression showed no difference between control and *GPC4* conditioned medium. $n = 1$. Error bars indicate minimum and maximum of technical replicates.

2.9 Hh signaling is impaired in differentiating shGpc4 mESCs

To further investigate the role of *Gpc4* as an Hh modulator during neural development, the *in vitro* differentiation system was analyzed in more detail. The luciferase assay revealed that upon knockdown of *Gpc4*, Hh signaling activity was decreased. However, about 60 % of the signaling activity remained in this system. Therefore, it was tested if the stimulation of the pathway by high doses of recombinant SHH might partially rescue the impaired neural differentiation observed in shGpc4 mESCs.

As a first step, the activation of the Hh signaling pathway by SHH was analyzed. ShGpc4 clones and control mESCs were differentiated for five days on MS5 cells (Fig 43 a)). From day 5 to day 8, medium which contained either vehicle or recombinant SHH was replaced daily. On day 8, cells were harvested and the mRNA expression of the two Hh downstream targets *Ptch1* and *Gli1* were analyzed by qPCR (Fig 43 b)). Upon SHH stimulation, shScr cells showed an upregulation of the Hh signaling pathway downstream targets *Ptch1* and *Gli1* (Fig 43 b)). The activation of the Hh signaling pathway led to an

increase of the neural precursor population demonstrated by the upregulation of *Nestin* on day 8 and day 14 (Fig 43 c) and d)). This effect was accompanied by a delayed differentiation to neurons on day 8 (Fig 43 c) and d)). The *Oct3/4* expression was unaffected by SHH stimulation.

In contrast, shGpc4 clones showed impaired upregulation of *Ptch1* and *Gli1* upon SHH treatment on day 8 (Fig 43 b)). Consistently, no SHH-mediated induction of *Nestin* was observed (Fig 43 c)). Also the expression of *Tubb3* was not altered by SHH treatment (Fig 43 c)). Similar results were obtained after two weeks of differentiation (Fig 43 d)).

Taken together, shGpc4 mESCs did not respond to SHH induction and did not show SHH-induced upregulation of *Nestin*. These results indicate that *Gpc4* might act as a positive modulator of Hh-mediated differentiation to neural precursor cells *in vitro*.

However, although SHH stimulation increased the neural precursor population in control cells, the development of neurons was first delayed on day 8 but normalized again on day 14. Therefore, although Hh signaling activity might be affected in shGpc4 cells, the observed impaired neural differentiation was most likely mediated by defects in other pathways than the Hh signaling pathway.

II. Results

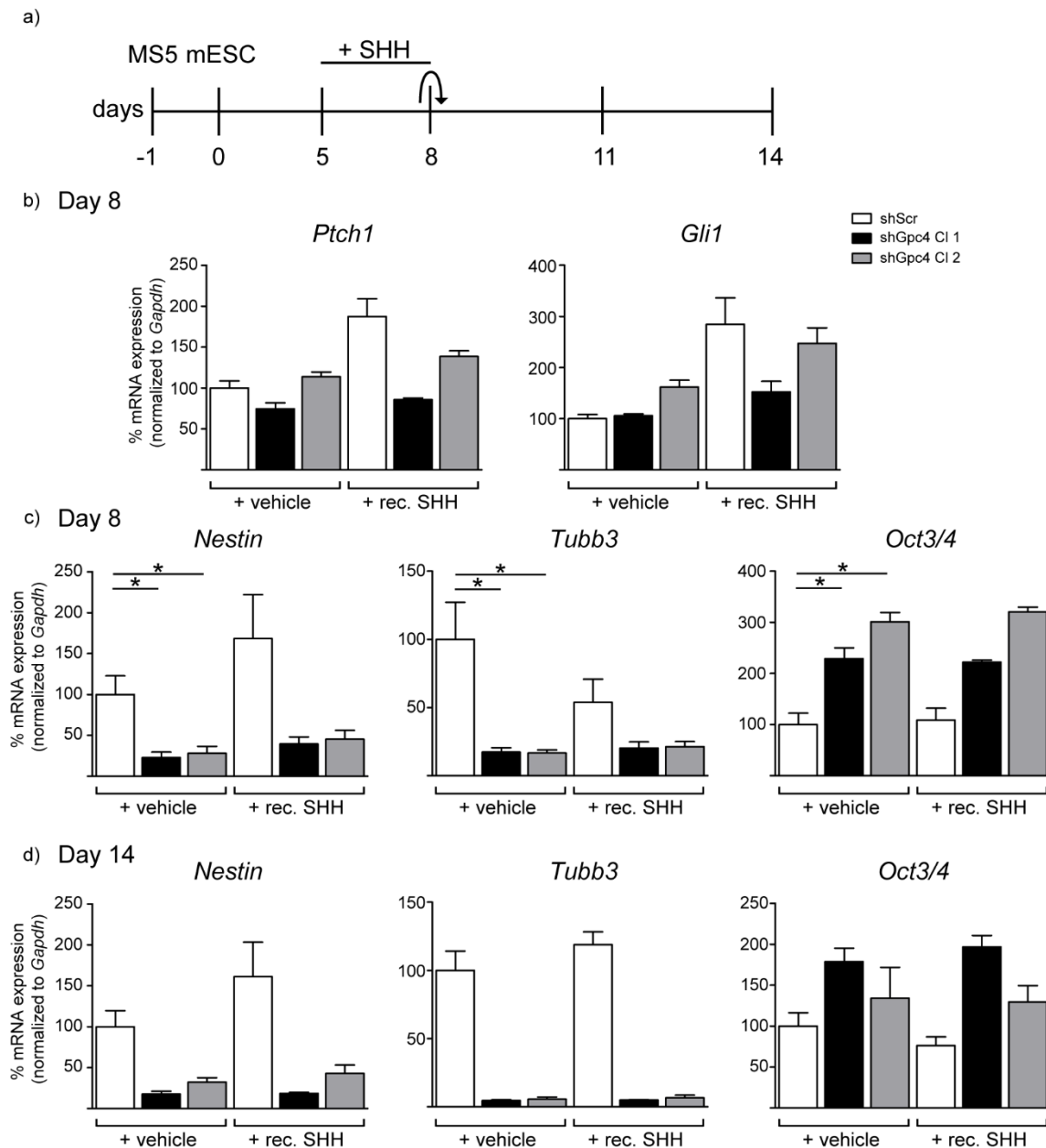


Figure 43 Hh signaling activity is impaired in differentiating shGpc4 mESCs. a) Differentiating mESCs were stimulated daily from day 5 to day 8 with recombinant SHH and analyzed on day 8 and day 14. b) shGpc4 mESCs lacked SHH-mediated activation of the Hh signaling pathway indicated by impaired upregulation of *Ptch1* and *Gli1*. $n = 3$. c) SHH stimulated neural precursor differentiation (*Nestin*) and delayed neural differentiation (*Tubb3*) in control, but not in shGpc4 mESCs on day 8. $n = 4$ d) Confirmation of impaired SHH-induced neural precursor differentiation in shGpc4 cells on day 14. $n = 3$.

Significant p-values: Day 8 + vehicle: ***Nestin***: shScr vs. shGpc4 CI 1 ($p = 0.0286$) vs. shGpc4 CI 2 ($p = 0.0286$); ***Tubb3***: shScr vs. shGpc4 CI 1 ($p = 0.0286$) vs. shGpc4 CI 2 ($p = 0.0286$); ***Oct3/4***: shScr vs. shGpc4 CI 1 ($p = 0.0286$) vs. shGpc4 CI 2 ($p = 0.0286$). $n = 4$.

2.10 Inhibition of Fgf signaling phenocopies *Gpc4* knockdown defects

Neural development requires the activity of a complex regulatory network of developmental signaling pathways including the Wnt, Hh and Fgf pathways. To investigate, which of these signaling pathways are required in the used neural differentiation model, a pharmacological approach was chosen. Therefore, wildtype mESCs were treated from day 1 to day 8 with different signaling pathway inhibitors, either alone or in combination (Fig 44 a)). For each inhibitor, three 10 fold concentration steps of the described half maximal inhibitory concentration (IC_{50}) value were tested. The activity of the Hh inhibitors at the used concentrations was confirmed by an independent cell system (in collaboration with Ms Elen Torres, PhD student in our group). On day 8, cells were fixed and neural differentiation efficiency was analyzed by stainings against B3 TUBULIN (Fig 44 b)). Treatment by the vehicle DMSO did not affect neural differentiation in the used concentrations. None of the used drugs impaired neural differentiation in concentrations of 0.01 fold to 1 fold of the IC_{50} . In addition, at 10 fold concentration, the Wnt inhibitor IWR-1-endo, which stabilizes the β -catenin destruction complex, had no effects on neural differentiation.

In contrast, two drugs suppressed neural differentiation at the 10 fold concentration. Gant61, which inhibits the Hh signaling pathway by directly targeting *Glis*, completely inhibited neural differentiation. However, apart from impaired differentiation, also the size of the colonies was strongly reduced by Gant61 treatment. This result indicates that not only neural differentiation was inhibited but suggests that also proliferation or cell death was altered. Importantly, treatment with another Hh signaling inhibitor, Cyclopamine, which acts at the level of SMO, did not inhibit neural differentiation.

The second drug which inhibited neural differentiation was SU5402, a potent Fgf-receptor antagonist. Although the colony size was also reduced in SU5402 treated cells, it was not changed when treated in combination with Cyclopamine. Because the latter had no effect alone, the inhibition of neural differentiation was considered to be mediated exclusively by SU5402 in the combinatorial condition. Taken together, these data suggest an important role of the Fgf signaling pathway in neural differentiation of mESCs. The inhibition of Fgf signaling strongly impaired neural differentiation, which is mimicking the loss-of-function of *Gpc4* in mESCs.

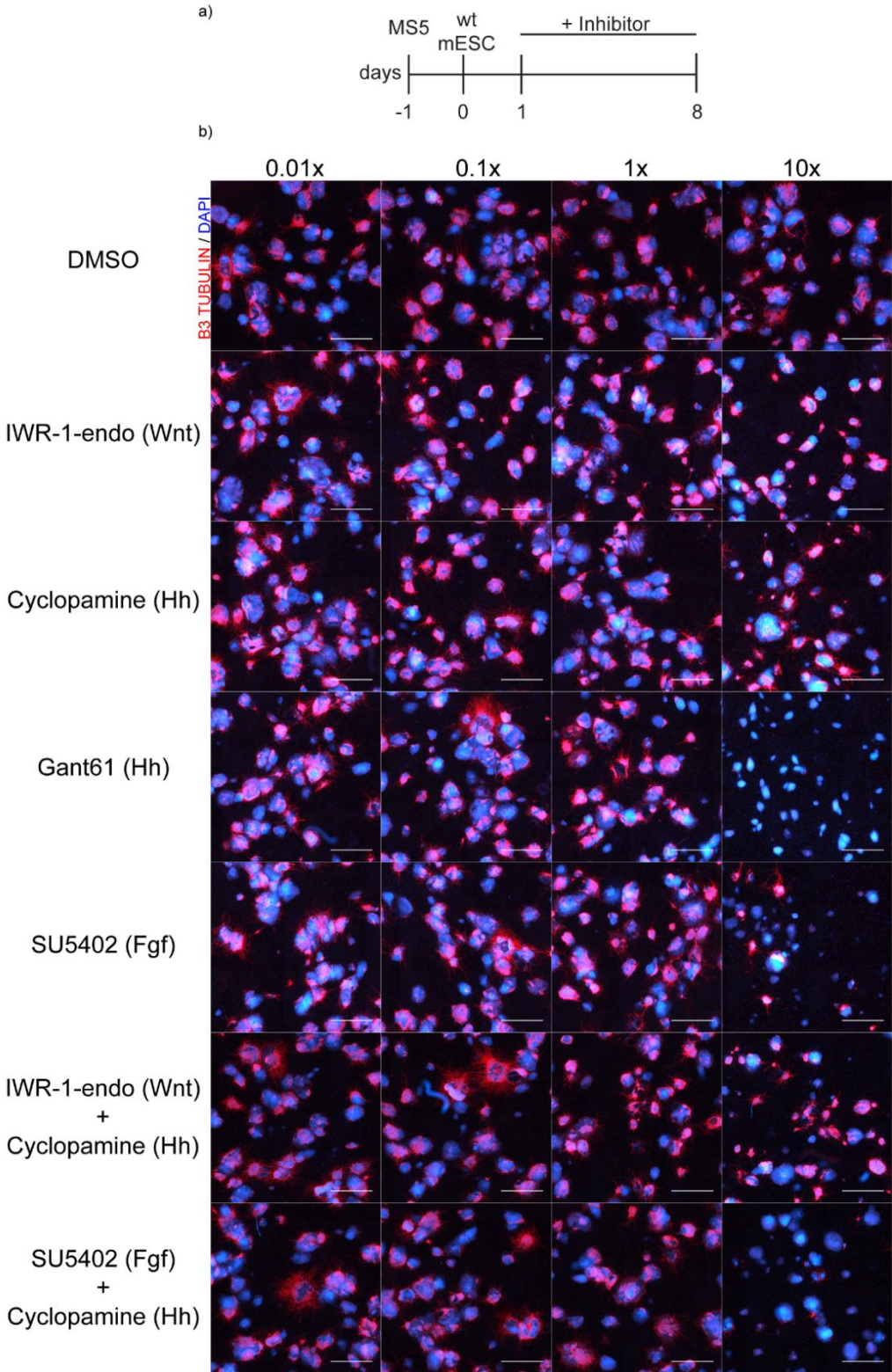


Figure 44 Inhibition of Fgf signaling phenocopies shGpc4 defects. a) wt mESCs were treated from day 1 to day 8 with signaling pathway inhibitors at four different concentrations. b) Treatment with Gant61 and SU5402 at the highest concentration inhibited neural differentiation, indicated by stainings against B3 TUBULIN. Scale bar: 500 μ m.

III. Discussion

Summary of the results

The aim of this thesis was to investigate the role of the extracellular matrix protein *Gpc4* during development of the mouse brain. First, the expression pattern of *Gpc4* mRNA and protein was analyzed during brain development. Strong expression in the anterior forebrain, specifically in the ventricular and sub ventricular zones of the cortex at E12.5 was observed. At E17.5, the expression pattern expanded to newly developing cortical layers where it remained expressed during adulthood, additionally to a high abundance in hippocampal structures. To analyze the role of *Gpc4 in vivo*, I created a loss-of-function mouse line (*Gpc4*^{-/-}) and analyzed it during embryogenesis. *Gpc4*^{-/-} embryos showed a broad spectrum of developmental defects ranging from embryos which died before E9.5, embryos with lethal forebrain defects to fertile adult animals. Within the group of severely affected embryos, an impaired separation of the anterior midline affecting the eyes (in 72 % of the embryos) and the developing cortex (in 24 % of the embryos) was observed. The incomplete separation of the anterior forebrain is defined as holoprosencephaly (HPE). Additionally, neural tube closure defects including exencephaly were often observed (in 24 % of the embryos). The expressivity of the observed phenotypes was strongly dependent on the genetic background of the mouse strain. Strong defects of *Gpc4*^{-/-} embryos were observed in a pure C57BL/6 inbred background. In contrast, *Gpc4*^{-/-} embryos with a mixed C57BL/6N x CD-1 genetic background showed only mild defects such as the lack of retina pigmentation. Furthermore, severe defects were detected with a higher prevalence in homozygous *Gpc4*^{-/-} females (68 %) compared to hemizygous *Gpc4*^{-/Y} males (8 %). Analysis of E12.5 *Gpc4*^{-/-} embryos with incomplete (semilobar) HPE revealed impaired neural precursor differentiation in the developing cortex, whereas the midline expression of PAX6 was not affected. Additionally, no differences in proliferation were observed in these embryos. Transcriptome analysis of E9.5 embryo heads identified the Wnt and the Hh signaling pathways as potentially misregulated in *Gpc4*^{-/-} embryos. *In situ* analysis of the diencephalic *Wnt1* domain revealed no altered expression pattern in E9.5 *Gpc4*^{-/-} embryos compared to controls. Hence, *Gpc4* seems not to repress Wnt signaling in the anterior forebrain. In contrast, Hh signaling was severely affected upon loss of *Gpc4 in vivo* and *in vitro*. Anteriorly truncated brains of E10.5 *Gpc4*^{-/-} embryos lacked the specific SHH domain AEP in the anterior forebrain whereas posterior regions were normally developed. Furthermore, the downregulation of *Gpc4* significantly reduced Hh signaling activation in an Hh reporter cell line. Consistent with these results, cleavage-resistant GPC4 protein was partially detected in primary cilia of MEFs, the main site of Hh signaling. Furthermore, single cell RNAseq of the human developing cortex revealed a strong co-expression of *GPC4* with the positive Hh modulator *BOC* suggesting a potential co-activity in Hh signaling. Taken

together, these data strongly suggest a role of *Gpc4* as a positive modulator of Hh signaling during mouse forebrain development. In vertebrates, the main site for Hh signaling is the primary cilium. Defects in the structure or function of this organelle are summarized as ciliopathies. A hallmark of ciliopathies is the high variability of expressivity and penetrance similar to *Gpc4*^{-/-} embryos. First analysis of primary cilia in the node of E7.5 embryos indicated that ciliogenesis was not affected in *Gpc4*^{-/-} embryos. Hence, the downstream function of signaling pathways rather than the formation of primary cilia seem to be impaired by the loss of *Gpc4*. However, for a final conclusion on the role of *Gpc4* on ciliogenesis during development, more animals will have to be analyzed.

Additionally to midline defects, a fraction of *Gpc4*^{-/-} embryos showed truncated anterior forebrains. Furthermore, empty deciduae of *Gpc4*^{-/-} mothers before E9.5 were frequently observed. These results suggested a very early role of *Gpc4*, potentially during neural plate induction. To study the role of *Gpc4* during early neural development, a mESC-based neural differentiation protocol was optimized. mESCs with a complete knockdown of *Gpc4* expression (shGpc4) showed no significant differences in proliferation, cell death and the expression of stem cell markers in the undifferentiated state. However, shGpc4 mESCs showed strongly impaired differentiation to neural precursor cells and neurons. Consistently, shGpc4 cells retained expression of stem cell markers. Neural development was neither delayed in shGpc4 mESCs nor did these cells differentiate to other germ layers. These results were in strong agreement with impaired neural differentiation in the developing cortex of E12.5 *Gpc4*^{-/-} embryos with alobar HPE.

Interestingly, also the weak expression of mesendoderm markers in differentiating control mESCs was impaired in shGpc4 mESCs. Hence, *Gpc4* might be generally required to leave the pluripotent state of embryonic stem cells rather than being specific for the neuroectoderm lineage. Although Hh signaling was impaired in differentiating shGpc4 cells, pharmacological studies revealed that Hh signaling was not mandatory for early neural induction *in vitro*. In contrast, the inhibition of Fgf signaling phenocopied neural differentiation defects observed in shGpc4 cells. These results suggest that *Gpc4* acts as a positive Fgf signaling modulator during early forebrain induction.

1. *Gpc4* modulates mouse forebrain development

The ECM plays an important role during embryo development by modulating the activity of key signaling pathways. One of the most abundant extracellular matrix proteins in the developing mouse brain is *Gpc4* whose orthologues have been identified to modulate Hh-, Wnt-, Fgf- and Bmp - signaling during non - mammalian development. Although all of these pathways are required for mammalian brain development, their modulation by the ECM remains poorly understood. To investigate the role of *Gpc4* during mouse brain development, the expression pattern of *Gpc4* in the brain was investigated and a *Gpc4* loss-of-function mouse line was analyzed.

1.1 *Gpc4* is specifically expressed in the developing anterior forebrain

In the early developing embryo (E6.5 – E7.5), strong expression of *Gpc4* mRNA was reported in the anterior visceral endoderm and the anterior neural ridge which are key signaling centers for the early induction of the future forebrain (Luxardi et al., 2007; Shimamura & Rubenstein, 1997). During further development, *Gpc4* expression expands to the midline epithelium, the eyes and to the ventricular and sub ventricular zones of the developing cortex (Ford-Perriss et al., 2003; Hagihara et al., 2000; Watanabe et al., 1995; Ybot-Gonzalez et al., 2005).

As a first step of my project, I confirmed the high abundance of *Gpc4* in the developing cortex by *in situ* hybridization and by staining against *Gpc4*-driven β -Galactosidase expression. Furthermore, GPC4 expression was analyzed on a protein level during brain development. Importantly, none of the tested commercial *Gpc4* antibodies detected exclusively GPC4, neither by stainings nor by western blot analysis. Because these antibodies were commonly used in recent studies, specificity of the obtained staining patterns should be reconsidered (N. J. Allen et al., 2012; de Wit et al., 2013; Ko et al., 2015). However, one non-commercial antibody was obtained (gift from Dr. Ussar, Helmholtz Zentrum München) which detected specifically the 37 kDa N-terminal cleavage fragment of GPC4 protein. Consistent with the mRNA expression pattern in the mouse brain, GPC4 protein was highly abundant in anterior regions of the developing brain including the eyes, the olfactory bulbs and the cortex. As expected from mRNA expression analysis, only low protein expression levels were observed in the mid- and hindbrain. Based on the high abundancy of GPC4 protein in the anterior brain, it was concluded that *Gpc4* might be specifically important for forebrain development.

1.2 The loss of *Gpc4*^{-/-} can cause HPE

To study the role of *Gpc4* during anterior brain development, I created a loss-of-function (*Gpc4*^{-/-}) mouse line. According to the observed expression pattern, *Gpc4*^{-/-} mice showed severe developmental defects in the developing anterior brain. Albeit the highly variable expressivity of the phenotype, which

will be discussed in chapter 1.5, the most commonly observed malformation in affected *Gpc4*^{-/-} embryos was the incomplete separation of the anterior forebrain (HPE). HPE is the most common developmental defect of the forebrain with an incidence of 1:250 in conceptuses and 1:16.000 in newborn infants (reviewed in Orioli & Castilla, 2010). 40 – 75 % of the described HPE cases show the severe alobar form of HPE (reviewed in Orioli & Castilla, 2010). In contrast, 80 % of *Gpc4*^{-/-} embryos with HPE showed the milder semilobar form of HPE with normal hemisphere separation posteriorly. This difference might be explained by an early loss of *Gpc4*^{-/-} embryos with severe alobar HPE, which therefore might have escaped analysis. Furthermore, the study population of epidemiological HPE studies (embryos, fetus and liveborns) might select for certain subtypes of HPE. Both possibilities will be discussed in the next chapter. In human HPE, midline defects of the face occur in about 80 % of the cases (Geng & Oliver, 2009). Consistently, cerebral misdevelopment of *Gpc4*^{-/-} mice was concomitant with strong craniofacial defects affecting the eyes (72 %) and the snout (24 %). Less frequently (1 – 10 %), defects in the mandibular have been described in human HPE cases which corresponds to 10 % observed in *Gpc4*^{-/-} mice (Lipinski, Godin, O'Leary-Moore, Parnell, & Sulik, 2010; Pauli, Pettersen, Arya, & Gilbert, 1983; Roessler & Muenke, 2010). Early human HPE studies suggested a correlation between developmental defects of the face and severity of HPE (reviewed Demyer, Zeman, & Palmer, 1964). Although a shortened snout was observed in some animals, no direct correlation between malformations of the face and the brain was observed in *Gpc4*^{-/-} mice. This was in line with newer human HPE studies with bigger cohorts weakening the suggested face-brain correlation (reviewed in Cohen, 1989). In *Gpc4*^{-/-} mice, misdeveloped eyes including microphthalmia and anophthalmia were much more reliable indicators of cortical defects, most likely because the eyes are the most accessible protrusion of the CNS.

1.3 Female *Gpc4*^{-/-} embryos have a higher phenotype penetrance

Interestingly, the analysis of 61 hemi-, hetero- and homozygous *Gpc4* loss-of-function embryos indicated a higher phenotype penetrance in homozygous *Gpc4*^{-/-} female embryos (68 %) compared to hemizygous *Gpc4*^{-/Y} males (8 %). A possible explanation could be the presence of potential protective modifier genes on the Y-chromosome, which compensate severe defects in hemizygous *Gpc4*^{-/Y} males. The most likely candidates would be other *Gpc* family members, however, no *Gpc* is located on the Y-chromosome. Furthermore, not all homozygous females are affected. Hence, other factors than protective Y-chromosomal genes might lead to the observed predominance in females. Consistent with my results, a significant predominance in women has been observed in a meta-analysis of human HPE cases (reviewed in Orioli & Castilla, 2010). However, this effect is highly variable between single studies. It was suggested that differences in the investigated study population (embryos, fetuses,

liveborns) could explain this variability (reviewed in Orioli & Castilla, 2010). Depending on the analyzed developmental stage, males with HPE might have been lost through spontaneous abortion and therefore escaped the analysis (Rasmussen, Moore, Khoury, & Cordero, 1996). This hypothesis was tested in *Gpc4*^{-/-} mice. The viable progeny of heterozygous breedings followed a mendelian distribution of *Gpc4* genotypes and sex, suggesting no early loss of hemizygous *Gpc4*^{-Y} males. Interestingly, also viable homozygous *Gpc4*^{-/-} females were detected at the expected mendelian ratio in this analysis. This result was unexpected due to the high phenotype penetrance (68 %) of homozygous *Gpc4*^{-/-} females. One possibility could be the limited number of 23 adult animals that were analyzed for their genotype due to the small litter sizes of C57BL/6 mice, which will be discussed in chapter 3.1. For a reliable exclusion of premature death of hemizygous *Gpc4*^{-Y} males, more animals should be included in this analysis. Taken together, homozygous *Gpc4*^{-/-} female embryos showed an eight times higher phenotype penetrance compared to hemizygous *Gpc4*^{-Y} males. However, the underlying reason leading to the difference remains elusive.

Interestingly, also heterozygous females showed a low penetrance of macroscopic defects (13 %). In females, usually one of the two X-chromosomes is transcriptionally inactivated by epigenetic silencing to achieve gene dosage compensation. The inactivation of one of the two X chromosomes is random, but once an X chromosome is inactivated it remains inactivated in all daughter cells. Therefore, *Gpc4*^{+/-} females show a mosaic expression pattern of one wildtype and one loss-of-function *Gpc4* allele which might explain the low phenotype penetrance of 13 %.

1.4 *Gpc4* controls different signaling pathways during mouse brain development

The separation of the single forebrain vesicle into the future cortical hemispheres and eye fields occurs shortly after gastrulation in the early developing embryo (around E8.0) (reviewed in Heavner & Pevny, 2012). Most identified genes associated to human HPE are members of the Hh signaling pathway including *SHH*, *PTCH1*, *GLI2* and *DISP1* (reviewed in Anna Petryk et al., 2015). However, members of the Nodal-, Retinoic acid-, Fgf- and Bmp -signaling pathways have also been linked to human HPE (Anderson et al., 2002; Brown et al., 1998; Gripp et al., 2000; A. Petryk et al., 2004; Roessler, Pei, et al., 2009).

To identify misregulated signaling pathways, which cause the observed defects in *Gpc4*^{-/-} embryos, the transcriptome of E9.5 heads was analyzed. The earliest developmental stage at which *Gpc4*^{-/-} embryos could be reliably distinguished from non-affected *Gpc4*^{-/-} embryos was at E9.5. To prevent a dilution of the transcriptome analysis by non-affected *Gpc4*^{-/-} embryos, the analysis of this stage was considered as the most promising approach. As expected, the most significantly downregulated genes in female *Gpc4*^{-/-} embryos included genes which are involved in forebrain and eye development

including *Lhx2*, *Alx3* and *Foxg1* (Manuel et al., 2010; Porter et al., 1997; Ribeiro-Bicudo, Queizi, Guion-Almeida, Legnaro, & Richieri-Costa, 2012).

Interestingly, one of the top downregulated genes in *Gpc4*^{-/-} embryos was *Six6*. *Six3*, another member of the *Six* family, has been identified as one of only 14 genes to cause HPE in humans (Wallis et al., 1999). It has been shown that *Six3* induces Hh signaling by activating Shh brain enhancer-2 (SBE2) in the anterior forebrain (Jeong et al., 2008). Interestingly, *Six3* also acts as a Wnt repressor in the developing anterior brain (Lagutin et al., 2003). SIX3 and SIX6 proteins share a high amount of functional domains and are both strongly expressed in the anterior neural plate suggesting a potential functional redundancy in early development (Conte, Morcillo, & Bovolenta, 2005).

In accordance to the important role of *Six3* in Hh and Wnt signaling, these pathways were the most significantly misregulated candidate pathways additionally to HIPPO signaling. As described in the introduction, Wnt- and Hh signaling pathways have been directly linked to early brain patterning (reviewed in Briscoe & Therond, 2013 and Ciani & Salinas, 2005). Therefore the role of these pathways was further investigated.

Although HIPPO signaling was the most significantly misregulated signaling pathways it has been mostly identified to regulate organ growth by cell proliferation and apoptosis rather than patterning organs (reviewed Saucedo & Edgar, 2007).

1.4.1 *Gpc4* does not repress Wnt signaling in the developing forebrain

A recent study discovered *Gpc4* as a positive regulator of canonical and non-canonical Wnt signaling *in vitro* (Sakane et al., 2012). Furthermore, the loss-of-function of *knypek*, the zebrafish *Gpc4/6* orthologue, caused severe craniofacial and forebrain defects including variable forms of cyclopia and shortening of the A-P axis (LeClair, Mui, Huang, Topczewska, & Topczewski, 2009; Topczewski et al., 2001). Since the expressivity of the cyclopia phenotype was further increased by additional loss of *Wnt11*, a member of the planar-cell-polarity Wnt signaling pathway, it was suggested that *knypek* acts as a positive regulator of non-canonical Wnt signaling during forebrain development (Topczewski et al., 2001). However, normal development of the mammalian anterior forebrain requires the inhibition of posteriorizing Wnt signaling by Wnt repressors including *Six3* (reviewed in Andoniadou & Martinez-Barbera, 2013). *Six3*^{-/-} embryos show HPE and forebrain truncations resulting in an anterior expansion of the diencephalic *Wnt1* domain (Lagutin et al., 2003). Therefore, *Six3* seems to repress Wnt signaling and activate Hh signaling during forebrain development (Jeong et al., 2008) (Lagutin et al., 2003). In contrast, *Gpc4*^{-/-} embryos showed no anterior expansion of *Wnt1* expression although the analyzed animals showed severe defects including an underdeveloped forebrain and impaired neural tube

closure. Thus, it was concluded that *Gpc4* most likely does not act as a Wnt repressor in the anterior forebrain.

1.4.2 Impaired Hh signaling most likely causes HPE in *Gpc4*^{-/-} embryos

Additionally to Wnt signaling, transcriptome analysis identified the Hh signaling pathway as potentially misregulated in *Gpc4*^{-/-} embryos. To analyze Hh activity in *Gpc4*^{-/-} embryos, the *Gpc4*^{-/-} line (with a pure C57BL/6N background) was crossed to a *Tg(GBS-GFP)* mouse line (with a FVB/N background), which visualizes Hh signaling by activation of *Gli*-induced GFP expression (Balaskas et al., 2012). Although a strong GFP signal was observed in the midline of the original *Tg(GBS-GFP)* embryos, no signal was detected in *GBS-GFP* positive embryos with the mixed FVB/N x C57BL/6N genetic background. This result was independent of the genotype of *Gpc4* which strongly suggests that the activity of the reporter system is dependent on the genetic background of the used mouse line. This phenomenon seems to be a common limitation of reporter mouse lines (personal communication Dr. Kathryn Anderson, NY, USA). The importance of the genetic background in genetically modified mice will be discussed in chapter 1.5.

The expression patterns of the Hh ligand *Shh* and the intracellular downstream target *Gli1* are highly similar during mouse development (Bae et al., 2011). Therefore, the SHH expression can be used as a readout for Hh signaling activity, which was analyzed in E10.5 embryos. In *Gpc4*^{-/-} mice, a loss of specific areas of the anterior forebrain, which included the anterior entopeduncular area (AEP) SHH domain, was observed. Importantly, the same specific expression domain is absent in loss-of-function mice of *Megalin*, a known positive modulator of *Ptc* (McCarthy et al., 2002; Spoelgen et al., 2005; Willnow et al., 1996). Furthermore, the functional role of *Gpc4* was analyzed in an Hh luciferase reporter mouse embryonic fibroblast (MEF) line (Taipale et al., 2000). MEFs express high levels of GPC4. Upon acute knockdown of *Gpc4*, a significant and concentration-dependent reduction of Hh signaling to 60 % was observed in MEFs that were either stimulated with recombinant SHH or SHH-conditioned medium. Interestingly, the functional impairment was not restored by the overexpression of GPC4, which will be discussed together with the mESC rescue experiments in chapter 3.5. Taken together, these data suggest a potential role of *Gpc4* as a positive Hh modulator during forebrain development.

Although most identified mutations in human HPE were found in direct members of the Hh signaling pathway, also Hh signaling pathway modulators are crucial for normal brain development. Several of these modulators including *Megalin*, *Cdo1*, *Gas1* and *Boc* have been identified on the cell-surface of receiving cells to positively modulate Hh signaling activity. Accordingly, HPE in humans can also be caused by loss-of-function mutations in the Hh modulator *Cdo1* (Bae et al., 2011). Like in *Gpc4*^{-/-}

embryos, the loss-of-function of *Megalin*, *Cdo1* or *Gas1* can cause HPE in mice with limited penetrance (B. L. Allen et al., 2007; Willnow et al., 1996; Zhang, Kang, et al., 2006). For instance, more than 80 % of *Cdo1*^{-/-} mouse embryos show severe forms of HPE with a strong dependency of the genetic background (Zhang, Kang, et al., 2006). This HPE phenotype was largely rescued by additional reduction of one *Ptc* allele suggesting a specific role in Hh signaling regulation (M. Hong & Krauss, 2013). In line with impaired cortical differentiation observed in *Gpc4*^{-/-} mice, adult *Cdo1*^{-/-} mice showed cortical thinning and impaired differentiation of *Cdo1*^{-/-} primary neurons (Oh et al., 2009) (Zhang, Yi, et al., 2006). The high similarity between the *Gpc4*^{-/-} phenotype and mutant mice with loss-of-function mutations in Hh modulators further supports the hypothesis of *Gpc4* as a positive Hh modulator on receiving cells during mouse forebrain development.

In line with this model is data of the *Gpc4* orthologue *dlp* in *Drosophila* (Desbordes & Sanson, 2003; Gallet et al., 2008). It was shown that *dlp* can bind to both, HH and PTC (Yan et al., 2010) and that *dlp* colocalizes with HH and PTC in endocytic vesicles of Hh receiving cells (Gallet et al., 2008). Blocking endocytosis impairs Hh signaling in *Drosophila* embryos and wing discs (Gallet et al., 2008; Gallet & Therond, 2005). Thus, it was suggested that *dlp* might increase Hh signaling by boosting the endocytosis of the HH-*dlp*-PTC complex (Yan et al., 2010). To investigate if *Gpc4* acts at the level of *Ptc* and/or at the level of the downstream receptor *Smo*, the Hh luciferase system was stimulated either with SHH or with purmorphamine. Purmorphamine is a small molecule which was reported to activate Hh signaling by targeting *Smo* (Sinha & Chen, 2006). Surprisingly, the stimulation with both activators was impaired upon knockdown of *Gpc4*. One possibility is that GPC4 might interact with SMO and therefore facilitate Hh signaling. However, no interaction between GPC4 and SMO has been reported so far. Alternatively, purmorphamine could still act over PTC, because no exclusivity of the Smo-purmorphamine interaction has been shown so far (Sinha & Chen, 2006). In the future, *Ptc*^{-/-} or *Smo*^{-/-} MEF cell lines should be analyzed for their Hh activity after knockdown of *Gpc4*.

Additionally to *Ptc* and *Smo*, *Gpc4* could also act at the level of *Ptc* co-receptors to modulate Hh signaling activity. Single cell RNAseq analysis of previously published data revealed that the expression pattern of the PTC co-receptor *BOC* strongly correlated with the expression of *GPC4* in the human developing cortex (Camp et al., 2015). In agreement with the *Gpc4* expression pattern in mice, both genes were strongly expressed in apical cells of the ventricular and sub ventricular zone, whereas *GPC6* was expressed less specifically also in other cortical layers. In mice, the loss-of-function of *Boc* alone does not cause HPE (Zhang et al., 2011). However, *Boc*^{-/-};*Cdo1*^{-/-} double-knockout mice show severe HPE in a *Cdo1*-phenotype resistant genetic mouse background (Zhang et al., 2011). It has been proposed before that *Cdo1* and *Boc* act as positive Hh modulators by stabilizing HH on the cell surface (Gallet et al., 2008; Yao et al., 2006). In contrast to this mode of action, overexpressed *dlp* did not

stabilize binding of HH on receiving cells, but was suggested to boost endocytosis and thereby increase Hh signaling (Yan et al., 2010). Hence, Hh signaling might be increased on the one hand by *BOC* which stabilizes HH on the cell surface and on the other hand by *GPC4* which boosts the endocytosis of the HH-PTC complex. Subsequently, both modulators might be required for optimal Hh signaling activity. However, *Gpc4*-mediated endocytosis would be more indispensable than Hh stabilization by *Boc*, because *Gpc4*^{-/-} embryos show severe HPE in contrast to *Boc*^{-/-} embryos (Zhang et al., 2011). It would be very interesting to analyze whether GPC4 directly binds to BOC and if this interaction is required for the *Gpc4*-mediated modulation of Hh signaling.

1.4.3 Other impaired signaling pathways might cause HPE

The presented data strongly suggest a role of *Gpc4* as a positive Hh modulator during forebrain development whose loss leads to severe forebrain developmental defects including HPE. Although most genetic causes of HPE have been detected in Hh signaling members, also mutations in Nodal-, Retinoic acid-, Bmp- and Fgf-signaling pathways have been linked to human HPE (Anderson et al., 2002; Brown et al., 1998; Gripp et al., 2000; A. Petryk et al., 2004; Roessler, Pei, et al., 2009). However, no modulation of Nodal- and Retinoic acid signaling by *Gpc4* or its orthologues has been reported so far. The *Gpc4* orthologue *knypek* was reported to act as a negative Bmp modulator during heart development (Strate, Tessadori, & Bakkers, 2015). However, no Bmp-mediated brain defects were reported in *knypek* mutants. Furthermore, human HPE can be caused by impaired Bmp signaling and not by a hyperactivity of this pathway. Hence, the observed forebrain defects of *Gpc4*^{-/-} embryos are most likely not caused by altered Bmp signaling. Interestingly, one *Gpc4*^{-/-} embryo showed an impaired separation of the heart ventricles which potentially might be caused by altered Bmp signaling. However, heart defects were only observed once, indicating a very limited role of *Gpc4* during mouse heart development.

Finally, the *Gpc4* orthologue in *Xenopus* was described to positively regulate Fgf signaling during brain development (Galli et al., 2003). The loss of *Xenopus Gpc4* caused severe forebrain truncations similar to *Gpc4*^{-/-} embryos, which will be discussed in chapter 1.4.5. However, no HPE-associated defects including cyclopia were described in this study. Therefore, *Gpc4* might act as a positive regulator of Fgf signaling during early neural plate initiation rather than during regulation of forebrain separation.

To reach a final conclusion about which impaired signaling pathway causes the HPE phenotype in *Gpc4*^{-/-} embryos, additional experiments will be necessary in the future. For instance, the phenotype could be rescued by a hyper activation of specific pathways. In case of Hh signaling, *Gpc4*^{-/-} mice could be crossed with *Ptc*^{-/+} or *Gli3*^{-/+} mice which show increased Hh signaling activity. A decrease in the HPE phenotype penetrance would clearly confirm that the observed defects were Hh-mediated.

1.4.4 Diabetes in *Gpc4*^{-/-} mothers might cause HPE in *Gpc4*^{-/-} embryos

Additionally to mutations in developmental genes, environmental risk factors have been identified to contribute to HPE. A main risk factor for HPE is maternal diabetes, especially with pregestational onset (Correa et al., 2008). Infants of diabetic mothers have a 1 – 2 % risk for HPE, which corresponds to a 200-fold increase compared to children of healthy mothers (Barr et al., 1983; Correa et al., 2008; Kousseff, 1999). Maternal and pregestational diabetes are characterized by increased blood sugar levels (hyperglycemia) due to decreasing insulin signaling, which can be caused by different mechanisms (reviewed in Vambergue & Fajardy, 2011). *Gpc4* has been shown to directly interact with the insulin receptor and to sensitize insulin signaling (Ussar, Bezy, Bluher, & Kahn, 2012). In pre-diabetic obesity, circulating GPC4 levels increase with the body mass index similar to insulin levels (K. Li et al., 2014; Ussar et al., 2012; Zhu et al., 2014). During late obesity with beginning diabetes, insulin signaling progressively decreases which is suggested to lead to less GPC4 cleavage and therefore less circulating GPC4 (Ussar et al., 2012). Because *Gpc4* acts as a positive insulin regulator, decreased levels of GPC4 further impairs insulin sensitivity and accelerates disease progression. Following this model of *Gpc4* as a positive insulin modulator, it is possible, that the loss of *Gpc4* causes impaired insulin signaling and therefore diabetes in adult *Gpc4*^{-/-} mice. Consequently, diabetes of *Gpc4*^{-/-} mothers might contribute to HPE observed in *Gpc4*^{-/-} embryos. It would be interesting to analyze potentially impaired insulin response in *Gpc4*^{-/-} mothers. These results could establish a molecular link between maternal diabetes and developmental brain defects.

1.4.5 *Gpc4*^{-/-} forebrain truncations and neural tube defects are not mediated by impaired Hh signaling

The data discussed so far suggest that *Gpc4* might either act as a positive modulator of Hh signaling on receiving cells during mouse forebrain development and/or as a positive insulin modulator in adult mice. Consequently, the loss-of-function of *Gpc4* causes HPE, presumably by impaired Hh signaling and/or maternal diabetes. However, *Gpc4*^{-/-} embryos showed also other severe brain defects including the absence of the anterior forebrain and impaired neural tube closure resulting in exencephaly. According to current models, both of these processes are not controlled by Hh signaling (reviewed in Andoniadou & Martinez-Barbera, 2013 and Murdoch & Copp, 2010).

One potential cause for forebrain truncation is the lack or impaired function of the anterior visceral endoderm (AVE), which induces the formation of the overlying anterior neural plate. Strong *Gpc4* expression has been described before in the AVE (Luxardi et al., 2007). Similar to the observed defects in *Gpc4*^{-/-} embryos, the removal of the AVE leads to a partial loss of the forebrain, which is not compatible with life (P. Thomas & Beddington, 1996). However, many of the top downregulated genes

in early *Gpc4*^{-/-} embryos including *Six3*, *Foxg1* and *Lhx2* are markers for the anterior neural plate and which are not expressed in the underlying AVE (Oliver et al., 1995; Shimamura & Rubenstein, 1997). In contrast, AVE markers including *Lefty1*, *Cer1*, *Hex* were not lost in *Gpc4*^{-/-} embryos (Belo et al., 1997; P. Q. Thomas, Brown, & Beddington, 1998; Yamamoto et al., 2004). Therefore, the AVE does not seem to be absent in the analyzed mice and consequently, *Gpc4* might not be directly involved in the induction of the AVE as a neural induction center. The loss of *Gpc4* might rather lead to impaired migration of the AVE and thereby cause defects in neural plate induction. One way to investigate whether *Gpc4* is involved in AVE migration would be to analyze its localization in *Gpc4*^{-/-} embryos.

Regarding neural tube defects, it was suggested before that *Gpc4* might not be involved in this process in mice due to an absent expression in the closing neural tube, marked by *Vangl2* (Ybot-Gonzalez et al., 2005). However, neural tube closure occurs at three different sites during development in a specific sequence (reviewed in Murdoch & Copp, 2010). In the described study, co-expression of *Gpc4* and *Vangl2* mRNA was only analyzed at the first closure site at the cervical-hindbrain boundary. In contrast, exencephaly detected in *Gpc4*^{-/-} embryos results from an incomplete neural tube closure of the second and third closure site at the forebrain/midbrain boundary and in the anterior forebrain respectively (reviewed in Murdoch & Copp, 2010). These data suggest that *Gpc4* might be involved in neural tube closure at anterior closure sites, where it is most abundantly expressed, but seems not to be required for posterior neural tube closure (Ybot-Gonzalez et al., 2005).

Consistent with *Gpc4*^{-/-} mouse embryos, forebrain truncations and anterior neural tube defects were reported before in *Gpc4* knockdown *Xenopus* embryos (Galli et al., 2003). In agreement with my results, dorsal forebrain domains were disrupted by increased cell death in *Xenopus* embryos. However, ventral domains expressing *Nkx2.1* were not affected in *Xenopus* in contrast to *Gpc4*^{-/-} mouse embryos. Treatment of wildtype *Xenopus* embryos with the Fgf-receptor inhibitor SU5402 phenocopied forebrain truncation and neural tube closure defects mediated by *Gpc4* knockdown (Galli et al., 2003). Hence, it was concluded that the loss of *Gpc4* leads to impaired Fgf signaling which causes both of these defects (Galli et al., 2003).

However, an independent parallel study of *Gpc4* knockdown in *Xenopus* confirmed neural tube closure defects, but did not observe forebrain truncations (Ohkawara et al., 2003). The authors suggested impaired non-canonical Wnt signaling during gastrulation movement as the underlying affected pathway (Ohkawara et al., 2003). In *Gpc4*^{-/-} mouse embryos with neural tube defects, I did not observe defects in canonical Wnt in the developing brain. However, non-canonical Wnt signaling was not investigated so far.

Taken together, the loss-of-function of *Gpc4* in *Xenopus* and mice can cause forebrain truncation and neural tube defects. Importantly, *Gpc4* might modulate Fgf- and non-canonical Wnt signaling which

can cause similar defects upon *Gpc4* knockdown in *Xenopus* (Galli et al., 2003; Ohkawara et al., 2003). These data indicate how closely connected different signaling pathways are during early embryo development. Because *Gpc4*^{-/-} mouse embryos show defects in forebrain processes which are controlled by different signaling pathways, it is most likely that *Gpc4* regulates Hh- and Fgf- signaling in a time- and tissue-specific manner during embryonic development.

1.5 Phenotype variability of *Gpc4*^{-/-} mice

1.5.1 Variability in human HPE

A hallmark of human HPE is the high variability of the disease expressivity and a reduced penetrance. Like *Gpc4*^{-/-} mouse embryos, other HPE mouse models including *Twsg1*^{-/-} (A. Petryk et al., 2004) and *Chordin*^{-/-}; *Noggin*^{+/-} double mutant mice (Anderson et al., 2002) show a broad spectrum of craniofacial defects similar to human HPE. In contrast to human loss of function of *SHH*, *Shh*^{-/-} mice show a complete penetrance of HPE and are therefore not considered as a traditional mouse model of human HPE (Chiang et al., 1996). Interestingly, haploinsufficiency of *SHH* does not cause HPE in humans. These observations led to the development of a non-linear threshold model of Hh signaling (Fig 45, reviewed by Anna Petryk et al., 2015). In this model, the variance of Hh signaling activity (σ_D) in the healthy and diseased state is similar. However, in the diseased state, Hh signaling activity is generally reduced compared to the healthy state. This reduced Hh signaling causes a broader variance of phenotype (σ_P) due to the non-linear correlation between Hh signaling and phenotype. This model is supported by experiments in avian embryos, where reduced intermediate levels of Hh signaling by pharmacological intervention resulted in a high variability of expressivity (reviewed by Anna Petryk et al., 2015 and J. K. Chen, Taipale, Cooper, & Beachy, 2002 and Cordero et al., 2004).

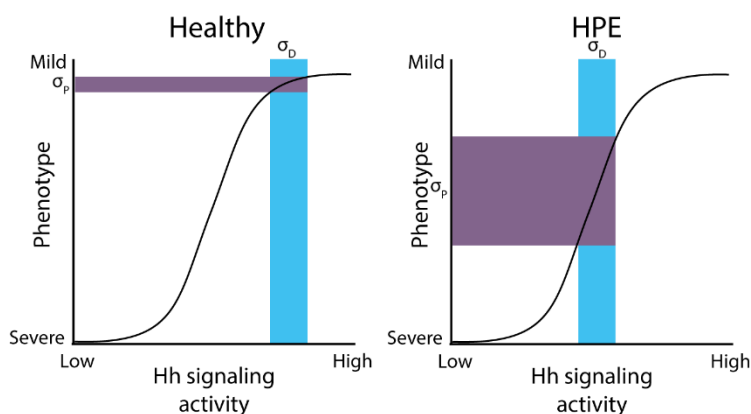


Figure 45 Non-linear Hh signaling activity may cause phenotype variation in *Gpc4*^{-/-} mice. σ_D : variance of Hh signaling activity; σ_P : variance of phenotype. Adapted from Anna Petryk et al., 2015.

Hh signaling activity can be modulated at many different levels including the abundance of various co-receptors of *Ptc*. The loss of function of these co-receptors in mice causes HPE with a high variability

(B. L. Allen et al., 2007; Cole & Krauss, 2003; Willnow et al., 1996; Zhang et al., 2011). My results suggest a new role of *Gpc4* as a positive modulator of Hh signaling in the mouse. Upon loss of function of *Gpc4*, Hh signaling activity might be reduced which causes a higher probability to develop Hh-mediated HPE. Following a “multiple hit” hypothesis of HPE pathogenesis (Ming et al., 2002), an HPE phenotype in *Gpc4*^{-/-} embryos might manifest itself when other factors including genetic modifiers contribute and finally lead to a pathogenic sub-threshold Hh activity.

1.5.2 Impact of genetic background of *Gpc4*^{-/-} mice

The genetic background of a genetically modified mouse line plays a major role in the manifestation of phenotypic outcomes. Therefore, a heterogeneous genetic background provides a major source for potential phenotype variability. In order to avoid this possibility, the used *Gpc4*^{-/-} mouse line was created and maintained on a pure C57BL/6N background. However, a broad spectrum of developmental defects was observed. Furthermore, the F1 generation of *Gpc4*^{-/-} animals with a mixed C57BL/6N x CD-1 genetic background showed only retinal defects.

In a recent study, another *Gpc4*^{-/-} mouse line was created independently and was used to investigate the role of *Gpc4* on excitatory synapses in the hippocampus (N. J. Allen et al., 2012). Interestingly, the authors reported breeding problems of *Gpc4*^{-/-} animals on a pure C57BL/6J genetic background with decreasing viability over generations. However, no further details about the cause of viability and potential developmental defects were reported. As a consequence, those animals were maintained and analyzed on a mixed C57BL/6J x 129 background with which they reached adulthood and showed mild defects in synaptic activity in hippocampal neurons (N. J. Allen et al., 2012).

These results indicate that the manifestation of developmental brain defects observed upon loss of *Gpc4* is highly dependent on genetic modifiers. It would be very interesting to study and identify these modulators of the *Gpc4* phenotype. One possibility would be to cross the *Gpc4*^{-/-} allele to other inbred strains and analyze their phenotype expressivity. New tools including whole genome databases of commonly used mouse strains (Keane et al., 2011) and maps of copy number variations might prove very useful for this approach (She, Cheng, Zollner, Church, & Eichler, 2008). The obtained predictive sequence variants could then be validated on the mRNA expression level by RNAseq in a whole genome scale leading to the identification of new *Gpc4*, and therefore, also new signaling pathway modulators.

1.5.3 Variability of *Gpc3*^{-/-} mice

Similar to *Gpc4*^{-/-} mice, variability of expressivity has also been observed in *Gpc3*^{-/-} mice. The phenotype variability was analyzed in detail in three independent loss-of-function lines on different 129 genetic sub strains (129/J; 129/SvJ; 129/Sv) (Cano-Gauci et al., 1999; Chiao et al., 2002; Paine-

Saunders et al., 2000). Increased body size of about 30 % was observed in all three mouse lines, independent of the genetic background. However, other malformations including polydactyly and differences in spleen size has been reported to be strain specific (Chiao et al., 2002). Additional to overgrowth, *Gpc3*^{-/-} mice showed increased postnatal death, which is thought to be mediated by breathing defects (Cano-Gauci et al., 1999). Consistent with my data, a pure 129 or C57BL/6 genetic background had a much higher incidence of postnatal death compared to genetic hybrids (Cano-Gauci et al., 1999; Chiao et al., 2002). However, even on a pure genetic background, postnatal death was incomplete in *Gpc3*^{-/-} embryos, leading to healthy adult phenotype escapers. These results suggest that *Gpcs* are highly prone for a high variability of phenotypes, which might be related to their lack of an intracellular domain, restricting their role to modifiers of signaling pathways.

1.5.4 Variability in defined genetic background and *Gpc* redundancy

Incomplete penetrance and variable expressivity was reported recently in many knockout lines even with a defined genetic background (Dickinson et al., 2016). These lines belonged to the 5000 knockout mouse lines created and analyzed by the International Mouse Phenotyping Consortium (Dickinson et al., 2016). The same standardized knockout-first vector system and defined genetic background was used to create the *Gpc4*^{-/-} line used in my project.

Variable expressivity has been suggested to be caused by cell-autonomous variation in gene expression of paralogues, other members of a gene family, providing functional redundancy (Dickinson et al., 2016). Variable expressivity might also be related to functional compensation by other gene family members. However, this hypothesis seems rather unlikely because the loss of *Gpc4* was not compensated by an upregulation of mRNA of other *Gpc* members. Similar observations have been reported for *Gpc1*^{-/-} mice in which no compensation by other *Gpcs* was observed (Jen et al., 2009). Regarding functional redundancy, the most likely candidates are *Gpc1* and *Gpc6*. *Gpc1* has a similar but less brain specific expression pattern than *Gpc4* in neuroepithelial cells of the developing forebrain (Jen et al., 2009; Litwack, Stipp, Kumbasar, & Lander, 1994). The loss of function of *Gpc1* caused a reduction of the brain size of about 10 – 15 %, but the patterning of brain structures was normal (Jen et al., 2009). Interestingly, the additional knockdown of *Gpc4* further decreased brain size of *Gpc1*^{-/-} embryos. It was therefore proposed that *Gpc1* and *Gpc4* act in the same signaling pathway in regulating the growth of mouse brain (Filmus et al., 2008; Jen et al., 2009). Although no mechanism was reported, reduced basal Extracellular Signal-regulated Kinase-1 (*ERK*) activity was observed and interpreted as impaired Fgf-signaling (Jen et al., 2009). Interestingly, analysis of mice carrying only the *Gpc4*^{LacZ} allele and thus functional *Gpc1*, showed no defects in brain development. This can be explained by the sole

analysis of male embryos and that the used *Gpc4^{LacZ}* allele was described as hypomorph and therefore expressed remaining *Gpc4* levels.

Furthermore, *Gpc6* might act redundantly to *Gpc4* due to a high conservation of their sequence potentially leading to a potentially conserved function. Indeed, both *Gpc4* and *Gpc6* have been described to strengthen synaptic activity in excitatory synapses of retinal ganglion cells (N. J. Allen et al., 2012). However, *Gpc6* is mainly expressed in bones where it is thought to regulate endochondral ossification and long-bone elongation (Tang et al., 2010). Consequently, *Gpc6^{-/-}* mice model omodysplasia and die prenatally presumably due to defects in Indian hedgehog signaling (Campos-Xavier et al., 2009).

In contrast to *Gpc6*, *Gpc2* shows strong expression in the anterior forebrain between E7.5 and E8.5 when the separation of the anterior forebrain occurs (Luxardi et al., 2007). However, mouse *Gpc2* and its orthologues have not been reported to be involved in brain development. Preliminary analysis of *Gpc2^{-/-}* mice, which I created during my PhD project, showed a general reduction of embryo body size at E10.5 but did not show brain-specific defects.

To investigate whether other *Gpc* family members act redundantly to the loss of *Gpc4* and if this effect contributes to the observed variability, double knockout mice would be required for future analysis.

1.5.5 Potential strategies to homogenize the *Gpc4^{-/-}* phenotype

Although the variable expressivity and reduced penetrance are hallmarks of HPE, these two characteristics have been the most challenging limitation in the analysis of *Gpc4^{-/-}* embryos. Therefore, a major aim for future experiments should be the homogenization and the increase of phenotype penetrance of *Gpc4^{-/-}* mice. Several strategies to reduce and understand the source for this variability have already been mentioned before, including the search for genetic modifiers and the analysis of *Gpc* double knockout mice. Although these strategies might reveal new insights in HPE and their underlying signaling pathway defects, they are also very labor intense. Hence, a pharmacological approach might be much faster in achieving a homogenized phenotype with higher penetrance. In the past, the exposure of HPE mouse models to teratogens including ethanol and retinoic acid was used to increase phenotype penetrance. Thus, the penetrance of severe HPE and neural tube defects of *Twsg^{-/-}* mice was increased from 17 % to 100 % by maternal exposure to retinoic acid (Billington et al., 2015). However, the exposure to retinoic acid might not be the ideal approach in *Gpc4^{-/-}* embryos because this chemical might selectively modulate signaling pathways, which would then complicate pathway analysis. Hence, the maternal exposure to ethanol might be a better approach. It has been shown before that the administration of ethanol to the mother on gestation day 7 is sufficient to cause HPE in wildtype mice (Higashiyama et al., 2007) and that low doses can increase the penetrance of HPE

in heterozygous *Shh*^{-/-};*Gli2*^{-/-} double-mutant mice (Kietzman, Everson, Sulik, & Lipinski, 2014). Therefore, this treatment might be a powerful approach to increase phenotype penetrance and homogenize expressivity. This would facilitate the analysis of the underlying affected pathways.

2. *GPC4* mutations in humans – Simpson-Golabi-Behmel-Syndrome

2.1 Hh-mediated overgrowth by mutations in *GPC4*

Simpson-Golabi-Behmel-Syndrome (SGBS) is an X-linked overgrowth syndrome with less than 250 cases reported (reviewed in Tenorio et al., 2014). The syndrome is categorized in a mild Type I form which is compatible with life, and a severe and usually lethal Type II form. Similar to *Gpc4*^{-/-} mice, the clinical phenotypic spectrum of SGBS is very broad (reviewed in Tenorio et al., 2014). It comprises body overgrowth, the misdevelopment of several organs including the skeleton, the heart, the kidney and the gastrointestinal tract (reviewed in Tenorio et al., 2014). Furthermore, mild midline defects of the face with a cleft lip have been reported in about 13 % of the cases (Morita, Kimoto, Ogawa, Omata, & Morita, 2011). Additionally SGBS patients have an increased risk for postnatal death of 18.5 % and to develop tumors including Wilms- and liver tumors (A. E. Lin, Neri, Hughes-Benzie, & Weksberg, 1999). Although loss-of-function mutations of *GPC3* have been identified as the main cause of SGBS, only about half of the patients carry mutations in this gene ((M. Li et al., 2001; A. E. Lin et al., 1999; Veugelers et al., 2000). In mice and humans, *GPC3* and *GPC4* form a genetic cluster and are both located in direct proximity on the X chromosome (Veugelers et al., 1998). In 2010, a family of SGBS patients has been identified who carried a gain-of-function duplication of *GPC4* Exon 1 – 9 and no mutations in the *GPC3* sequence (Waterson, Stockley, Segal, & Golabi, 2010). Hence, the loss-of-function of *GPC3* causes the same phenotypic spectrum as the gain-of-function of *GPC4* in humans.

Several aspects of SGBS including body overgrowth and postnatal death can be modeled in *Gpc3*^{-/-} mice. The observed overgrowth is thought to be a consequence of hyper active Hh signaling (Chiao et al., 2002) rather than increased insulin growth factor signaling as proposed before (Pilia et al., 1996). Hence, the current hypothesis suggests that overgrowth and increased tumor risk upon loss of *GPC3* are consequences of hyper activation of Hh signaling (M. I. Capurro et al., 2008). Therefore, *Gpc3* is proposed as a negative regulator of Hh signaling in humans and mice. Importantly, considering that the gain-of-function of *GPC4* can also cause SGBS, *Gpc4* would act as a positive Hh regulator in humans. This hypothesis is in strong agreement with my results suggesting *Gpc4* as a positive modulator of Hh signaling during brain development in mammals.

In contrast to body overgrowth, brain defects are very rare in SGBS, probably due to a low expression of *GPC3* in the developing brain (Luxardi et al., 2007). Only one case of SGBS was reported with severe CNS defects in which the corpus callosum was absent, the cerebellum was underdeveloped and the

lateral ventricles were dilatated (Mujezinovic et al., 2016). Interestingly, this patient carried not only a loss-of-function mutation of *GPC3* but also a duplication of *GPC4* leading to its gain-of-function. Therefore, a duplication of *GPC4* cannot only cause typical forms of SGBS, potentially by hyper activation of Hh signaling, but additionally causes a malformation of the brain. The mutation of two *Gpcs*, the loss of *Gpc3* as a negative and the duplication of *Gpc4* as a positive modulator, might lead to excessive Hh signaling and therefore to a misdevelopment of the brain.

2.2 Severe forms of SGBS are caused by impaired ciliogenesis

In contrast to SGBS Type I, the Type II form of the disease comprises much more severely affected patients who usually die soon after birth due to respiratory defects (reviewed in Tenorio et al., 2014). Due to early miscarriage of these misdeveloped embryos, only 10 cases have been described so far (Brzustowicz, Farrell, Khan, & Weksberg, 1999; Terespolsky, Farrell, Siegel-Bartelt, & Weksberg, 1995). Interestingly, SGBS Type II patients show severe CNS misdevelopment such as macrocephaly additionally to body overgrowth. So far, no mutations in *Gpcs* have been discovered in this form. However, loss-of-function mutations in the X-linked *OFD1* gene can cause SGBS Type II additionally to other syndromes with similar phenotypic features including Oral-facial-digital syndrome and Joubert syndrome (Budny et al., 2006). *OFD1* acts at the distal ends of centrioles and plays a major role in ciliogenesis by recruiting ciliar transport proteins and stabilizing centriolar microtubules (reviewed in Singla, Romaguera-Ros, Garcia-Verdugo, & Reiter, 2010). Consistently, *Ofd1*^{-/-} mice have defects in left-right-patterning due to a lack of primary cilia in the node (Ferrante et al., 2006). Furthermore, SGBS Type II patients show impaired ciliary motility in the lung causing respiratory problems which finally lead to death (Budny et al., 2006).

Collectively, similar congenital abnormalities can be caused either by mutations in *OFD1*, causing impaired ciliogenesis, or by mutations in *GPC3* and *GPC4*. Therefore, the developmental defects observed in *Gpc4*^{-/-} mice might be caused by an impaired function of signaling pathways which require primary cilia, or by impaired primary cilia formation itself.

Hh signaling requires the presence of primary cilia during embryo development (Huangfu et al., 2003). The downstream receptor *Smo* has to undergo lateral movement to the ciliary membrane upon Hh activation (Milenkovic, Scott, & Rohatgi, 2009). Furthermore, the intraflagellar transport proteins, which establish and maintain the primary cilium, are thought to be required for the modulation of the activator to the repressor form of *Glis* in the tip of the primary cilium (Huangfu et al., 2003). To act as a positive modulator of Hh signaling at receiving cells as proposed before, *GPC4* has to be located in close proximity to Hh receptors. Consistent with this requirement, I observed GPC4 protein expression in basal bodies and throughout the cilium in a subset of primary cilia *in vitro*. Therefore, *Gpc4* might

potentially interact with *Ptc* and/or its co-receptor *Boc* to modulate Hh signaling as discussed in the chapter 1.4.2.

Furthermore, I investigated a more general role of *Gpc4* on primary cilia formation *in vivo*. In favor for such a general role is the very broad phenotypic range of *Gpc4*^{-/-} embryos and neural tube closure defects which are hallmarks of ciliopathies (reviewed in Waters & Beales, 2011). However, other characteristics of ciliopathies including a (partial) inversion of visceral organs (*situs inversus*) and polydactyly have not been observed in *Gpc4*^{-/-} mice. Although primary cilia were detected in the node of *Gpc4*^{-/-} embryos, they appeared smaller than in controls. The observed differences could be explained by differences in developmental stages between 1 – 2 hours, indicated by a slightly smaller node structure in *Gpc4*^{-/-} embryos. Therefore, it will be interesting to investigate whether ciliogenesis is affected in better stage-matched *Gpc4*^{-/-} embryos. So far, most described genes causing ciliopathies are coding for intraflagellar transport proteins involved in vesicular trafficking to the primary cilium (reviewed in the introduction and in Waters & Beales, 2011). If defects in ciliogenesis were found upon loss of *Gpc4*, it would be the first identified cell-surface bound protein regulating ciliogenesis.

Taken together, gain-of-function mutations in *GPC4* have been associated to the overgrowth syndrome SGBS Type I, which has been proposed to be caused by a hyper activation of Hh signaling in mice (M. I. Capurro et al., 2008). Furthermore, the only described SGBS patients with CNS defects carried mutations in *GPC4* additionally to *GPC3* (Mujezinovic et al., 2016). Consistently, *Gpc4*^{-/-} mice show severe midline defects and loss of ventral SHH domains reminiscent of impaired Hh signaling in the forebrain. These combined data from mouse and human studies further support the hypothesis that *Gpc4* might act as a positive regulator of Hh signaling during development with strong requirement in the developing anterior forebrain.

3. *Gpc4* is required for early stem cell differentiation

3.1 Limitations of early *Gpc4*^{-/-} embryo analysis

Gpc4^{-/-} embryos showed severe malformations of the early developing forebrain. Although HPE was the most common misdevelopment, other early defects including the truncation of the forebrain were observed. These data suggest that *Gpc4* might also be involved in early forebrain induction. The analysis of early developmental stages of mouse embryos is very challenging. During my project, I encountered four main limitations of early *Gpc4*^{-/-} embryo analysis. First, the litter sizes of the used C57BL/6 inbred mouse strain is typically about half compared to the outbred CD-1 mouse line which is often used for early development analysis (Rennie et al., 2012). Second, C57BL/6 mice are about 30 % smaller than CD-1 mice, making it more difficult to prepare embryos and determine reliably vaginal plugs in females (Kulandavelu et al., 2006). Third, the developmental stage between embryos of the same pregnancy varies naturally. This becomes especially challenging in early development, when embryos with two hours developmental difference become already incomparable. Fourth, due to the broad phenotype expressivity and reduced penetrance, it was not possible to predict potential developmental defects from the genotype of an embryo. Taken together, although many embryos between E7.5 and E8.5 were analyzed, these limitations made a conclusion of early affected signaling pathways of *Gpc4*^{-/-} embryos highly challenging.

3.2 Early brain development is modeled by neural *in vitro* differentiation protocol

To circumvent these limitations, a mouse embryonic stem cell differentiation protocol was optimized which models early neural development *in vitro* (Barberi et al., 2003). In this model, mESCs were co-cultured for one week on MS5 cells, which induced neural fate. Subsequently, neural precursor cells were replated and matured to neurons as a monolayer for another week. Importantly, this protocol mimicked key developmental stages of brain development indicated by the loss of stem cell markers and the progressive upregulation of neural precursor markers and mature neuron markers. The *in vitro* differentiation of mESCs to a specific lineage is usually accompanied by a low rate of non-specific cell types. In my protocol, low expression of the astrocyte marker *Gfap* was observed only after two weeks. Additionally, no expression of endodermal genes and low expression of mesodermal genes was detected. However, due to the more than 128-fold higher expression of neuronal genes compared to non-neuronal markers, the optimized protocol can be considered as highly specific to the neuronal lineage. The expression pattern of the *Gpc* family members was highly diverse during the early neural differentiation suggesting different functions of *Gpcs* in neural fate decision. *Gpc4* mRNA was expressed at intermediate levels in undifferentiated mESCs. During differentiation, the expression was strongly upregulated in neural precursor cells and was downregulated in mature neurons. This

expression pattern is consistent with a previous study, which reported strong *GPC4* expression in primary mouse neural precursor cells, which was downregulated during neural maturation (Hagihara et al., 2000). Strong *Gpc4* mRNA expression was also observed in neural precursor cells of the ventricular and sub ventricular zones but not in differentiated neurons of the developing mouse cortex (Hagihara et al., 2000; Watanabe et al., 1995). Interestingly, we observed a similar expression pattern of *GPC4* in the human developing cortex by RNAseq analysis of single cortical cells as discussed in the chapter 1.4.1. The conserved expression pattern in the human brain suggest that also the function of *Gpc4* is conserved during human brain development.

3.3 *Gpc4* is not required for mESC maintenance

To investigate the role of *Gpc4* during early neural induction, the expression of *Gpc4* in mESCs was downregulated by shRNA below the detection limit of western blot analysis. In the undifferentiated state (in the presence of LIF) sh*Gpc4* mESCs grew more densely packed within single colonies compared to wildtype and shScr control cells. Hence, it was hypothesized, that *Gpc4* might be involved in the regulation of stem cell maintenance or in spontaneous differentiation. However, the expression of stem cell markers including *Oct3/4*, *Nestin* and *Sox2* was not altered in sh*Gpc4* cells. These results are consistent with a previous report, which also did not detect altered gene expression in undifferentiated *Gpc4* knockdown mESCs (Fico et al., 2012).

As discussed in chapter 2.1, gain-of-function mutations in *GPC4* can cause developmental body overgrowth in SGBS (Waterson et al., 2010). Conversely, the loss of *Gpc4* could cause impaired proliferation in sh*Gpc4* mESCs. However, no alteration in proliferation was determined. Furthermore, no differences in cell death were observed. The lack of a strong phenotype in undifferentiated sh*Gpc4* cells might also be explained by functional redundancy of *Gpc6* as the most closely related *Gpc* family member to *Gpc4* (reviewed in Filmus et al., 2008). However, *Gpc6* is not expressed in mESCs. Hence, although *Gpc4* is expressed in mESCs, my data suggest that it does not modulate signaling pathways which are required for the maintenance of embryonic stem cells including proliferation and cell death. The analysis of *Gpc4*^{-/-} mice indicated impaired Hh signaling upon loss of *Gpc4*. However, it has been reported before that although Hh signaling is active in human ESCs (hESCs) at basal levels, it is not required for hESC maintenance (Wu, Choo, Yap, & Chan, 2010). Consistently, impaired Hh signaling in sh*Gpc4* cells would not cause defects in this state as the activity of this pathway is not required. In summary, these results suggest that *Gpc4* is dispensable for stem cell maintenance.

3.4 *Gpc4* is required for early mESC differentiation

Although stem cell maintenance was not altered upon loss of *Gpc4*, severe impairment of neural differentiation was observed in shGpc4 cells. Importantly, already the early induction to the neural precursor stage was impaired, indicated by strongly reduced expression of *Nestin* on day 8. One explanation for impaired neural differentiation was a potential developmental delay upon loss of *Gpc4*. To test this hypothesis, cells were differentiated for an additional week. Also after two weeks, no increase in neural precursors was observed. Consistently, both shGpc4 lines lacked almost completely mature neurons. Therefore, it was concluded that the loss of *Gpc4* did not lead to a delay of neural developmental. Alternatively, the impaired function of *Gpc4* could lead to the differentiation of cell types with a similar, but non-neuronal lineage (e.g. astrocytes) or even to other germ layer(s). However, no increase in astrocyte or non-ectoderm lineage markers was observed. Instead, astrocyte markers and early mesendoderm markers were completely lost in shGpc4 cells compared to control cells. Consistently, stem cell markers remained highly expressed during differentiation in these cells. These results strongly suggest that *Gpc4* might modulate signaling pathways which are generally required to leave the stem cell maintenance state rather than for a specific neural differentiation.

A highly similar phenotype to shGpc4 mESCs has been reported before in *Ext1*^{-/-} mESCs (Kraushaar, Yamaguchi, & Wang, 2010; X. Lin et al., 2000). The *Ext1* gene encodes for the exostosin glycosyltransferase 1, which is mandatory for the biosynthesis of HS GAG chains which are covalently bound also to *Gpc4*. Like shGpc4 mESCs, the loss of *Ext1* in mESC did not affect stem cell marker expression in the presence of LIF indicating that HS GAG chains were dispensable for stem cell maintenance. However, *Ext1*^{-/-} cells completely failed spontaneous differentiation to all three germ layers, kept a dense morphology and retained the expression of stem cell markers. Interestingly, differentiation defects reported in *Ext1*^{-/-} mESCs were more severe than in shGpc4 cells. *Ext1*^{-/-} cells lacked completely differentiation whereas shGpc4 cells showed strongly reduced but still remaining expression levels of neural markers. Hence, even though *Gpc4* might be an important HSPG member, which is required for the exit of the self-renewing stem cell state, it is probably not the only one. Furthermore, because differentiation defects are observed upon loss of HS GAG chains, the GAG chains of *Gpc4* are expected to be essential in the function of *Gpc4* in promoting mESC differentiation. The importance of correct glycosylation in *Gpc4* function will be discussed in the next chapter.

The role of *Gpc4* during mESCs differentiation has been investigated in a recent study (Fico et al., 2012; Fico et al., 2014). As discussed in the previous chapter, no differences in stem cell marker expression were observed in mESCs with downregulated levels of *Gpc4* in the presence of LIF, which is consistent with my results. In contrast to my shGpc4 cells, the reduction of *Gpc4* by a hypomorph *Gpc4* gene-trap allele facilitated differentiation to meso- and ectoderm and suppressed tumorigenic properties of

mESCs (Fico et al., 2012). The authors therefore concluded that *Gpc4* might be required for self-renewal of embryonic and neural stem cells by facilitating canonical Wnt signaling. In a follow-up study of this group, the same mESC line was reported to have a highly specific effect on neuronal subpopulation specification. Reduced levels of *Gpc4* specifically increased the differentiation to ventral midbrain dopaminergic neurons, which are degenerated in Parkinson's disease patients (Fico et al., 2014).

The opposing effects of *Gpc4* knockdown on stem cell differentiation observed in my results and in the previously published data might be explained by differences in *Gpc4* knockdown efficiency. Both of my sh*Gpc4* mESC lines were completely deficient of GPC4 protein, which was below the detection limit of western blot analysis. In contrast, most experiments in the studies of Fico and colleagues were performed with a *Gpc4* gene trap line which showed 30 % residual GPC4 expression (Fico et al., 2012). Similar discrepancies in stem cell maintenance and differentiation phenotypes were also observed in *Ext1*^{-/-} mESCs. As described before, the complete loss of *Ext1* expression retains stem cell markers and prevents differentiation (Kraushaar et al., 2010). In contrast, incomplete knockdown of *Ext1* expression shows the opposite effect of increased spontaneous differentiation (Sasaki et al., 2008).

Considering these results, the functional modulation of cell fate by glycosylated cell-surface proteins might be highly dependent on the abundance of these ECM members. To verify this hypothesis for *Gpc4*, the heterogeneous *Gpc4* knockdown population was analyzed before selecting single sh*Gpc4* clones. In this cell population, GPC4 protein expression was reduced to 16 %. However, neural differentiation efficiency was only marginally reduced to about 90 % compared to about 5 % in the two sh*Gpc4* clones. Therefore, it might be possible that the signaling pathways which regulate the balance between self-renewal and differentiation are modulated differently in complete- and residually-expressing *Gpc4* mESCs, leading to the observed discrepancies in the phenotypes.

Importantly, this level of regulation seems also be conserved *in vivo*. It has been shown before in *Gpc4* knockdown experiments in *Xenopus* that the severity of developmental defects strongly depends on the *Gpc4* knockdown efficiency (Galli et al., 2003). Furthermore, remaining *Gpc4* expression might also explain why no brain defects were observed in hypomorph *Gpc4*^{LacZ} mice (Jen et al., 2009).

This regulation step might also be conserved in human stem cells. In a recent study, *GPC4* was suggested to be required for the differentiation to astrocytes, but not to neurons (Oikari et al., 2016). Also in this study, *GPC4* mRNA expression was only downregulated to 30 %. Hence, also the difference to these results might be explained by different levels of *Gpc4* expression. However, it cannot be excluded that *GPC4* might also have additional or other function in humans compared to mice.

3.5 Released GPC4 does not rescue defects which are caused by the loss of *Gpc4*

To rescue the impaired neural differentiation of sh*Gpc4* mESCs, several strategies were pursued. *Gpc4* could be strongly overexpressed and detected on the protein level in human embryonic kidney cells (HEK) and neuroblastoma (N2a) cells. In mESCs, high levels of *EF1a* promoter-driven *Gpc4* mRNA expression was observed. However, no overexpression of the GPC4 protein could be detected. Interestingly, I also did not achieve overexpression of *GPC4* in human neural stem cells. The underlying reason for this cell line difference remains unclear. One possibility could be that the overexpression of *Gpc4* in stem cells leads to cell death, whereby *Gpc4* overexpressing cells would be lost in the analyzed cell lysate. However, no increased cell death was observed after *Gpc4* transduction. Interestingly, Fico and colleagues could rescue their observed phenotype in mESCs by *Actin*-driven *Gpc4* expression. However, rescued *Gpc4* expression levels were only reported on mRNA levels but not on protein levels (Fico et al., 2012).

To circumvent this limitation, a mutant form of GPC4 was overexpressed in HEK cells which carried an HA-Tag at the extracellular N-terminus and a destroyed GPI-anchor site at the C-terminus leading to the release of GPC4 to the medium. Although the conditioned medium contained high amounts of the 37 kDa GPC4 fragment, it did not rescue neural differentiation defects of sh*Gpc4* mESCs. Several possibilities might cause this observation. One explanation could be that the overexpressed GPC4 was not active. This could either be caused by the N-terminal HA-tag of GPC4 or by the cleavage of the full-length protein leading only to the 37 kDa N-terminal fragment in conditioned medium. Because an N-terminal HA-tag did not impair rescue activity of *dlp* in *Drosophila*, defects in tagged mouse GPC4 seems unlikely (Williams et al., 2010). Furthermore, it has been shown before, that cleaved and full-length GPC4 have different protein binding characteristics (Ko et al., 2015). However, also in wildtype mESCs only the N-terminal fragment of GPC4 is detected, suggesting that the 37 kDa fragment might be the most relevant form of GPC4 in mESCs. Another possibility might be an inadequate glycosylation state of the overexpressed GPC4. The HS GAG chain composition changes enormously during differentiation and becomes increasingly sulfated in a lineage-specific manner (Hirano et al., 2012; Johnson et al., 2007; Nairn et al., 2007). Therefore, GPC4 which is produced in HEK cells might carry inadequately modified HS chains. Furthermore, neural differentiation might require a constant adaptation of HS chain composition due to changing responses to different signaling pathways. A wrong sugar code might therefore lead to a non-functional GPC4 protein. To prevent this potential limitation in the future, GPC4 could be overexpressed in the immortalized neural precursor cell line TSM (Chun & Jaenisch, 1996). These cells are thought to provide a biosynthetic background similar to the ventricular zone of the developing cortex (Hagihara et al., 2000; Hecht, Weiner, Post, & Chun, 1996; Weiner, Hecht, & Chun, 1998).

Assuming that GPC4 acts as a co-receptor, it is very likely that GPC4 needs to be cell-surface anchored for its function during stem cell differentiation. Consistent with this hypothesis, it was reported in different studies that *Drosophila dlp* acts on Hh signaling-receiving cells and that membrane tethering of *dlp* is required for this function (Desbordes & Sanson, 2003; Gallet et al., 2008; Williams et al., 2010). Whether GPC4 specifically requires the GPI-anchor or if a general tethering on the cell surface is sufficient, remains unclear (Gallet et al., 2008; Williams et al., 2010). Independent of that, non-anchored GPC4 would lack the close proximity to its modulated signaling pathway receptors, and would therefore not be functional to rescue shGpc4 defects in differentiating mESCs. To test the activity of different GPC4 forms, a direct readout for recombinant GPC4 function would be required. Importantly, also the reintroduction of *Gpc4* in acutely knocked-down MEFs did not rescue impaired Hh signaling. To exclude potential effects of the N-terminal HA-Tag of GPC4, an untagged wildtype form was overexpressed, but also showed no rescue ability. In contrast to my results, Hh activity in *Drosophila* cell culture was rescued by the overexpression *dlp*, also with an N-terminally tagged form of *dlp* (Williams et al., 2010). In my rescue experiments, *Gpc4* mRNA was about 2.5 fold upregulated compared to endogenous expression levels. It has been reported in *Drosophila* that the Hh co-receptor *lhog* has biphasic activity depending on its expression level (Yan et al., 2010). Hence, too much or too little *lhog* expression leads to reduced Hh signaling *in vitro* and *in vivo* (Yan et al., 2010). To investigate if this effect might also be true for *Gpc4*, intermediate overexpression levels of GPC4 should be tested to rescue impaired Hh signaling upon *Gpc4* knockdown.

3.6 Impaired Hh signaling does not cause differentiation defects in shGpc4 mESCs

The analysis of *Gpc4*^{-/-} embryos suggested that impaired Hh- and Fgf signaling cause brain defects during different stages of development. To verify the role of *Gpc4* as a positive Hh modulator in an additional model, the Hh response in differentiating mESCs was investigated. Consistent with my previous results in mice and functional Hh experiments, differentiating shGpc4 cells showed strongly impaired Hh signaling response during neural differentiation. Hence, also these results support the potential role of *Gpc4* as a positive Hh modulator in mammals. However, as discussed in chapter 3.4, shGpc4 strongly retained stem cell fate and showed impaired differentiation to neural precursor cells. Hence, decreased Hh response of shGpc4 cells might be a secondary effect of alternative cell identity caused by impaired differentiation which could lead to a different set up of signaling pathway members. To address this hypothesis, *Ptc* expression of non-Hh-stimulated cells was analyzed but was not altered in shGpc4 cells. These data suggest that impaired Hh signaling in shGpc4 cells is not caused by differences in *Ptc* abundancy. However, other Hh signaling pathway members might be differently expressed in stem cell-like shGpc4 cells and differentiating neural precursor control cells and therefore

cause impaired Hh signaling. To exclude potential differences in Hh response due to differences in cell identity, the downstream activity of SHH-stimulated mESCs and differentiating cells could be compared side by side. However, because the cell identity changes continuously during differentiation, Hh signaling responsiveness might already change during the two days of SHH stimulation.

As discussed before in chapter 3.3, Hh signaling is not required for stem cell maintenance in hESCs (Wu et al., 2010). To analyze the role of Hh signaling during neural differentiation in my model, the neural differentiation efficiency after Hh activity modulation was analyzed. Neither the stimulation of Hh signaling, nor its inhibition affected the expression of neuronal markers in control cells. These data suggest that although the activation of the Hh signaling pathway is impaired in shGpc4 cells, this defect might not be the main cause for the observed differentiation defects. Consistent with these results, Hh signaling is thought to be required for forebrain patterning rather than for its early induction (reviewed in Andoniadou & Martinez-Barbera, 2013). Accordingly, the stimulation of Hh signaling has been used to induce ventral fate during neural stem cell differentiation rather than for a general neural induction (Barberi et al., 2003; Kriks et al., 2011).

3.7 Impaired Fgf signaling in shGpc4 mESCs might cause differentiation defects

The defects in Hh activity observed in shGpc4 cells most likely do not explain their impaired ability to differentiate to neurons. To identify the signaling pathways which are required for neural differentiation in my model, wild-type mESCs were treated with inhibitors of different signaling pathways.

The inhibition of Wnt signaling was expected to increase neural differentiation as Wnt signaling has been suggested to maintain pluripotency in mESCs and to prevent neuronal differentiation (Aubert, Dunstan, Chambers, & Smith, 2002; Fico et al., 2012). However, no differences in the neural population were observed upon inhibition of Wnt signaling. This could be due to a saturated neural differentiation by the co-culture on MS5 cells. Another explanation could be that the analysis of B3 TUBULIN stainings as a readout might not be sensitive enough to identify small changes of neural differentiation. However, according to the previously reported role in stem cell maintenance, differentiation defects of shGpc4 defects would be caused by increased Wnt signaling. This would require that *Gpc4* acts as a negative modulator of Wnt signaling. Because so far *Gpc4* has only been reported to positively modulate Wnt signaling, it seems very unlikely that shGpc4 defects result from increased Wnt signaling (Ohkawara et al., 2003; Sakane et al., 2012).

In contrast to the inhibition of Wnt signaling, the Fgf receptor inhibitor SU5402 almost completely inhibited neural differentiation and thereby phenocopied shGpc4 defects. The role of Fgf signaling in mESCs differentiation has been investigated in several studies (Kraushaar et al., 2010; Kunath et al.,

2007) (reviewed in Chuang, Tung et al. 2015). *FGF4*-induced activation of *Erk1/2* promotes mESC differentiation by facilitating the exit from the self-renewing state (Kunath et al., 2007). Consistently, *Fgf4*^{-/-} and *Erk2*^{-/-} mESCs retain pluripotency and fail to differentiate to meso- or endoderm (Kunath et al., 2007). Furthermore, it was reported that *Fgf1*, *Fgf2* and *Fgf4* were able to enhance neurogenesis of mESCs (C. W. Chen et al., 2010). These findings suggest that Fgf signaling plays not only an important role in neural differentiation but generally controls the exit from the self-renewal state of mESCs. Importantly, also shGpc4 cells showed not only impaired differentiation to neuroectoderm. Also low amounts of non-specific mesoderm differentiation observed in control cells were lost in shGpc4 cells. These results strongly support the hypothesis that *Gpc4* is required for the exit of the self-renewal state by positively modulating Fgf signaling. Because differentiation defects in shGpc4 cells were less severe than in *Fgf4*^{-/-} or *Erk2*^{-/-} cells, *Gpc4* seems to be an important but not the only modulator of Fgf signaling in mESCs.

Interestingly, there is a strong link between Fgf-mediated differentiation and HS GAG chains. It was shown recently, that HS chains are mandatory for Fgf-mediated differentiation (Kraushaar et al., 2010). Like the loss-of-function of *Erk2* and *Fgf4*, *Ext*^{-/-} mESCs fail to exit the self-renewal state and therefore do not differentiate as discussed in chapter 3.4 (Kraushaar et al., 2010; Kunath et al., 2007).

These data suggest that the GAG chains of *Gpc4* might play an important role in the modulation of Fgf-mediated differentiation. Accordingly, it was reported that recombinant GPC4 binds to FGF2 (bFGF) in a GAG chain dependent manner (Hagihara et al., 2000). Importantly, an impairment of bFGF-stimulated proliferation of neural precursor in shGpc4 cells might explain, why differentiation defects are more pronounced in the second week of differentiation and therefore after bFGF stimulation.

To confirm impaired Fgf signaling in shGpc4 cells, it would be interesting to measure the phosphorylation levels of *Erk1/2* as a readout for downstream Fgf activity in shGpc4 mESCs. Furthermore, it would be exciting to activate the Fgf signaling pathway in shGpc4 mESCs and thereby potentially rescue the observed differentiation defects. Because signaling on the cell surface is expected to be impaired by the loss of *Gpc4*, the Fgf pathway could be stimulated downstream of *Erk2* by E-2-benzylidene-3-(cyclohexylamino)-2,3-dihydro-1H-inden-1-one (BCI) (Molina et al., 2009). The rescue with BCI would prove that the loss of function of *Gpc4* impairs Fgf-mediated neural differentiation.

4. Conclusion

The development of the mammalian brain requires a tight regulation of different signaling pathways, which have been described to be modulated by *Gpc4* orthologues in non-mammals. Hence, the loss of *Gpc4* orthologues impairs various developmental processes which causes severe misdevelopment of the brain and other organs. In *Gpc4*-deficient zebrafish embryos, variable forms of cyclopia were observed whereas forebrain truncations were reported upon downregulation of *Gpc4* in *Xenopus* embryos (Galli et al., 2003; Topczewski et al., 2001).

In my PhD project, I confirmed the previously reported expression pattern of *Gpc4* specifically in the developing anterior brain of mice. Accordingly, *Gpc4*^{-/-} mice showed severe malformations of the developing brain which were highly similar to the brain defects reported in non-mammals – including HPE and forebrain truncations. These results confirm a highly conserved and essential role of *Gpc4* also during mammalian brain development.

My analysis of *Gpc4*^{-/-} mouse embryos and differentiating *Gpc4* knockdown mESCs strongly suggests that *Gpc4* positively modulates the Hh- and Fgf signaling pathways during different stages of mouse forebrain development. These insights are summarized in a working model of *Gpc4* during brain development (Fig 46). During very early brain development, *Gpc4* might regulate Fgf signaling during the induction of the anterior neural plate. This hypothesis is strongly supported by forebrain truncations of *Gpc4*^{-/-} embryos and impaired neural induction in mESCs, which was phenocopied by Fgf inhibition. At a later stage, *Gpc4* is involved in the separation of the forebrain into two cortical hemispheres. During this process, *Gpc4* might modulate Hh signaling, presumably together with the positive Hh modulator *Boc*. Consequently, the loss of *Gpc4* can cause HPE and anteriorly truncated SHH domains in embryos as well as impaired Hh signaling activity *in vitro*.

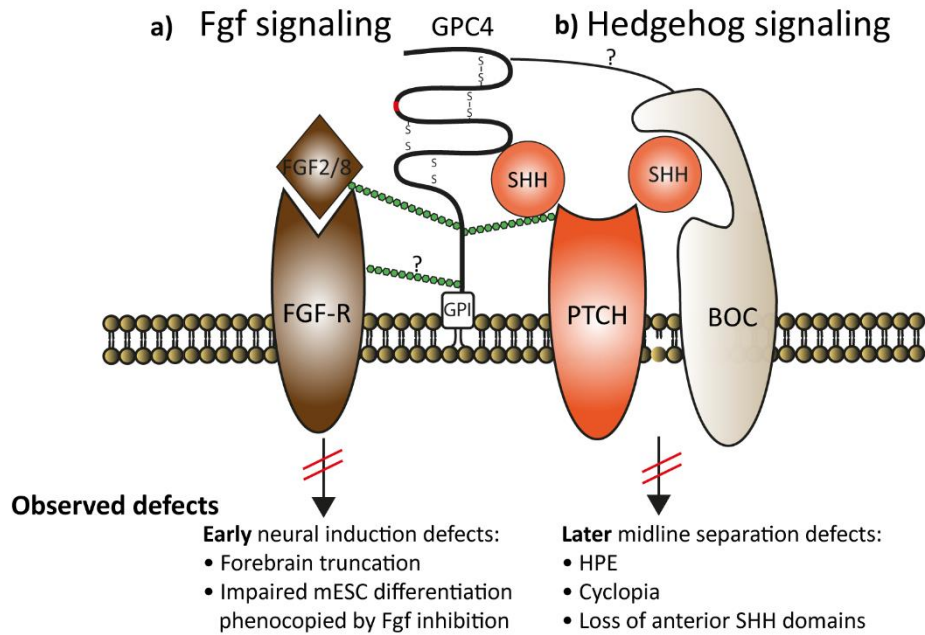


Figure 46 Working model of *Gpc4* during forebrain development. a) During early forebrain induction, *Gpc4* might positively regulate Fgf signaling. GPC4 binds to FGF2 and might also interact with FGF8 and the Fgf-receptor (Hagihara et al., 2000). Consequently, the loss of *Gpc4* might cause impaired Fgf signaling resulting in forebrain truncation. This role is supported by impaired differentiation of *Gpc4* knockdown mESCs, which is phenocopied by Fgf inhibition. b) During later forebrain separation into two cortical hemispheres, *Gpc4* seems to control Hh signaling. The loss of *Gpc4* causes HPE with cyclopia and a loss of anterior SHH domains. Furthermore, *Gpc4* orthologues can bind to SHH and PTC and boost their endocytosis (Yan et al., 2010). The positive Hh modulator BOC binds to PTC and stabilizes SHH on the cell surface (B. L. Allen et al., 2011). Due to a strong co-expression of GPC4 with BOC in the human developing cortex, these modulators might interact to positively regulate Hh signaling.

In the discussion, I suggested several experiments to further investigate the role of *Gpc4* during brain development. Out of these, the following three approaches appear to be the most relevant:

First, the role of *Gpc4* in Fgf and Hh signaling should be investigated in more detail *in vitro*. Impaired Fgf signaling in sh*Gpc4* mESCs might be rescued by BCI, which would strongly support the hypothesis that defects in Fgf signaling cause forebrain truncations in *Gpc4*^{-/-} embryos. Furthermore, the interaction between *Gpc4* and *Boc* should be studied. If *Gpc4* regulated Hh signaling indirectly by the modulation of *Boc*, these results would establish a new level of indirect Hh signaling regulation.

Second, impaired Fgf and Hh signaling should be confirmed in early *Gpc4*^{-/-} embryos. These experiments will require a high penetrance and low variability of the *Gpc4*^{-/-} phenotype, which might be achieved by the administration of low doses of ethanol during pregnancy. Only a stable early phenotype offers the possibility to analyze the localization and activity of early signaling centers and therefore affected pathways.

Third, the role of *Gpc4* as a potential mediator between diabetes in mothers and HPE in embryos should be analyzed. Diabetes in mothers is an environmental risk factor to develop HPE in humans (Barr et al., 1983; Correa et al., 2008; Kousseff, 1999). Importantly, *Gpc4* seems to have a crucial role in both of these defects, by sensitizing insulin signaling and by modulating forebrain development (Ussar et al., 2012). To investigate a functional connection between diabetes and HPE in *Gpc4*^{-/-} mice, *Gpc4*^{-/-} mothers should be investigated for diabetes hallmarks.

In my project, I showed that the extracellular matrix protein *Gpc4* plays an important role during mouse forebrain development. Due to a conserved expression pattern in the human developing cortex, a similar function of *GPC4* in humans is very likely. Although *GPC4* loss-of-function mutations in the rare SGB-Syndrome might have minor impact on our society, impaired *GPC4* function might play a central role in diabetes-mediated developmental malformations. Regarding the exponential growth of diabetes in our modern society, understanding the role of *Gpc4* as a potential mediator of diabetes-induced brain defects might be highly relevant for the future.

IV. Materials and methods

1. Materials

1.1 Equipment

Name	Source
Agilent 2100 Bioanalyzer	Agilent (Santa Clara, USA)
Agarose gel chamber	Midi 450 (Harnischmacher, Kassel, Germany) Typ Mini (neoLab, Heidelberg, Germany)
Spectramax M5	Molecular devices (Sunnyvale, USA)
Cameras	AxioCam MRc5 (Carl Zeiss AG, Göttingen) AxioCam HRm (Carl Zeiss AG, Göttingen)
Centrifuges	5418 R (Eppendorf AG, Hamburg) 5418 (Eppendorf AG, Hamburg) Rotina 420 R (Andreas Hettich GmbH & Co.KG, Tuttlingen, Germany) LSE Mini Microcentrifuge (Corning, Corning, USA) Avanti J-30I (Beckman Coulter, München, Germany)
Cryotome	CM 3050S (Leica, Wetzlar, Germany)
Freezer (-20 °C)	Liebherr Hausgeräte Ochsenhausen GmbH (Ochsenhausen, Germany)
Freezer (-80 °C)	New Brunswick Scientific, (New Brunswick, USA)
Fridge	Liebherr Hausgeräte Ochsenhausen (Ochsenhausen, Germany)
FUSION Xpress System	Peqlab (Erlangen, Germany)
GeneChip Scanner 3000 7G	Affymetrix (Santa Clara, USA)
Heating plate	RCT basic (IKA -Werke GmbH, Staufen)
Ice machine	Ziegra Eismaschine (Isernhagen, Germany)
Incubator	CB 210 (Binder, Neckarsulm, Germany)
Incubation systems/ovens	Shaking incubator; 37 °C bacteria (Shel Lab, Sheldon Manufacturing, Cornelius, USA) TH-30 and SM-30; 32 °C bacteria (Edmund Bühler, Hechingen, Germany) Thermomixer comfort (Eppendorf AG, Hamburg, Germany) Shake'n'Stack (ThermoHybaid, Thermo Fisher Scientific Inc., Waltham, USA)
Microplate reader	Centro LB 960 (Berthold Technologies, Bad Wildbad, Germany)
Microscopes	Zeiss Lumar.V12. MRc5 camera (Carl Zeiss Microscopy, Jena, Germany)

IV. Materials and methods

	Joel JSM-6300F (Tokyo, Japan)
	LSM510 META (Carl Zeiss Microscopy, Jena, Germany)
	Operetta microscope (PerkinElmer, Waltham, USA)
	EVOS FL auto Cell Imaging System (Thermo Fisher Scientific, Rockford, USA)
	TCS SP5 (Leica, Wetzlar, Germany)
	DMIL LED (Leica, Wetzlar, Germany)
	Mirax Desk slide scanner (Carl Zeiss Microscopy, Jena, Germany)
Microwave 700 W	Severin Elektrogeräte (Sundern, Germany)
Nanodrop ND-1000	Thermo Fisher Scientific (Rockford, USA)
Spectrophotometer	
PCR machines	Quantstudio 12k Flex real-time PCR system (Thermo Fisher Scientific, Rockford, USA)
	Mastercycler Nexus Gradient (Eppendorf AG, Hamburg, Germany)
pH meter	pH211 Microprocessor pH Meter (HANNA instruments, Kehl am Rhein, Germany)
Pipetboy	accu-jet and accu-jet pro (Brand GmbH & Co. KG, Wertheim, Germany)
Power supply	PowerPac HC High-Current (Bio-Rad, Hercules, USA)
Sput coater K575	Emitech (Ashford, UK)
Pumps	LABOPORT (neoLab Migge Laborbedarf-Vertriebs GmbH, Heidelberg, Germany)
Roller	Mixer SRT1 (Bibby Scientific (Stuart), Staffordshire, UK)
SHAKER	DOS-10L (neoLab, Heidelberg, Germany)
SkyScan 1172	Bruker SkyScan (Kontich, Belgium)
Stirrer	STIR (VWR international GmbH, Darmstadt, Germany)
Vortexer	Vortex Genie 2 (Scientific Industries, New York, USA)
Water bath	JB Aqua 12 Plus (Grant Instruments, Cambridge, UK)
Western Blot Gel	Mini-PROTEAN Tetra Vertical (Bio-Rad, Hercules, USA)
Electrophoresis chamber	

1.2 Consumables

Name	Source
10 cm bacterial plates	Thermo Fisher Scientific, Rockford, USA
50 ml / 15 ml Falcons	#352070, #352095 (Corning, Coning, USA)
6-well plates cell culture	Nunc (#150288, Thermo Fisher Scientific, Rockford, USA)
6-/ 12-/ 24-/ 48-well plates	#353043 (Corning, Coning, USA)
8-well glass chambers	Sarstedt, Nümbrecht, Germany
96-well plates (straight/conical), nunc	Thermo Fisher Scientific, Rockford, USA
96-well plates Cell Carrier (6005558)	PerkinElmer, Waltham, USA
Cell scraper	Sarstedt, Nümbrecht, Germany
Counting chamber (cells)	Neubauer (LO-Laboroptik GmbH, Friedrichsdorf)
Cover slips	VWR, Radnor, USA
Eppendorf Tubes (1,5 ml / 5 ml), safe-lock	Eppendorf AG, Hamburg, Germany
fat marker	VWR, Radnor, USA
Glass slides (Superfrost Plus)	Thermo Fisher Scientific, Rockford, USA
Glass vials (ISH)	A. Hartenstein
Glassware	Schott-Duran, Mainz, Germany
Nitrogen	Linde AG, München, Germany
Nescofilm	Thermo Fisher Scientific, Rockford, USA
Parafilm	VWR, Radnor, USA
Pipette filter tips	TipOne (Starlab GmbH, Hamburg, Germany)
Pipette tips	Eppendorf AG, Hamburg, Germany
Pipettes (5/10/25/50ml)	Greiner GmbH, Frickenhausen, Germany
Tissue-Tek Oct	VWR, Radnor, USA
WB protein standard	Thermo Fisher Scientific, Rockford, USA
Whatman paper	GE Healthcare, Little Chalfont, UK

1.3 Kits

Name	Source
Affymetrix Mouse Gene ST 2.0 arrays	Affymetrix, Santa Clara, USA
Agilent RNA 6000 Pico Kit	Agilent, Santa Clara, USA
Dual-luciferase assays (E1910)	Promega, Fitchburg, USA
ECL Western Blotting Detection System	GE Healthcare, Little Chalfont, UK

Encore Biotin Module	Nugen, San Carlos, USA
Illustra GFX PCR DNA and Gel Band Purification Kit	GE Healthcare, Little Chalfont, UK
Illustra MicroSpin G-50 Columns	GE Healthcare, Little Chalfont, UK
Ovation PicoSL WTA System V2	Nugen, San Carlos, USA
Pierce BCA Protein Assay Kit	Thermo Fisher Scientific, Rockford, USA
PrimeTime qPCR Assays	Integrated DNA Technologies, San Jose, USA
Q5 Site-directed mutagenesis Kit.	New England Biolabs, Ipswich, USA
QIAGEN Plasmid Maxi Kit	Qiagen, Hilden, Germany
QIAprep Spin Miniprep	Qiagen, Hilden, Germany
QIAshredder	Qiagen, Hilden, Germany
RNeasy Mini Kit	Qiagen, Hilden, Germany
SuperScript III kit	Thermo Fisher Scientific, Rockford, USA
TUNEL (<i>In Situ</i> Cell Death Detection Kit, Fluorescein)	Roche, Basel, Switzerland
Wizard® Genomic DNA Purification Kit	Promega, Fitchburg, USA
Xfect	Takara Bio, Mountain View, USA

1.4 Chemicals

Name	Source
Accutase (A6964)	Sigma-Aldrich, Steinheim, Germany
Acetic acid (glacial)	Sigma-Aldrich, Steinheim, Germany
Acetic Anhydride (A6404)	Sigma-Aldrich, Steinheim, Germany
Acrylamide, 40%	Bio-Rad, Hercules, USA
Agarose	Biozym Scientific GmbH, Hess. Oldendorf
Ammonium peroxodisulfate (APS; A3678-25G)	Carl Roth, Karlsruhe, Germany
Ampicillin (10835269001)	Sigma-Aldrich, Steinheim, Germany
Anti-Digoxigenin-AP Fab fragments	Sigma-Aldrich, Steinheim, Germany
B-27	Thermo Fisher Scientific, Rockford, USA
BCIP	Sigma-Aldrich, Steinheim, Germany
Benzyl Alcohol	Sigma-Aldrich, Steinheim, Germany
Benzyl Benzoate	Sigma-Aldrich, Steinheim, Germany
Blocking reagent (11096176001)	Sigma-Aldrich, Steinheim, Germany
BM purple AP Substrate	Sigma-Aldrich, Steinheim, Germany
BSA (A7030)	Sigma-Aldrich, Steinheim, Germany

IV. Materials and methods

CutSmart Buffer 10x	New England Biolabs, Ipswich, USA
Denhardt's solution (750018)	Thermo Fisher Scientific, Rockford, USA
Diethylpyrocarbonate (DEPC), approx. 97 %	Sigma-Aldrich, Steinheim, Germany
DIG RNA labeling mix (11277073910)	Roche, Basel, Switzerland
Dimethylsulfoxide (DMSO), >99.9 % (D5879)	Sigma-Aldrich, Steinheim, Germany
Dimethylsulfoxide (DMSO), Cell culture (D2650)	Sigma-Aldrich, Steinheim, Germany
Dithiothreitol (DTT; D0632)	Sigma-Aldrich, Steinheim, Germany
DMEM High Glucose (21969-035)	Thermo Fisher Scientific, Rockford, USA
dNTPs	Thermo Fisher Scientific, Rockford, USA
EDTA (0.5 M, pH 8.0)(15575020)	Thermo Fisher Scientific, Rockford, USA
EM microscopy fix (15950)	EMS, Hatfield, USA
Ethanol, EtOH 100 %	Carl Roth, Karlsruhe, Germany
Fast SYBR Green Master Mix 2x	Thermo Fisher Scientific, Rockford, USA
FBS (heat inactivated, 16140071)	Thermo Fisher Scientific, Rockford, USA
FBS mESC approved (16141079)	Thermo Fisher Scientific, Rockford, USA
Fibronectin (FN, F0287)	Sigma-Aldrich, Steinheim, Germany
Formaldehyde 36 %	Sigma-Aldrich, Steinheim, Germany
Formamide (>99,5 %; 6749.1)	Carl Roth, Karlsruhe, Germany
G418 (Geneticin, 50mg/ml) (10131-035)	Thermo Fisher Scientific, Rockford, USA
Gelatine 0.1%	Pan Biotech, Aidenbach, Germany
GeneRuler 100 bp DNA Ladder	Thermo Fisher Scientific, Rockford, USA
GeneRuler 1kb DNA Ladder	Thermo Fisher Scientific, Rockford, USA
Glutaraldehyde (25 %; G6257)	Sigma-Aldrich, Steinheim, Germany
Glycerol (G9891)	Sigma-Aldrich, Steinheim, Germany
Glycine (3908)	Sigma-Aldrich, Steinheim, Germany
H ₂ O ₂ 30 %	Carl Roth, Karlsruhe, Germany
HCl (2 M; T134.1)	Carl Roth, Karlsruhe, Germany
Heparin (9041-08-1)	Sigma-Aldrich, Steinheim, Germany
Herring Sperm (D1815)	Promega, Fitchburg, USA
Isopropanol, 100 %	Merck KGaA, Darmstadt, Germany
Kanamycin (K-1377)	Sigma-Aldrich, Steinheim, Germany
Knockout DMEM (10829-018)	Thermo Fisher Scientific, Rockford, USA
Knockout serum replacement (10828-028)	Thermo Fisher Scientific, Rockford, USA
Laminin (LAM, L2020)	Sigma-Aldrich, Steinheim, Germany

IV. Materials and methods

LB-Agar (244520)	BD, Franklin Lakes, USA
Levamisole (A4341)	Applichem, Gatersleben, Germany
L-glutamine (25030024)	Thermo Fisher Scientific, Rockford, USA
LIF (ESG1107)	Millipore, Schwalbach, Germany
Lugol's solution	Carl Roth, Karlsruhe, Germany
Magnesium chloride (25108.260)	VWR, Radnor, USA
Maleic acid (M0375)	Sigma-Aldrich, Steinheim, Germany
MEMs non-essential amino acids (M7145)	Sigma-Aldrich, Steinheim, Germany
Methanol, MeOH 100 % (34485)	Carl Roth, Karlsruhe, Germany
Milk powder	Carl Roth, Karlsruhe, Germany
Mowiol	Sigma-Aldrich, Steinheim, Germany
N-2 (17502-048)	Thermo Fisher Scientific, Rockford, USA
NBT	Sigma-Aldrich, Steinheim, Germany
Neurobasal	Thermo Fisher Scientific, Rockford, USA
Paraformaldehyde 16% (43368.9M)	VWR, Radnor, USA
PBS (cell culture)	Thermo Fisher Scientific, Rockford, USA
Penicillin/Streptomycin	Thermo Fisher Scientific, Rockford, USA
Polyornithin (PO, P3655)	Sigma-Aldrich, Steinheim, Germany
Polyvinylalcohol (PVA, A2255)	Applichem, Gatersleben, Germany
Protease inhibitor cocktail, 1 × Complete	Roche, Basel, Switzerland
Proteinase K	Roche, Basel, Switzerland
Puromycin (P8833)	Sigma-Aldrich, Steinheim, Germany
RNaseZAP	Sigma-Aldrich, Steinheim, Germany
RNAasin (RNAse inhibitor) (03335399001)	Roche, Basel, Switzerland
Serum goat (NGS) (16210-072)	Thermo Fisher Scientific, Rockford, USA
Serum Sheep (S-2263)	Sigma-Aldrich, Steinheim, Germany
SHH, C24II, human (130-095-727)	Miltenyi Biotec, Bergisch Gladbach, Germany
SOC medium	New England Biolabs, Ipswich, USA
Sodium Azid (NaN ₃)	Sigma-Aldrich, Steinheim, Germany
Sodium chloride (NaCl, 3957)	Sigma-Aldrich, Steinheim, Germany
Sodium citrate	Sigma-Aldrich, Steinheim, Germany
Sodium desoxycholate (97 %)	Sigma-Aldrich, Steinheim, Germany
Sodiumdodecylsulphate (SDS, N071.1)	Carl Roth, Karlsruhe, Germany
Sucrose	VWR, Radnor, USA

SYBR Safe DNA Gel Stain 1x	Thermo Fisher Scientific, Rockford, USA
Taqman Fast Advanced Mastermix	Thermo Fisher Scientific, Rockford, USA
TEMED (2367.3)	Carl Roth, Karlsruhe, Germany
Triethanolamine (TEA, A5932)	Applichem, Gatersleben, Germany
Tris Base (4855)	Carl Roth, Karlsruhe, Germany
Tri-sodium-citrat (>99 %, 3580.2)	Carl Roth, Karlsruhe, Germany
Triton X-100 (Roth)	Carl Roth, Karlsruhe, Germany
tRNA (Yeast extract, R8759)	Sigma-Aldrich, Steinheim, Germany
Trypsin-EDTA 0.25 %	Thermo Fisher Scientific, Rockford, USA
TWEEN-20 (P2287)	Sigma-Aldrich, Steinheim, Germany
β -mercaptoethanol (14.3 M)	Thermo Fisher Scientific, Rockford, USA
β -mercaptoethanol (cell culture, 55 mM, 21985-023)	Thermo Fisher Scientific, Rockford, USA
X-gal	Thermo Fisher Scientific, Rockford, USA

1.5 Buffers and solutions

Immunostainings

Pearmeabilization and staining buffer (sections) 1 % BSA, 0.2 % Triton X-100 in PBS

Pearmeabilization buffer (cells) 0.5 % BSA, 0.3 % Triton X-100 in PBS

Staining buffer (cells) 1 % BSA in PBS

In situ

10% PVA 20 g PVA powder, 200 ml H₂O MilliQ, Heat at 180 °C on hot plate while stirring until clear. Do not allow to boil, for 200ml

20 x SSC 175 g NaCl, 88.2 g Sodium citrate, adjust pH 7.0, Fill up to 1 l with H₂O_{DEPC}, for 1 l

50% Formamide, 5x SSC 100 ml Formamide, 50 ml 20x SSC, 50 ml H₂O MilliQ, for 200ml

Acetylation solution 5.32 ml Triethanolamine (TEA)(viscous), 0.64 ml Concentrated HCl (mix before adding AcA), 1 ml Acetic Anhydride (add AcA just before using), Fill up to 400 ml with H₂O_{DEPC}, for 400 ml, fume hood, prepare fresh

IV. Materials and methods

anti-DIG antibody mix	Anti-Digoxigenin-AP Fab fragments (1:2500) in Buffer 1 + 10% heat inactivated goat serum, prepare fresh
Blocking solution	10 ml NGS in 100 ml of Buffer 1, Store at -20 °C, for 100 ml
Buffer 1	100 ml 1 M Tris-HCl pH 7.5, 37.5 ml 4 M NaCl, Fill up to 1 l with MilliQ H ₂ O
Fixative solution	44.44 ml 36% formaldehyde, 40 ml PBS _{DEPC} , Fill up to 400ml with H ₂ O _{DEPC} , fume hood, for 400 ml, prepare fresh
NTMT 2x	25 ml 4 M NaCl, 100 ml 1 M Tris-HCl pH 9.5, 50 ml 1 M MgCl ₂ , 10 ml 10 % Tween-20, 315 ml H ₂ O MilliQ, for 500 ml
Prehybridization buffer	50ml: 25 ml Formamide, 12.5 ml 20x SSC, 1.25 ml tRNA (10mg/ml), 2.5 ml 100x Denhardt's solution, 2.5 ml 500 mg / ml Herring Sperm, 6.25 ml H ₂ O _{DEPC}
Staining solution	3.5 µl NBT, 3.5 µl BCIP, in 1:1 mix of 2x NTMT and 10 % PVA solution, for 1 ml, prepare fresh

Western Blot

1 x Transfer Buffer	Dissolve 6.06 g Tris base, 28.83 g Glycine, 400 ml 100 % MeOH in 2 l H ₂ O
10 % APS	Dissolve 5 g Ammonium peroxodisulfate powder in 45 ml H ₂ O, store aliquots at -20 °C
10 x TBS(-T)	Dissolve 60.3 g Tris base, 87.66 g NaCl in 1l H ₂ O
4x SDS Loading Buffer	Dissolve 0.4 g SDS, 900 µl 5 M DTT, 2 ml Glycerol, 2 ml 0.5 M Tris, spoon tip of Bromphenol Blue, pH: 6.8 in 5 ml H ₂ O
5 x Running Buffer	Dissolve 15.1 g Tris base, 72 g Glycine, 5 g SDS in 1l H ₂ O
Blocking solution	Dissolve 5 g milk powder in 100 ml TBS-T
ECL solution	Mix A and B solution 1:1 just before usage
Harsh stripping buffer	Dissolve 20 ml SDS 10%, 12.5 ml Tris HCl pH 6.8 0.5M, 67.5 ml MilliQ H ₂ O, 0.8 ml 14.5M β-mercaptoethanol in 100 ml H ₂ O
RIPA buffer	150 mM sodium chloride, 1.0 % Igepal (NP-40), 0.5 % sodium deoxycholate, 0.1 % sodium dodecyl sulfate (SDS), 50mM Tris, pH 8.0; add freshly protease inhibitor

Whole mount immunostainings

BABB	33% Benzyl Alcohol, 66 % Benzyl Benzoate (in 50ml Falcon)
Blocking Solution	5 % heat-inactivated normal horse serum (NHS), 75 % PBS, 20 % DMSO
Dent's Bleach	33 % H ₂ O ₂ , 66 % Dent's Fix
Dent's Fix	20 % DMSO, 80 % MeOH

Lac-Z staining

Lac-Z staining solution	PBS containing 0.02 % NP-40, 2 mM MgCl ₂ , 5 mM K ₃ [Fe(CN) ₆], 5 mM K ₄ [Fe(CN) ₆]x6H ₂ O, 0.01 % sodium deoxycholate, 1 mg/ml X-gal)
Washing buffer	0.02 % NP-40 in PBS

1.6 Enzymes

Name	Source
DNase I (RNase-free) (04716728001)	Roche, Basel, Switzerland
MyTaq polymerase	Bioline, Luckenwalde, Germany
Restriction Enzyme HindIII-HF	New England Biolabs, Ipswich, USA
Restriction Enzyme Sall	New England Biolabs, Ipswich, USA
RNA Polymerase T3 (11031163001)	Roche, Basel, Switzerland
RNA Polymerase T7 (10881767001)	Roche, Basel, Switzerland
α-Dig Alkaline Phosphatase	Sigma-Aldrich, Steinheim, Germany

1.7 Software

Name	Source
Affymetrix Expression console v.1.4.1.46	Affymetrix, Santa Clara, USA
Bioconductor v. 2.6	https://www.bioconductor.org/
CARMAweb v. 1.5.18	https://carmaweb.genome.tugraz.at/carma/
GePS	Genomatix, Germany
GraphPad Prism 5.0	GraphPad Software, La Jolla, USA
Harmony	PerkinElmer, Waltham, USA
ImageJ v.1.47	https://imagej.nih.gov/ij/
Ingenuity Pathway Analysis	Qiagen, Hilden, Germany
Quantstudio Software	Thermo Fisher Scientific, Rockford, USA
R v. 2.11.0	https://cran.r-project.org/bin/windows/base/old/2.11.0/
SkyScan NRECON software suite	Bruker SkyScan, Kontich, Belgium
SoftmaxPro 7	Molecular Devices, Sunnyvale, USA
Vector NTI	Thermo Fisher Scientific, Rockford, USA

1.8 Primary antibodies

Name	Species	Dilution WB	Dilution IC	Source
Arl13b (17711-1-AP)	rabbit polyclonal		1:1000	Proteintech
Gpc4	rabbit polyclonal	1:1000		Gift from Dr. Ussar, Helmholtz Zentrum München
HA-Tag (901502)	mouse IgG1		1:100	Biolegend
Map2 (M9942)	mouse IgG1		1:1000	Sigma-Aldrich
Oct3/4 (036SC-5279)	mouse IgG2b		1:200	Santa Cruz
Shh (SC9024)	rabbit polyclonal		1:200	Santa Cruz
B Actin (GTX26276)	mouse IgG1	1:10.000		GeneTex
B3 Tubulin (MMS-435P)	mouse IgG2a		1:1000	Biolegend

1.9 Secondary antibodies

Name	Conjugate	Dilution WB	Dilution IC	Company
goat anti-mouse IgG (H+L)	HRP	1:2500		Sigma
rabbit anti-goat IgG (H+L)	HRP	1:2500		Sigma
goat anti-rabbit IgG (H+L)	HRP	1:2500		Jackson Labs
donkey anti-mouse IgG 488 (H+L)	fluorescent		1:500	Molecular Probes
donkey anti-mouse IgG 555 (H+L)	fluorescent		1:500	Molecular Probes
donkey anti-goat IgG 488 (H+L)	fluorescent		1:500	Molecular Probes
donkey anti-goat IgG 555 (H+L)	fluorescent		1:500	Molecular Probes
donkey anti-rabbit IgG 488 (H+L)	fluorescent		1:500	Molecular Probes
donkey anti-rabbit IgG 555 (H+L)	fluorescent		1:500	Molecular Probes

1.10 Bacteria and bacteria culture media

Bacteria

NEB 5-alpha Competent *E. coli* NEB

IV. Materials and methods

Bacteria culture media

Ampicillin:	dissolve 1 g Ampicillin powder in 10 ml H ₂ O (final conc. 100 mg/ml), sterile filtration, prepare 1 ml aliquots and store at -20 °C
LB-Agar:	dissolve 16 g in 400 ml H ₂ O, boil for 1 min until it is completely dissolved, autoclave and store at RT or 4 °C
LB-Agar-plates:	cook LB-Agar in the microwave, cool down to 50 – 55 °C, add antibiotics, fill Agar into 10 cm dishes and store at 4 °C
LB-Medium:	dissolve 10 g Tryptone, 10 g Yeast extract, 5 g NaCl in 1 l H ₂ O, autoclave and store on 4 °C

1.11 Eukaryotic cell lines and cell media

Eukaryotic cell lines

E14tg2a	mouse embryonic stem cells, (ATCC, CRL-1821)
Primary MEFs	primary mouse embryonic fibroblasts isolated on E13.5
HEK293T	human embryonic kidney cells
MS5	mouse stromal cell line, gift from Dr. Studer, Sloan Kettering Institute, New York, USA
HEK293T-SHH-N	HEK293T cells with stable secretion of SHH-N, gift from Dr. Uhmman, University of Göttingen, Germany
Light II NIH-3T3	NIH-3T3 MEFs with stable insertion of Hedgehog Luciferase reporter and Renilla (Taipale et al., 2000), gift from Dr. Uhmman, University of Göttingen, Germany

Eukaryotic cell culture media

Conditioned SHH	HEK293T-SHH-N or control line conditioned medium 1:1 dilution with MEF stimulation medium
Freezing medium	10 % DMSO, 30 % FBS, 60 % cell line specific medium
KSR	Knockout DMEM, 15 % Knockout serum replacement, 2x Pen/Strep, 1x L-Glutamine, 1x MEM Non-Essential Amino Acids, 10 µM β-Mercaptoethanol
Light II maintenance	DMEM High Glucose 10 % FCS 1 % Pen/Strep, 0.4 mg/ml G-418 and 0.15 mg/ml Zeocin
MEF & HEK	DMEM High Glucose, 10 % heat-inactivated FBS, 1x Pen/Strep, 1x L-Glutamine

MEF starvation	DMEM High Glucose, 0.5 % heat-inactivated FBS, 1x Pen/Strep, 1x L-Glutamine
MEF stimulation	DMEM High Glucose, 2 % heat-inactivated FBS, 1x Pen/Strep, 1x L-Glutamine supplemented with 500 ng/ml C24II human SHH or control vehicle
mESC	DMEM High Glucose, 15 % mESC approved FBS, 2x Pen/Strep, 1x L-Glutamine, 1x MEM Non-Essential Amino Acids, 100 μ M β -Mercaptoethanol, 1000 Units/ml medium LIF
MS5	Alpha-Mem, 10 % heat-inactivated FBS, 1x Pen/Strep
N2-B-27	Neurobasal, 1x N2, 1x B-27, 1x L-Glutamine

1.12 Mouse lines

BALB/C	inbred strain (Helmholtz Zentrum München)
C57BL/6N	inbred strain (Helmholtz Zentrum München)
CD-1	outbred strain (Helmholtz Zentrum München)
<i>Tg(pPGKneobpA)3Ems/J</i> ; C57BL/6J background	inbred strain (Helmholtz Zentrum München)
<i>Tg(CAG-Flpe)2Arte</i> ; C57BL/6 background	inbred strain (Helmholtz Zentrum München)
<i>Gt(ROSA)26Sor^{tm16(cre)Arte}</i> ; C57BL/6NTac background	inbred strain (Helmholtz Zentrum München)
<i>Tg(GBS-GFP)</i> ; FVB/N background	gift from Prof. Lickert, Helmholtz Zentrum München, created by (Balaskas et al., 2012)

2. Methods

2.1 Embryology

2.1.1 Ethics statement

Animals were handled and housed according to the German Federal guidelines for the use and care of laboratory animals. All experimental procedures were approved by the Helmholtz Zentrum München Institutional Animal Care and Use Committee and conducted in adherence to the guidelines of the Regierung von Oberbayern.

2.1.2 Husbandry and matings

Mice were kept in a day-night cycle (06.00 – 18:00). To determine the embryonic stages, animals were put together in the afternoon. The next morning, female mice were checked for the presence of a vaginal plug. Noon of the day of the plug was considered as embryonic day 0.5 (E0.5).

2.1.3 Generation of *Gpc4* loss-of-function mice

Gpc4 loss-of-function mice were created in collaboration with EUCOMM, Munich, Germany. If not indicated otherwise, all mouse lines were kept on a C57BL/6N background. *Gpc4* loss-of-function mice were created using the EUCOMM knockout-first conditional vector allele, clone EPD0430_5_E03, which targets Exon 3 (Skarnes et al., 2011). Transgenic mESCs (JM8A3.N1 agouti) were injected in BALB/C donor blastocysts and reimplanted in BALB/C carrier females. One chimeric male with 90 % chimerism was born. This male was mated with wildtype C57BL/6N females to establish the *Gpc4* knockout-first mouse line (*Gpc4*^{tm1a(EUCOMM)Wtsi} allele). The line was further crossed with *Gt(ROSA)26Sor*^{tm16(cre)Arte} transgenic mice for *Cre*-mediated removal of Exon 3 (*Gpc4*^{tm1b(EUCOMM)Wtsi} allele). Out of 51 animals, one hemizygous knockout male reached the adult stage and was fertile. This animal was backcrossed with wildtype C57BL/6N females to remove the *Cre* allele. After the complete loss of GPC4 protein was confirmed, the *Gpc4*^{tm1b(EUCOMM)Wtsi} mouse line was referred to as *Gpc4*^{-/-}. To exclude potential effects of the remaining *LacZ* cassette on the *Gpc4*^{tm1b(EUCOMM)Wtsi} allele, another *Gpc4* loss-of-function line was generated. Hence, the *Gpc4* knockout-first line (*Gpc4*^{tm1a(EUCOMM)Wtsi} allele) was crossed with the *Tg(CAG-Flpe)2Arte* line to remove the *LacZ* cassette (*Gpc4*^{tm1c(EUCOMM)Wtsi} allele). The resulting animals were subsequent crossed with *Gt(ROSA)26Sor*^{tm16(cre)Arte} mice leading to the removal of *Gpc4* Exon 3 without a *LacZ* cassette (*Gpc4*^{tm1d(EUCOMM)Wtsi} allele). No differences in the phenotype were observed between the two *Gpc4* loss-of-function mouse lines.

2.1.4 Genotyping

Tissue from ear marks was used for genotyping the *Gpc4* transgenic mice. DNA was isolated and purified using the Wizard Genomic DNA Purification Kit. Genomic DNA (gDNA) was eluted in 20 µl H₂O. Polymerase chain reaction (PCR) was set up with MyTaq polymerase like summarized below. The PCR reaction was performed on a Mastercycler Nexus gradient.

	Volume in µl		Temp in °C	Time	Cycles
5x Coral Master Mix	4	Initial Denature	95	3 min	1
gDNA	1	Denature	95	30 sec	35
H ₂ O	14	Annealing	60	30 sec	
Forward Primer (25µM)	0.4	Extension	72	30 sec	
Reverse Primer (25µM)	0.4	Final Extension	72	10 min	1
MyTaq Polymerase	0.2	Cooling	10	infinite	1
<hr/>					
20					

The following primers were used for genotyping:

Allele	Forward (5'-3')	Reverse (5'-3')	Size in bps
<i>Gpc4</i> wt	CTTAGGTCATAATCAGGAGGCTT GG	CACATAGTAGCGCTTCAACTCA ACG	912
<i>Gpc4</i> knockout-first	CTTAGGTCATAATCAGGAGGCTT GG	CAACGGGTTCTTCTGTTAGTCC	500
<i>Gpc4</i> ^{-/-}	ACCGCTGGGATCTGCCATTG	TCCCTGTGGCAGTTACGGT	1186
<i>Sry</i> (Gender)	TGGGACTGGTGACAATTGTC	GAGTACAGGTGTGCAGCTCT	402
<i>Myogenin</i> (loading control)	TTACGTCCATCGTGGACAGC	TGGGCTGGGTGTTAGCCTTA	246

The size of PCR products was determined by gel electrophoresis on a 2 % agarose gel in 1 x TAE buffer supplemented with 1 x SYBR Safe DNA Gel Stain. DNA products were separated by their size (90 V, 40 min) by a PowerPac HC High-Current power supply. GeneRuler 100 bp DNA Ladder was used as a size standard. Products were visualized on a FUSION Xpress System.

2.1.5 *In situ* hybridization on histological sections

The protocol was provided by Anna Truckenbrodt, IDG, Helmholtz Zentrum München and is based on (Schaeren-Wiemers & Gerfin-Moser, 1993). *Gpc4* mRNA expression analysis was supported by Anna Truckenbrodt.

Solutions are summarized in Materials section 1.5 “Buffers and solutions”.

Procedure

Day 1

Sections were thawed (30 min, RT). Slides were incubated in fixative (10 min, RT,) and washed (PBS_{DEPC}, 3 x 5 min, RT). Slides were incubated in acetylation solution (10 min, RT, shaking), washed (PBS_{DEPC}, 3 x 5 min, RT) and incubated with hybridization buffer (at least 2 h, RT). Probe was denatured (75 °C, 10 min), vortexed and placed on ice. 100 µl diluted probe were added per slide. Sections were covered with nescofilm and slides were incubated in a humidified chamber on a filter paper soaked with 5X SSC, 50% formamide at 70 °C overnight. 0.2X SSC solution was pre-warmed (70 °C, ON).

Day 2

Slides were washed (5x SSC, 1 x 5 min, RT) while the nescofilm fell off. Slides were further washed (0.2x SSC, 2 x 30 min, 70 °C) and then another time in 0.2X SSC, (5 minutes, RT). Lastly, slides were washed in Buffer 1 solution (5 min, RT). Afterwards, sections were incubated with blocking solution (800 µl/slide, at least 1 h, RT). Then, anti-DIG antibody mix was added (100 µl/slide), followed by a coverslip and finally, sections were placed in a humidified chamber at 4 °C, overnight.

Day 3

Slides were washed (buffer 1 solution, 3 x 5 min, RT) while the coverslips fell off. Slides were further washed (1x NTMT, 2 x 10 min, RT). Staining solution was added (800 µl/slide) and slides were placed in a humidified chamber and incubated (37 °C, in the dark). If the staining was continued the next day, slides were washed (1x NTMT, 3 x 10 min, RT, in the dark), stored (4 °C, ON, in the dark) and further incubated with staining solution on the next day. Staining was stopped by washing (H₂O, 3 x 5 min), slides were air dried and mounted with Aquatex. Tissue sections were scanned with a Mirax Desk slide-scanner.

2.1.6 X-ray micro-computed tomography (µ – CT)

µ-CT analysis of mouse embryos was performed in collaboration with Dr. Sandholzer, ISF, Helmholtz Zentrum München. Embryos were fixed according to their developmental stage (4 % PFA, E12.5: ON, E14.5 and E17.5 heads: 2 days, E17.5 and P0 whole embryos: 1 week, 4 °C). For contrasting the soft tissue, all specimens were incubated in 5 ml Eppendorf tubes filled with Lugol's solution (E12.5: 24 h, E14.5: 72 h, E17.5: 1 week, P0: 2 weeks) according to described methods (Metscher, 2009). Scans were carried out on a SkyScan 1172. A flat field correction was performed prior to scanning using the SkyScan control software to correct for variations in the pixel sensitivity of the CCD detector. Depending on the size, embryos were scanned at 5.9 µm (E12.5 and E14.5) or 9.0 µm (E17.5 and P0) camera pixel resolution using 80 kV voltage, 100 µA current and a 0.5 mm aluminium filter, resulting in 480 projection images.

2.1.7 µ-CT data analysis

The resulting µ-CT projection images were reconstructed using the SkyScan NRECON software suite with a uniform attenuation coefficient to produce cross-sectional images of the specimens. Subsequently, the cross-sections were processed with ImageJ v.1.47 (Schneider, Rasband, & Eliceiri, 2012) and 3-D models were rendered using the Fiji '3D viewer' plugin (Schmid, Schindelin, Cardona, Longair, & Heisenberg, 2010).

2.1.8 Scanning electron microscopy

Imaging of primary cilia in the node by scanning electron microscopy was performed in collaboration with Dr. Aichler and Gabriele Mettenmeier, Institute of Pathology, Helmholtz Zentrum München. Embryos (E7.5, early to late head fold) were fixed in Formaldehyde/Glutaraldehyde, 3% each in 0.1 M Sodium Cacodylate Buffer, pH 7.4. Dehydration was performed in a graded series of EtOH. Embryos were critical-point dried from CO₂ by a routine procedure and sput-coated by the K575 sput coater with 40 nm platinum. Coated specimens were examined in a field emission scanning microscope (Joel JSM-6300F) with a voltage of 10kV in secondary electron mode.

2.1 Generation of viral *Gpc4* knockdown and overexpression particles

2.1.1 Re-transformation of sh*Gpc4* and shScr constructs

Lentiviral shRNA vectors (pLKO.1) against the *Gpc4* sequence GCCACTGGTTTAAGCAATGTT (Clone TRCN0000109465) and a scrambled shRNA (shSCR) control vector targeting the sequence AGGTTAAGTCGCCCTCG were used (gifts from Dr. Ussar, Helmholtz Zentrum München). One aliquot of competent bacteria (50 µl) per construct was thawed for 10 min on ice. About 1 ng of DNA was mixed with the bacteria and incubated for 5 min on ice. The mixture was heat shocked (42 °C, 40 sec) and immediately afterwards put on ice for 5 min. 200 µl SOC medium was added and one drop was plated on selective LB dishes. Plates were incubated over night at 37 °C and single clones were expanded.

2.1.2 Growth of bacteria

5 ml of LB medium containing 0.1 mg/ml ampicillin were inoculated with a single bacterial clone. Thereby, the colony was touched by a sterile pipette tip and added into the tube containing the LB medium. The tube was shaken at 37 °C overnight. To obtain large amounts for plasmid DNA preparations, 100 ml LB medium containing 0.1 mg/ml ampicillin were inoculated and incubated at 37 °C on a shaker overnight.

2.1.3 Plasmid DNA preparation

Plasmids DNA was extracted by QIAprep Spin Miniprep and QIAGEN Plasmid Maxi Kit according to manufacturer's manual.

2.1.4 Lentivirus production

For virus production, HEK293T cells were transfected with 30 µg/10 cm dish total DNA (50 % shRNA-Vector, 33 % Delta8.9 and 12 % VSV-G) according to the Xfect manual. Two 10 cm dishes were transfected for each virus. 4 h after transfection, medium was replaced (10 ml/10cm plate). After 48 h, viral supernatant was harvested, sterile filtered (0.33 µm) and centrifuged (50.000 g, 1.5 h, 4 °C). The virus pellet from two 10 cm dishes was resuspended in 300 µl PBS and stored in 20 µl aliquots (-80 °C).

2.2 Cell culture

All eukaryotic cells were grown in an incubator with stable conditions of 37 °C and 5 % CO₂.

2.2.1 Production of irradiated mouse embryonic fibroblasts

Primary neomycin resistant mouse embryonic fibroblasts (MEFs) were prepared from E13.5 mouse embryos of the C57BL/6J-Tg(pPGKneobpA)3Ems/J mouse line. Embryos were dissected in ice-cold sterile PBS. The head, tail and inner organs were removed. The remaining tissue of several embryos were pooled and cut in small pieces with a scissor in 1 ml/embryo cold sterile PBS. Tissue pieces were further minced by passing the tissue-containing solution 10 x through a G16 needle. The solution was transferred to a 50 ml falcon containing double amount of MEF medium and was centrifuged (1500 rpm, 5 min). Cells were resuspended in 10 ml/embryo and 10 ml cell solution were seeded in one 0.1 % gelatin pre-coated 10 cm cell culture dish. After 3 – 4 days, MEFs migrated out of the tissue pieces and reached about 80 % confluency. They were rinsed once with PBS, trypsinized (3 ml/10 cm dish, 0.25% Trypsin, 5 min, 37°C) and neutralized with MEF medium (7 ml/10 cm dish). The suspension was transferred to falcons and placed under the hood for 5 – 10 min to allow sinking of big tissue particles. The supernatant was transferred to a new falcon and centrifuged (1500 rpm, 5 min). Cells were either frozen for later expansion or reseeded for further expansion. These cells were considered as passage 0.

To produce non-proliferative MEFs by irradiation, cells were expanded on 0.1% gelatin pre-coated 15 cm dishes by splitting in a ratio of 1:3 until cells reached confluency at passage 4. Cells were rinsed with PBS, trypsinized (0.25 % Trypsin, 10 ml/15 cm dish, 5 min, 37°C) and neutralized with 10 ml MEF medium. Pooled cells were centrifuged (1500 rpm, 5 min), resuspended in 30 ml MEF medium in a 50 ml falcon and counted. Cells were then irradiated by exposure to 30 gray of γ – radiation (Helmholtz Zentrum München). Afterwards, cells were centrifuged (1500 rpm, 5 min), and resuspended in freezing medium in concentrations of 3.5 x 10⁶/ml and 7 x 10⁶/ml. 1 ml/vial was frozen.

2.2.2 Production of irradiated MS5 cells

To produce non-proliferative MS5 cells, one vial of non-irradiated MS5 cells was seeded in a 225 cm flask (gift from Dr. Studer, New York). Cells were split at a confluency of 60 – 70 %. Hence, cells were rinsed with PBS, trypsinized (0.25 % Trypsin, 10 ml/225 cm flask, 37°C) and neutralized with 10 ml MS5 medium. Cells were centrifuged (1000 rpm, 5 min), resuspended and seeded in a ratio of 1:5 to 1:8 on 225 cm flasks. Cells were split once again after 2 – 4 days. For irradiation, cells were rinsed once with PBS, trypsinized, centrifuged (1200 rpm, 5 min), resuspended in 30 ml MS5 medium in a 50 ml falcon and counted. Cells were irradiated by exposure to 45 gray γ – radiation (Helmholtz Zentrum München). Afterwards, cells were centrifuged (1200 rpm, 5 min), and resuspended in freezing medium in concentrations of 2.5×10^6 /ml and 5×10^6 /ml. 1 ml/vial was frozen.

2.2.3 Freezing and thawing of cells

For freezing of cells after trypsinization and centrifugation, cell pellets were resuspended in freezing medium (10 % DMSO, 30 % FCS, 60 % cell type-specific medium). 1 ml of cell solution was transferred to a cryo vial and immediately frozen in isopropanol containing freezing containers. Vials were kept at -80 °C for at least 4 h before they were transferred to a N₂ tank for long term storage.

Cells were thawed in a water bath at 37 °C and transferred to 4 ml cell type specific medium in a 15 ml falcon. Suspension was centrifuged (1200 rpm, 3 min), resuspended in cell type-specific medium and seeded.

2.2.4 mESC maintenance

E14tg2a mESC (CRL-1821) were obtained from ATCC (Manassas, USA) and grown on irradiated MEFs which were seeded at a density of 4×10^4 /cm² on 0.1 % gelatin pre-coated plates. The next day, cells were rinsed once with PBS, and the medium was changed to mESC medium. mESCs were thawed and seeded on irradiated MEFs. 2 – 3 days after thawing, cells were regularly split every other day in a ratio of 1:20 corresponding to approximately 4×10^4 /cm². Cells were maintained for at least 7 days after thawing before neural differentiation. For high content analysis of undifferentiated mESCs, cells were grown feeder-free for 3 passages on 0.1 % gelatin pre-coated plates. Hence, cell pellets were resuspended in 2 ml mESC medium after centrifugation, added to a 6 cm dish and incubated (30 min, 37 °C). Afterwards, the MEF-cleared mESC supernatant was transferred to a new 0.1 % gelatin pre-coated plate and cells were maintained at a high density. For proliferation and cell death analysis, 8×10^4 cells/cm² were seeded and grown for 48 h hours. Cells were fixed and stained against the proliferation marker phospho-Histone 3 (PHH3) or analyzed for cell death by TUNEL.

2.2.5 Generation of *Gpc4* knockdown mESCs

Gpc4 knockdown and control cells were generated by transducing low-passage mESCs with sh*Gpc4* and shSCR lentiviral particles (20 μ l virus/6 cm dish) for 24 h. The next morning, cells were washed (4 x PBS) and split in a ratio of 1:20. 48 h after transduction, cells were selected for 7 days in mESC medium containing 1 μ g/ml puromycin. For clonal selection, transduced cells were first cleared from MEF as described in the previous chapter. MEF-cleared mESC supernatant was seeded on a new 0.1 % gelatin pre-coated 6-well. After confluency was reached, 2 cells/96-well were seeded. The knockdown efficiency of 18 sh*Gpc4* clones was analyzed by qPCR. Two clones with a high knockdown efficiency of *Gpc4* were selected, expanded and the loss of GPC4 protein was confirmed by western blot analysis.

2.2.6 mESC differentiation

mESCs were differentiated to neuroectoderm by an optimized MS5 co-culture protocol (Barberi et al., 2003). 5×10^4 cells/cm² irradiated MS5 cells were seeded on 0.1 % gelatin coated plates to establish a monolayer. The next day (day 0), MS5 cells were rinsed once with PBS to remove remaining serum and 5×10^3 mESC were plated and grown for 8 days in knockout serum replacement medium (KSR). KSR medium was changed on day 3 and daily from day 5 until day 8.

To reduce cell death during further differentiation, cells were gently dissociated on day 8 and replated as a monolayer. Hence, cells were rinsed once with PBS, dissociated by Accutase (1 ml/6 cm dish, 20 min, 37°C) followed by pipetting 20 x up and down with a P1000 pipette. Cell solution was transferred to a 15 ml falcon containing 2 ml differentiation medium (N2/B-27). After centrifugation (1200 rpm, 3 min), cells were counted with a Neubauer counting chamber and resuspended at a concentration of 1×10^6 /ml. Before replating, plates were pre-coated with polyornithine (PO, 15 μ g/ml, 100 μ l/96-well, 37°C, ON), rinsed (PBS, 3x) and coated with laminin (LAM, 5 μ g/ml, 100 μ l/96-well) and fibronectin (FN, 2 μ g/ml, 100 μ l/96-well) for at least 2 h at 37 °C. Subsequently, wells were rinsed once with PBS and pre-filled with 100 μ l/96-well N2/B-27 supplemented with bFGF (20 ng/ml). Cells were then replated at high density (3×10^5 /cm² corresponding to 1×10^5 /96-well in 100 μ l medium). Medium was changed every other day until day 11. From day 12 until day 14, neurons were matured by removing bFGF (N2/B-27).

2.2.7 Treatment of *Gpc4* knockdown mESCs with GPC4 conditioned medium

2.2.7.1 Creation of GPC4 conditioned medium

80 % confluent HEK293T cells were transfected by Xfect with pCDH-CMV-*Gpc4* Δ GPI-EF1a-Puro (gift from Dr. Ussar, Helmholtz Zentrum München) or with pCDH-CMV-empty-EF1a-puro as control. The

overexpressed mutated form of mouse *Gpc4* carried two 6xHis-Tags, one on each terminus of the *Gpc4* sequence which destroys the GPI anchor and therefore leads to a soluble, non-anchored form of the GPC4 protein. After four hours, cells were rinsed once with PBS and then KSR medium was added for 48 h (8 ml/10 cm dish). Cell supernatant was sterile filtered (0.33 μm) and GPC4 abundance in the supernatant was confirmed by western blot analysis. Thereby, 30 μl conditioned medium and 10 μl 4x SDS Loading Buffer were mixed, heated and loaded per well as described in the western blot section. For treatment, the conditioned medium was diluted 1:1 with fresh KSR and was stored (4 °C).

2.2.7.2 Treatment with GPC4 conditioned medium

500 mESCs/24-well of each line were seeded on MS5 cells in KSR medium as described before. On day 2, 5, 6 and 7, medium was replaced by GPC4- or control conditioned KSR medium. 500 μl /24-well was added on day 2 and day 5. 1 ml/24-well was added on day 6 and day 7. On day 8, mRNA was harvested and gene expression was analyzed by qPCR.

2.2.8 Inhibition of *in vitro* neural differentiation by signaling pathway inhibitors

500 wt mESCs/24-well were seeded in KSR medium as described before. On day 1, medium was exchanged containing signaling pathway inhibitors (compound) or DMSO vehicle in four concentrations (Table 4). The compound-containing medium was changed every other day until day 8. Then, cells were fixed and stained against B3 TUBULIN and DAPI as described in the immunocytochemistry section. About 80 % of the area of each 24-well were automatically imaged by the EVOS FL auto Cell Imaging System. The activity of Cyclopamine and Gant61 in the indicated concentration range was confirmed in another cell system (in collaboration with Ms Elen Torres, PhD student of our group).

Compound	Concentration			
	0.01 x	0.1 x	1 x	10 x
DMSO	0.004 %	0.04 %	0.4 %	4 %
IWR-1-endo (Wnt)	0.006 μM	0.06 μM	0.6 μM	6 μM
Cyclopamine (Hh)	0.048 μM	0.48 μM	4.8 μM	48 μM
Gant61 (Hh)	0.022 nM	0.22 nM	2.2 nM	22 nM
SU5402 (Fgf)	0.03 μM	0.3 μM	3 μM	30 μM

Table 4 Inhibition of *in vitro* neural differentiation by signaling pathway inhibitors. Four different concentrations of the EC₅₀ of each drug (1 x) were tested for their potential to inhibit neural differentiation.

2.2.9 Luciferase assay

2.2.9.1 Creation of SHH conditioned medium

HEK293T-SHH is a stable transfected cell line which secretes SHH-N (gift from Dr. Uhmman, University of Göttingen, Germany). SHH conditioned medium was created according to previous studies (Linder et al., 2015). Cells were thawed in normal HEK medium. After three days in culture, the medium was changed to a selection medium (0.4 mg/ml G418) and cells were expanded. For the condition medium with SHH, cells were starved for 24 h in HEK starvation medium containing 2 % FBS without G418. At 80 % confluency, this medium was replaced by HEK medium containing 2 % FBS (10 ml/10 cm dish). After 24 h, supernatant was collected. Cells were split in normal HEK medium containing 10 % FBS without G418 to recover from starvation. At 80 % confluency of the next passage, the conditioning was repeated as described before. Control HEK medium was harvested accordingly. Conditioned medium from both harvest rounds were pooled, sterile filtered (0.33 μ m), diluted 1:1 with fresh medium and stored at 4 °C.

2.2.9.2 Luciferase analysis

Light II NIH-3T3 MEFs are stably transfected cells expressing a *Gli*-responsive firefly luciferase reporter and a constitutively expressed renilla luciferase (Taipale et al., 2000) (gift from Dr. Uhmman, University of Göttingen, Germany). Cells were maintained in Light II maintenance medium. Antibiotics of the medium were removed 2 days before cells were seeded for luciferase experiments. 5×10^4 cells/cm² were seeded in a 96-well plate with 200 μ l medium/well. The next morning, cells were transduced with shGpc4 or shSCR lentiviral particles accordingly. Therefore, 100 μ l medium of each well was removed, pooled in an Eppendorf tube and 5 μ l virus/well was added. The virus-containing medium was mixed and 95 μ l/96-well were re-added and incubated for 24 h. The next day, cells were rinsed (4 x PBS) and starved in 200 μ l/96-well MEF starvation medium containing 0.5 % FBS for 24h. The next day, the medium was changed to MEF stimulation medium containing 2 % FBS and recombinant C-24 human SHH or PBS vehicle. For stimulation with conditioned medium, 1:1 diluted medium was added accordingly. Cells were stimulated with 100 μ l/96-well twice for 24 h each. Afterwards, the dual-luciferase reporter assay was performed. Therefore, cells were rinsed once with PBS, 30 μ l/96-well passive lysis buffer was added and incubated (30 min, RT, shaker). In the meanwhile, the microplate reader was set up and primed with room temperature firefly and renilla substrate according to the manufacture's manual. 50 μ l of each substrate was consecutively added and the signal intensity was measured by the program "Dlr2" (2 sec waiting time, 5 sec exposure time). The ratio of firefly to renilla signal was calculated and fold induction was determined by normalizing signals to the signal of the non-stimulated, non-transduced cells. The *Gpc4* knockdown efficiency of viral transduction was

determined by qPCR. Therefore, 100µl/96-well RLT buffer were added and the mRNA of two wells for each condition were pooled to obtain sufficient mRNA amounts. RNA preparation and qPCR analysis was performed as described in 2.3.1 and 2.3.1.2.

2.2.10 GPC4 expression in primary cilia

8-well glass chambers were pre-coated with laminin (LAM, 5 µg/ml, 37 °C, ON, 300µl/well) and rinsed once with PBS. Light II NIH-3T3 MEFs were seeded (5×10^4 cells/cm²) and grown in 300 µl medium/well overnight. The next morning, medium was reduced to 200 µl/well and cells were transduced with 18 µl/well pCDH-CMV-empty or pCDH-CMV-HA-GPC4-AISA virus for 24 h. The next morning, the medium was carefully changed to starvation medium containing 0.5 % FBS for 60 h (300 µl/well). The knockdown efficiency was confirmed by PCR. The cells were fixed after starvation (4 % PFA, 20 min), washed (4 x PBS, 5 min each) and stained first for cell-surface HA-tagged GPC4. Hence, cells were incubated with blocking solution without detergents (1 % BSA, 3 % heat-inactivated donkey serum, in PBS, 1h, RT) and incubated with anti-HA antibody (1:300, in blocking solution, 1h, RT). After washing (3 x 5min), the secondary antibody was added (1:500, 1 h, RT) in PBS containing 1 % BSA. Subsequently, cilia were visualized by staining against Arl13b (1:1000) using standard stainings as described in the immunocytochemistry section (2.4.2). Nuclei were stained by DAPI.

2.3 Molecular Biology

2.3.1 RNA isolation

Brain and cell samples were homogenized using QIAshredder. Total RNA was isolated employing the RNeasy Mini Kit including digestion of genomic DNA. Total RNA was eluted in 20 – 30 µl elution buffer.

2.3.2 cDNA synthesis

cDNA was generated using the SuperScript III kit, adding 1.0 – 1.5 µg total RNA to 20 µl total volume using oligo-dT primers. Due to limited amounts of tissue, 600 ng cDNA were generated from E9.5 microarray samples.

2.3.1 mRNA expression analysis by PCR

mRNA expression of specific genes was analyzed by two methods. In a conventional approach, the intensity of RT-PCR products were analyzed by fluorescence excitation in an agarose gel. Additionally, quantitative real time PCR (qPCR) was used to quantify expression patterns.

2.3.1.1 Conventional PCR analysis

To determine the mRNA expression by conventional PCR analysis, the same PCR protocol and chemicals were used as described for the genotyping PCR in 2.1.4 except that 0.2 μ l undiluted cDNA was used instead of 1 μ l gDNA for each reaction. Master mixes were created for each cDNA to minimize technical variability. Used primers and cycle numbers are summarized below. All primers were designed with Primer-BLAST (Ye et al., 2012), except for *Gpc4* (endo) (Fico et al., 2012).

Gene	Forward Primer (5'-3')	Reverse Primer (5'-3')	Size in bps	Cycles
<i>Acta2</i>	TTCATTGGGATGGAGTCAGCG	TTCCTGACCACTAGAGGGGG	570	35
<i>Gapdh</i>	AATGCATCCTGCACCACCACC	GGAGGCCATGTAGGCCATGAG	555	28
<i>Gfap</i>	GCGCTCAATGCTGGCTTCAA	ACGCAGCCAGGTTGTTCTCT	346	35
<i>Gpc1</i>	TGGGGACCTGTATACGCAGA	ACACCGCCAATGACTCTC	557	28
<i>Gpc2</i>	GGGCGGATATCTGGATGGTC	TCATTCAAGGAGCCCACGAC	468	35
<i>Gpc3</i>	CCAACATGCTGCTCAAGAAA	CTTGGGGAAACTGCCAAATA	432	28
<i>Gpc4</i> (endo + exo)	CTGTTTGCAGTGACAGGAA	CTGCATGGGCACCACCGGC	310	35
<i>Gpc4</i> (endo)	CTGCTTCCATCGGGTCTCATTCTG	AGGTCCTGGCTGCAACAAATGCGC	725	28
<i>Gpc5</i>	CACGGAACCTACGACGTTGA	TCTCCCCGTAACAACCTGGA	498	35
<i>Gpc6</i>	GAGGACTGTGTGGAGGACCAT	AGATTCTCTTCTCTGCGGTC	466	35
<i>Gsc</i>	CTACACGGGGACTCGCTCTA	AAACCAGACCTCCACCTTCTC	513	35
<i>Map2</i>	GGAAAACCACAGCAGCAAGTG	CATTCTTCAGGTCCGGCAGT	495	35
<i>Nestin</i>	GGTAGGGCTAGAGGACCCAA	GGTAGAGGCCCAAGGGAGTA	593	35
<i>Oct3/4</i>	ATTTGCCAAGCTCCTGAAGCAG	TTGATCGCTTGCCCTTCTGG	422	35
<i>T</i>	TGAAGGTGGCTGTTGGGTAG	GCCACCCCCATTGGGAATA	799	35

2.3.1.2 qPCR analysis

qPCR analysis was performed on a Quantstudio 12k Flex real-time PCR system using 10 μ l/386-well. Relative expression levels were calculated by the $\Delta\Delta$ Ct method using *Gapdh* as a reference gene. To verify gene expression of candidate genes, which were detected by microarray analysis, PrimeTime qPCR Assays in combination with the Taqman Fast Advanced Mastermix were used (summarized below). For one reaction, the following amounts were used:

IV. Materials and methods

	Volume in μ l
2x Master Mix	5
cDNA	0.2
IDT Assay	1
H ₂ O	3.8
<hr/>	
Total	10

Gene	Assay ID
<i>Aldh1a3</i>	Mm.PT.58.11310697
<i>Lhx2</i>	Mm.PT.58.32109564
<i>Sox5</i>	Mm.PT.58.29673690
<i>Alx1</i>	Mm.PT.58.42897104
<i>Alx3</i>	Mm.PT.58.626702
<i>Dlk1</i>	Mm.PT.58.30309372
<i>Gapdh</i>	Mm.PT.39a.1
<i>Six3</i>	Mm.PT.58.14013039
<i>Six6</i>	Mm.PT.58.43583201
<i>Wnt7b</i>	Mm.PT.58.21675366

For all other genes, quantitative mRNA expression was analyzed by 2x Fast SYBR Green Master Mix. For each cDNA, master mixes were created to minimize technical variability. For one reaction, the following amounts were used:

	Volume in μ l
2x Master Mix	5
cDNA (1:10)	0.2
Forward Primer (1.5 μ M)	0.5
Reverse Primer (1.5 μ M)	0.5
H ₂ O	3.8
<hr/>	
	10

IV. Materials and methods

For qPCR, the following primers were used:

Gene	Forward Primer (5'-3')	Reverse Primer (5'-3')	Source
<i>Gapdh</i>	CCCACTGAAGGGCATCTTGGGCT AC	GGGTGGGTGGTCCAGGGTTTCTT AC	(Ye et al., 2012)
<i>Gli1</i>	GCTTGGATGAAGGACCTTGTG	GCTGATCCAGCCTAAGGTTCTC	(M. I. Capurro et al., 2008)
<i>Gpc4</i>	GGCAGCTGGCACTAGTTTG	AACGGTGCTTGGGAGAGAG	(Gesta et al., 2006)
<i>Nanog</i>	GAAATCCCTTCCCTCGCCATC	CTCAGTAGCAGACCCTTGTAAGC	(Ye et al., 2012)
<i>Nestin</i>	TCTCTTCCCCCTTGCCTAAT	GGCTCTGACCTCTGCATTTT	(Ye et al., 2012)
<i>Oct3/4</i>	GGCTTCAGACTTCGCCTTCT	TGGAAGCTTAGCCAGGTTTCG	(Ye et al., 2012)
<i>Ptch1</i>	CAAGTGTCGTCCGGTTTGC	CTGTACTIONCCGAGTCGGAGGAA	(M. I. Capurro et al., 2008)
<i>Sox2</i>	GATCAGCATGTACCTCCCCG	CTGGGCCATGTGCAGTCTAC	(Ye et al., 2012)
<i>Tubb3</i>	TAGACCCAGCGGCAACTAT	GTTCCAGGTTCCAAGTCCACC	(Spandidos, Wang, Wang, & Seed, 2010)

2.3.2 *In situ* probe generation

To visualize *Gpc4* and *Wnt1* mRNA expression in mouse tissue, *in situ* probes were generated. Therefore, vectors were linearized using the following restriction enzymes:

Gene	Vector	Antibiotic	Enzyme for AS Probe	RNA Polymerase	Origin
<i>Gpc4</i>	pCMV-Sport6	Ampicillin	Sall	T7	Source Bioscience, Nottingham, UK
<i>Wnt1</i>	pBlueScript Sk II	Ampicillin	HindIII	T7	IDG, Helmholtz Zentrum München

10 µg total DNA were digested in 100 µl total volume containing 10 µl 10 x CutSmart Buffer and 2 µl restriction enzyme for 2 h at 37 °C. Enzymes were inactivated by heat according to manufacturer's manual. 1 µl was used to confirm linearization of the vector on a 1 % agarose gel. Linearized DNA was subsequently purified by illustra GFX PCR DNA and Gel Band Purification Kit and eluted in 20 µl Nuclease-free H₂O. *In vitro* transcription was performed according to manufacturer's manual. 1 µg template was added to 20 µl reaction volume using the following amounts:

	Volume in μ l
Nuclease-free H ₂ O	14-X
10x transcription buffer	2
RNAse inhibitor	1
DNA Template	x
Dig RNA labeling mix	2
T7 RNA polymerase	1
Total	20

The mixtures were incubated at 37 °C for 2 h. 2 μ l of RNase-free DNase I were added and incubated at 37 °C for 15 min to digest the template vector DNA. Reactions were stopped by adding 0.2 M EDTA (pH 8.0). 1 μ l was used to verify *in vitro* transcription of probes on a 1 % agarose gel. Afterwards, probes were purified by illustra MicroSpin G-50 columns. Therefore, columns were vortexed, the lower-part was cut off and columns were centrifuged (3000 rpm, 1min). Reaction mix was pipetted in the center of the column and centrifuged (3000 rpm, 2 min). Eluate was diluted with 1 ml of pre hybridization buffer and stored at -20 °C.

2.3.3 Generation of the pCDH-HA-Gpc4-AISA construct

The cleavage resistant overexpression plasmid pCDH-CMV-HA-Gpc4-AISA was created in collaboration with Ms Theresa Bäcker, PhD student in our group. To achieve this, a site-directed mutation was generated in the original pCDH-CMV-HA-Gpc4 construct (gift from Dr. Ussar, Helmholtz Zentrum München) which exchanged the wt *Gpc4* sequence R³⁵¹ISR³⁵⁴ to the cleavage resistant mutant A³⁵¹ISA³⁵⁴ (AISA) as described before (de Wit et al., 2013). The mutation was created by PCR using the Q5 Site-directed mutagenesis Kit with following primers on the wt *Gpc4* template: Forward (5'-3'): tctgccTCCATCTCTGAAAGTGCCTTC and Reverse (5'-3'): aattgcTCCAGCTGGGAGAGGCTT. Primers were designed with the online tool <http://nebasechanger.neb.com/>. PCR was conducted as described in 2.1.4 using 65 °C annealing temperature. Correctness of the sequence was confirmed by Sanger sequencing.

2.3.1 Sanger sequencing

DNA sequence of plasmids was confirmed by Sanger sequencing. Sequencing was performed by GATC Biotech, Konstanz, Germany. 800 ng DNA in 20 μ l and 200 pmol sequencing primers were used. Sequences were analyzed by Vector NTI.

2.3.2 Microarray expression profiling

Microarray analysis of E9.5 mouse embryos was performed in collaboration with Dr. Irmeler, IEG, Helmholtz Zentrum München. RNA quality of microarray samples was assessed using the Agilent 2100 Bioanalyzer in combination with the Agilent RNA 6000 Pico Kit. Only high quality samples (RIN>7) were included in microarray analyses. Total RNA (30 ng) was amplified using the Ovation PicoSL WTA System V2 in combination with the Encore Biotin Module. cDNA was hybridized on Affymetrix Mouse Gene ST 2.0 arrays containing about 35,000 probe sets. Staining and scanning were performed on a GeneChip Scanner 3000 7G according to the Affymetrix expression protocol including minor modifications as suggested in the Encore Biotin protocol.

2.3.3 Microarray statistical transcriptome analysis.

Expression console (v.1.4.1.46, Affymetrix) was used for quality control and to obtain annotated normalized robust multi-array average (RMA) gene-level data (standard settings including median polish and sketch-quantile normalization). Statistical analyses were performed by utilizing the statistical programming environment R (R Development Core Team, 2010) implemented in CARMAweb (CARMAweb version 1.5.18 – uses R version 2.11.0 together with Bioconductor version 2.6; (Rainer, Sanchez-Cabo, Stocker, Sturn, & Trajanoski, 2006). Genewise testing for differential expression was done employing the limma t-test and Benjamini-Hochberg multiple testing correction (FDR < 10%). Heatmaps were generated with CARMAweb and cluster dendrogram with the R scripts hclust, diana, and agnes. Array data has been submitted to GEO (GSE83857). GO term analyses were performed with GePS and significant terms ($p < 0.01$) were determined. The pathway analyses were generated through the use of QIAGEN's INGENUITY Pathway Analysis.

2.3.1 Human single cell RNAseq analysis

The single cell transcriptome analysis of the developing human brain was performed in collaboration with Dr. Camp and Dr. Treutlein, Max Planck Institute for Evolutionary Anthropology, Leipzig, Germany. Data analysis was performed by Dr. Camp on previously published data including a detailed description of the methods (Camp et al., 2015). In short, 226 single-cell transcriptomes of 12- and 13 weeks postconception human neocortex specimens were analyzed. Single cells were categorized to the expression pattern of specific cortical zones (ventricular zone (VZ), inner/outer sub ventricular zone (I/O-SVZ), cortical plate (CP)). Therefore, single cells represented the diverse neural precursor- and neuronal subpopulations at different neural maturation stages of the developing human cortex.

For the Gpc expression analysis, the transcriptome of each single cell was analyzed for its Gpc expression. The result was plotted in aligned cells from ventral cortical- to dorsal cortical zones. For

correlation analysis, the mRNA expression pattern of *Gpc4* was compared to similar patterns of other genes.

2.4 Methods in protein biochemistry

2.4.1 Western blot analysis

2.4.1.1 Protein extraction from cells

Cells and tissues were rinsed once with ice cold PBS and scraped off culture dish plates with a cell scraper in ice cold PBS. Solution was transferred to an Eppendorf tube, centrifuged (1200 rpm, 3 min) and supernatant discarded. Cell pellet was lysed with 100 – 300 μ l RIPA buffer supplemented freshly with 5 mM EDTA and 1 \times Complete protease inhibitor cocktail. Lysates were incubated (on ice, 20 min) with occasional vortexing steps, centrifuged (13.000 rpm, 40 min, 4 $^{\circ}$ C) and supernatant was transferred to a new tube and stored (-20 $^{\circ}$ C).

2.4.1.2 Protein extraction from tissue

Embryos were dissected in ice cold PBS. Whole brains or brain areas were shredded with a scalpel and transferred to Eppendorf tubes. Tissues were homogenized in 500 μ l RIPA buffer supplemented freshly with 5 mM EDTA and 1 \times Complete protease inhibitor cocktail by grinding several times up and down with a pellet pestle. Afterwards, lysates were incubated (on ice, 20 min) with occasional vortexing steps, centrifuged (13.000 rpm, 40 min, 4 $^{\circ}$ C) and supernatant was transferred to new tube and stored (-20 $^{\circ}$ C).

2.4.1.3 Total protein concentration determination (BCA)

Total protein amount of supernatant was determined by Pierce BCA Protein Assay Kit. Samples were diluted 1:1 with H₂O in a total volume of 10 μ l/96-well. 200 μ l/well BCA solution was added and incubated (30 min, 37 $^{\circ}$ C). Protein concentration was detected by colorimetry measurements at 562 nm using a Spectramax M5 system.

2.4.1.4 Gel and buffer preparation

For two 10 % separating gels the following composition was used:

16 ml of 10% separating gel:		10 ml of 4% stacking gel:	
7.7 ml	MiliQ H ₂ O	6.3 ml	MiliQ H ₂ O
4 ml	40 % Acrylamide	1 ml	40 % Acrylamide
4 ml	1.5 M Tris pH 8.8	2.5 ml	0.5 M Tris pH 6.8
160 µl	10 % SDS	100 µl	10 % SDS
160 µl	10 % APS	100 µl	10 % APS
16 µl	TEMED	10 µl	TEMED

The separating gel mixture was filled into two sealed glass plates and covered with 70 % EtOH. After polymerization, the EtOH was decanted and completely removed with Whatman paper. Afterwards, the stacking gel mixture was added and the 1.5 mm comb was inserted.

The required buffers and solutions are summarized in Materials section.

2.4.1.5 Sample preparation

10 – 20 µg total protein were mixed with 10 µl 4x SDS Loading Buffer in a total volume of 40 µl. Samples were denatured (95 °C, 5 min) and kept on ice.

2.4.1.6 Western blot procedure

Gel chamber (Mini-PROTEAN Tetra Vertical Electrophoresis Cell) was filled with running buffer, combs were removed and pockets of the stacking gel were washed by 200 µl tips. 40 µl total volume were loaded on the gels. 7 µl page ruler was used as a standard to identify molecular weight of the proteins of interest. The proteins were separated at a constant voltage of 90 V for approximately 1.5 h (PowerPac™ HC High-Current power supply). After gel electrophoresis, the gel was released from the glass plates and equilibrated in transfer buffer for 5 min. The PVDF membrane was activated in MeOH for 1 min and kept in transfer buffer. Subsequently, proteins were transferred on a PVDF membrane by a wet blot. Setup of the wet blot was like the following:

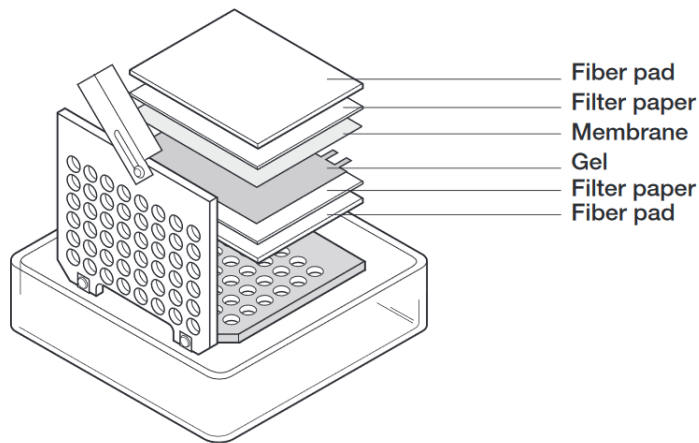


Figure 47 Western blot set up. Adapted from Mini Trans-Blot Electroblotting Transfer Cell Instruction Manual, Bio-Rad, USA.

Gel electrophoresis was performed at constant current of 0.08 A, 10 h at 4 °C with a magnetic stirring fish inside the chamber. After transfer, membranes were calibrated (PBS-T, 5 min) and blocked (5 % Milk powder in PBS-T, 1 h, RT). Afterwards, membranes were probed with primary antibodies (in PBS-T, ON, 4 °C). After washing (PBS-T, 3 x 5 min), Horseradish peroxidase-conjugated (HRP) secondary antibodies were used (1:2500, 1 h, RT). Membranes were washed (3 x 5 min) and incubated for 5 min with ECL Western Blotting Detection System. Protein expression was analyzed on a FUSION Xpress System. Membranes were stripped for re-probing with the harsh stripping buffer (45 min, 50 °C), rinsed with tap water (10 min), re-blocked and incubated with the B Actin antibody as described before.

2.4.2 Immunocytochemistry stainings

After fixation (4 % PFA, 20 min), cells were washed (3 x 5 min), permeabilized (0.5 % BSA; 0.3 % Triton X-100, 1 h, RT) and washed again (3 x 5 min). Afterwards, cells were incubated with primary antibodies in staining buffer, containing 1 % BSA in PBS (ON, 4°C). After washing (3 x 5 min), fluorophore-conjugated secondary antibodies were added (Alexa488, Alexa555 or Alexa647; 1 h, RT, in the dark). Nuclei were visualized by staining with 4',6-Diamidin-2-phenylindol (DAPI) (1:100, 20 min, RT). For long-term storage at 4 °C, cells were preserved with PBS containing 0.002 % NaN₃ to prevent bacterial contaminations.

2.4.1 Cell death analysis

Cell death analysis of mESCs was performed according to the manual of the *In Situ* Cell Death Detection Kit.

2.4.1 LacZ staining

For visualization of *Gpc4*-driven β -Galactosidase by conversion of X-gal (5 – bromo – 4 – chloro – 3 - indolyl β – D - galactoside) substrate, a modified protocol of Dr. Silvia Engert, ISF, Helmholtz Zentrum München, was used (Engert et al., 2013).

Adult brains were dissected in ice cold PBS, fixed (4 % PFA, ON) and cryopreserved as described in the next chapter. 40 μ m brain sections were cut, washed (PBS containing 0.02 % NP-40, 3 x 10 min) and stained in *LacZ* staining solution (PBS containing 0.02 % NP-40, 2 mM MgCl₂, 5 mM K₃[Fe(CN)₆], 5 mM K₄[Fe(CN)₆]x6H₂O, 0.01 % sodium deoxycholate, 1 mg/ml X-gal). The staining was carried out over night at 37 °C. After staining, sections were washed (PBS containing 0.02 % NP-40, 3 x 10 min) and postfixed (4 % formaldehyde, 4 °C). The expression was documented on a Zeiss Lumar.V12. MRc5 camera.

2.4.1 Whole mount immunohistochemistry

The whole mount immunohistochemistry protocol was provided by Dr. Rosa Hüttl, ISF, Helmholtz Zentrum München and was published before (Huber et al., 2005).

Solutions are summarized in Materials section “1.5 Buffers and solutions”.

Procedure

All staining steps were conducted in Eppendorf tubes except for the clearing step.

Fixation

E10.5 Embryos were fixed (4 % PFA, 4 °C, rotating, ON), washed (PBS, 3 x 5 min, rotating) and bleached (Dent’s Bleach, 4°C, 24 h). Afterwards, embryos were rinsed (5 x MeOH) and post-fixed (Dent’s Fix, at least 24 h, 4°C). Embryos can be stored in this solution.

Antibody incubation

Embryos were rinsed (3 x PBS), washed hourly (3 x PBS) and incubated with primary antibody against Shh (1:200, in blocking solution, RT, 3 – 5 days, rotating). Afterwards, embryos were rinsed (3 x PBS), washed hourly (5 x PBS) and secondary antibody was added (1:250, in blocking solution, RT, 2 days, dark, rotating). Then, embryos were rinsed (3 x PBS) and washed hourly (5 x PBS).

Clearing (in dark)

50 % of PBS were replaced with MeOH and incubated (10 min, RT). Embryos were washed (MeOH, 3 x 20 min) and then 50 % of MeOH were replaced with BABB and incubated (10 min, RT). Afterwards, embryos were cleared in 100 % BABB (use of lowest possible volume to avoid tissue loss). Embryos were imaged and stored in BABB in the dark.

Imaging

Whole mount stainings were imaged on the laser scanning microscope LSM510 META.

2.4.2 Immunohistochemistry stainings

Embryos were fixed in 4 % PFA (E12.5: 1 h, E15.5: 2 h, >E17.5: ON; 4°C), washed (PBS, 2 x 5 min,) and cryopreserved in 30 % sucrose at 4 °C until the tissue sank down. Usually the next day, embryos were embedded in Tissue-Tek and frozen (-80 °C). Tissue blocks were fixed to the cryostat using Tissue-Tek and sectioned at a thickness of 12 µm on a CM 3050S cryotome. Histological sections were melted on glass slides, dried (RT, 30 min) and stored (-80 °C). For staining, slides were thawed (30 min, RT) and washed (PBS, 3 x 5 min). Tissues were surrounded by a fat pen and permeabilized (1 % BSA; 0.2 % Triton X-100, 1 h, RT). Then tissues were incubated with primary antibodies in permeabilization buffer (ON, 4°C). After washing (3 x 5 min), fluorophore-conjugated secondary antibodies (Alexa488, Alexa555 or Alexa647) were used according to primary hosts (in permeabilization buffer, 1 h, RT, in the dark). Nuclei were visualized by staining with 4',6-Diamidin-2-phenylindol (DAPI) (1:100, 20 min, RT).

2.4.1 Fluorescence microscopy

Fluorescent stainings were analyzed by different microscopes. Cells and histological sections were analyzed on an EVOS FL Cell Imaging System. For whole mount staining, the laser scanning microscope LSM510 META was used. Cilia were analyzed on a Leica TCS SP5.

2.4.2 High-content imaging analysis

For high-content imaging analysis, cells were seeded on Cell Carrier 96-well plates with optically clear bottoms. Plates were recorded using the automated Operetta microscope with a 10 x objective for MAP2 detection and with a 20 x objective for *PHH3* detection. For each condition, 3 wells of 3 independent differentiations/passages were analyzed. The center images of each well (15 images for 10 x recordings, 21 images for 20 x recordings) were analyzed with the Harmony software. For the analysis of MAP2, a region of interest (ROI) was defined for each image based on a fixed level of MAP2 staining intensity (dsRed). Furthermore, a ROI for all nuclei was selected by staining intensity of DAPI. Then, the MAP2 ROI was normalized to the DAPI ROI for each image and the mean value was calculated for each well. For proliferation analysis by PHH3 staining, single nuclei were defined by nuclear staining (DAPI). Within this population, positively and negatively stained nuclei subpopulations were selected based on PHH3 staining intensity (Alexa488). Then, the number of OCT3/4 or PHH3 positive nuclei was normalized to the total number of nuclei.

2.5 Statistical evaluation

If not otherwise indicated, results were calculated as mean ± SEM and tested for normal distribution using GraphPad Prism 5.0. If data followed normal distribution, differences of statistical significance

were determined with the Student's t-test. For data with significant differences in their variances, the Welch's correction was applied. If data values were not normally distributed, the Mann-Whitney test was used. P-values below 0.05 were considered as statistically significant. * $p < 0.05$, ** $p < 0.01$, *** $p < 0.001$.

List of figures

Figure 1 The three compartments of the ECM of the CNS.....	2
Figure 2 Glypican structure.	4
Figure 3 Wnt signaling.....	6
Figure 4 Release of HH from secreting cells.....	8
Figure 5 Hh signaling pathway	9
Figure 6 Hh signaling modulators on signal receiving cells.....	10
Figure 7 <i>Gpc4</i> mRNA expression during mouse embryo development.	12
Figure 8 Anterior neural induction by inhibition of posterior signals.	15
Figure 9 A-P forebrain specification by Wnt and Fgf signaling.....	15
Figure 10 Dorso-ventral patterning of the anterior brain.....	16
Figure 11 Mouse model of HPE.	17
Figure 12 Signaling pathway activity on primary cilium.....	19
Figure 13 Structure and disease-associated compartments of the primary cilium.	20
Figure 14 <i>Gpc4</i> expression in the developing and the adult brain.	24
Figure 15 Generation of <i>Gpc4</i> loss-of-function mice.....	26
Figure 16 Confirmation of <i>Gpc4</i> knockout in mice.....	27
Figure 17 Reabsorbed embryos in <i>Gpc4</i> ^{-/-} mothers.....	28
Figure 18 Overview of developmental defects in <i>Gpc4</i> ^{-/-} embryos.	30
Figure 19 μ-CT analysis of <i>Gpc4</i> ^{-/-} embryos.	32
Figure 20 Phenotype penetrance analysis of <i>Gpc4</i> ^{-/-} embryos.....	35
Figure 21 <i>Gpc4</i> ^{-/-} phenotype expressivity is dependent on the genetic background.....	36
Figure 22 <i>Gpc4</i> ^{-/-} mice show impaired neural differentiation in lateral ventricles.....	37
Figure 23 Wnt and Hh are misregulated candidate pathways in <i>Gpc4</i> ^{-/-} embryos.....	38
Figure 24 <i>Gpc4</i> does not act as an anterior repressor of Wnt signaling	40
Figure 25 <i>Gpc4</i> ^{-/-} embryos lack forebrain SHH domains.....	41
Figure 26 Hh signaling is impaired upon loss of <i>Gpc4</i> <i>in vitro</i>	43
Figure 27 Impaired Hh activity upon <i>Gpc4</i> knockdown also by purmorphamine stimulation.	44
Figure 28 Overexpression of <i>Gpc4</i> did not rescue Hh signaling activity.	44
Figure 29 <i>BOC</i> mRNA expression correlates with <i>GPC4</i> in the human developing cortex.	45
Figure 30 Cleavage resistant HA- <i>GPC4</i> can be expressed in primary cilia.	47
Figure 31 E7.5 <i>Gpc4</i> ^{-/-} embryos develop primary cilia in the node.....	49
Figure 32 Optimization of a neural differentiation protocol for mESCs.	51
Figure 33 Generation of <i>Gpc4</i> knockdown mESCs.....	54

Figure 34 shGpc4 mESCs do not show altered levels of proliferation. 55

Figure 35 shGpc4 mESCs do not show altered levels of cell death. 55

Figure 36 Impaired neural differentiation of shGpc4 cells on day 8. 56

Figure 37 Impaired neural differentiation is not the result of increased colony numbers. 57

Figure 38 Impaired neural differentiation is not the result of developmental delay. 58

Figure 39 MAP2 quantification on day 14 of neural differentiation. 59

Figure 40 OCT3/4 quantification on day 14 of neural differentiation. 60

Figure 41 Impaired mesoderm differentiation of shGpc4 mESCs. 61

Figure 42 GPC4 treatment of shGpc4 mESCs does not rescue neural differentiation defects. 62

Figure 43 Hh signaling activity is impaired in differentiating shGpc4 mESCs. 64

Figure 44 Inhibition of Fgf signaling phenocopies shGpc4 defects. 66

Figure 45 Non-linear Hh signaling activity may cause phenotype variation in *Gpc4*^{-/-} mice. 78

Figure 46 Working model of *Gpc4* during forebrain development. 94

Figure 47 Western blot set up. 125

List of tables

Table 1 *Gpc4* mRNA expression during mouse embryo development. 13

Table 2 Human HPE-associated gene loci. 18

Table 3 Phenotype expressivity of *Gpc4*^{-/-} embryos. 34

Table 4 Inhibition of *in vitro* neural differentiation by signaling pathway inhibitors. 115

List of abbreviations

ADE	Anterior definitive endoderm
AA	Ascorbic Acid
AEP	Anterior entopeduncular area
AF	Anterior forebrain
AME	Axial mesendoderm
A-P	Anterior-posterior
AVE	Anterior visceral endoderm
BMP	Bone morphogenetic protein
BSA	Bovine serum albumine
CA1	Region I of hippocampus proper
CNS	Central nervous system
CSPG	Chondroitin sulfate proteoglycans
DAPI	4',6-Diamidin-2-phenylindol
DG	Dentate gyrus
DNA	Desoxyribonucleic acid
dNTP	Desoxynucleotide
D-V	Dorsal-ventral
E	Embryonic day
EC	Neural ectoderm
ECM	Extracellular matrix
EDTA	Ethylendiamintetraacetic acid
En2 SA	<i>Engrailed-2</i> splice acceptor
ES	Early streak
EtOH	Ethanol
EUCOMM	European Conditional Mouse Mutagenesis Program
FCS	Fetal calf serum
Fgf	Fibroblast growth factor
Flp	<i>LoxP-flippase</i>
<i>Fzd</i>	Frizzled (Wnt receptor)
GAG	Glycosaminoglycan
GBS	Gli binding site
gDNA	Genomic DNA

List of abbreviations

GFP	Green fluorescent protein
<i>Gpc</i>	Glypican
GPI	Glycosylphosphatidylinositol
HA-Tag	Influenza hemagglutinin-Tag
HEK	Human embryonic kidney
hESC	Human embryonic stem cell
HH	Hedgehog
HH-N	N-terminal, activae HH
hiPSC	Human induced pluripotent stem cell
HPE	Holoprosencephaly
HRP	Horseradish Peroxidase
HS	Heparan sulfate
HSPG	Heparan sulfate proteoglycans
IC	Immunocytochemistry
ISH	<i>In situ</i> hybridization
kDa	Kilo dalton
LHF	Late head fold
LIF	Leukemia inhibitory factor
LoxP	Locus of X-over P1
MEF	Mouse embryonic fibroblast
mESC	Mouse embryonic stem cell
MGE	Medial ganglionic eminence domain
mRNA	Messenger ribonuclein acid
NEO	Neomycin (selection cassette)
nm	Nanometer
np	Notochordal plate
NPC	Neural precursor cell
NTD	Neural tube defects
OB	Olfactory bulbs
P	Postnatal day
pA	SV40 polyadenylation
PCR	Polymerase chain reaction
PFA	Paraformaldehyde
PHH3	Phospho-Histone 3

List of abbreviations

pm	Purmorphamine
PS	Primitive streak
PSC (h/m)	(Human/mouse) Pluripotent stem cells
qPCR	Quantitative polymerase chain reaction
RMA	Robust multi-array average
RNA	Ribonucleic acid
rpm	Rounds per minute
RT	Room temperature
SDS	Sodium dodecylsulfate
SEM	Standard error of the mean
Shh	Sonic Hedgehog
Smo	Smoothed
SVZ	Sub ventricular zone
T	Brachyury
TCF	T-cell factor
TE	Tris/EDTA buffer
TH	Tyrosine Hydroxylase
TUNEL	TdT-mediated dUTP-biotin nick end labeling
VZ	Ventricular zone
WB	Western blot
Wnt	Wingless/INT proteins
wt	Wildtype

References

- Agarwal, S., Holton, K. L., & Lanza, R. (2008). Efficient Differentiation of Functional Hepatocytes from Human Embryonic Stem Cells. *Stem Cells*, *26*(5), 1117-1127. doi:10.1634/stemcells.2007-1102
- Akiyama, T., Kamimura, K., Firkus, C., Takeo, S., Shimmi, O., & Nakato, H. (2008). Dally regulates Dpp morphogen gradient formation by stabilizing Dpp on the cell surface. *Dev Biol*, *313*(1), 408-419. doi:10.1016/j.ydbio.2007.10.035
- Allen, B. L., & Rapraeger, A. C. (2003). Spatial and temporal expression of heparan sulfate in mouse development regulates FGF and FGF receptor assembly. *J Cell Biol*, *163*(3), 637-648. doi:10.1083/jcb.200307053
- Allen, B. L., Song, J. Y., Izzi, L., Althaus, I. W., Kang, J. S., Charron, F., . . . McMahon, A. P. (2011). Overlapping roles and collective requirement for the coreceptors GAS1, CDO, and BOC in SHH pathway function. *Dev Cell*, *20*(6), 775-787. doi:10.1016/j.devcel.2011.04.018
- Allen, B. L., Tenzen, T., & McMahon, A. P. (2007). The Hedgehog-binding proteins Gas1 and Cdo cooperate to positively regulate Shh signaling during mouse development. *Genes Dev*, *21*(10), 1244-1257. doi:10.1101/gad.1543607
- Allen, N. J., Bennett, M. L., Foo, L. C., Wang, G. X., Chakraborty, C., Smith, S. J., & Barres, B. A. (2012). Astrocyte glypicans 4 and 6 promote formation of excitatory synapses via GluA1 AMPA receptors. *Nature*, *486*(7403), 410-414. doi:10.1038/nature11059
- Anderson, R. M., Lawrence, A. R., Stottmann, R. W., Bachiller, D., & Klingensmith, J. (2002). Chordin and noggin promote organizing centers of forebrain development in the mouse. *Development*, *129*(21), 4975-4987.
- Andoniadou, C. L., & Martinez-Barbera, J. P. (2013). Developmental mechanisms directing early anterior forebrain specification in vertebrates. *Cell Mol Life Sci*, *70*(20), 3739-3752. doi:10.1007/s00018-013-1269-5
- Aubert, J., Dunstan, H., Chambers, I., & Smith, A. (2002). Functional gene screening in embryonic stem cells implicates Wnt antagonism in neural differentiation. *Nat Biotechnol*, *20*(12), 1240-1245. doi:10.1038/nbt763
- Ayers, K. L., Gallet, A., Staccini-Lavenant, L., & Therond, P. P. (2010). The long-range activity of Hedgehog is regulated in the apical extracellular space by the glypican Dally and the hydrolase Notum. *Dev Cell*, *18*(4), 605-620. doi:10.1016/j.devcel.2010.02.015
- Bae, G. U., Domene, S., Roessler, E., Schachter, K., Kang, J. S., Muenke, M., & Krauss, R. S. (2011). Mutations in CDON, encoding a hedgehog receptor, result in holoprosencephaly and defective interactions with other hedgehog receptors. *Am J Hum Genet*, *89*(2), 231-240. doi:10.1016/j.ajhg.2011.07.001
- Balaskas, N., Ribeiro, A., Panovska, J., Dessaud, E., Sasai, N., Page, K. M., . . . Ribes, V. (2012). Gene regulatory logic for reading the Sonic Hedgehog signaling gradient in the vertebrate neural tube. *Cell*, *148*(1-2), 273-284. doi:10.1016/j.cell.2011.10.047
- Bandtlow, C. E., & Zimmermann, D. R. (2000). Proteoglycans in the developing brain: new conceptual insights for old proteins. *Physiol Rev*, *80*(4), 1267-1290.
- Barberi, T., Klivenyi, P., Calingasan, N. Y., Lee, H., Kawamata, H., Loonam, K., . . . Studer, L. (2003). Neural subtype specification of fertilization and nuclear transfer embryonic stem cells and application in parkinsonian mice. *Nat Biotechnol*, *21*(10), 1200-1207. doi:10.1038/nbt870
- Barr, M., Jr., Hanson, J. W., Currey, K., Sharp, S., Toriello, H., Schmickel, R. D., & Wilson, G. N. (1983). Holoprosencephaly in infants of diabetic mothers. *J Pediatr*, *102*(4), 565-568.
- Beachy, P. A., Hymowitz, S. G., Lazarus, R. A., Leahy, D. J., & Siebold, C. (2010). Interactions between Hedgehog proteins and their binding partners come into view. *Genes Dev*, *24*(18), 2001-2012. doi:10.1101/gad.1951710
- Belenkaya, T. Y., Han, C., Yan, D., Opoka, R. J., Khodoun, M., Liu, H., & Lin, X. (2004). Drosophila Dpp morphogen movement is independent of dynamin-mediated endocytosis but regulated by

- the glypican members of heparan sulfate proteoglycans. *Cell*, 119(2), 231-244. doi:10.1016/j.cell.2004.09.031
- Belo, J. A., Bouwmeester, T., Leyns, L., Kertesz, N., Gallo, M., Follettie, M., & De Robertis, E. M. (1997). Cerberus-like is a secreted factor with neuralizing activity expressed in the anterior primitive endoderm of the mouse gastrula. *Mechanisms of Development*, 68(1–2), 45-57. doi:http://dx.doi.org/10.1016/S0925-4773(97)00125-1
- Bignami, A., Hosley, M., & Dahl, D. (1993). Hyaluronic acid and hyaluronic acid-binding proteins in brain extracellular matrix. *Anat Embryol (Berl)*, 188(5), 419-433.
- Billington, C. J., Jr., Schmidt, B., Marcucio, R. S., Hallgrimsson, B., Gopalakrishnan, R., & Petryk, A. (2015). Impact of retinoic acid exposure on midfacial shape variation and manifestation of holoprosencephaly in *Twsg1* mutant mice. *Dis Model Mech*, 8(2), 139-146. doi:10.1242/dmm.018275
- Bonnans, C., Chou, J., & Werb, Z. (2014). Remodelling the extracellular matrix in development and disease. *Nat Rev Mol Cell Biol*, 15(12), 786-801. doi:10.1038/nrm3904
- Bouwmeester, T., Kim, S., Sasai, Y., Lu, B., & De Robertis, E. M. (1996). Cerberus is a head-inducing secreted factor expressed in the anterior endoderm of Spemann's organizer. *Nature*, 382(6592), 595-601. doi:10.1038/382595a0
- Briscoe, J., & Therond, P. P. (2013). The mechanisms of Hedgehog signalling and its roles in development and disease. *Nat Rev Mol Cell Biol*, 14(7), 416-429. doi:10.1038/nrm3598
- Brown, S. A., Warburton, D., Brown, L. Y., Yu, C. Y., Roeder, E. R., Stengel-Rutkowski, S., . . . Muenke, M. (1998). Holoprosencephaly due to mutations in *ZIC2*, a homologue of *Drosophila* odd-paired. *Nat Genet*, 20(2), 180-183. doi:10.1038/2484
- Brzustowicz, L. M., Farrell, S., Khan, M. B., & Weksberg, R. (1999). Mapping of a new SGBS locus to chromosome Xp22 in a family with a severe form of Simpson-Golabi-Behmel syndrome. *Am J Hum Genet*, 65(3), 779-783. doi:10.1086/302527
- Budny, B., Chen, W., Omran, H., Fliegau, M., Tzschach, A., Wisniewska, M., . . . Ropers, H. H. (2006). A novel X-linked recessive mental retardation syndrome comprising macrocephaly and ciliary dysfunction is allelic to oral-facial-digital type I syndrome. *Hum Genet*, 120(2), 171-178. doi:10.1007/s00439-006-0210-5
- Camp, J. G., Badsha, F., Florio, M., Kanton, S., Gerber, T., Wilsch-Brauninger, M., . . . Treutlein, B. (2015). Human cerebral organoids recapitulate gene expression programs of fetal neocortex development. *Proc Natl Acad Sci U S A*, 112(51), 15672-15677. doi:10.1073/pnas.1520760112
- Campos-Xavier, A. B., Martinet, D., Bateman, J., Belluoccio, D., Rowley, L., Tan, T. Y., . . . Bonafe, L. (2009). Mutations in the heparan-sulfate proteoglycan glypican 6 (GPC6) impair endochondral ossification and cause recessive omodysplasia. *Am J Hum Genet*, 84(6), 760-770. doi:10.1016/j.ajhg.2009.05.002
- Cano-Gauci, D. F., Song, H. H., Yang, H., McKerlie, C., Choo, B., Shi, W., . . . Filmus, J. (1999). Glypican-3-Deficient Mice Exhibit Developmental Overgrowth and Some of the Abnormalities Typical of Simpson-Golabi-Behmel Syndrome. *J Cell Biol*, 146(1), 255-264. doi:10.1083/jcb.146.1.255
- Capurro, M., Martin, T., Shi, W., & Filmus, J. (2014). Glypican-3 binds to Frizzled and plays a direct role in the stimulation of canonical Wnt signaling. *J Cell Sci*, 127(Pt 7), 1565-1575. doi:10.1242/jcs.140871
- Capurro, M., Shi, W., Izumikawa, T., Kitagawa, H., & Filmus, J. (2015). Processing by convertases is required for glypican-3-induced inhibition of Hedgehog signaling. *J Biol Chem*, 290(12), 7576-7585. doi:10.1074/jbc.M114.612705
- Capurro, M. I., Li, F., & Filmus, J. (2009). Overgrowth of a mouse model of Simpson-Golabi-Behmel syndrome is partly mediated by Indian hedgehog. *EMBO Rep*, 10(8), 901-907. doi:10.1038/embor.2009.98
- Capurro, M. I., Shi, W., & Filmus, J. (2012). LRP1 mediates Hedgehog-induced endocytosis of the GPC3-Hedgehog complex. *J Cell Sci*, 125(Pt 14), 3380-3389. doi:10.1242/jcs.098889

- Capurro, M. I., Xiang, Y. Y., Lobe, C., & Filmus, J. (2005). Glypican-3 promotes the growth of hepatocellular carcinoma by stimulating canonical Wnt signaling. *Cancer Res*, *65*(14), 6245-6254. doi:10.1158/0008-5472.CAN-04-4244
- Capurro, M. I., Xu, P., Shi, W., Li, F., Jia, A., & Filmus, J. (2008). Glypican-3 inhibits Hedgehog signaling during development by competing with patched for Hedgehog binding. *Dev Cell*, *14*(5), 700-711. doi:10.1016/j.devcel.2008.03.006
- Chambers, S. M., Fasano, C. A., Papapetrou, E. P., Tomishima, M., Sadelain, M., & Studer, L. (2009). Highly efficient neural conversion of human ES and iPS cells by dual inhibition of SMAD signaling. *Nat Biotechnol*, *27*(3), 275-280. doi:10.1038/nbt.1529
- Chen, C. W., Liu, C. S., Chiu, I. M., Shen, S. C., Pan, H. C., Lee, K. H., . . . Su, H. L. (2010). The signals of FGFs on the neurogenesis of embryonic stem cells. *J Biomed Sci*, *17*, 33. doi:10.1186/1423-0127-17-33
- Chen, J. K., Taipale, J., Cooper, M. K., & Beachy, P. A. (2002). Inhibition of Hedgehog signaling by direct binding of cyclopamine to Smoothened. *Genes Dev*, *16*(21), 2743-2748. doi:10.1101/gad.1025302
- Chen, X., Tukachinsky, H., Huang, C. H., Jao, C., Chu, Y. R., Tang, H. Y., . . . Salic, A. (2011). Processing and turnover of the Hedgehog protein in the endoplasmic reticulum. *J Cell Biol*, *192*(5), 825-838. doi:10.1083/jcb.201008090
- Chiang, C., Litingtung, Y., Lee, E., Young, K. E., Corden, J. L., Westphal, H., & Beachy, P. A. (1996). Cyclopia and defective axial patterning in mice lacking Sonic hedgehog gene function. *Nature*, *383*(6599), 407-413. doi:10.1038/383407a0
- Chiao, E., Fisher, P., Crisponi, L., Deiana, M., Dragatsis, I., Schlessinger, D., . . . Efstratiadis, A. (2002). Overgrowth of a mouse model of the Simpson-Golabi-Behmel syndrome is independent of IGF signaling. *Dev Biol*, *243*(1), 185-206. doi:10.1006/dbio.2001.0554
- Chuang, J.-H., Tung, L.-C., & Lin, Y. (2015). Neural differentiation from embryonic stem cells in vitro: An overview of the signaling pathways. *World Journal of Stem Cells*, *7*(2), 437-447. doi:10.4252/wjsc.v7.i2.437
- Chuang, P. T., & McMahon, A. P. (1999). Vertebrate Hedgehog signalling modulated by induction of a Hedgehog-binding protein. *Nature*, *397*(6720), 617-621. doi:10.1038/17611
- Chun, J., & Jaenisch, R. (1996). Clonal cell lines produced by infection of neocortical neuroblasts using multiple oncogenes transduced by retroviruses. *Mol Cell Neurosci*, *7*(4), 304-321. doi:10.1006/mcne.1996.0023
- Ciani, L., & Salinas, P. C. (2005). WNTs in the vertebrate nervous system: from patterning to neuronal connectivity. *Nat Rev Neurosci*, *6*(5), 351-362.
- Cohen, M. M., Jr. (1989). Perspectives on holoprosencephaly: Part I. Epidemiology, genetics, and syndromology. *Teratology*, *40*(3), 211-235. doi:10.1002/tera.1420400304
- Cole, F., & Krauss, R. S. (2003). Microform holoprosencephaly in mice that lack the Ig superfamily member Cdon. *Curr Biol*, *13*(5), 411-415.
- Coles, C. H., Shen, Y., Tenney, A. P., Siebold, C., Sutton, G. C., Lu, W., . . . Aricescu, A. R. (2011). Proteoglycan-specific molecular switch for RPTPsigma clustering and neuronal extension. *Science*, *332*(6028), 484-488. doi:10.1126/science.1200840
- Conte, I., Morcillo, J., & Bovolenta, P. (2005). Comparative analysis of Six3 and Six6 distribution in the developing and adult mouse brain. *Developmental Dynamics*, *234*(3), 718-725. doi:10.1002/dvdy.20463
- Corbit, K. C., Shyer, A. E., Dowdle, W. E., Gaulden, J., Singla, V., Chen, M. H., . . . Reiter, J. F. (2008). Kif3a constrains beta-catenin-dependent Wnt signalling through dual ciliary and non-ciliary mechanisms. *Nat Cell Biol*, *10*(1), 70-76. doi:10.1038/ncb1670
- Cordero, D., Marcucio, R., Hu, D., Gaffield, W., Tapadia, M., & Helms, J. A. (2004). Temporal perturbations in sonic hedgehog signaling elicit the spectrum of holoprosencephaly phenotypes. *J Clin Invest*, *114*(4), 485-494. doi:10.1172/jci19596

- Correa, A., Gilboa, S. M., Besser, L. M., Botto, L. D., Moore, C. A., Hobbs, C. A., . . . Reece, E. A. (2008). Diabetes mellitus and birth defects. *Am J Obstet Gynecol*, *199*(3), 237 e231-239. doi:10.1016/j.ajog.2008.06.028
- Cortes, C. R., Metzis, V., & Wicking, C. (2015). Unmasking the ciliopathies: craniofacial defects and the primary cilium. *Wiley Interdiscip Rev Dev Biol*, *4*(6), 637-653. doi:10.1002/wdev.199
- Cragg, B. (1979). Brain extracellular space fixed for electron microscopy. *Neurosci Lett*, *15*(2-3), 301-306.
- Creanga, A., Glenn, T. D., Mann, R. K., Saunders, A. M., Talbot, W. S., & Beachy, P. A. (2012). Scube/You activity mediates release of dually lipid-modified Hedgehog signal in soluble form. *Genes Dev*, *26*(12), 1312-1325. doi:10.1101/gad.191866.112
- Croen, L. A., Shaw, G. M., & Lammer, E. J. (2000). Risk factors for cytogenetically normal holoprosencephaly in California: a population-based case-control study. *Am J Med Genet*, *90*(4), 320-325.
- Dani, N., Nahm, M., Lee, S., & Broadie, K. (2012). A targeted glycan-related gene screen reveals heparan sulfate proteoglycan sulfation regulates WNT and BMP trans-synaptic signaling. *PLoS Genet*, *8*(11), e1003031. doi:10.1371/journal.pgen.1003031
- De Cat, B., & David, G. (2001). Developmental roles of the glypicans. *Semin Cell Dev Biol*, *12*(2), 117-125. doi:10.1006/scdb.2000.0240
- de Wit, J., O'Sullivan, M. L., Savas, J. N., Condomitti, G., Caccese, M. C., Vennekens, K. M., . . . Ghosh, A. (2013). Unbiased discovery of glypican as a receptor for LRRTM4 in regulating excitatory synapse development. *Neuron*, *79*(4), 696-711. doi:10.1016/j.neuron.2013.06.049
- Demyer, W., Zeman, W., & Palmer, C. G. (1964). THE FACE PREDICTS THE BRAIN: DIAGNOSTIC SIGNIFICANCE OF MEDIAN FACIAL ANOMALIES FOR HOLOPROSENCEPHALY (ARHINENCEPHALY). *Pediatrics*, *34*, 256-263.
- Desbordes, S. C., & Sanson, B. (2003). The glypican Dally-like is required for Hedgehog signalling in the embryonic epidermis of Drosophila. *Development*, *130*(25), 6245-6255. doi:10.1242/dev.00874
- Dickinson, M. E., Flenniken, A. M., Ji, X., Teboul, L., Wong, M. D., White, J. K., . . . Murray, S. A. (2016). High-throughput discovery of novel developmental phenotypes. *Nature*, advance online publication. doi:10.1038/nature19356
- Dupe, V., Rochard, L., Mercier, S., Le Petillon, Y., Gicquel, I., Bendavid, C., . . . David, V. (2011). NOTCH, a new signaling pathway implicated in holoprosencephaly. *Hum Mol Genet*, *20*(6), 1122-1131. doi:10.1093/hmg/ddq556
- Engert, S., Burtscher, I., Liao, W. P., Dulev, S., Schotta, G., & Lickert, H. (2013). Wnt/beta-catenin signalling regulates Sox17 expression and is essential for organizer and endoderm formation in the mouse. *Development*, *140*(15), 3128-3138. doi:10.1242/dev.088765
- Eugster, C., Panakova, D., Mahmoud, A., & Eaton, S. (2007). Lipoprotein-heparan sulfate interactions in the Hh pathway. *Dev Cell*, *13*(1), 57-71. doi:10.1016/j.devcel.2007.04.019
- Ferrante, M. I., Zullo, A., Barra, A., Bimonte, S., Messaddeq, N., Studer, M., . . . Franco, B. (2006). Oral-facial-digital type I protein is required for primary cilia formation and left-right axis specification. *Nat Genet*, *38*(1), 112-117. doi:10.1038/ng1684
- Fico, A., De Chevigny, A., Egea, J., Bosl, M. R., Cremer, H., Maina, F., & Dono, R. (2012). Modulating Glypican4 suppresses tumorigenicity of embryonic stem cells while preserving self-renewal and pluripotency. *Stem Cells*, *30*(9), 1863-1874. doi:10.1002/stem.1165
- Fico, A., de Chevigny, A., Melon, C., Bohic, M., Kerkerian-Le Goff, L., Maina, F., . . . Cremer, H. (2014). Reducing glypican-4 in ES cells improves recovery in a rat model of Parkinson's disease by increasing the production of dopaminergic neurons and decreasing teratoma formation. *J Neurosci*, *34*(24), 8318-8323. doi:10.1523/JNEUROSCI.2501-13.2014
- Filmus, J., & Capurro, M. (2014). The role of glypicans in Hedgehog signaling. *Matrix Biol*, *35*, 248-252. doi:10.1016/j.matbio.2013.12.007

- Filmus, J., Capurro, M., & Rast, J. (2008). Glypicans. *Genome Biol*, 9(5), 224. doi:10.1186/gb-2008-9-5-224
- Fliegauf, M., Benzing, T., & Omran, H. (2007). When cilia go bad: cilia defects and ciliopathies. *Nat Rev Mol Cell Biol*, 8(11), 880-893. doi:http://www.nature.com/nrm/journal/v8/n11/supinfo/nrm2278_S1.html
- Ford-Perriss, M., Turner, K., Guimond, S., Apedaile, A., Haubeck, H. D., Turnbull, J., & Murphy, M. (2003). Localisation of specific heparan sulfate proteoglycans during the proliferative phase of brain development. *Dev Dyn*, 227(2), 170-184. doi:10.1002/dvdy.10298
- Fratzl, P., Misof, K., Zizak, I., Rapp, G., Amenitsch, H., & Bernstorff, S. (1998). Fibrillar structure and mechanical properties of collagen. *J Struct Biol*, 122(1-2), 119-122. doi:10.1006/jsbi.1998.3966
- Fujise, M., Takeo, S., Kamimura, K., Matsuo, T., Aigaki, T., Izumi, S., & Nakato, H. (2003). Dally regulates Dpp morphogen gradient formation in the Drosophila wing. *Development*, 130(8), 1515-1522.
- Gallet, A., Staccini-Lavenant, L., & Therond, P. P. (2008). Cellular trafficking of the glypican Dally-like is required for full-strength Hedgehog signaling and wingless transcytosis. *Dev Cell*, 14(5), 712-725. doi:10.1016/j.devcel.2008.03.001
- Gallet, A., & Therond, P. P. (2005). Temporal modulation of the Hedgehog morphogen gradient by a patched-dependent targeting to lysosomal compartment. *Dev Biol*, 277(1), 51-62. doi:10.1016/j.ydbio.2004.09.005
- Galli, A., Roure, A., Zeller, R., & Dono, R. (2003). Glypican 4 modulates FGF signalling and regulates dorsoventral forebrain patterning in Xenopus embryos. *Development*, 130(20), 4919-4929. doi:10.1242/dev.00706
- Geng, X., & Oliver, G. (2009). Pathogenesis of holoprosencephaly. *J Clin Invest*, 119(6), 1403-1413. doi:10.1172/jci38937
- Gerdes, J. M., Davis, E. E., & Katsanis, N. (2009). The vertebrate primary cilium in development, homeostasis, and disease. *Cell*, 137(1), 32-45. doi:10.1016/j.cell.2009.03.023
- Gerdes, J. M., Liu, Y., Zaghoul, N. A., Leitch, C. C., Lawson, S. S., Kato, M., . . . Katsanis, N. (2007). Disruption of the basal body compromises proteasomal function and perturbs intracellular Wnt response. *Nat Genet*, 39(11), 1350-1360. doi:10.1038/ng.2007.12
- Gesta, S., Bluher, M., Yamamoto, Y., Norris, A. W., Berndt, J., Kralisch, S., . . . Kahn, C. R. (2006). Evidence for a role of developmental genes in the origin of obesity and body fat distribution. *Proc Natl Acad Sci U S A*, 103(17), 6676-6681. doi:10.1073/pnas.0601752103
- Gori, F., Lerner, U., Ohlsson, C., & Baron, R. (2015). A new WNT on the bone: WNT16, cortical bone thickness, porosity and fractures. *Bonekey Rep*, 4, 669. doi:10.1038/bonekey.2015.36
- Gripp, K. W., Wotton, D., Edwards, M. C., Roessler, E., Ades, L., Meinecke, P., . . . Elledge, S. J. (2000). Mutations in TGIF cause holoprosencephaly and link NODAL signalling to human neural axis determination. *Nat Genet*, 25(2), 205-208. doi:10.1038/76074
- Guilak, F., Cohen, D. M., Estes, B. T., Gimble, J. M., Liedtke, W., & Chen, C. S. (2009). Control of Stem Cell Fate by Physical Interactions with the Extracellular Matrix. *Cell Stem Cell*, 5(1), 17-26. doi:http://dx.doi.org/10.1016/j.stem.2009.06.016
- Guo, J., Higginbotham, H., Li, J., Nichols, J., Hirt, J., Ghukasyan, V., & Anton, E. S. (2015). Developmental disruptions underlying brain abnormalities in ciliopathies. *Nat Commun*, 6, 7857. doi:10.1038/ncomms8857
- Hagihara, K., Watanabe, K., Chun, J., & Yamaguchi, Y. (2000). Glypican-4 is an FGF2-binding heparan sulfate proteoglycan expressed in neural precursor cells. *Dev Dyn*, 219(3), 353-367. doi:10.1002/1097-0177(2000)9999:9999::AID-DVDY1059>3.0.CO;2-#
- Hahn, H., Wojnowski, L., Zimmer, A. M., Hall, J., Miller, G., & Zimmer, A. (1998). Rhabdomyosarcomas and radiation hypersensitivity in a mouse model of Gorlin syndrome. *Nat Med*, 4(5), 619-622.
- Harkness, L., Christiansen, H., Nehlin, J., Barington, T., Andersen, J. S., & Kassem, M. (2008). Identification of a membrane proteomic signature for human embryonic stem cells

- independent of culture conditions. *Stem Cell Res*, 1(3), 219-227.
doi:10.1016/j.scr.2008.06.001
- Heavner, W., & Pevny, L. (2012). Eye Development and Retinogenesis. *Cold Spring Harb Perspect Biol*, 4(12), a008391. doi:10.1101/cshperspect.a008391
- Hébert, J. M., & Fishell, G. (2008). The genetics of early telencephalon patterning: some assembly required. *Nature reviews. Neuroscience*, 9(9), 678-685. doi:10.1038/nrn2463
- Hecht, J. H., Weiner, J. A., Post, S. R., & Chun, J. (1996). Ventricular zone gene-1 (vzg-1) encodes a lysophosphatidic acid receptor expressed in neurogenic regions of the developing cerebral cortex. *J Cell Biol*, 135(4), 1071-1083.
- Heisenberg, C. P., Houart, C., Take-Uchi, M., Rauch, G. J., Young, N., Coutinho, P., . . . Stemple, D. L. (2001). A mutation in the Gsk3-binding domain of zebrafish Masterblind/Axin1 leads to a fate transformation of telencephalon and eyes to diencephalon. *Genes Dev*, 15(11), 1427-1434. doi:10.1101/gad.194301
- Higashiyama, D., Saitsu, H., Komada, M., Takigawa, T., Ishibashi, M., & Shiota, K. (2007). Sequential developmental changes in holoprosencephalic mouse embryos exposed to ethanol during the gastrulation period. *Birth Defects Res A Clin Mol Teratol*, 79(7), 513-523. doi:10.1002/bdra.20367
- Hirano, K., Sasaki, N., Ichimiya, T., Miura, T., Van Kuppevelt, T. H., & Nishihara, S. (2012). 3-O-sulfated heparan sulfate recognized by the antibody HS4C3 contributes [corrected] to the differentiation of mouse embryonic stem cells via fas signaling. *PLoS One*, 7(8), e43440. doi:10.1371/journal.pone.0043440
- Hogan, B. L. (1996). Bone morphogenetic proteins in development. *Curr Opin Genet Dev*, 6(4), 432-438.
- Hong, M., & Krauss, R. S. (2013). Rescue of holoprosencephaly in fetal alcohol-exposed Cdon mutant mice by reduced gene dosage of Ptch1. *PLoS One*, 8(11), e79269. doi:10.1371/journal.pone.0079269
- Hong, S., Hwang, D.-Y., Yoon, S., Isacson, O., Ramezani, A., Hawley, R. G., & Kim, K.-S. (2007). Functional Analysis of Various Promoters in Lentiviral Vectors at Different Stages of In Vitro Differentiation of Mouse Embryonic Stem Cells. *Mol Ther*, 15(9), 1630-1639. doi:10.1038/sj.mt.6300251
- Hosaka, M., Nagahama, M., Kim, W. S., Watanabe, T., Hatsuzawa, K., Ikemizu, J., . . . Nakayama, K. (1991). Arg-X-Lys/Arg-Arg motif as a signal for precursor cleavage catalyzed by furin within the constitutive secretory pathway. *J Biol Chem*, 266(19), 12127-12130.
- Houart, C., Caneparo, L., Heisenberg, C., Barth, K., Take-Uchi, M., & Wilson, S. (2002). Establishment of the telencephalon during gastrulation by local antagonism of Wnt signaling. *Neuron*, 35(2), 255-265.
- Huangfu, D., Liu, A., Rakeman, A. S., Murcia, N. S., Niswander, L., & Anderson, K. V. (2003). Hedgehog signalling in the mouse requires intraflagellar transport proteins. *Nature*, 426(6962), 83-87. doi:10.1038/nature02061
- Huber, A. B., Kania, A., Tran, T. S., Gu, C., De Marco Garcia, N., Lieberam, I., . . . Kolodkin, A. L. (2005). Distinct roles for secreted semaphorin signaling in spinal motor axon guidance. *Neuron*, 48(6), 949-964. doi:10.1016/j.neuron.2005.12.003
- Hynes, R. O., & Naba, A. (2012). Overview of the matrisome--an inventory of extracellular matrix constituents and functions. *Cold Spring Harb Perspect Biol*, 4(1), a004903. doi:10.1101/cshperspect.a004903
- Izzi, L., Levesque, M., Morin, S., Laniel, D., Wilkes, B. C., Mille, F., . . . Charron, F. (2011). Boc and Gas1 each form distinct Shh receptor complexes with Ptch1 and are required for Shh-mediated cell proliferation. *Dev Cell*, 20(6), 788-801. doi:10.1016/j.devcel.2011.04.017
- Jen, Y. H., Musacchio, M., & Lander, A. D. (2009). Glypican-1 controls brain size through regulation of fibroblast growth factor signaling in early neurogenesis. *Neural Dev*, 4, 33. doi:10.1186/1749-8104-4-33

- Jeong, Y., Leskow, F. C., El-Jaick, K., Roessler, E., Muenke, M., Yocum, A., . . . Epstein, D. J. (2008). Regulation of a remote Shh forebrain enhancer by the Six3 homeoprotein. *Nat Genet*, *40*(11), 1348-1353. doi:10.1038/ng.230
- Johnson, C. E., Crawford, B. E., Stavridis, M., Ten Dam, G., Wat, A. L., Rushton, G., . . . Merry, C. L. (2007). Essential alterations of heparan sulfate during the differentiation of embryonic stem cells to Sox1-enhanced green fluorescent protein-expressing neural progenitor cells. *Stem Cells*, *25*(8), 1913-1923. doi:10.1634/stemcells.2006-0445
- Kakugawa, S., Langton, P. F., Zebisch, M., Howell, S. A., Chang, T. H., Liu, Y., . . . Vincent, J. P. (2015). Notum deacylates Wnt proteins to suppress signalling activity. *Nature*, *519*(7542), 187-192. doi:10.1038/nature14259
- Kattman, S. J., Witty, A. D., Gagliardi, M., Dubois, N. C., Niapour, M., Hotta, A., . . . Keller, G. (2011). Stage-Specific Optimization of Activin/Nodal and BMP Signaling Promotes Cardiac Differentiation of Mouse and Human Pluripotent Stem Cell Lines. *Cell Stem Cell*, *8*(2), 228-240. doi:http://dx.doi.org/10.1016/j.stem.2010.12.008
- Kawasaki, H., Mizuseki, K., Nishikawa, S., Kaneko, S., Kuwana, Y., Nakanishi, S., . . . Sasai, Y. (2000). Induction of midbrain dopaminergic neurons from ES cells by stromal cell-derived inducing activity. *Neuron*, *28*(1), 31-40. doi:http://dx.doi.org/10.1016/S0896-6273(00)00083-0
- Keane, T. M., Goodstadt, L., Danecek, P., White, M. A., Wong, K., Yalcin, B., . . . Adams, D. J. (2011). Mouse genomic variation and its effect on phenotypes and gene regulation. *Nature*, *477*(7364), 289-294. doi:http://www.nature.com/nature/journal/v477/n7364/abs/nature10413.html#supplementary-information
- Kietzman, H. W., Everson, J. L., Sulik, K. K., & Lipinski, R. J. (2014). The teratogenic effects of prenatal ethanol exposure are exacerbated by Sonic Hedgehog or GLI2 haploinsufficiency in the mouse. *PLoS One*, *9*(2), e89448. doi:10.1371/journal.pone.0089448
- Kim, M. S., Saunders, A. M., Hamaoka, B. Y., Beachy, P. A., & Leahy, D. J. (2011). Structure of the protein core of the glypican Dally-like and localization of a region important for hedgehog signaling. *Proc Natl Acad Sci U S A*, *108*(32), 13112-13117. doi:10.1073/pnas.1109877108
- Kinder, S. J., Tsang, T. E., Wakamiya, M., Sasaki, H., Behringer, R. R., Nagy, A., & Tam, P. P. (2001). The organizer of the mouse gastrula is composed of a dynamic population of progenitor cells for the axial mesoderm. *Development*, *128*(18), 3623-3634.
- Kirkpatrick, C. A., Dimitroff, B. D., Rawson, J. M., & Selleck, S. B. (2004). Spatial regulation of Wingless morphogen distribution and signaling by Dally-like protein. *Dev Cell*, *7*(4), 513-523. doi:10.1016/j.devcel.2004.08.004
- Ko, J. S., Pramanik, G., Um, J. W., Shim, J. S., Lee, D., Kim, K. H., . . . Ko, J. (2015). PTPsigma functions as a presynaptic receptor for the glypican-4/LRRTM4 complex and is essential for excitatory synaptic transmission. *Proc Natl Acad Sci U S A*, *112*(6), 1874-1879. doi:10.1073/pnas.1410138112
- Kousseff, B. G. (1999). Gestational diabetes mellitus (class A): a human teratogen? *Am J Med Genet*, *83*(5), 402-408.
- Kraushaar, D. C., Yamaguchi, Y., & Wang, L. (2010). Heparan sulfate is required for embryonic stem cells to exit from self-renewal. *J Biol Chem*, *285*(8), 5907-5916. doi:10.1074/jbc.M109.066837
- Kraushaar, D. C., Yamaguchi, Y., & Wang, L. (2015). Heparan sulfate is required for embryonic stem cells to exit from self-renewal. *J Biol Chem*, *290*(38), 23023. doi:10.1074/jbc.A109.066837
- Kreuger, J., Perez, L., Giraldez, A. J., & Cohen, S. M. (2004). Opposing activities of Dally-like glypican at high and low levels of Wingless morphogen activity. *Dev Cell*, *7*(4), 503-512. doi:10.1016/j.devcel.2004.08.005
- Kriks, S., Shim, J.-W., Piao, J., Ganat, Y. M., Wakeman, D. R., Xie, Z., . . . Studer, L. (2011). Dopamine neurons derived from human ES cells efficiently engraft in animal models of Parkinson's disease. *Nature*, *480*(7378), 547-551.

- doi:<http://www.nature.com/nature/journal/v480/n7378/abs/nature10648.html#supplementary-information>
- Kulandavelu, S., Qu, D., Sunn, N., Mu, J., Rennie, M. Y., Whiteley, K. J., . . . Adamson, S. L. (2006). Embryonic and neonatal phenotyping of genetically engineered mice. *ILAR J*, *47*(2), 103-117.
- Kunath, T., Saba-El-Leil, M. K., Almousailleakh, M., Wray, J., Meloche, S., & Smith, A. (2007). FGF stimulation of the Erk1/2 signalling cascade triggers transition of pluripotent embryonic stem cells from self-renewal to lineage commitment. *Development*, *134*(16), 2895-2902. doi:10.1242/dev.02880
- Kwok, J. C., Dick, G., Wang, D., & Fawcett, J. W. (2011). Extracellular matrix and perineuronal nets in CNS repair. *Dev Neurobiol*, *71*(11), 1073-1089. doi:10.1002/dneu.20974
- Lagutin, O. V., Zhu, C. C., Kobayashi, D., Topczewski, J., Shimamura, K., Puelles, L., . . . Oliver, G. (2003). Six3 repression of Wnt signaling in the anterior neuroectoderm is essential for vertebrate forebrain development. *Genes Dev*, *17*(3), 368-379. doi:10.1101/gad.1059403
- Lammer, E. J., Chen, D. T., Hoar, R. M., Agnish, N. D., Benke, P. J., Braun, J. T., . . . et al. (1985). Retinoic acid embryopathy. *N Engl J Med*, *313*(14), 837-841. doi:10.1056/nejm198510033131401
- Lanoue, L., Dehart, D. B., Hinsdale, M. E., Maeda, N., Tint, G. S., & Sulik, K. K. (1997). Limb, genital, CNS, and facial malformations result from gene/environment-induced cholesterol deficiency: further evidence for a link to sonic hedgehog. *Am J Med Genet*, *73*(1), 24-31.
- Lau, L. W., Cua, R., Keough, M. B., Haylock-Jacobs, S., & Yong, V. W. (2013). Pathophysiology of the brain extracellular matrix: a new target for remyelination. *Nat Rev Neurosci*, *14*(10), 722-729. doi:10.1038/nrn3550
- Le Dreau, G., & Marti, E. (2012). Dorsal-ventral patterning of the neural tube: a tale of three signals. *Dev Neurobiol*, *72*(12), 1471-1481. doi:10.1002/dneu.22015
- LeClair, E. E., Mui, S. R., Huang, A., Topczewska, J. M., & Topczewski, J. (2009). Craniofacial skeletal defects of adult zebrafish Glypican 4 (knypek) mutants. *Dev Dyn*, *238*(10), 2550-2563. doi:10.1002/dvdy.22086
- Ledin, J., Staatz, W., Li, J. P., Gotte, M., Selleck, S., Kjellen, L., & Spillmann, D. (2004). Heparan sulfate structure in mice with genetically modified heparan sulfate production. *J Biol Chem*, *279*(41), 42732-42741. doi:10.1074/jbc.M405382200
- Lee, H., Shamy, G. A., Elkabetz, Y., Schofield, C. M., Harrision, N. L., Panagiotakos, G., . . . Studer, L. (2007). Directed differentiation and transplantation of human embryonic stem cell-derived motoneurons. *Stem Cells*, *25*(8), 1931-1939. doi:10.1634/stemcells.2007-0097
- Li, F., Shi, W., Capurro, M., & Filmus, J. (2011). Glypican-5 stimulates rhabdomyosarcoma cell proliferation by activating Hedgehog signaling. *J Cell Biol*, *192*(4), 691-704. doi:10.1083/jcb.201008087
- Li, K., Xu, X., Hu, W., Li, M., Yang, M., Wang, Y., . . . Yang, G. (2014). Glypican-4 is increased in human subjects with impaired glucose tolerance and decreased in patients with newly diagnosed type 2 diabetes. *Acta Diabetol*, *51*(6), 981-990. doi:10.1007/s00592-014-0652-5
- Li, M., Shuman, C., Fei, Y. L., Cutiongco, E., Bender, H. A., Stevens, C., . . . Weksberg, R. (2001). GPC3 mutation analysis in a spectrum of patients with overgrowth expands the phenotype of Simpson-Golabi-Behmel syndrome. *Am J Med Genet*, *102*(2), 161-168.
- Lin, A. E., Neri, G., Hughes-Benzie, R., & Weksberg, R. (1999). Cardiac anomalies in the Simpson-Golabi-Behmel syndrome. *Am J Med Genet*, *83*(5), 378-381.
- Lin, X., Wei, G., Shi, Z., Dryer, L., Esko, J. D., Wells, D. E., & Matzuk, M. M. (2000). Disruption of Gastrulation and Heparan Sulfate Biosynthesis in EXT1-Deficient Mice. *Dev Biol*, *224*(2), 299-311. doi:<http://dx.doi.org/10.1006/dbio.2000.9798>
- Linder, B., Weber, S., Dittmann, K., Adamski, J., Hahn, H., & Uhmman, A. (2015). A Functional and Putative Physiological Role of Calcitriol in Patched1/Smoothed Interaction. *J Biol Chem*, *290*(32), 19614-19628. doi:10.1074/jbc.M115.646141

- Lipinski, R. J., Godin, E. A., O'Leary-Moore, S. K., Parnell, S. E., & Sulik, K. K. (2010). Genesis of teratogen-induced holoprosencephaly in mice. *Am J Med Genet C Semin Med Genet*, *154c*(1), 29-42. doi:10.1002/ajmg.c.30239
- Litwack, E. D., Stipp, C. S., Kumbasar, A., & Lander, A. D. (1994). Neuronal expression of glypican, a cell-surface glycosylphosphatidylinositol-anchored heparan sulfate proteoglycan, in the adult rat nervous system. *J Neurosci*, *14*(6), 3713-3724.
- Liu, A., & Niswander, L. A. (2005). Bone morphogenetic protein signalling and vertebrate nervous system development. *Nat Rev Neurosci*, *6*(12), 945-954. doi:10.1038/nrn1805
- Lum, L., Yao, S., Mozer, B., Rovescalli, A., Von Kessler, D., Nirenberg, M., & Beachy, P. A. (2003). Identification of Hedgehog pathway components by RNAi in *Drosophila* cultured cells. *Science*, *299*(5615), 2039-2045. doi:10.1126/science.1081403
- Luxardi, G., Galli, A., Forlani, S., Lawson, K., Maina, F., & Dono, R. (2007). Glypicans are differentially expressed during patterning and neurogenesis of early mouse brain. *Biochem Biophys Res Commun*, *352*(1), 55-60. doi:10.1016/j.bbrc.2006.10.185
- Ma, Y., Erkner, A., Gong, R., Yao, S., Taipale, J., Basler, K., & Beachy, P. A. (2002). Hedgehog-mediated patterning of the mammalian embryo requires transporter-like function of Dispatched. *Cell*, *111*(1), 63-75.
- Mann, R. K., & Beachy, P. A. (2004). Novel lipid modifications of secreted protein signals. *Annu Rev Biochem*, *73*, 891-923. doi:10.1146/annurev.biochem.73.011303.073933
- Manuel, M., Martynoga, B., Yu, T., West, J. D., Mason, J. O., & Price, D. J. (2010). The transcription factor Foxg1 regulates the competence of telencephalic cells to adopt subpallial fates in mice. *Development*, *137*(3), 487-497. doi:10.1242/dev.039800
- Marklund, M., Sjodal, M., Beehler, B. C., Jessell, T. M., Edlund, T., & Gunhaga, L. (2004). Retinoic acid signalling specifies intermediate character in the developing telencephalon. *Development*, *131*(17), 4323-4332. doi:10.1242/dev.01308
- Martinelli, D. C., & Fan, C. M. (2007). Gas1 extends the range of Hedgehog action by facilitating its signaling. *Genes Dev*, *21*(10), 1231-1243. doi:10.1101/gad.1546307
- McCarthy, R. A., Barth, J. L., Chintalapudi, M. R., Knaak, C., & Argraves, W. S. (2002). Megalin functions as an endocytic sonic hedgehog receptor. *J Biol Chem*, *277*(28), 25660-25667. doi:10.1074/jbc.M201933200
- Mecham, R. P. (2012). Overview of extracellular matrix. *Curr Protoc Cell Biol*, Chapter 10, Unit 10.11. doi:10.1002/0471143030.cb1001s57
- Metscher, B. D. (2009). MicroCT for developmental biology: a versatile tool for high-contrast 3D imaging at histological resolutions. *Dev Dyn*, *238*(3), 632-640. doi:10.1002/dvdy.21857
- Milenkovic, L., Scott, M. P., & Rohatgi, R. (2009). Lateral transport of Smoothed from the plasma membrane to the membrane of the cilium. *J Cell Biol*, *187*(3), 365-374. doi:10.1083/jcb.200907126
- Ming, J. E., Kaupas, M. E., Roessler, E., Brunner, H. G., Golabi, M., Tekin, M., . . . Muenke, M. (2002). Mutations in PATCHED-1, the receptor for SONIC HEDGEHOG, are associated with holoprosencephaly. *Human Genetics*, *110*(4), 297-301. doi:10.1007/s00439-002-0695-5
- Molina, G., Vogt, A., Bakan, A., Dai, W., Queiroz de Oliveira, P., Znosko, W., . . . Tsang, M. (2009). Zebrafish chemical screening reveals an inhibitor of Dusp6 that expands cardiac cell lineages. *Nat Chem Biol*, *5*(9), 680-687. doi:10.1038/nchembio.190
- Morita, Y., Kimoto, N., Ogawa, H., Omata, T., & Morita, N. (2011). Simpson-Golabi-Behmel syndrome associated with cleft palate. *J Craniofac Surg*, *22*(5), 1917-1918. doi:10.1097/SCS.0b013e31822ea73c
- Mouw, J. K., Ou, G., & Weaver, V. M. (2014). Extracellular matrix assembly: a multiscale deconstruction. *Nat Rev Mol Cell Biol*, *15*(12), 771-785. doi:10.1038/nrm3902
- Mujezinovic, F., Krgovic, D., Blatnik, A., Zagradisnik, B., Vipotnik, T. V., Golec, T., . . . Vokac, N. K. (2016). Simpson-Golabi-Behmel syndrome: a prenatal diagnosis in a foetus with GPC3 and GPC4 gene microduplications. *Clin Genet*, *90*(1), 99-101. doi:10.1111/cge.12725

- Mummery, C. L., Zhang, J., Ng, E. S., Elliott, D. A., Elefanty, A. G., & Kamp, T. J. (2012). Differentiation of human embryonic stem cells and induced pluripotent stem cells to cardiomyocytes: a methods overview. *Circ Res*, *111*(3), 344-358. doi:10.1161/CIRCRESAHA.110.227512
- Murdoch, J. N., & Copp, A. J. (2010). The relationship between sonic Hedgehog signaling, cilia, and neural tube defects. *Birth Defects Res A Clin Mol Teratol*, *88*(8), 633-652. doi:10.1002/bdra.20686
- Nairn, A. V., Kinoshita-Toyoda, A., Toyoda, H., Xie, J., Harris, K., Dalton, S., . . . Linhardt, R. J. (2007). Glycomics of proteoglycan biosynthesis in murine embryonic stem cell differentiation. *J Proteome Res*, *6*(11), 4374-4387. doi:10.1021/pr070446f
- Nicholson, C., & Sykova, E. (1998). Extracellular space structure revealed by diffusion analysis. *Trends Neurosci*, *21*(5), 207-215.
- Nozawa, Y. I., Lin, C., & Chuang, P. T. (2013). Hedgehog signaling from the primary cilium to the nucleus: an emerging picture of ciliary localization, trafficking and transduction. *Curr Opin Genet Dev*, *23*(4), 429-437. doi:10.1016/j.gde.2013.04.008
- Oh, J.-E., Bae, G.-U., Yang, Y.-J., Yi, M.-J., Lee, H.-J., Kim, B.-G., . . . Kang, J.-S. (2009). Cdo promotes neuronal differentiation via activation of the p38 mitogen-activated protein kinase pathway. *The FASEB Journal*, *23*(7), 2088-2099. doi:10.1096/fj.08-119255
- Ohkawara, B., Yamamoto, T. S., Tada, M., & Ueno, N. (2003). Role of glypican 4 in the regulation of convergent extension movements during gastrulation in *Xenopus laevis*. *Development*, *130*(10), 2129-2138.
- Oikari, L. E., Okolicsanyi, R. K., Qin, A., Yu, C., Griffiths, L. R., & Haupt, L. M. (2016). Cell surface heparan sulfate proteoglycans as novel markers of human neural stem cell fate determination. *Stem Cell Research*, *16*(1), 92-104. doi:http://dx.doi.org/10.1016/j.scr.2015.12.011
- Okada, T., Okumura, Y., Motoyama, J., & Ogawa, M. (2008). FGF8 signaling patterns the telencephalic midline by regulating putative key factors of midline development. *Dev Biol*, *320*(1), 92-101. doi:http://dx.doi.org/10.1016/j.ydbio.2008.04.034
- Oliver, G., Mailhos, A., Wehr, R., Copeland, N. G., Jenkins, N. A., & Gruss, P. (1995). Six3, a murine homologue of the sine oculis gene, demarcates the most anterior border of the developing neural plate and is expressed during eye development. *Development*, *121*(12), 4045-4055.
- Olsen, C. L., Hughes, J. P., Youngblood, L. G., & Sharpe-Stimac, M. (1997). Epidemiology of holoprosencephaly and phenotypic characteristics of affected children: New York State, 1984-1989. *Am J Med Genet*, *73*(2), 217-226.
- Orioli, I. M., & Castilla, E. E. (2010). Epidemiology of holoprosencephaly: Prevalence and risk factors. *Am J Med Genet C Semin Med Genet*, *154C*(1), 13-21. doi:10.1002/ajmg.c.30233
- Paine-Saunders, S., Viviano, B. L., Zupicich, J., Skarnes, W. C., & Saunders, S. (2000). glypican-3 controls cellular responses to Bmp4 in limb patterning and skeletal development. *Dev Biol*, *225*(1), 179-187. doi:10.1006/dbio.2000.9831
- Panakova, D., Sprong, H., Marois, E., Thiele, C., & Eaton, S. (2005). Lipoprotein particles are required for Hedgehog and Wingless signalling. *Nature*, *435*(7038), 58-65. doi:http://www.nature.com/nature/journal/v435/n7038/supinfo/nature03504_S1.html
- Pauli, R. M., Pettersen, J. C., Arya, S., & Gilbert, E. F. (1983). Familial agnathia-holoprosencephaly. *Am J Med Genet*, *14*(4), 677-698. doi:10.1002/ajmg.1320140411
- Petryk, A., Anderson, R. M., Jarcho, M. P., Leaf, I., Carlson, C. S., Klingensmith, J., . . . O'Connor, M. B. (2004). The mammalian twisted gastrulation gene functions in foregut and craniofacial development. *Dev Biol*, *267*(2), 374-386. doi:10.1016/j.ydbio.2003.11.015
- Petryk, A., Graf, D., & Marcucio, R. (2015). Holoprosencephaly: signaling interactions between the brain and the face, the environment and the genes, and the phenotypic variability in animal models and humans. *Wiley Interdisciplinary Reviews: Developmental Biology*, *4*(1), 17-32. doi:10.1002/wdev.161

- Pilia, G., Hughes-Benzie, R. M., MacKenzie, A., Baybayan, P., Chen, E. Y., Huber, R., . . . Schlessinger, D. (1996). Mutations in GPC3, a glypican gene, cause the Simpson-Golabi-Behmel overgrowth syndrome. *Nat Genet*, *12*(3), 241-247. doi:10.1038/ng0396-241
- Pineda-Alvarez, D. E., Roessler, E., Hu, P., Srivastava, K., Solomon, B. D., Siple, C. E., . . . Muenke, M. (2012). Missense substitutions in the GAS1 protein present in holoprosencephaly patients reduce the affinity for its ligand, SHH. *Hum Genet*, *131*(2), 301-310. doi:10.1007/s00439-011-1078-6
- Porter, F. D., Drago, J., Xu, Y., Cheema, S. S., Wassif, C., Huang, S. P., . . . Westphal, H. (1997). Lhx2, a LIM homeobox gene, is required for eye, forebrain, and definitive erythrocyte development. *Development*, *124*(15), 2935-2944.
- Poulain, F. E., & Yost, H. J. (2015). Heparan sulfate proteoglycans: a sugar code for vertebrate development? *Development*, *142*(20), 3456-3467. doi:10.1242/dev.098178
- R Development Core Team. (2010). R: A language and environment for statistical computing.
- Rahimov, F., Ribeiro, L. A., de Miranda, E., Richieri-Costa, A., & Murray, J. C. (2006). GLI2 mutations in four Brazilian patients: how wide is the phenotypic spectrum? *Am J Med Genet A*, *140*(23), 2571-2576. doi:10.1002/ajmg.a.31370
- Rainer, J., Sanchez-Cabo, F., Stocker, G., Sturn, A., & Trajanoski, Z. (2006). CARMAweb: comprehensive R- and bioconductor-based web service for microarray data analysis. *Nucleic Acids Res*, *34*(Web Server issue), W498-503. doi:10.1093/nar/gkl038
- Rallu, M., Corbin, J. G., & Fishell, G. (2002). Parsing the prosencephalon. *Nat Rev Neurosci*, *3*(12), 943-951. doi:10.1038/nrn989
- Rasmussen, S. A., Moore, C. A., Khoury, M. J., & Cordero, J. F. (1996). Descriptive epidemiology of holoprosencephaly and arhinencephaly in metropolitan Atlanta, 1968-1992. *Am J Med Genet*, *66*(3), 320-333. doi:10.1002/(sici)1096-8628(19961218)66:3<320::aid-ajmg16>3.0.co;2-o
- Rennie, M. Y., Detmar, J., Whiteley, K. J., Jurisicova, A., Adamson, S. L., & Sled, J. G. (2012). Expansion of the fetoplacental vasculature in late gestation is strain dependent in mice. *American Journal of Physiology - Heart and Circulatory Physiology*, *302*(6), H1261-H1273. doi:10.1152/ajpheart.00776.2011
- Ribeiro-Bicudo, L. A., Queizi, R. G., Guion-Almeida, M. L., Legnaro, C., & Richieri-Costa, A. (2012). Exclusion of mutations in TGIF, ALX3, and ALX4 genes in patients with the syndrome of frontonasal dysgenesis, callosal agenesis, basal encephalocele, and eye anomalies. *Am J Med Genet A*, *158a*(5), 1233-1235. doi:10.1002/ajmg.a.35305
- Ribeiro, L. A., Murray, J. C., & Richieri-Costa, A. (2006). PTCH mutations in four Brazilian patients with holoprosencephaly and in one with holoprosencephaly-like features and normal MRI. *Am J Med Genet A*, *140*(23), 2584-2586. doi:10.1002/ajmg.a.31369
- Ribeiro, L. A., Queizi, R. G., Nascimento, A., Bertolacini, C. P., & Richieri-Costa, A. (2010). Holoprosencephaly and holoprosencephaly-like phenotype and GAS1 DNA sequence changes: Report of four Brazilian patients. *Am J Med Genet A*, *152a*(7), 1688-1694. doi:10.1002/ajmg.a.33466
- Roessler, E., Belloni, E., Gaudenz, K., Jay, P., Berta, P., Scherer, S. W., . . . Muenke, M. (1996). Mutations in the human Sonic Hedgehog gene cause holoprosencephaly. *Nat Genet*, *14*(3), 357-360. doi:10.1038/ng1196-357
- Roessler, E., Du, Y. Z., Mullor, J. L., Casas, E., Allen, W. P., Gillesen-Kaesbach, G., . . . Muenke, M. (2003). Loss-of-function mutations in the human GLI2 gene are associated with pituitary anomalies and holoprosencephaly-like features. *Proc Natl Acad Sci U S A*, *100*(23), 13424-13429. doi:10.1073/pnas.2235734100
- Roessler, E., Ermilov, A. N., Grange, D. K., Wang, A., Grachtchouk, M., Dlugosz, A. A., & Muenke, M. (2005). A previously unidentified amino-terminal domain regulates transcriptional activity of wild-type and disease-associated human GLI2. *Hum Mol Genet*, *14*(15), 2181-2188. doi:10.1093/hmg/ddi222

- Roessler, E., Ma, Y., Ouspenskaia, M. V., Lacbawan, F., Bendavid, C., Dubourg, C., . . . Muenke, M. (2009). Truncating loss-of-function mutations of DISP1 contribute to holoprosencephaly-like microform features in humans. *Hum Genet*, *125*(4), 393-400. doi:10.1007/s00439-009-0628-7
- Roessler, E., & Muenke, M. (2010). The molecular genetics of holoprosencephaly. *Am J Med Genet C Semin Med Genet*, *154c*(1), 52-61. doi:10.1002/ajmg.c.30236
- Roessler, E., Pei, W., Ouspenskaia, M. V., Karkera, J. D., Velez, J. I., Banerjee-Basu, S., . . . Muenke, M. (2009). Cumulative ligand activity of NODAL mutations and modifiers are linked to human heart defects and holoprosencephaly. *Mol Genet Metab*, *98*(1-2), 225-234. doi:10.1016/j.ymgme.2009.05.005
- Ronen, G. M., & Andrews, W. L. (1991). Holoprosencephaly as a possible embryonic alcohol effect. *Am J Med Genet*, *40*(2), 151-154. doi:10.1002/ajmg.1320400206
- Rozario, T., & DeSimone, D. W. (2010). The extracellular matrix in development and morphogenesis: a dynamic view. *Dev Biol*, *341*(1), 126-140. doi:10.1016/j.ydbio.2009.10.026
- Rubenstein, J. L., Shimamura, K., Martinez, S., & Puelles, L. (1998). Regionalization of the prosencephalic neural plate. *Annu Rev Neurosci*, *21*, 445-477. doi:10.1146/annurev.neuro.21.1.445
- Sakane, H., Yamamoto, H., Matsumoto, S., Sato, A., & Kikuchi, A. (2012). Localization of glypican-4 in different membrane microdomains is involved in the regulation of Wnt signaling. *J Cell Sci*, *125*(2), 449-460. doi:10.1242/Jcs.091876
- Sasaki, N., Okishio, K., Ui-Tei, K., Saigo, K., Kinoshita-Toyoda, A., Toyoda, H., . . . Nishihara, S. (2008). Heparan Sulfate Regulates Self-renewal and Pluripotency of Embryonic Stem Cells. *Journal of Biological Chemistry*, *283*(6), 3594-3606. doi:10.1074/jbc.M705621200
- Saucedo, L. J., & Edgar, B. A. (2007). Filling out the Hippo pathway. *Nat Rev Mol Cell Biol*, *8*(8), 613-621.
- Schaeren-Wiemers, N., & Gerfin-Moser, A. (1993). A single protocol to detect transcripts of various types and expression levels in neural tissue and cultured cells: in situ hybridization using digoxigenin-labelled cRNA probes. *Histochemistry*, *100*(6), 431-440. doi:10.1007/bf00267823
- Schmid, B., Schindelin, J., Cardona, A., Longair, M., & Heisenberg, M. (2010). A high-level 3D visualization API for Java and ImageJ. *BMC Bioinformatics*, *11*, 274. doi:10.1186/1471-2105-11-274
- Schneider, C. A., Rasband, W. S., & Eliceiri, K. W. (2012). NIH Image to ImageJ: 25 years of image analysis. *Nat Methods*, *9*(7), 671-675.
- She, X., Cheng, Z., Zollner, S., Church, D. M., & Eichler, E. E. (2008). Mouse segmental duplication and copy number variation. *Nat Genet*, *40*(7), 909-914. doi:http://www.nature.com/ng/journal/v40/n7/suppinfo/ng.172_S1.html
- Shimamura, K., Hartigan, D. J., Martinez, S., Puelles, L., & Rubenstein, J. L. (1995). Longitudinal organization of the anterior neural plate and neural tube. *Development*, *121*(12), 3923-3933.
- Shimamura, K., & Rubenstein, J. L. (1997). Inductive interactions direct early regionalization of the mouse forebrain. *Development*, *124*(14), 2709-2718.
- Shiratori, H., & Hamada, H. (2006). The left-right axis in the mouse: from origin to morphology. *Development*, *133*(11), 2095-2104. doi:10.1242/dev.02384
- Siddiqui, T. J., Tari, P. K., Connor, S. A., Zhang, P., Dobie, F. A., She, K., . . . Craig, A. M. (2013). An LRRTM4-HSPG complex mediates excitatory synapse development on dentate gyrus granule cells. *Neuron*, *79*(4), 680-695. doi:10.1016/j.neuron.2013.06.029
- Singla, V., Romaguera-Ros, M., Garcia-Verdugo, J. M., & Reiter, J. F. (2010). Odf1, a Human Disease Gene, Regulates the Length and Distal Structure of Centrioles. *Developmental Cell*, *18*(3), 410-424. doi:http://dx.doi.org/10.1016/j.devcel.2009.12.022
- Sinha, S., & Chen, J. K. (2006). Purmorphamine activates the Hedgehog pathway by targeting Smoothened. *Nat Chem Biol*, *2*(1), 29-30. doi:http://www.nature.com/nchembio/journal/v2/n1/suppinfo/nchembio753_S1.html

- Skarnes, W. C., Rosen, B., West, A. P., Koutourakis, M., Bushell, W., Iyer, V., . . . Bradley, A. (2011). A conditional knockout resource for the genome-wide study of mouse gene function. *Nature*, *474*(7351), 337-342. doi:<http://www.nature.com/nature/journal/v474/n7351/abs/10.1038-nature10163-unlocked.html#supplementary-information>
- Song, H. H., Shi, W., Xiang, Y. Y., & Filmus, J. (2005). The loss of glypican-3 induces alterations in Wnt signaling. *J Biol Chem*, *280*(3), 2116-2125. doi:10.1074/jbc.M410090200
- Spandidos, A., Wang, X., Wang, H., & Seed, B. (2010). PrimerBank: a resource of human and mouse PCR primer pairs for gene expression detection and quantification. *Nucleic Acids Res*, *38*(Database issue), D792-799. doi:10.1093/nar/gkp1005
- Spoelgen, R., Hammes, A., Anzenberger, U., Zechner, D., Andersen, O. M., Jerchow, B., & Willnow, T. E. (2005). LRP2/megalin is required for patterning of the ventral telencephalon. *Development*, *132*(2), 405-414. doi:10.1242/dev.01580
- Strate, I., Tessadori, F., & Bakkers, J. (2015). Glypican4 promotes cardiac specification and differentiation by attenuating canonical Wnt and Bmp signaling. *Development*, *142*(10), 1767-1776. doi:10.1242/dev.113894
- Sugahara, K., & Mikami, T. (2007). Chondroitin/dermatan sulfate in the central nervous system. *Current Opinion in Structural Biology*, *17*(5), 536-545. doi:10.1016/j.sbi.2007.08.015
- Taipale, J., Chen, J. K., Cooper, M. K., Wang, B., Mann, R. K., Milenkovic, L., . . . Beachy, P. A. (2000). Effects of oncogenic mutations in Smoothed and Patched can be reversed by cyclopamine. *Nature*, *406*(6799), 1005-1009. doi:10.1038/35023008
- Takahashi, K., & Yamanaka, S. (2006). Induction of Pluripotent Stem Cells from Mouse Embryonic and Adult Fibroblast Cultures by Defined Factors. *Cell*, *126*(4), 663-676. doi:<http://dx.doi.org/10.1016/j.cell.2006.07.024>
- Takaoka, K., & Hamada, H. (2012). Cell fate decisions and axis determination in the early mouse embryo. *Development*, *139*(1), 3-14. doi:10.1242/dev.060095
- Takaoka, K., Yamamoto, M., & Hamada, H. (2011). Origin and role of distal visceral endoderm, a group of cells that determines anterior-posterior polarity of the mouse embryo. *Nat Cell Biol*, *13*(7), 743-752. doi:10.1038/ncb2251
- Tam, P. P., & Steiner, K. A. (1999). Anterior patterning by synergistic activity of the early gastrula organizer and the anterior germ layer tissues of the mouse embryo. *Development*, *126*(22), 5171-5179.
- Tang, T., Li, L., Tang, J., Li, Y., Lin, W. Y., Martin, F., . . . de Sauvage, F. J. (2010). A mouse knockout library for secreted and transmembrane proteins. *Nat Biotechnol*, *28*(7), 749-755. doi:10.1038/nbt.1644
- Tani, E., & Ametani, T. (1971). Extracellular distribution of ruthenium red-positive substance in the cerebral cortex. *J Ultrastruct Res*, *34*(1), 1-14.
- Tenorio, J., Arias, P., Martinez-Glez, V., Santos, F., Garcia-Minaur, S., Nevado, J., & Lapunzina, P. (2014). Simpson-Golabi-Behmel syndrome types I and II. *Orphanet J Rare Dis*, *9*, 138. doi:10.1186/s13023-014-0138-0
- Terespolsky, D., Farrell, S. A., Siegel-Bartelt, J., & Weksberg, R. (1995). Infantile lethal variant of Simpson-Golabi-Behmel syndrome associated with hydrops fetalis. *Am J Med Genet*, *59*(3), 329-333. doi:10.1002/ajmg.1320590310
- Theil, T., Aydin, S., Koch, S., Grotewold, L., & Ruther, U. (2002). Wnt and Bmp signalling cooperatively regulate graded Emx2 expression in the dorsal telencephalon. *Development*, *129*(13), 3045-3054.
- Thomas, P., & Beddington, R. (1996). Anterior primitive endoderm may be responsible for patterning the anterior neural plate in the mouse embryo. *Current Biology*, *6*(11), 1487-1496. doi:[http://dx.doi.org/10.1016/S0960-9822\(96\)00753-1](http://dx.doi.org/10.1016/S0960-9822(96)00753-1)
- Thomas, P. Q., Brown, A., & Beddington, R. S. (1998). Hex: a homeobox gene revealing peri-implantation asymmetry in the mouse embryo and an early transient marker of endothelial cell precursors. *Development*, *125*(1), 85-94.

- Timmer, J. R., Wang, C., & Niswander, L. (2002). BMP signaling patterns the dorsal and intermediate neural tube via regulation of homeobox and helix-loop-helix transcription factors. *Development*, *129*(10), 2459-2472.
- Topczewski, J., Sepich, D. S., Myers, D. C., Walker, C., Amores, A., Lele, Z., . . . Solnica-Krezel, L. (2001). The zebrafish glypican knypek controls cell polarity during gastrulation movements of convergent extension. *Dev Cell*, *1*(2), 251-264.
- Traister, A., Shi, W., & Filmus, J. (2008). Mammalian Notum induces the release of glypicans and other GPI-anchored proteins from the cell surface. *Biochemical Journal*, *410*(3), 503-511. doi:10.1042/bj20070511
- Tukachinsky, H., Kuzmickas, R. P., Jao, C. Y., Liu, J., & Salic, A. (2012). Dispatched and scube mediate the efficient secretion of the cholesterol-modified hedgehog ligand. *Cell Rep*, *2*(2), 308-320. doi:10.1016/j.celrep.2012.07.010
- Ussar, S., Bezy, O., Bluher, M., & Kahn, C. R. (2012). Glypican-4 enhances insulin signaling via interaction with the insulin receptor and serves as a novel adipokine. *Diabetes*, *61*(9), 2289-2298. doi:10.2337/db11-1395
- Vambergue, A., & Fajardy, I. (2011). Consequences of gestational and pregestational diabetes on placental function and birth weight. *World Journal of Diabetes*, *2*(11), 196-203. doi:10.4239/wjd.v2.i11.196
- Veugelers, M., Cat, B. D., Muyltermans, S. Y., Reekmans, G., Delande, N., Frints, S., . . . David, G. (2000). Mutational analysis of the GPC3/GPC4 glypican gene cluster on Xq26 in patients with Simpson-Golabi-Behmel syndrome: identification of loss-of-function mutations in the GPC3 gene. *Hum Mol Genet*, *9*(9), 1321-1328.
- Veugelers, M., De Cat, B., Ceulemans, H., Bruystens, A. M., Coomans, C., Durr, J., . . . David, G. (1999). Glypican-6, a new member of the glypican family of cell surface heparan sulfate proteoglycans. *J Biol Chem*, *274*(38), 26968-26977.
- Veugelers, M., Vermeesch, J., Watanabe, K., Yamaguchi, Y., Marynen, P., & David, G. (1998). GPC4, the gene for human K-glypican, flanks GPC3 on xq26: deletion of the GPC3-GPC4 gene cluster in one family with Simpson-Golabi-Behmel syndrome. *Genomics*, *53*(1), 1-11. doi:10.1006/geno.1998.5465
- Wallis, D. E., Roessler, E., Hehr, U., Nanni, L., Wiltshire, T., Richieri-Costa, A., . . . Muenke, M. (1999). Mutations in the homeodomain of the human SIX3 gene cause holoprosencephaly. *Nat Genet*, *22*(2), 196-198. doi:10.1038/9718
- Watanabe, K., Yamada, H., & Yamaguchi, Y. (1995). K-glypican: a novel GPI-anchored heparan sulfate proteoglycan that is highly expressed in developing brain and kidney. *J Cell Biol*, *130*(5), 1207-1218.
- Waters, A. M., & Beales, P. L. (2011). Ciliopathies: an expanding disease spectrum. *Pediatr Nephrol*, *26*(7), 1039-1056. doi:10.1007/s00467-010-1731-7
- Waterson, J., Stockley, T. L., Segal, S., & Golabi, M. (2010). Novel duplication in glypican-4 as an apparent cause of Simpson-Golabi-Behmel syndrome. *Am J Med Genet A*, *152A*(12), 3179-3181. doi:10.1002/ajmg.a.33450
- Weiner, J. A., Hecht, J. H., & Chun, J. (1998). Lysophosphatidic acid receptor gene vzg-1/lpA1/edg-2 is expressed by mature oligodendrocytes during myelination in the postnatal murine brain. *J Comp Neurol*, *398*(4), 587-598.
- Williams, E. H., Pappano, W. N., Saunders, A. M., Kim, M. S., Leahy, D. J., & Beachy, P. A. (2010). Dally-like core protein and its mammalian homologues mediate stimulatory and inhibitory effects on Hedgehog signal response. *Proc Natl Acad Sci U S A*, *107*(13), 5869-5874. doi:10.1073/pnas.1001777107
- Williamson, D., Selfe, J., Gordon, T., Lu, Y. J., Pritchard-Jones, K., Murai, K., . . . Shipley, J. (2007). Role for amplification and expression of glypican-5 in rhabdomyosarcoma. *Cancer Res*, *67*(1), 57-65. doi:10.1158/0008-5472.CAN-06-1650

- Willnow, T. E., Hilpert, J., Armstrong, S. A., Rohlmann, A., Hammer, R. E., Burns, D. K., & Herz, J. (1996). Defective forebrain development in mice lacking gp330/megalyn. *Proc Natl Acad Sci U S A*, *93*(16), 8460-8464.
- Wilson, N. H., & Stoeckli, E. T. (2013). Sonic hedgehog regulates its own receptor on postcrossing commissural axons in a glypican1-dependent manner. *Neuron*, *79*(3), 478-491. doi:10.1016/j.neuron.2013.05.025
- Winter, T. C., Kennedy, A. M., & Woodward, P. J. (2015). Holoprosencephaly: A Survey of the Entity, with Embryology and Fetal Imaging. *RadioGraphics*, *35*(1), 275-290. doi:doi:10.1148/rg.351140040
- Wu, S. M., Choo, A. B., Yap, M. G., & Chan, K. K. (2010). Role of Sonic hedgehog signaling and the expression of its components in human embryonic stem cells. *Stem Cell Res*, *4*(1), 38-49. doi:10.1016/j.scr.2009.09.002
- Yamamoto, M., Saijoh, Y., Perea-Gomez, A., Shawlot, W., Behringer, R. R., Ang, S.-L., . . . Meno, C. (2004). Nodal antagonists regulate formation of the anteroposterior axis of the mouse embryo. *Nature*, *428*(6981), 387-392. doi:http://www.nature.com/nature/journal/v428/n6981/supinfo/nature02418_S1.html
- Yan, D., & Lin, X. (2007). Drosophila glypican Dally-like acts in FGF-receiving cells to modulate FGF signaling during tracheal morphogenesis. *Dev Biol*, *312*(1), 203-216. doi:10.1016/j.ydbio.2007.09.015
- Yan, D., Wu, Y., Yang, Y., Belenkaya, T. Y., Tang, X., & Lin, X. (2010). The cell-surface proteins Dally-like and Ihog differentially regulate Hedgehog signaling strength and range during development. *Development*, *137*(12), 2033-2044. doi:10.1242/dev.045740
- Yang, Y., Drossopoulou, G., Chuang, P. T., Duprez, D., Marti, E., Bumcrot, D., . . . Tickle, C. (1997). Relationship between dose, distance and time in Sonic Hedgehog-mediated regulation of anteroposterior polarity in the chick limb. *Development*, *124*(21), 4393-4404.
- Yao, S., Lum, L., & Beachy, P. (2006). The ihog cell-surface proteins bind Hedgehog and mediate pathway activation. *Cell*, *125*(2), 343-357. doi:10.1016/j.cell.2006.02.040
- Ybot-Gonzalez, P., Copp, A. J., & Greene, N. D. (2005). Expression pattern of glypican-4 suggests multiple roles during mouse development. *Dev Dyn*, *233*(3), 1013-1017. doi:10.1002/dvdy.20383
- Ye, J., Coulouris, G., Zaretskaya, I., Cutcutache, I., Rozen, S., & Madden, T. L. (2012). Primer-BLAST: a tool to design target-specific primers for polymerase chain reaction. *BMC Bioinformatics*, *13*, 134. doi:10.1186/1471-2105-13-134
- Zhang, W., Hong, M., Bae, G. U., Kang, J. S., & Krauss, R. S. (2011). Boc modifies the holoprosencephaly spectrum of Cdo mutant mice. *Dis Model Mech*, *4*(3), 368-380. doi:10.1242/dmm.005744
- Zhang, W., Kang, J. S., Cole, F., Yi, M. J., & Krauss, R. S. (2006). Cdo functions at multiple points in the Sonic Hedgehog pathway, and Cdo-deficient mice accurately model human holoprosencephaly. *Dev Cell*, *10*(5), 657-665. doi:10.1016/j.devcel.2006.04.005
- Zhang, W., Yi, M. J., Chen, X., Cole, F., Krauss, R. S., & Kang, J. S. (2006). Cortical thinning and hydrocephalus in mice lacking the immunoglobulin superfamily member CDO. *Mol Cell Biol*, *26*(10), 3764-3772. doi:10.1128/mcb.26.10.3764-3772.2006
- Zhu, H. J., Pan, H., Cui, Y., Wang, X. Q., Wang, L. J., Li, N. S., . . . Gong, F. Y. (2014). The changes of serum glypican4 in obese patients with different glucose metabolism status. *J Clin Endocrinol Metab*, *99*(12), E2697-2701. doi:10.1210/jc.2014-2018
- Zimmer, B., Piao, J., Ramnarine, K., Tomishima, Mark J., Tabar, V., & Studer, L. (2016). Derivation of Diverse Hormone-Releasing Pituitary Cells from Human Pluripotent Stem Cells. *Stem Cell Reports*, *6*(6), 858-872. doi:http://dx.doi.org/10.1016/j.stemcr.2016.05.005
- Zimmermann, D. R., & Dours-Zimmermann, M. T. (2008). Extracellular matrix of the central nervous system: from neglect to challenge. *Histochem Cell Biol*, *130*(4), 635-653. doi:10.1007/s00418-008-0485-9

Appendix

Curriculum vitae

Name: Stefan Weiß
Geburtsdatum: 30.07.1986
Geburtsort: Tirschenreuth
Nationalität: Deutsch

Promotion:

2012 – 2017: **Promotion**
WZW der Technischen Universität München
Betreuerin: Dr. Sabrina Desbordes
Doktorvater: Prof. Dr. Wolfgang Wurst
Institut für Entwicklungsgenetik, Helmholtz Zentrum München

Studium:

2009 – 2011 **Master of Science in Cellular & Molecular Neuroscience**
Universität Tübingen
Masterarbeit: "The potential role of mitochondrial A β in Alzheimer's disease"
Betreuer: Dr. Baumann, Prof. Jucker
Hertie Institut für klinische Hirnforschung, Tübingen

2006 – 2009 **Bachelor of Science in Biologie**
Universität Regensburg
Bachelorarbeit: „Psychosocial stress and its impact on the functionality of the adrenal gland in the mouse“
Betreuer: Dr. Reber, Prof. Neumann
Lehrstuhl für Neurobiologie und Tierphysiologie, Universität Regensburg

Ausbildung

1997 – 2006 Stiftland-Gymnasium Tirschenreuth
1993 – 1997 Marien Grundschule Tirschenreuth

List of conference contributions

Annual Meeting ISSCR San Francisco, USA, June 2016

(Poster)

ISSCR Symposium „Stem cell models of neural regeneration and disease“, Dresden, February 2016

(Talk)

Annual Meeting German Stem Cell Network (GSCN), Heidelberg, November 2014

MipTec Conference, Basel, Switzerland, October 2014

PharmaIQ ‘Cell-based assays’, Munich, December 2013

World conference on regenerative medicine, Leipzig, October 2013

Acknowledgements

At first, I want to thank Prof. Dr. Wolfgang Wurst who gave me the opportunity to do my PhD project at the institute for developmental genetics (IDG) and at the Wissenschaftszentrum Weihenstephan (WZW).

I would also like to thank Dr. Micha Drukker (ISF) for the continuous guidance as a member of my thesis committee as well as my second thesis examiner Prof. Dr. Angelika Schnieke (WZW).

Special thanks go to my direct supervisor and group leader Dr. Sabrina Desbordes. You introduced me to the fascinating world of stem cells and the extracellular matrix and gave your encouraging advice whenever I needed one. I am especially thankful for the unlimited trust to let me work independently and for your support of my project with all possible resources. I think we were a great and productive team!

Furthermore, I want to thank my closest colleagues and friends Elen Torres, Theresa Bäcker, Tanja Orschmann and Anna Truckenbrodt. Not only the unlimited trouble shootings and scientific discussions but also the warm atmosphere made me feel being a member of a very special team. Thank you for the great time I could spend with you, including the numerous weekends.

For the big support with my mouse work, I want to thank Jakob Reber and Xheva Halitaj. Your work allowed me to advance much faster my project and to train my coordination skills.

Additionally, I want to thank my collaboration partners including Dr. Kenji Schorpp and Dr. Kamyar Hadian (TOX), Dr. Siegfried Ussar (IDO), Dr. Michael Sandholzer (ISF), Dr. Martin Irmeler and PD Dr. Beckers (IEG), Dr. Silvia Engert (ISF), Dr. Michaela Aichler and Gabriele Mettenleiter (AAP), Dr. Camp and Dr. Treutlein (MPI Leipzig) and the mouse facility team, coordinated by Daniela Würzinger (AVM). This project would not have been possible without their continuous contribution and ideas.

Especially, I want to thank my girlfriend Maïke for her endless support throughout the whole PhD project and especially during the last months of the thesis. Your patience, motivation and feedback together with your great food helped me to finish this project in my best possible way. Thank you so much for being there for me!

Finally, I want to thank my parents and my brother for their persistent support during the last four years. You always get me back on track in challenging phases during this project but also celebrated good times with me. A big thanks for your unlimited believe in whatever I did so far.